Regulation of G-protein coupled PLC signalling by PI4KIIIα in *Drosophila* photoreceptors

A Thesis

Submitted to the

Tata Institute of Fundamental Research, Mumbai

for the degree of Doctor of Philosophy

in Biology

by

Sruthi S. Balakrishnan

National Centre for Biological Sciences, Bangalore

Tata Institute of Fundamental Research, Mumbai

November, 2019

Declaration

This thesis is a presentation of my original research work. Wherever contributions of others are involved, every effort is made to indicate this clearly, with due reference to the literature, and acknowledgement of collaborative research and discussions.
The work was done under the guidance of Dr. Raghu Padinjat, at the Tata Institute of Fundamental Research, Mumbai.

Sruthi S. Balakrishnan
National Centre for Biological Sciences-TIFR, Bangalore

In my capacity as supervisor of the candidate's thesis, I certify that the above statements are true to the best of my knowledge.

Dr. Raghu Padinjat
National Centre for Biological Sciences-TIFR, Bangalore

Date : 01/11/2019

Certificate

I certify that this thesis entitled "**Regulation of G-protein coupled PLC signalling by PI4KIIIα in *Drosophila* photoreceptors**" comprises research work carried out by **Sruthi S. Balakrishnan** at National Centre for Biological Sciences under the supervision of **Dr. Raghu Padinjat** during the period 2012 - 2019 for the degree of Doctor of Philosophy of the Tata Institute of Fundamental Research (TIFR). The results presented in this thesis have not been submitted previously to this or any other University for a PhD or any other degree.

Head of Academics
National Centre for Biological Sciences
Tata Institute of Fundamental Research
Bangalore

Publication

Balakrishnan Sruthi S., Basu Urbashi, Shinde Dhananjay, Thakur Rajan, Jaiswal Manish, Padinjat Raghu. Regulation of PI4P levels by PI4KIIIα during G-protein coupled PLC signaling in *Drosophila* photoreceptors. *Journal of Cell Science*. 2018 Aug; 131(15) doi: 10.1242/jcs.217257. PubMed PMID:29980590.

Acknowledgments

I would first like to thank my thesis advisor, Dr. Raghu Padinjat, for his guidance and support. This thesis and all the work within would not have come to fruition without his mentorship. I would also like to thank my thesis committee members, Dr. Akash Gulyani and Dr. Sandeep Krishna, for their valuable comments and advice that helped massively improve this work.

Nearly every member of the lab, past and present, has helped me over these past seven years, be it as mentors or fellow journeymen along the PhD voyage. My thanks to the senior members - Rajan, Shweta, Sourav and Sudipto - for being kind and patient teachers and bearing with my countless missteps and questions. My forays into mass spectrometry would not have been successful without fellow spectrometrists Avishek, Panda and Sanjeev, who did most of the legwork and allowed me to reap the benefits. I am extremely grateful to Dr. Dhananjay Shinde, always ready to face my endless complaints and without whose patience and guidance the latter half of my PhD would not have been possible. I thank Aastha, Amruta, Bishal, Harini, Rohit, Sankhanil, Shirish and Vishnu for the many insights, discussions (especially flyroom ones), dances and edible treats that kept me going through this journey. A special note of thanks to Urbashi, my partner in crime for all things PI4K, whose formidably positive attitude has often tided the both of us through tough spells. I would like to thank Swarna, my companion in thesis writing, for the remarkably engaging conversations that are always a welcome treat. I also thank her for producing Jia, the three-foot marvel who filled a lot of my evenings with curiosity and crocodiles (and often curiosity about crocodiles).

My time in NCBS has been immensely enriched by several people outside the lab. My two years in the Parijata hostel were made memorable thanks to the many late night chat/movie sessions with my Int. PhD batchmates - Akshay, Aparna, Avishek, Leanna, Payel and Vishal. Many thanks to the board game group - Chaitra, Ebi, Jyothi, Pritha, Rohit, Snehal and Sree Krishna - for

allowing guest appearances and spontaneous pow-wows. An extra heaping of gratitude is due to Chaitra for simply being the effervescent entity that she is and always finding a solution to any problem. A similarly measured dose goes to Aparna for all the brilliant birthday bashes, books, coffee, conversations (usually about books and coffee) and eerie parallels in our lives. I will always be grateful to Dinesh for his constant companionship, cooking and computer capabilities that got me through the bulk of my PhD. My thanks to Nitesh and Shivansh for the innumerable discussions about history, technology and a plethora of other things that never failed to intrigue. A shout out to the drama clubs at NCBS (StageCraft) and IISc (Rangmanch), with whom I shared brief associations that were vastly rewarding.

I am very thankful to my friends outside NCBS - Chaitra, Dhisha, Harshitha, Kaveri, Shwetha and Soujanya - for reminding me about the "outside" world from time to time. Many thanks to my parents for their neverending support and continual supply of good food. Special thanks to my little sister for offering to catch flies from the fruit bowl at home to speed up my research.

The academic office at NCBS has never failed to help when called upon; an additional note of thanks to Mrs. Vishalakshi K S for keeping tabs on us and facing the onslaught of doubts and paperwork with a smile.

Finally, I would like to thank the entire NCBS community for fostering an environment that has allowed independent thinking and personal growth on exceptional levels.

List of Figures

List of Tables

Contents

Acronyms

^{32}-P ^{32}-phosphorus. 5

ANOVA Analysis of Variance. 66

AP-1 adaptor protein - 1. 14

ASD autism spectrum disorders. 191

ATP adenosine triphosphate. 6

BDNF brain-derived neurotrophic factor. 192

CDP cytidine diphosphate. 5

CDP-DAG cytidine diphosphate - diacylglycerol. 23

CERT ceramide transport protein. 13

CO_2 carbon dioxide. 59

DAG diacylglycerol. 7

DAPI 4', 6 - diamidino - 2 - phenylindole. 63

DPP Deep Pseudopupil. 54

EFR3 eighty five requiring 3. 17

EGFR epidermal growth factor receptor. 15

ER endoplasmic reticulum. 11

ERG electroretinogram. 54

FAPP2 four phosphate adaptor protein 2. 13

FGF fibroblast growth factor. 14

fMLP N-formyl-methionine-leucyl-phenylalanine. 9

GFP green fluorescent protein. 54

GGA Golgi localised, Gamma adaptin ear containing, ARF binding protein. 14

GMR Glass Multimer Reporter. 69

GOLPH3 Golgi phosphoprotein 3. 14

GPCR G-protein coupled receptor. 7

GTPases guanosine triphosphatases. 7

HA haemagglutinin. 50

HPLC high performance liquid chromatography. 4

INAD inactivation no afterpotential D. 79

IP_3 inositol - 1,4,5 - trisphosphate. 7

LC-MS liquid chromatography - mass spectrometry. 87

LPWS Lower Phase Wash Solution. 55

OCRL oculocerebral renal syndrome of Lowe. 9

ORP OSBP related protein. 14

OSBP oxysterol binding protein. 13

Osh OSBP homologue. 14

P4M PI4P binding of SidM. 50

PA phosphatidic acid. 23

PBS Phosphate Buffered Saline. 55

PDGF platelet derived growth factor. 15

PE Phosphatidylethanolamine. 56

PEB Phosphoinositide Elution Buffer. 55

PH pleckstrin homology. 94

PI Phosphatidylinositol. 4

PI(3,4)P_2 phosphatidylinositol 3,4 - bisphosphate. 4

PI(3,4,5)P_3 phosphatidylinositol 3,4,5 - trisphosphate. 5

PI(3,5)P_2 phosphatidylinositol 3,5 - bisphosphate. 4

PI(4,5)P_2 phosphatidylinositol 4,5 - bisphosphate. 4

PI3P phosphatidylinositol 3 - phosphate. 4

PI4K phosphatidylinositol 4 - kinase. 15

PI4P phosphatidylinositol 4 - phosphate. 4

PI5P phosphatidylinositol 5 - phosphate. 4

PIP phosphatidylinositol phosphate. 87

PIP4K phosphatidylinositol 5 - phosphate 4 - kinase. 187

PIP5K phosphatidylinositol 4 - phosphate 5 - kinase. 17

PIP_2 phosphatidylinositol bisphosphate. 87

PLC phospholipase C. 6

PLD phospholipase D. 187

PM plasma membrane. 11

PS phosphatidylserine. 14

PSSM Position Specific Scoring Matrix. 64

PTEN phosphatase and tensin homologue. 9

PUFA polyunsaturated fatty acids. 161

Q-PCR Quantitative Polymerase Chain Reaction. 52

RDGB retinal degeneration B. 23

RNAi ribonucleic acid interference. 19

SMC sub-microvillar cisternae. 23

TGN trans-Golgi network. 14

TLC thin layer chromatography. 4

TMS Trimethylsilyl. 55

TRP transient receptor potential. 22

TRPL transient receptor potential like. 22

TTC7 tetratricopeptide containing protein 7. 17

UAS upstream activating sequence. 46

UPLC Ultra Performance Liquid Chromatography. 56

VSP voltage sensitive phosphatase. 185

WT wild-type. 46

Chapter 1

Introduction

1.1 Phosphoinositides

One of the fundamental tenets of living systems is their ability to sense changes in the environment and respond accordingly. Be it differences in temperature, pressure or availability of food, organisms have developed means of detecting variations and modulating their behaviours to adapt to the change. At the cellular level, environmental perturbations are sensed by receptors present at the plasma membrane. Eukaryotic cells carry different kinds of receptors, each attuned to specific external signals. These receptors communicate information to the cell, which is processed in the form of a signal transduction cascade and allows the cell to respond to the external perturbations (Grecco et al., 2011).

Signal transduction events are often triggered by the action of enzymes which have been activated by receptors. The substrates for these enzymes could be either proteins or lipids. Lipids, although they largely play a structural role in the form of membranes, also function in the cell as signalling intermediates (Sunshine and Iruela-Arispe, 2017). The phosphoinositide lipids offer a good example of signalling lipids that mediate cellular responses such as smooth muscle contraction and neurotransmission (Balla et al., 2012). These lipids form a small fraction of total cellular lipids, comprising only about 15% of the total phospholipid content (Slack et al., 1978). They fall in the class of glycerophospholipids, with a head group of inositol attached to the glycerol backbone through a phosphodiester bond. The lipid phosphatidylinositol (PI) is the parent lipid from which all the phosphoinositides are derived, as the hydroxyl groups of the inositol ring can be phosphorylated at the third,

fourth and fifth positions, either individually or in combination **(Fig.1.1)** (Balakrishnan et al., 2015).

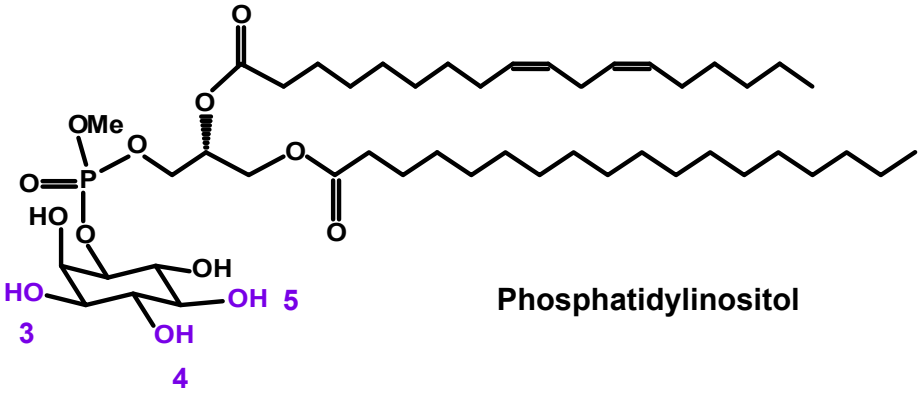

Figure 1.1 : Phosphatidylinositol
Chemical structure of phosphatidylinositol, the parent lipid that gives rise to all other phosphoinositides. The three hydroxyl groups that can be phosphorylated are marked in purple.

This allows the generation of seven different phosphoinositide lipids, depending on the position of the attached phosphate groups. These comprise of three monophosphorylated species (PI3P, PI4P, PI5P), three bisphosphorylated species [PI(3,4)P_2, PI(4,5)P_2, (PI(3,5)P_2] and one trisphosphorylated species [PI(3,4,5)P_3] **(Fig.1.2)**. The positions one, two and six cannot be phosphorylated owing to steric hindrance from the glycerol moiety. The addition and removal of phosphate groups is carried out by lipid kinases and phosphatases, respectively (Sasaki et al., 2009). The interconversion of phosphoinositides from one form to another is one of the main properties that enable them to perform their cellular functions. Some of the enzymatic reactions that facilitate such interconversions are outlined in **Fig.1.2**.

1.1.1 Subcellular localisations and abundances of phosphoinositides

Each of the seven different phosphoinositide species, along with their parent lipid PI, have been observed at different cellular locations, where they serve distinct purposes. The subcellular localisations of the lipids were mostly deciphered using lipid-binding probes, which are protein domains tagged to a fluorophore, that selectively bind certain phosphoinositides based on the

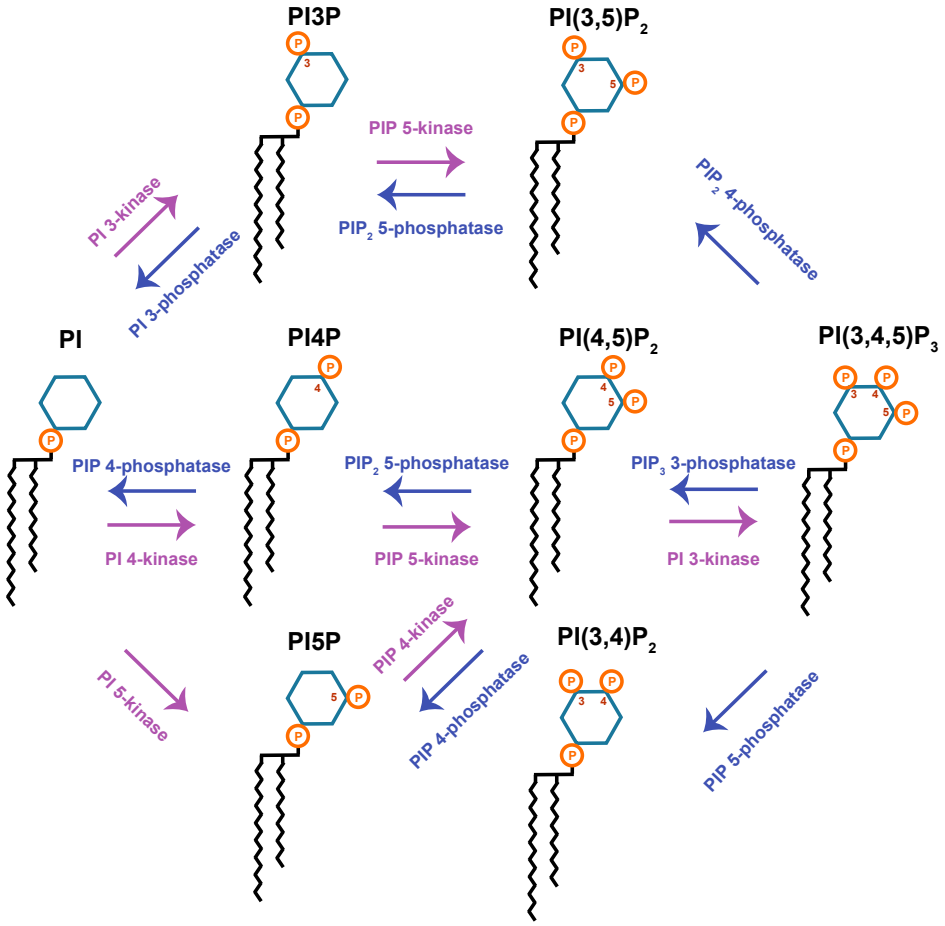

Figure 1.2 : Phosphoinositides
Phosphatidylinositol can be phosphorylated at three different positions, either individually or combinatorially, to produce the seven phosphoinositides shown here. The inositol ring is marked in teal and phosphate groups are marked in orange, with the positions numbered in red. The different phosphoinositides can undergo interconversions through the action of lipid kinases (purple) or phosphatases (blue). The reactions listed here are a subset of those for which there is evidence from cell culture studies.

inositol head group (Várnai et al., 2017). The concentrations of these lipids at specific membranes is governed by the presence and/or absence of the enzymes that metabolise them (Yang et al., 2018). Earlier studies routinely used either thin layer chromatography (TLC) or high performance liquid chromatography (HPLC) to quantify radiolabelled lipids, whereas more recently liquid chromatography has been coupled with mass spectrometry (LC-MS) to measure cellular phosphoinositides (Pettitt et al., 2006).

Phosphatidylinositol (PI) is present at the endoplasmic reticulum, as seen from experiments using subcellular fractionation assays. The enzyme which synthesises it, PI synthase, is also present at the same membrane (Bleasdale et al., 1979). PI only accounts for ~2.5% of the total phospholipids (Fridriksson et al., 1999), but forms the majority species of cellular phosphoinositides itself, with recent reports of it constituting more than 90% of the total pool (Traynor-Kaplan et al., 2017).

With respect to the monophosphorylated forms, phosphatidylinositol 4 - phosphate (PI4P) is perhaps the most abundant of the three, comprising ~5% of the total phosphoinositide population (Gunnarsson et al., 1997). PI4P has been reported to be present at equivalent concentrations both at the Golgi apparatus and the plasma membrane, with a small fraction present on endocytic vesicles and phagosomes as well (Hammond et al., 2014; Wang et al., 2015). The lipid phosphatidylinositol 3 - phosphate (PI3P) is present in far lower amounts, accounting for barely 0.2% of all phosphoinositides (Stephens et al., 2000). PI3P localises to the endosomal membranes, where it confers compartment identity to the vesicle and aids in recruiting adaptor proteins (Gillooly, 2000). The last of the monophosphorylated forms, phosphatidylinositol 5 - phosphate (PI5P), is the least abundant and also the least studied species. PI5P has been reported to be present at the nucleus and on internal vesicles, making up a mere 0.002% of total phosphoinositides (Jones et al., 2006; Sarkes and Rameh, 2010).

Among the bisphosphorylated species, phosphatidylinositol 4,5 - bisphosphate ($PI(4,5)P_2$) occurs at the highest concentration, accounting for close to 5% of all phosphoinositides (Gunnarsson et al., 1997). $PI(4,5)P_2$ is predominantly found at the plasma membrane of cell, where it is required for both signalling and other housekeeping functions (Várnai and Balla, 1998). The lipid phosphatidylinositol 3,4 - bisphosphate ($PI(3,4)P_2$) is a very minor class of lipid found on endosomal membranes and the plasma membrane, where it regulates cell signalling and maturation of endosomes (Kimber et al., 2002). It forms ~0.02% of the phosphoinositide pool (Stephens et al., 1991; Hawkins et al., 1992). The third species, phosphatidylinositol 3,5 - bispho-

sphate ($PI(3,5)P_2$), is a marker of late endosomal membranes and regulates membrane trafficking events. It is also a very low abundance lipid, comprising about 0.03% of phosphoinositides (Jin et al., 2008).

The final species is the trisphosphorylated form, phosphatidylinositol 3,4,5 - trisphosphate ($PI(3,4,5)P_3$), which is also a signalling lipid. $PI(3,4,5)P_3$ is present at the plasma membrane of cells, constituting only ~0.004% of the total celluar phosphoinositides (Stephens et al., 1991; Hawkins et al., 1992; Venkateswarlu et al., 1999).

1.1.2 Brief history of phosphoinositides

Phosphoinositides as a category of glycerophospholipids in eukaryotic cells was first reported by Klenk and colleagues in 1939, when the ether soluble extracts of soybean were analysed (Klenk and Sakai, 1939). In mammalian tissues, Folch further characterised these compounds from bovine brain extracts, where "inositol phosphatide" was isolated by chloroform-methanol extraction. These studies also attempted to derive the structure of the compound, but were not able to establish the nature of the linkage between the inositol group and the glycerol moiety (Folch, 1949a,b). The structure was finally deciphered by two independent groups, using soybean extracts of high purity to remove the nitrogenous contaminants that had been previously confounding (Hawthorne and Chargaff, 1954; Okuhara and Nakayama, 1954). These findings were soon followed by reports of the ubiquity of these lipids, having been found in liver, lung, brain tissue and erythrocytes (McKibbin, 1956; Dawson et al., 1960; Tomlinson and Ballou, 1961; Bleasdale et al., 1979).

After characterising the lipids, attention shifted to their synthesis. The pathway for the incorporation of myo-inositol into a cytidine diphosphate (CDP)-activated diacylglycerol backbone was elucidated by Agranoff and colleagues (Agranoff, 1958), laying the foundation for studies on the synthesis of derivatives of phosphatidylinositol. Agranoff was also the scientist famously responsible for drawing up the analogy of a myo-inositol ring to a turtle, which was particularly helpful in remembering the numbering of hydroxyl groups in keeping with the three-dimensional "chair" conformation of myo-inositol. The raised head of the turtle represents the axial hydroxyl (the back of the chair), while the limbs and tail represent the equatorial hydroxyls (Agranoff, 1978).

The discovery of enzymes that synthesise phosphoinositides from PI began with the observation that the radiolabelled phosphorus [^{32}-phosphorus (^{32}-

P)] in [γ-^{32}P]ATP was incorporated into the phosphoinositides of erythrocyte ghosts and agonist-stimulated pancreatic slices, implying that there was an active regeneration of these lipids immediately after stimulation (Hokin and Hokin, 1952, 1964). Further studies performed using rat liver and bovine brain tissue described a lipid kinase, associated with the plasma membrane, that could phosphorylate PI by utilising adenosine triphosphate (ATP) as the source of phosphate (Colodzin and Kennedy, 1965; Michell and Hawthorne, 1965; Kai et al., 1966). These were followed by more comprehensive attempts to identify the subcellular localisation of this enzymatic activity, with different studies reporting it to be on the plasma membrane (Harwood and Hawthorne, 1969) as well as lysosomal membranes (Collins and Wells, 1982) of rat liver tissue. We now know that these reports correspond to current identifications of the production of PI4P from PI, both at the plasma membrane (Nakatsu et al., 2012) and at the lysosome (Sridhar et al., 2012), albeit by different isoforms of the same enzyme.

Hokin and Hokin's observation of ^{32}P incorporation into the phosphoinositides of agonist-stimulated pancreatic tissue opened a field of inquiry into the function of lipids as signalling intermediates (Hokin and Hokin, 1952). Parallel reports of the breakdown of phosphoinositides in the brain (Sloane-Stanley, 1953) lead to the identification of phospholipase C (PLC), an enzyme that drives many different types of signalling pathways by hydrolysing phosphoinositides (Thompson and Dawson, 1964). Later demonstrations of phosphoinositide breakdown in response to agonists such as vasopressin, carbachol and angiotensin further strengthened the role of these lipids in signal transduction (Billah and Michell, 1979; Prpic and Extong, 1982; Berridge et al., 1983; Creba et al., 1983). These studies set the scene for future investigations into phosphoinositides as mediators of cell signalling.

1.2 PLC-mediated GPCR signalling

When a receptor present on the plasma membrane of a cell is activated by an external agent, signal transduction events serve to propagate information further into the cell, allowing it to undergo physiological changes in accordance with the external event. The physiological response varies depending on the combination of signal, receptor and transduction cascade and there are set combinations of these events tailored to specific scenarios (Berridge, 2008).

1.2.1 GPCR signalling

An example of a very well-characterised signal transduction pathway is G-protein coupled receptor (GPCR) signalling. In such pathways, a multi-pass transmembrane receptor at the plasma membrane senses stimuli and conveys the message to downstream elements. The receptor is coupled to a G-protein, which is activated when a ligand binds the receptor. The associated G-protein has three subunits - α, β and γ. Once activated, in most cases the subunits split into G_α and $G_{\beta\gamma}$, either of which can carry forward the signal, depending on the specific pathway that has been activated (Gomperts et al., 2002). The heterotrimeric G-protein has functional variants depending on the final cellular output, ranging from inhibitory (such as Gi and Go) to activating (such as Gs and Gq). The G-protein, once split into its subunits, can activate or inhibit the main effector of the signalling pathway, which is usually an enzyme. The effectors that drive GPCR signalling are generally guanosine triphosphatases (GTPases), adenyl cyclases or lipid-metabolising enzymes. They generate secondary messengers that further amplify the signal within the cell, driving the reaction forward (Dupré et al., 2012).

1.2.2 G-protein coupled PLC signalling

Perhaps one of the most closely examined GPCR pathways is the phospholipase C (PLC) beta mediated pathway. This kind of signal transduction is required for physiological phenomena such as neurotransmission (Weiss and Putney, 1981), smooth muscle contraction (Billah and Michell, 1979) and response to hormonal changes (Prpic and Extong, 1982). When the external stimulus (acetylcholine, norepinephrine, etc.) is sensed by the GPCR, the cognate G-protein is activated. In most scenarios, the G-protein is heterotrimeric Gq, which upon activation is dissociated into its components, Gq_α and $Gq_{\beta\gamma}$. The small subunit Gq_α triggers PLCβ, which hydrolyses a specific plasma membrane lipid known as phosphatidylinositol-4,5-bisphosphate, commonly abbreviated as PI(4,5)P_2. This reaction produces the secondary messengers diacylglycerol (DAG) and inositol - 1,4,5 - trisphosphate (IP_3), which amplify the signal and enable the cell to execute its physiological response **(Fig.1.3)** (Berridge, 1984; Rhee, 2001).

The key reaction in the above-described cascade is the hydrolysis of PI(4,5)P_2 by PLCβ. This lipid belongs to the class of signalling lipids known as phosphoinositides described in the earlier section. These are phosphorylated derivatives of the glycerophospholipid phosphatidylinositol (PI), with the number denoting the position of phosphorylation on the inositol ring **(Fig.1.4)**. PI(4,5)P_2, therefore, is a doubly phosphorylated derivative of PI,

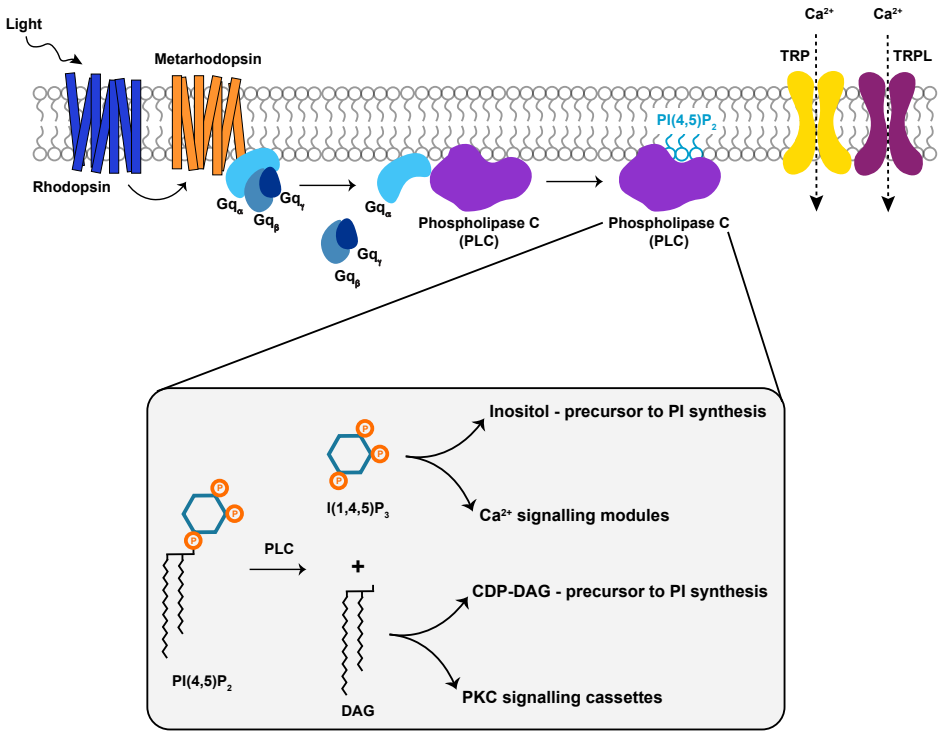

Figure 1.3 : PLC-mediated GPCR signalling
An example of a PLC-mediated GPCR signalling where the GPCR rhodopsin is activated by a light stimulus. Upon activation, rhodopsin undergoes a conformational change to become metarhodopsin. This photoisomer activates the cognate G-protein, which is the heterotrimeric Gq. Gq dissociates into its subunits - Gq_α and $Gq_{\beta\gamma}$. Gq_α then triggers the enzyme phospholipase C (PLC), which hydrolyses the plasma membrane lipid phosphatidylinositol-4,5-bisphosphate [PI(4,5)P_2]. PI(4,5)P_2 hydrolysis by PLC generates the second messengers diacylglycerol (DAG) and inositol-1,4,5-trisphosphate (IP_3). These messengers drive the signal forward in the cell and instruct it to execute the relevant physiological response.

with the phosphate groups present at positions 4 and 5 **(Fig.1.4)**. In this thesis, PI(4,5)P_2 will be further abbreviated and referred to as PIP_2.

Although some PLC isoforms have been shown to hydrolyse lipids other than PIP_2, such as PI and PI4P (Zhang et al., 2013), the specificity of the PLCβ isoform towards PIP_2 is extremely high (Deer et al., 1995; Kadamur and Ross, 2013). PIP_2 is also a rather low abundance lipid, accounting for only 5% of the total cellular phosphoinositides (Gunnarsson et al., 1997). This implies that there is a potential risk of activated PLCβ utilising all the PIP_2 present on the plasma membrane within a small time frame (Biddlecome et al., 1996). Therefore, during signalling it is vital for the cell to maintain enough PIP_2 at the plasma membrane for PLCβ to act upon, as insufficient amounts of PIP_2 will cause the signal to run down and leave the cell unable to respond efficiently to the stimulus (Hardie and Postma, 2008). This requirement is complicated by the fact that PLCβ has a very high rate of catalysis, completely consuming all the PIP_2 molecules on the plasma membrane within ~10 minutes (Biddlecome et al., 1996; Hardie et al., 2004). Since the cell has only limited amounts of PIP_2 at any given point, during a signalling event the synthesis of PIP_2 must keep pace with its hydrolysis, or the cell risks stalling signal transduction.

1.2.3 PIP_2 metabolism

Depending on the cell type and signalling context, PIP_2 can either be broken down by PLCβ or further phosphorylated by a lipid kinase, known as phosphatidylinositol 3-kinase (PI3K), to form PI(3,4,5)P_3 (Hawkins et al., 1992). The latter reaction is required to drive cellular responses such as the production of reactive oxygen species by neutrophils stimulated by chemoattractants like N-formyl-methionine-leucyl-phenylalanine (fMLP) (Stephens et al., 1991; Arcaro and Wymann, 1993). In the converse scenario, PI(3,4,5)P_3 can be dephosphorylated by a lipid phosphatase known as phosphatase and tensin homologue (PTEN) to regenerate PIP_2, a reaction that is vital for the control of cell growth (Maehama and Dixon, 1998). In fact, mutations in PTEN that abrogate its function have been found in primary tumours as well as brain, breast and prostate cancer cell lines (Li, 1997).

Aside from serving as an agent of PI(3,4,5)P_3 regulation, PIP_2 is also a substrate for lipid phosphatases such as TMEM55A/B, which dephosphorylate it at the fourth position to form PI5P and are thought to help in the regulation of nuclear PI5P levels (Zou et al., 2007). PIP_2 can also be dephosphorylated at the fifth position by phosphatases oculocerebral renal syndrome of Lowe (OCRL) and synaptojanin to form PI4P. Synaptojanin knockout mice have

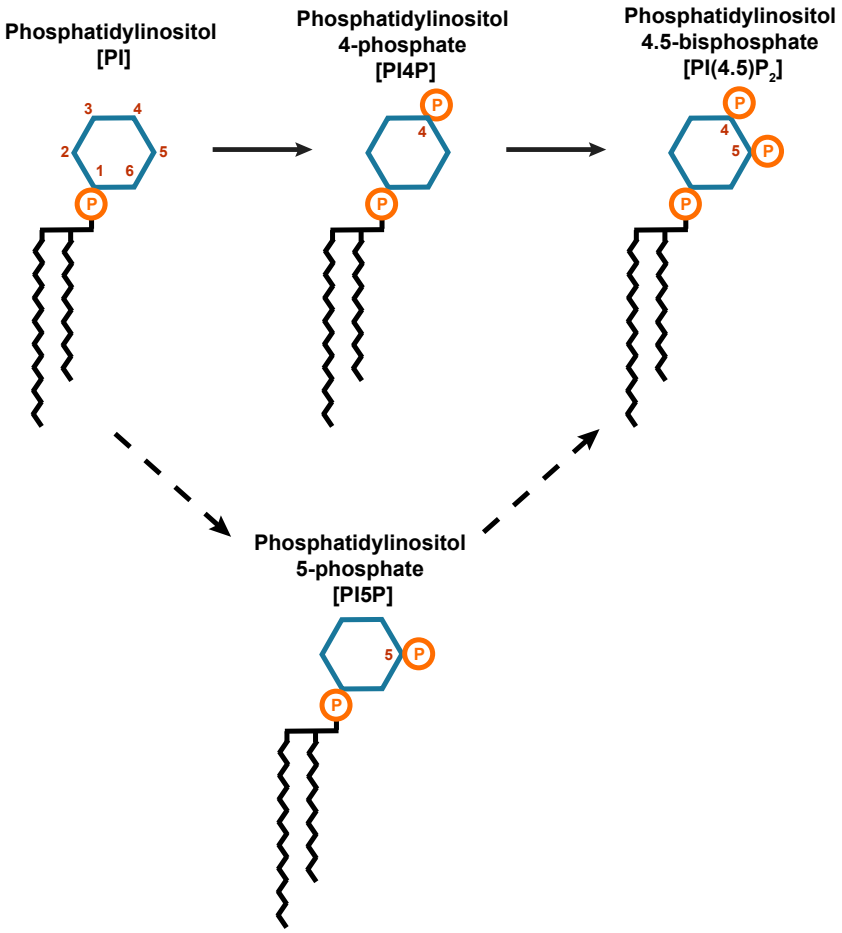

Figure 1.4 : Synthesis of PI(4,5)P_2
PI(4,5)P_2 is synthesised by the sequential action of specific lipid kinases, depending on the starting point. In the first sequence, PI is phosphorylated at the fourth position by a PI 4-kinase to produce PI4P. This PI4P is then further phosphorylated at the fifth position by a PI4P 5-kinase to form PI(4,5)P_2. Alternatively, PI can be phosphorylated at the fifth position to form PI5P, which is then acted upon by a PI5P 4-kinase to generate PI(4,5)P_2. In cells, it appears that the former pathway is the dominant one as PI4P is present in greater abundance at the plasma membrane as compared to PI5P.

been shown to have defective synaptic vesicle recycling events (Guo et al., 1999; Kim et al., 2002) whereas mutations in OCRL are responsible for the occurrence of Lowe's syndrome, a developmental disorder affecting the brain, kidneys and eyes (Attree et al., 1992; Zhang et al., 1998).

PIP_2 is synthesised from PI by the sequential action of specific lipid kinases (Stephens et al., 1991). The most common method is where PI is first phosphorylated at the fourth position by a PI 4-kinase. The PI4P thus generated is further phosphorylated by a PI4P 5-kinase at the fifth position, making PIP_2 (King et al., 1987, 1989). The alternate method of making PI5P first and then PIP_2 is also possible by the action of a PI5P 4-kinase (Rameh et al., 1997) **(Fig.1.4)**. Given that PI4P is the more abundant monophosphorylated lipid, it is generally assumed that the former route is the one preferred by cells (King et al., 1987; Hinchliffe et al., 1998).

Although there are multiple methods of making and breaking PIP_2, the required combination is set by context. During agonist-stimulation, it has been shown in mammalian cell culture systems that PIP_2 is made by the sequential action of a PI 4-kinase and PI4P 5-kinase (Stephens et al., 1993). However, it is important to note that in most cell types, the substrate for PI 4-kinase, i.e., PI, is usually present on the endoplasmic reticulum (ER) (Bishop and Strickland, 1970). PI4P and PIP_2, on the other hand, are present at the plasma membrane (PM) (Várnai and Balla, 1998; Hammond et al., 2014). This means that there exists some mechanism to transport either PI or PI4P from the ER to the plasma membrane. We know from studies in both mammalian cells and *Drosophila* that a PI transfer protein moves PI from the ER to the plasma membrane and that this function is required for PIP_2 synthesis during PLC signalling (Helmkamp et al., 1974; Thomas et al., 1993; Yadav et al., 2015; Kim et al., 2016). Additionally, the whole sequence of PI transfer and phosphorylation by the lipid kinases must happen on a timescale that allows sustained signalling. These spatial and temporal constraints on PIP_2 synthesis imply a high level of coordination between different organelles and lipid-metabolising enzymes. Such tightly regulated processes would need to be closely monitored to avoid any errors that could potentially halt signalling and deter cellular responses.

The control of PIP_2 metabolism is further convoluted by the fact that PIP_2 is a multi-functional lipid. Apart from signalling, it regulates more basic cellular functions such as endocytosis (Haucke, 2005) and anchoring of cytoskeletal elements (Lassing and Lindberg, 1985), all of which occur at the plasma membrane itself. This implies that the cell has a means of functionally demarcating different pools of PIP_2, which could be achieved through mech-

anisms such as targetted synthesis or compartmentalisation of the membrane (Kolay et al., 2016).

1.2.4 Testing models of PIP_2 metabolism in whole organisms

While we currently have insight into the regulation of PIP_2 synthesis in mammalian cells, this data largely comes from cell culture studies (Tóth et al., 2016; Várnai and Balla, 1998; Balla et al., 2008). In such experiments, the amount of agonist used to elicit signalling is typically orders larger than is physiologically relevant. Moreover, it is important to exercise caution when extrapolating results obtained from cell culture studies to similar phenomena in whole organisms.

An example of such a disconnect is presented by the case of Vitamin D as a potential chemotherapeutic agent against pancreatic cancer. This effect of vitamin D has been studied since the mid-90s, chiefly using pancreatic cancer cell lines as an experimental system (Zugmaier et al., 1996; Kawal et al., 1997; Pettersson et al., 2000). Multiple follow-ups in humans did not provide any conclusive results. In fact, different sets of studies have reported directly contrasting results, with one group demonstrating reduced risk and the other showing increased risk of the cancer when healthy individuals were treated with vitamin D (Skinner, 2006; Stolzenberg-Solomon et al., 2010; Wolpin et al., 2012). Such conflicting results prompted an investigation of the phenomenon in a genetically uniform population of mice in order to eliminate genetic difference arising from heterogeneous cohorts of human subjects. When vitamin D was administered to a population of mice suffering from drug-induced pancreatic cancer, no therapeutic effects were observed in the mice (Iqbal, 2018).

Given that such discrepancies exist, it is important to test models drawn from cell culture studies in whole organism systems. In this thesis, I examine a specific aspect of PIP_2 resynthesis during visual signalling in *Drosophila melanogaster*. *Drosophila* eyes provide a well-characterized system in which to test the current model of PIP_2 metabolism during endogenous PLC signalling (Hardie and Raghu, 2001; Raghu et al., 2012). The ease of genetic manipulation and robust signalling readouts allow one to assess the requirement of specific genes during the process of PIP_2 resynthesis (Pak, 2010).

1.3 Cellular functions and metabolism of PI4P

Phosphatidylinositol 4-phosphate (PI4P) was possibly the very first monophosphorylated derivative of PI to be identified. A study in 1949 reported the isolation of a "diphosphoinositide" from bovine brain extracts (Folch, 1949a), which was eventually followed by the observation that this lipid was an important intermediate in the synthesis of PIP_2 in bovine brains (Brockerhoff and Ballou, 1962). The process of its enzymatic synthesis from PI, using ATP as a source of phosphate, was outlined very soon after with the description of a lipid kinase, also isolated from bovine brain tissue (Colodzin and Kennedy, 1965). Although earlier thought to be merely a precursor for the synthesis of PIP_2, we now know that PI4P is required for a host of other cellular functions as well, ranging from vesicular transport to maintenance of membrane homeostasis (Venditti et al., 2016).

1.3.1 Cellular functions of PI4P

In a typical eukaryotic cell, PI4P is enriched in the Golgi apparatus and plasma membrane. It has also been reported to be present on endosomal structures and phagosomes as well (Hammond et al., 2014; Levin et al., 2017). At the Golgi apparatus, one of the roles of PI4P is regulation of sphingolipid synthesis. This function is performed through its association with proteins such as ceramide transport protein (CERT), which transfers ceramide from the ER to the Golgi, where it is converted to sphingomyelin (Hanada et al., 2003). PI4P also binds to and regulates four phosphate adaptor protein 2 (FAPP2), an intermediate protein required for the synthesis of glycosphingolipids (D'Angelo et al., 2007). In both the above cases, the enrichment of PI4P at the trans-Golgi network is thought to serve as a localisation signal for these proteins to the membrane. A third class of PI4P-regulated proteins is formed by oxysterol binding protein (OSBP) and its related proteins (Levine and Munro, 2002; Chung et al., 2015b). These transfer proteins perform a counter-transport of cholesterol and PI4P between the ER and Golgi membranes, maintaining a gradient of cholesterol along the endomembrane system. The transfer of PI4P from the Golgi apparatus to the ER is irreversible, as it is dephosphorylated by Sac1 upon reaching the ER. This irreversible transfer possibly provides a directionality to the transfer activity of OSBP, allowing it to sustain the cholesterol gradient across membranes (Mesmin, 2013).

Another major function of PI4P is to regulate vesicle formation and anterograde trafficking from the Golgi apparatus. The concentrated presence of

PI4P at the trans-Golgi network (TGN) recruits adaptors such as Golgi localised, Gamma adaptin ear containing, ARF binding protein (GGA) (Wang et al., 2007) and adaptor protein - 1 (AP-1) (Wang et al., 2003) to the membrane, aiding the formation and sorting of secretory vesicles. PI4P also serves as an identifier of the Golgi apparatus by binding to and recruiting proteins such as Golgi phosphoprotein 3 (GOLPH3). Interfering with the binding of GOLPH3 to PI4P results in irregular Golgi morphologies and impaired anterograde trafficking (Dippold et al., 2009; Xing et al., 2016).

Aside from its constitutive presence at the Golgi apparatus, PI4P occurs transiently on lysosomal membranes as well. The *in situ* formation of PI4P on lysosomes is required for the recycling of protein components from lysosomes targetted for degradation (Sridhar et al., 2012). A similar phenomenon is also seen on the membranes of autophagosomes prior to fusing with lysosomes (Wang et al., 2015). In fact, a study tracking PI4P on phagosomes showed that it is present on nascent phagosomes, replaced by PI3P during maturation and then reappears on the late phagosomal and phagolysosomal membrane. The reoccurrence of PI4P on the late phagosome probably serves to recruit Rab7 to the membrane, marking the fate of the vesicle (Levin et al., 2017). Such an interplay of phosphoinositide signatures is also seen over the life cycle of endosomal vesicles and aids in the recruitment of adaptor proteins and Rab GTPases to the vesicle membranes (He et al., 2017).

At the plasma membrane, PI4P not only works as a precursor to PIP_2, but has independent functions in membrane homeostasis and signalling. Recent studies on OSBP related protein (ORP) and OSBP homologue (Osh) proteins have unveiled a role for the counter-transport of PI4P and phosphatidylserine (PS) between the plasma membrane and ER as a means of controlling lipid levels, similar to the lipid-exchange cycle seen at the ER-Golgi interface. The mammalian ORP5/8 proteins (Osh6/7 in yeast) bind to and transfer PI4P from the plasma membrane to the ER, where it is promptly dephosphorylated to PI by the action of the Sac1 phosphatase. There is a simultaneous transfer of PS from the ER to the plasma membrane, where it is thought to regulate membrane fluidity and thereby, conformations of membrane proteins (Chung et al., 2015c; von Filseck et al., 2015).

The signalling functions of PI4P at the plasma membrane are largely regulated by the lipid kinases that synthesise it from PI. There is evidence that PI4P at the plasma membrane is required for fin development in zebrafish. During development, fibroblast growth factor (FGF) is thought to stimulate production of PI4P, which serves as a precursor for the formation of $PI(3,4,5)P_3$. This in turn regulates a balance between Akt and MAPK sig-

nalling pathways, which determines apoptotic or proliferative fates for the cell (Ma et al., 2009). PI4P has also been implicated in *Drosophila* embryonic development, possibly by interacting with the Hippo signalling module. A 2011 study showed that heterozygous loss-of-function mutants for a PI 4-kinase had mislocalised Hippo signalling targets, indicating a role for the enzyme in regulating developmental pathways (Yan et al., 2011).

In response to agonist-stimulation of cultured cells, it is known that PIP_2 levels undergo a drop, followed by a recovery as the signal is attenuated (Creba et al., 1983; Willars et al., 1998; Balla et al., 2008). What is important to note is that in each of these cases, the levels of PI4P closely mirror those of PIP_2, indicating that PI4P levels are regulated on par with PIP_2 levels. More recently, it has been shown that inhibiting PI4P synthesis by using a chemical blocker for PI 4-kinase in mammalian cells reduces both epidermal growth factor receptor (EGFR) and PLC signalling readouts, suggesting a role for the lipid in modulating cell signalling events (Tóth et al., 2016).

1.3.2 Metabolism of PI4P

PI4P is synthesised from PI by the action of phosphatidylinositol 4 - kinase (PI4K). The activity of such kinases were studied and identified in the 1960s, using bovine brain and rat liver tissue as source material (Colodzin and Kennedy, 1965; Hokin and Hokin, 1952; Michell et al., 1967). Initially thought to be a single enzyme, work from the late 1980s showed that there were two kinds of PI4Ks in animal tissues (Endemann et al., 1987; Li et al., 1989). We now know that there are four isoforms of PI4K in mammals, grouped into two classes. The class II enzymes - PI4KIIα and PI4KIIβ - are sensitive to inhibition by adenosine. The class III enzymes - PI4KIIIα and PI4KIIIβ - on the other hand, are sensitive to inhibition by wortmannin. Each isoform has a distinct localisation and cellular function, as listed in Table 1.1 and described below.

Both the class II isoforms possess palmitoylation motifs (Lu et al., 2012). In fact, PI4KIIα is targetted to the Golgi apparatus and some endosomal structures on this basis. At the Golgi apparatus, PI4KIIα makes the major PI4P pool and thereby regulates vesicular transport (Balla et al., 2002; Minogue, 2006). PI4KIIβ, despite also possessing a palmitoylation motif, appears to be partially cytosolic in terms of localisation. It is likely recruited to the plasma membrane when required, such as when platelet derived growth factor (PDGF) signalling is activated (Wei et al., 2002).

The class III enzymes do not possess any obvious membrane targetting sig-

Table 1.1 :
Phosphatidylinositol 4-kinases

Enzyme	**Chemical Inhibitors**	**Subcellular Localisation**	**Function**	***Drosophila* Gene**
PI4KIIα (PI4K2A)	Adenosine, LY294002	Golgi apparatus, endosomes	Maintain Golgi apparatus PI4P, vesicular transport, recruit adaptor proteins	CG2929
PI4KIIβ (PI4K2B)	Adenosine, LY294002	Cytosol, plasma membrane, endoplasmic reticulum, Golgi apparatus	Regulate cellular response to growth factor signalling	-
PI4KIIIα (PI4KA)	Wortmannin, Phenylarsine oxide (PAO), A1	Cytosol, plasma membrane	Maintain plasma membrane PI4P, regulate signalling	CG10260
PI4KIIIβ (PI4KB)	Wortmannin, Phenylarsine oxide (PAO)	Golgi apparatus, lysosomes	Maintain Golgi apparatus PI4P, vesicular transport, cholesterol/PI4P exchange cycle, lysosome maturation	CG7004

nals, but both isoforms are localised to their respective membranes through interactions with other proteins. PI4KIIIα interacts with two highly conserved proteins - eighty five requiring 3 (EFR3) and tetratricopeptide containing protein 7 (TTC7) - and forms a complex at the plasma membrane, where it synthesises PI4P (Baird et al., 2008; Nakatsu et al., 2012). This plasma membrane pool of PI4P is required for plasma membrane identity, as disrupting the production of this pool causes the mislocalisation of certain plasma membrane resident proteins in mammalian cells (Hammond et al., 2012; Nakatsu et al., 2012). It is also required to sustain signalling events at the plasma membrane, as chemical inhibition of PI4KIIIα decreases cellular activity in response to agonist-stimulation (Balla et al., 2008; Tóth et al., 2016). The second member of the class III kinases, PI4KIIIβ, appears to localise to the Golgi apparatus via interactions with ACBD3, Rab11 and Arf1, although the exact nature of the interactions is not clear (Chalupska et al., 2019). At the trans-Golgi network, PI4KIIIβ makes PI4P that directly feeds into the OSBP/Osh-mediated lipid exchange cycle (de Saint-Jean et al., 2011), apart from regulating other vesicular processes such as delivery of enzymes to lysosomes (Jović et al., 2012). In yeast, the enzyme PIK1, which is the orthologue of PI4KIIIβ, is also required for the trafficking of Atg9, a protein component of autophagosomes, to their target compartments (Wang et al., 2012). A similar function has also been demonstrated in mammalian cells, where PI4KIIIβ is present on lysosomal membranes and controls the exit of recycled components from the lysosome (Sridhar et al., 2012).

Both the class III isoforms have been shown to be required for host infections by viruses belonging to the families of Flaviviridae (Hepatitis C) (Berger et al., 2009; Reiss et al., 2013), Picornaviridae (Polio) (Arita et al., 2011) and Coronaviridae (Coxsackie) (Hsu et al., 2010). The viruses use PI4P produced by the group III PI4Ks to rewire lipid metabolism and create viral replication compartments, allowing them to infect the host cell without detection. Inhibition of group III PI4Ks prevents efficient host entry of the virus, offering promising drug targets for eventual treatments. The reason for the preference of class III is possibly because they are also linked to the sterol exchange cycle mediated by OSBP, since sterol enriched membranes are a feature of viral replication compartments (Strating and van Kuppeveld, 2017).

Moving on to other metabolic fates, PI4P can be converted to PIP_2 by the action of phosphatidylinositol 4 - phosphate 5 - kinase (PIP5K). This reaction generates the majority of the PIP_2 at the plasma membrane (King et al., 1989). The activity of PIP5Ks is often upregulated in response to stimuli, as in the case of Wnt signalling. Stimulation of HEK293T cells with Wnt3a results in the coordinated activation of both PI4KIIα and PIP5KI, causing

a surge in PI4P and PIP_2 synthesis. This eventually leads to the stabilisation of β-catenin, regulating the physiological effects of Wnt stimulation (Pan et al., 2008; Qin et al., 2009). PI4P can also be dephosphorylated to PI by the action of Sac1, which is a 4-phosphatase usually present at the endoplasmic reticulum. The production of PI from PI4P at the ER, through the action of Sac1, is thought to be part of the OSBP/Osh-mediated exchange cycle between the endoplasmic reticulum and either the plasma membrane or the Golgi apparatus (Mesmin, 2013; Antonny et al., 2018). Sac1 is also thought to work in *trans*, acting upon PI4P at the plasma membrane by stretching across an ER-PM contact site. This was demonstrated in yeast, where it appeared that Sac1 preferred the PI4P pool generated by the plasma membrane PI4KIIIα, as opposed to the Golgi pool generated by PI4KIIIβ (Foti et al., 2001). A more recent study in mammalian cells, however, showed that Sac1 preferentially works at the ER, only gaining the ability to access plasma membrane PI4P when a linker is added to the protein (Zewe et al., 2018). Whether by acting in *trans* or in *cis*, Sac1 appears to maintain overall PI4P homeostasis in the cell, as temperature-sensitive loss-of-function mutants in *Drosophila* show elevated PI4P levels and abnormal eye development (Del Bel et al., 2018).

In this thesis, I will focus on the synthesis of PI4P from PI by the enzyme PI4KIIIα, since it has a direct bearing on the maintenance of PI4P levels at the plasma membrane. The synthesis of PI4P at the plasma membrane most likely feeds into PIP_2 synthesis, which is essential for sustaining a PLC signalling response. Therefore, in the next section, I will elaborate on the possible role of PI4KIIIα in regulating PLC signalling.

1.4 Cellular roles of PI4KIIIα

The existence of two groups of PI4Ks was first established in 1987, when two distinct PI 4-kinase activities were isolated from bovine brain tissue. One group was sensitive to adenosine (class II) and the other was not (class III), although both performed the same catalytic reaction (Endemann et al., 1987). The class III PI4Ks were further resolved into PI4KIIIα and PI4KIIIβ based on genetic experiments in yeast, where mutations for the individual genes had distinct physiological effects (Flanagan et al., 1993; Yoshida et al., 1994a,b).

The yeast PI4KIIIα (*stt4*) was first isolated in a test for sensitivity to the anti-fungal drug staurosporine. Temperature-sensitive loss-of-function mutants for *stt4* showed a high degree of sensitivity to the drug, a lack of PI

4-kinase activity and lower amounts of PI4P than their wild-type controls. The protein was cloned and characterised, demonstrating a PI 4-kinase activity and establishing it as one of the PI4Ks in yeast. Further experiments confirmed the findings and placed its activity upstream of the yeast PIP5K (*mss4*) (Yoshida et al., 1994a,b).

Parallel experiments in mammalian cells involved cloning and characterising a large protein that displayed PI 4-kinase activity (Nakagawa et al., 1996). This protein was larger than the other PI4Ks purified so far (230kD vs. 55kD and 92kD) and bore homology to the yeast STT4 protein. Systematic ribonucleic acid interference (RNAi)-mediated knockdown studies against each PI4K isoform indicated that the 230kD PI4K function was required to produce PI4P at the plasma membrane, whereas the other PI4Ks appeared to function at the Golgi apparatus (Balla et al., 2005).

The PI4KIIIα protein in mammals has a domain organisation very similar to that of the PI 3-kinases. At the N-terminus, it has an SH3 domain and a proline-rich region, both of which likely aid in plasma membrane localisation. Towards the C-terminus, it has a lipid kinase unique (LKU) region, earlier thought to be characteristic only of PI 3-kinases, but possessed by the class III PI 4-kinases as well. It also has a PH domain, likely for binding to PI, and a catalytic domain. All of these features are present across both yeast and metazoan systems, pointing to a high degree of conservation of the gene (Nakagawa et al., 1996).

Following experiments that identified the PI4K isoform that likely works at the plasma membrane, further investigations were conducted regarding the physiological relevance. Several studies from mammalian cell culture systems demonstrated that PI4KIIIα was the most important contributor to PI4P at the plasma membrane (Balla et al., 2008, 2005; Nakatsu et al., 2012). Complete deletions of PI4KIIIα led to embryonic lethality in mice, implying a strong developmental role for the gene. Conditional knockout MEFs for PI4KIIIα displayed reduced PI4P and PIP_2 levels (Nakatsu et al., 2012), suggesting that PI4P produced by PI4KIIIα has a role in cellular development and compositional homeostasis at the plasma membrane. These cells also showed a disruption of plasma membrane identity, with several plasma membrane resident proteins mislocalised to endomembranes. PI4KIIIα has been implicated in brain development, as kinase-inactivating point mutations in the gene have been associated with polymicrogyria and resulting foetal lethality (Pagnamenta et al., 2015).

Apart from its functions in cellular homeostasis, it was shown that PI4KIIIα activity is required to produce PI4P pools that are involved in plasma mem-

brane signalling events. Experiments in cell culture systems showed a clear dependence of PLC-mediated GPCR signalling efficiency on PI4KIIIα presence. When either AngII or M3 muscarinic receptor is expressed in cells and stimulated using an agonist, PLC signalling is activated. This causes a detectable drop in PIP_2 levels followed by a recovery to basal levels as the agonist is washed out. When PI4KIIIα was specifically inhibited in cells expressing these receptors, the recovery of PIP_2 levels at the plasma membrane post agonist washout was diminished. This in turn attenuated the signalling output, implying that the signalling response was tied to PI4KIIIα activity. These studies also demonstrated that the overall PI4P levels were reduced in cells where PI4KIIIα was inhibited. Not only that, the recovery of PI4P at the plasma membrane following agonist stimulation was also delayed in these cells, corresponding to the effect seen on PIP_2 levels (Balla et al., 2008; Tóth et al., 2016). The key interpretation that came from such experiments was that blocking PI4KIIIα negatively impacts PLC-mediated GPCR signalling in mammalian cells, most likely by controlling the synthesis of PI4P and PIP_2 at the cell membrane.

1.4.1 Mechanism of localisation of PI4KIIIα to the plasma membrane

Having shown that PI4KIIIα activity is required to make PI4P at the plasma membrane, it was apparent that the enzyme was also most likely present at the same membrane. Indeed, in yeast cells, it was very clearly demonstrated that the enzyme is present in "pik (PI kinase) patches" at the plasma membrane. These patches were non-uniformly distributed along the membrane, but they did not consist of PI4KIIIα alone. Instead, it was seen that PI4KIIIα resides at these patches by virtue of its interaction with two other proteins - Efr3 and Ypp1 (Audhya and Emr, 2002; Baird et al., 2008).

The mechanism by which these two interactors aid in localising PI4KIIIα to the plasma membrane was revealed in a 2014 study, where structural data about Efr3 and Ypp1 were used to infer the details. It was shown that the yeast Efr3 possesses a patch of basic amino acids that localise it to the plasma membrane. The unstructured C-terminus of Efr3 interacts with Ypp1, which in turn pulls PI4KIIIα along with it to the membrane. This complex of three proteins can be regulated based on the phosphorylation status of the Efr3 C-terminus, with high levels of phosphorylation inhibiting interactions with Ypp1. With respect to the phosphoinositide levels, this study showed that preventing formation of the protein complex reduced the levels of PI4P in yeast, implying that the protein interactions were required for PI4KIIIα

activity (Wu et al., 2014).

Both Efr3 and Ypp1 are conserved in mammalian cells. Ypp1 is referred to as TTC7 in mammals and hence, I will use that nomenclature going forward. Given that PI4KIIIα activity at the plasma membrane was demonstrated at the plasma membrane in mammalian cells as well, it stood to reason that the mechanisms of localisation to the plasma membrane might also be conserved between yeast and mammals. This was first validated in 2012, when a study in mouse fibroblasts showed that PI4KIIIα is transiently recruited to the plasma membrane through its interaction with Efr3 and TTC7 (Nakatsu et al., 2012). Unlike yeast, there were no constitutive patches of the complex present at the membrane, but the mechanism of complex formation appeared to be very similar (Baskin et al., 2016). The transient nature of the complex points to a more tightly controlled presence of PI4KIIIα at the plasma membrane.

Additionally, over the past five years, other protein interactors of PI4KIIIα have been identified in mammals. Proteins such as TMEM150A and FAM126A may modulate the architecture of the complex, allowing for a greater degree of regulation (Baskin et al., 2016; Chung et al., 2015a; Lees et al., 2017).

1.5 Using *Drosophila* photoreceptors as a model system

The compound eyes of *Drosophila* have been an object of study right from the early 20th century (Hamilton, 1922; Haskins and Enzmann, 1936; Hecht, 1934; McEwen, 1918). Starting with classical experiments that outlined eye colour inheritance in fruit flies, our current knowledge extends deep into the genetics, structure and physiology of the eye (Morgan, 1910; Mishra and Knust, 2019). Notably, the *Drosophila* eye has been instrumental in working out the molecular elements of cellular signalling cascades, especially those of PLC-mediated GPCR signalling (Hotta and Benzer, 1969; Stark et al., 1976; Scott and Zuker, 1998; Pak, 2010). The existence of a such a well characterised system makes it ideal to study the nuances of signalling and its regulation. V

Each eye of a fruit fly is comprised of approximately 700-800 subunits known as ommatidia. Each ommatidium, in turn, consists of 8 photoreceptor cells, along with other accessory and pigment cells. Photoreceptors are the primary sensory neurons that transduce visual information to deeper optical neurons, making them the equivalent of rods and cones in human eyes. Pho-

toreceptors are polarised cells, with their apical plasma membrane thrown into folds known as microvilli. The microvilli of a single photoreceptor form a long columnar structure known as the rhabdomere, which is the main light-sensitive region of the cell **(Fig.1.5)**. The rhabdomere also houses all of the molecular components involved in phototransduction, the process of translating a visual stimulus to a cellular signal. It is built to maximise sensitivity to light, making it capable of sensing and responding even to single photons (Hardie and Postma, 2008).

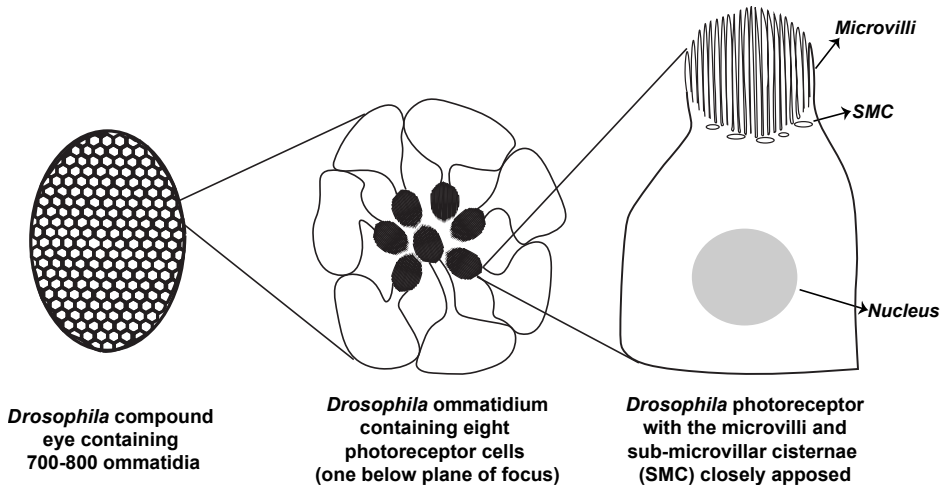

Figure 1.5 : Organisation of the *Drosophila* eye
The compound eye of *Drosophila melanogaster* is comprised of 700-800 subunits called ommatidia. Each ommatidium consists of eight photoreceptor cells, of which seven are visible in a cross-section. Photoreceptors are polarised cells whose apical plasma membrane is thrown into folds known as microvilli. The microvilli of a single photoreceptor form a long columnar structure called the rhabdomere, which is the main light-sensitive region of the cell and houses all the molecular components required for phototransduction. Closely apposed to the base of the rhabdomere are the sub-microvillar cisternae (SMC) which houses some of the molecular components required for resynthesis of $PI(4,5)P_2$ at the plasma membrane.

When light hits a photoreceptor, the GPCR rhodopsin, present at the rhabdomere, is stimulated. A resulting conformational change in rhodopsin activates the associated heterotrimeric G protein Gq, which splits into the components Gq_{α} and $Gq_{\beta\gamma}$. Gq_{α} then triggers PLCβ, which promptly hydrolyses PIP_2 present at the plasma membrane. This causes transient receptor potential (TRP) and transient receptor potential like (TRPL) channels to open,

ushering a large number of calcium ions into the cell. The cell becomes depolarised as a result and the signal is transmitted to deeper neuronal layers in the optical lobe of the fly **(Fig.1.3)** (Hardie and Raghu, 2001).

The hydrolysis of PIP_2 on the rhabdomere, which is essentially a modified plasma membrane, initiates a chain of events in the associated endoplasmic reticulum as well. The sub-microvillar cisternae (SMC) is a modified smooth ER compartment that is closely apposed to the rhabdomere. As mentioned in Section 1.2, PIP_2 resynthesis during PLC signalling requires the coordinated action of molecules between both the plasma membrane and ER. In the case of *Drosophila* photoreceptors, the molecular components of this process are distributed between the rhabdomere and the SMC (Raghu et al., 2012).

Upon PIP_2 hydrolysis at the rhabdomere, the resulting DAG is converted to phosphatidic acid (PA) by a DAG kinase encoded by the gene *rdgA* (Inoue et al., 1989). PA, thought to be transferred from the rhabdomere to the SMC, is converted to cytidine diphosphate - diacylglycerol (CDP-DAG) by the enzyme CDP-DAG synthase, encoded by the gene *cds* (Wu et al., 1995). PA can also be acted upon by a PA-phosphatase, encoded by the gene *lazaro* to remake DAG (Garcia-Murillas et al., 2006). The CDP-DAG intermediate is acted upon by the enzyme PI synthase, encoded by the gene *pis*, which produces PI at the SMC (Wang and Montell, 2006). PI is transported from the SMC to the rhabdomere by the PI-transfer protein retinal degeneration B (RDGB), encoded by the gene *rdgB* (Yadav et al., 2015). It is then phosphorylated successively by a PI 4-kinase and then an eye-enriched PIP 5-kinase (*dPIP5K*) to regenerate PIP_2 (Chakrabarti et al., 2015) **(Fig.1.6)**. As can be noted in **Fig.1.6**, the gene encoding PI 4-kinase function in *Drosophila* photoreceptors has not yet been annotated. This gap in the cycle forms one of the bases for the scientific questions addressed in this thesis.

The ease of genetic manipulations and abundance of phenotypic readouts in fruit flies made it possible to unravel the individual units of PIP_2 resynthesis, making the system well suited for analysing the finer points of control in the pathway. Importantly, the *Drosophila* genome usually encodes only a single copy of each gene, excluding the possibility of compensatory effects from other copies in the case of genetic manipulation studies.

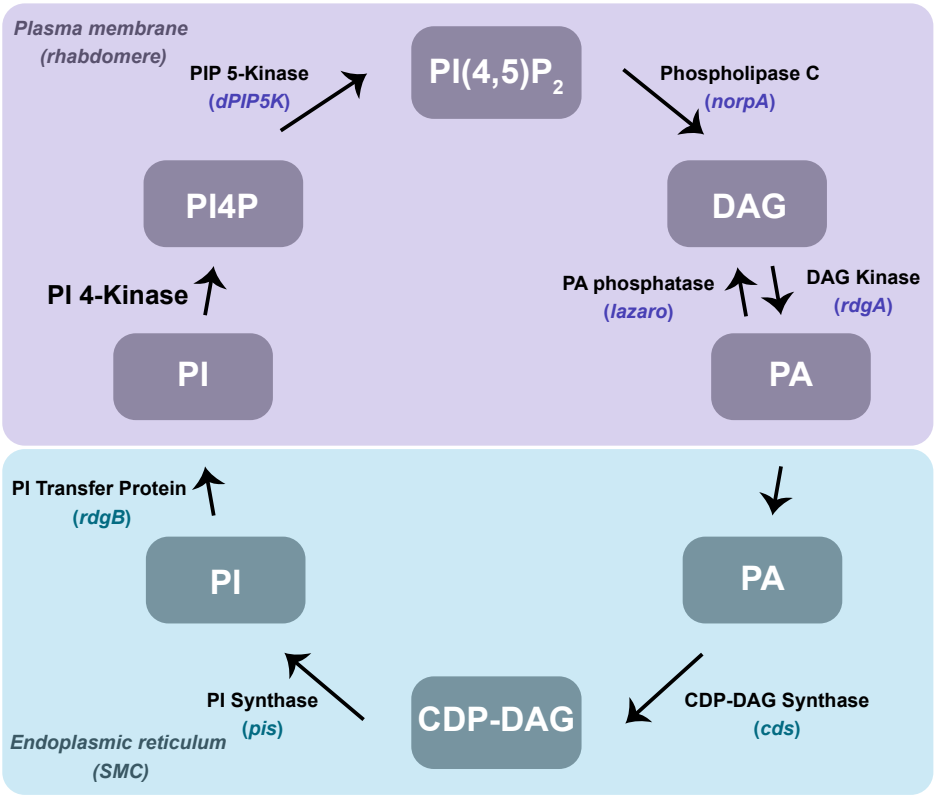

Figure 1.6 : The PI(4,5)P_2 cycle in *Drosophila* photoreceptors
The reactions of the PI(4,5)P_2 cycle in *Drosophila* photoreceptors are distributed between two membranes - the plasma membrane (rhabdomere - purple) and endoplasmic reticulum (SMC - blue). The lipid intermediates are marked in gray boxes, the enzymes carrying out each reaction are listed in black and the genes encoding each enzyme are listed in italics below the enzyme.

1.6 Current knowledge about PI4KIIIα in *Drosophila*

The *Drosophila* PI4KIIIα gene was first identified in the year 2000 as part of an attempt to map the *Drosophila* orthologues of mammalian kinases and phosphatases (Morrison et al., 2000). Based on amino acid sequence similarity and conservation of key residues, the gene CG10260 was annotated as PI4KIIIα. The functions of PI4KIIIα in *Drosophila* have not been very well characterised, although existing studies indicate a strong role in developmental processes (Yan et al., 2011; Tan et al., 2014).

Complete deletions of PI4KIIIα are cell lethal, implying an essential function of the gene in development (Yan et al., 2011; Tan et al., 2014). The oocytes of heterozygotic loss-of-function mutants for PI4KIIIα are incorrectly polarised, owing to an improper localisation of the Gurken protein. The follicle cells of these oocytes also display misregulation of Hippo signalling targets *expanded* and *diap1*, accompanied by mislocalisation of the Merlin protein (Yan et al., 2011). These phenotypes mirror those seen when components of the Hippo pathway are perturbed, implying an interaction of PI4KIIIα with the Hippo signalling module, which in itself has been well-documented in regulating cellular development (Staley and Irvine, 2012).

A role for PI4KIIIα in oogenesis was confirmed when it was seen that induction of germ line clones for a deletion mutant of the gene prevents the flies from laying eggs (Tan et al., 2014). The study also demonstrated that, in the germ line clones, F-actin is mislocalised and phospho-Moesin levels are low, indicating that the cytoskeleton in these cells is disorganised. The structural integrity of the plasma membrane is disrupted in clones lacking PI4KIIIα, but not in those lacking the other PI4K isoforms. A second significant result from this study is that the PI4P and PIP_2 levels are reduced in the plasma membranes of the germ line clones. Therefore, in *Drosophila* oocytes, PI4KIIIα is required to ensure plasma membrane integrity, most likely through the maintenance of PI4P and PIP_2 levels at the membrane.

With respect to the determinants of PI4KIIIα localisation, the proteins Efr3 and TTC7 are present in flies as well. In both yeast and mammalian cells, Efr3 and TTC7 bind to and recruit PI4KIIIα to the plasma membrane (Baird et al., 2008; Nakatsu et al., 2012). The fly orthologue of Efr3 was shown to physically interact with PI4KIIIα in a 2017 study. This complex was also linked to the accumulation of beta amyloid peptides, a key causative agent of Alzheimer's disease. Downregulating PI4KIIIα and the *Drosophila* Efr3 facilitates greater clearance of beta amyloid peptides from cells, offering a

potential therapeutic target for the treatment of associated diseases (Zhang et al., 2017). A more recent study has shown that PI4KIIIα works in concert with a PI transfer protein known as Vibrator to control the asymmetric division of neuronal stem cells. It is thought to do so by producing PI4P at the plasma membrane, which regulates the anchoring of a myosin light chain to the cell cortex (Koe et al., 2018).

Till date, there has not been a comprehensive demonstration of a role for PI4KIIIα in PLC-mediated GPCR signalling in *Drosophila*. While there exists data from mammalian cell culture systems, it is important to demonstrate these findings in a whole organism context. *Drosophila* phototransduction provides an excellent system in which to test this hypothesis, allowing for unambiguous genetic manipulation and ease of interpretation.

1.7 Main questions to be addressed in this thesis

The key questions that will be addressed in this study are outlined below:

1. What is effect of removing PI4KIIIα on *Drosophila* phototransduction? How does the electrical response to light change, if at all, when the photoreceptors are depleted of PI4KIIIα? Is the role of PI4KIIIα during phototransduction a function of its kinase activity?
2. What is the effect of removing PI4KIIIα on the levels of PI4P and PIP_2 in photoreceptors? How are the total phosphoinositide levels affected and how does it impact the rate of PIP_2 resynthesis during visual signalling?
3. What is the relationship of PI4KIIIα with other members of the PIP_2 resynthesis cascade, namely *rdgB* and *dPIP5K*?
4. Is the PI4KIIIα protein complex a conserved phenomenon? Are both Efr3 and TTC7 required for *Drosophila* phototransduction as well? How does removing these interactors impact PI4P and PIP_2 levels?

In addition to the above questions, we also attempted to resolve an issue of enzymatic activity previously ascribed to the *Drosophila* orthologue of Efr3 (Huang et al., 2004). To do so, we asked the following question:

5. Does Efr3 function as a DAG lipase in the context of *Drosophila* phototransduction?

Bibliography

B. W. Agranoff. The Enzymatic Synthesis of Inositol Phosphatide. 233(5): 8, 1958.

B. W. Agranoff. Cyclitol confusion. *Trends in Biochemical Sciences*, 3: 283–285, 1978.

B. Antonny, J. Bigay, and B. Mesmin. The Oxysterol-Binding Protein Cycle: Burning Off PI(4)P to Transport Cholesterol. *Annual Review of Biochemistry*, 87(1):809–837, June 2018. ISSN 0066-4154, 1545-4509. doi: 10.1146/annurev-biochem-061516-044924.

A. Arcaro and M. P. Wymann. Wortmannin is a potent phosphatidylinositol 3-kinase inhibitor: The role of phosphatidylinositol 3,4,5-trisphosphate in neutrophil responses. *Biochemical Journal*, 296(2):297–301, Dec. 1993. ISSN 0264-6021, 1470-8728. doi: 10.1042/bj2960297.

M. Arita, H. Kojima, T. Nagano, T. Okabe, T. Wakita, and H. Shimizu. Phosphatidylinositol 4-Kinase III Beta Is a Target of Enviroxime-Like Compounds for Antipoliovirus Activity. *J. VIROL.*, 85:9, 2011.

O. Attree, I. M. Olivos, I. Okabe, L. C. Bailey, D. L. Nelson, R. A. Lewis, R. R. Mclnnes, and R. L. Nussbaum. The Lowe's oculocerebrorenal syndrome gene encodes a protein highly homologous to inositol polyphosphate-5-phosphatase. *Nature*, 358(6383):239–242, July 1992. ISSN 0028-0836, 1476-4687. doi: 10.1038/358239a0.

A. Audhya and S. D. Emr. Stt4 PI 4-Kinase Localizes to the Plasma Membrane and Functions in the Pkc1-Mediated MAP Kinase Cascade. *Developmental Cell*, 2(5):593–605, May 2002. ISSN 1534-5807. doi: 10.1016/S1534-5807(02)00168-5.

D. Baird, C. Stefan, A. Audhya, S. Weys, and S. D. Emr. Assembly of the PtdIns 4-kinase Stt4 complex at the plasma membrane requires Ypp1 and Efr3. *J Cell Biol*, 183(6):1061–1074, Dec. 2008. ISSN 0021-9525, 1540-8140. doi: 10.1083/jcb.200804003.

S. S. Balakrishnan, U. Basu, and P. Raghu. Phosphoinositide signalling in Drosophila. *Biochimica et Biophysica Acta (BBA) - Molecular and Cell Biology of Lipids*, 1851(6):770–784, June 2015. ISSN 1388-1981. doi: 10.1016/j.bbalip.2014.10.010.

A. Balla, G. Tuymetova, M. Barshishat, M. Geiszt, and T. Balla. Characterization of Type II Phosphatidylinositol 4-Kinase Isoforms Reveals Association of the Enzymes with Endosomal Vesicular Compartments. *Journal*

of Biological Chemistry, 277(22):20041–20050, May 2002. ISSN 0021-9258, 1083-351X. doi: 10.1074/jbc.M111807200.

A. Balla, G. Tuymetova, A. Tsiomenko, P. Várnai, and T. Balla. A Plasma Membrane Pool of Phosphatidylinositol 4-Phosphate Is Generated by Phosphatidylinositol 4-Kinase Type-III Alpha: Studies with the PH Domains of the Oxysterol Binding Protein and FAPP1. *Molecular Biology of the Cell*, 16(3):1282–1295, Jan. 2005. ISSN 1059-1524, 1939-4586. doi: 10.1091/mbc.E04-07-0578.

A. Balla, Y. J. Kim, P. Varnai, Z. Szentpetery, Z. Knight, K. M. Shokat, and T. Balla. Maintenance of Hormone-sensitive Phosphoinositide Pools in the Plasma Membrane Requires Phosphatidylinositol 4-Kinase IIIα. *Molecular Biology of the Cell*, 19(2):711–721, Jan. 2008. ISSN 1059-1524, 1939-4586. doi: 10.1091/mbc.E07-07-0713.

T. Balla, M. Wymann, and J. D. York, editors. *Phosphoinositides II: The Diverse Biological Functions*. Number Tomas Balla ... ed. ; 2 in Phosphoinositides. Springer, Dordrecht, 2012. ISBN 978-94-007-3014-4 978-94-007-3015-1. OCLC: 830746386.

J. M. Baskin, X. Wu, R. Christiano, M. S. Oh, C. M. Schauder, E. Gazzerro, M. Messa, S. Baldassari, S. Assereto, R. Biancheri, F. Zara, C. Minetti, A. Raimondi, M. Simons, T. C. Walther, K. M. Reinisch, and P. De Camilli. The leukodystrophy protein FAM126A (hyccin) regulates PtdIns(4)P synthesis at the plasma membrane. *Nature Cell Biology*, 18 (1):132–138, Jan. 2016. ISSN 1476-4679. doi: 10.1038/ncb3271.

K. L. Berger, J. D. Cooper, N. S. Heaton, R. Yoon, T. E. Oakland, T. X. Jordan, G. Mateu, A. Grakoui, and G. Randall. Roles for endocytic trafficking and phosphatidylinositol 4-kinase III alpha in hepatitis C virus replication. *Proceedings of the National Academy of Sciences*, 106(18):7577–7582, May 2009. ISSN 0027-8424, 1091-6490. doi: 10.1073/pnas.0902693106.

M. J. Berridge. Inositol trisphosphate and diacylglycerol as second messengers. *Biochemical Journal*, 220(2):345–360, June 1984. ISSN 0264-6021, 1470-8728. doi: 10.1042/bj2200345.

M. J. Berridge. Module 2: Cell Signalling Pathways. In *Cell Signalling Biology*, volume 6, page csb0001002. 2008.

M. J. Berridge, R. M. C. Dawson, C. P. Downes, J. P. Heslop, and R. F. Irvine. Changes in the levels of inositol phosphates after agonist-dependent hydrolysis of membrane phosphoinositides. *Biochemical Journal*, 212(2): 473–482, May 1983. ISSN 0264-6021, 1470-8728. doi: 10.1042/bj2120473.

G. H. Biddlecome, G. Berstein, and E. M. Ross. Regulation of Phospholipase C-b1 by Gq and m1 Muscarinic Cholinergic Receptor. *Journal of Biological Chemistry*, 271:11, 1996.

M. M. Billah and R. H. Michell. Phosphatidylinositol metabolism in rat hepatocytes stimulated by glycogenolytic hormones. Effects of angiotensin, vasopressin, adrenaline, ionophore A23187 and calcium-ion deprivation. *Biochemical Journal*, 182(3):661–668, Sept. 1979. ISSN 0264-6021, 1470-8728. doi: 10.1042/bj1820661.

H. H. Bishop and K. P. Strickland. On the specificity of cytidine diphosphate diglycerides in monophosphoinositide biosynthesis by rat brain preparations. *Canadian Journal of Biochemistry*, 48(3):269–277, Mar. 1970. ISSN 0008-4018. doi: 10.1139/o70-048.

J. E. Bleasdale, P. C. MacDonald, P. Wallis, and J. M. Johnston. CHARACTERIZATION OF THE FORWARD AND REVERSE REACTIONS CATALYZED BY CDP-DIACYLGLYCEROL:INOSITOL TRANSFERASE IN RABBIT LUNG TISSUE. *Biochimica et Biophysica Acta*, 575:135–147, 1979.

H. Brockerhoff and C. E. Ballou. Phosphate Incorporation in Brain Phosphoinositides.pdf. *Journal of Biological Chemistry*, 1962.

P. Chakrabarti, S. Kolay, S. Yadav, K. Kumari, A. Nair, D. Trivedi, and P. Raghu. A dPIP5K Dependent Pool of Phosphatidylinositol 4,5 Bisphosphate (PIP2) Is Required for G-Protein Coupled Signal Transduction in Drosophila Photoreceptors. *PLOS Genetics*, 11(1):e1004948, Jan. 2015. ISSN 1553-7404. doi: 10.1371/journal.pgen.1004948.

D. Chalupska, B. Różycki, J. Humpolickova, L. Faltova, M. Klima, and E. Boura. Phosphatidylinositol 4-kinase IIIβ (PI4KB) forms highly flexible heterocomplexes that include ACBD3, 14-3-3, and Rab11 proteins. *Scientific Reports*, 9(1), Dec. 2019. ISSN 2045-2322. doi: 10.1038/s41598-018-37158-6.

J. Chung, F. Nakatsu, J. M. Baskin, and P. D. Camilli. Plasticity of PI4KIIIα interactions at the plasma membrane. *EMBO reports*, 16(3):312–320, Mar. 2015a. ISSN 1469-221X, 1469-3178. doi: 10.15252/embr.201439151.

J. Chung, F. Torta, K. Masai, L. Lucast, H. Czapla, L. B. Tanner, P. Narayanaswamy, M. R. Wenk, F. Nakatsu, and P. D. Camilli. PI4P/phosphatidylserine countertransport at ORP5- and ORP8-mediated ER–plasma membrane contacts. *Science*, 349(6246):428–432, July 2015b. ISSN 0036-8075, 1095-9203. doi: 10.1126/science.aab1370.

J. Chung, F. Torta, K. Masai, L. Lucast, H. Czapla, L. B. Tanner, P. Narayanaswamy, M. R. Wenk, F. Nakatsu, and P. De Camilli. PI4P/phosphatidylserine countertransport at ORP5- and ORP8-mediated ER-plasma membrane contacts. *Science*, 349(6246):428–432, July 2015c. ISSN 0036-8075, 1095-9203. doi: 10.1126/science.aab1370.

C. A. Collins and W. Wells. Identification of PhosphatidylinositolKinase in Rat Liver Lysosomal Membranes. page 6, 1982.

M. Colodzin and E. P. Kennedy. Biosynthesis of Diphosphoinositide in Brain.pdf. *Journal of Biological Chemistry*, 1965.

J. A. Creba, C. P. Downes, P. T. Hawkins, G. Brewster, R. H. Michell, and C. J. Kirk. Rapid breakdown of phosphatidylinositol 4-phosphate and phosphatidylinositol 4,5-bisphosphate in rat hepatocytes stimulated by vasopressin and other Ca^{2+} -mobilizing hormones. *Biochemical Journal*, 212(3):733–747, June 1983. ISSN 0264-6021, 1470-8728. doi: 10.1042/bj2120733.

G. D'Angelo, E. Polishchuk, G. D. Tullio, M. Santoro, A. D. Campli, A. Godi, G. West, J. Bielawski, C.-C. Chuang, A. C. van der Spoel, F. M. Platt, Y. A. Hannun, R. Polishchuk, P. Mattjus, and M. A. De Matteis. Glycosphingolipid synthesis requires FAPP2 transfer of glucosylceramide. *Nature*, 449(7158):62–67, Sept. 2007. ISSN 0028-0836, 1476-4687. doi: 10.1038/nature06097.

R. M. C. Dawson, N. Hemington, and D. B. Lindsay. The phospholipids of the erythrocyte 'ghosts' of various species. *Biochemical Journal*, 77(2):226–230, Nov. 1960. ISSN 0264-6021, 1470-8728. doi: 10.1042/bj0770226.

M. de Saint-Jean, V. Delfosse, D. Douguet, G. Chicanne, B. Payrastre, W. Bourguet, B. Antonny, and G. Drin. Osh4p exchanges sterols for phosphatidylinositol 4-phosphate between lipid bilayers. *The Journal of Cell Biology*, 195(6):965–978, Dec. 2011. ISSN 0021-9525, 1540-8140. doi: 10.1083/jcb.201104062.

J. L. R. Deer, J. B. Hurley, and S. L. Yarfitz. G Protein Control of Drosophila Photoreceptor Phospholipase C. *Journal of Biological Chemistry*, 270(21):12623–12628, May 1995. ISSN 0021-9258, 1083-351X. doi: 10.1074/jbc.270.21.12623.

L. M. Del Bel, N. Griffiths, R. Wilk, H.-C. Wei, A. Blagoveshchenskaya, J. Burgess, G. Polevoy, J. V. Price, P. Mayinger, and J. A. Brill. The phosphoinositide phosphatase Sac1 regulates cell shape and microtubule

stability in the developing *Drosophila* eye. *Development*, page dev.151571, May 2018. ISSN 0950-1991, 1477-9129. doi: 10.1242/dev.151571.

H. C. Dippold, M. M. Ng, S. E. Farber-Katz, S.-K. Lee, M. L. Kerr, M. C. Peterman, R. Sim, P. A. Wiharto, K. A. Galbraith, S. Madhavarapu, G. J. Fuchs, T. Meerloo, M. G. Farquhar, H. Zhou, and S. J. Field. GOLPH3 Bridges Phosphatidylinositol-4- Phosphate and Actomyosin to Stretch and Shape the Golgi to Promote Budding. *Cell*, 139(2):337–351, Oct. 2009. ISSN 00928674. doi: 10.1016/j.cell.2009.07.052.

D. J. Dupré, T. E. Hébert, and R. Jockers, editors. *GPCR Signalling Complexes – Synthesis, Assembly, Trafficking and Specificity*, volume 63 of *Subcellular Biochemistry*. Springer Netherlands, Dordrecht, 2012. ISBN 978-94-007-4764-7 978-94-007-4765-4. doi: 10.1007/978-94-007-4765-4.

G. Endemann, S. N. Dunn, and L. C. Cantley. Bovine brain contains two types of phosphatidylinositol kinase. *Biochemistry*, 26(21):6845–6852, Oct. 1987. ISSN 0006-2960, 1520-4995. doi: 10.1021/bi00395a039.

C. Flanagan, E. Schnieders, A. Emerick, R. Kunisawa, A. Admon, and J. Thorner. Phosphatidylinositol 4-kinase: Gene structure and requirement for yeast cell viability. *Science*, 262(5138):1444–1448, Nov. 1993. ISSN 0036-8075, 1095-9203. doi: 10.1126/science.8248783.

J. Folch. Brain Diphosphoinositide, A New Phosphatide Having Inositol Metadiphosphate as a Constituent.pdf. *Journal of Biological Chemistry*, 1949a.

J. Folch. Complete Fractionation of Brain Cephalin - Isolation from IT of Phospatidylserine, Phosphatidylethanolamine and Diphosphoinositide.pdf. *Journal of Biological Chemistry*, 1949b.

M. Foti, A. Audhya, and S. D. Emr. Sac1 Lipid Phosphatase and Stt4 Phosphatidylinositol 4-Kinase Regulate a Pool of Phosphatidylinositol 4-Phosphate That Functions in the Control of the Actin Cytoskeleton and Vacuole Morphology. *Molecular Biology of the Cell*, 12(8):2396–2411, Aug. 2001. ISSN 1059-1524, 1939-4586. doi: 10.1091/mbc.12.8.2396.

E. K. Fridriksson, P. A. Shipkova, E. D. Sheets, D. Holowka, B. Baird, and F. W. McLafferty. Quantitative Analysis of Phospholipids in Functionally Important Membrane Domains from RBL-2H3 Mast Cells Using Tandem High-Resolution Mass Spectrometry †. *Biochemistry*, 38(25):8056–8063, June 1999. ISSN 0006-2960, 1520-4995. doi: 10.1021/bi9828324.

I. Garcia-Murillas, T. Pettitt, E. Macdonald, H. Okkenhaug, P. Georgiev,

D. Trivedi, B. Hassan, M. Wakelam, and P. Raghu. Lazaro Encodes a Lipid Phosphate Phosphohydrolase that Regulates Phosphatidylinositol Turnover during Drosophila Phototransduction. *Neuron*, 49(4):533–546, Feb. 2006. ISSN 08966273. doi: 10.1016/j.neuron.2006.02.001.

D. J. Gillooly. Localization of phosphatidylinositol 3-phosphate in yeast and mammalian cells. *The EMBO Journal*, 19(17):4577–4588, Sept. 2000. ISSN 14602075. doi: 10.1093/emboj/19.17.4577.

B. D. Gomperts, I. M. Kramer, and Tatham. *Signal Transduction*. Elsevier Academic Press, USA, 1 edition, 2002. ISBN 0-12-289631-9.

H. E. Grecco, M. Schmick, and P. I. Bastiaens. Signaling from the Living Plasma Membrane. *Cell*, 144(6):897–909, Mar. 2011. ISSN 00928674. doi: 10.1016/j.cell.2011.01.029.

T. Gunnarsson, L. Ekblad, A. Karlsson, P. Michelsen, G. Odham, and B. Jergil. Separation of Polyphosphoinositides Using Normal-Phase High-Performance Liquid Chromatography and Evaporative Light Scattering Detection or Electrospray Mass Spectrometry. *Analytical Biochemistry*, 254(2):293–296, Dec. 1997. ISSN 00032697. doi: 10.1006/abio.1997.2430.

S. Guo, L. E. Stolz, S. M. Lemrow, and J. D. York. *SAC1* -like Domains of Yeast *SAC1* , *INP52* , and *INP53* and of Human Synaptojanin Encode Polyphosphoinositide Phosphatases. *Journal of Biological Chemistry*, 274 (19):12990–12995, May 1999. ISSN 0021-9258, 1083-351X. doi: 10.1074/jbc.274.19.12990.

W. F. Hamilton. A Direct Method of Testing Color Vision in Lower Animals.pdf. *Proceedings of the National Academy of Sciences*, 8, 1922.

G. R. V. Hammond, M. J. Fischer, K. E. Anderson, J. Holdich, A. Koteci, T. Balla, and R. F. Irvine. PI4P and PI(4,5)P2 Are Essential But Independent Lipid Determinants of Membrane Identity. *Science*, 337(6095): 727–730, Aug. 2012. ISSN 0036-8075, 1095-9203. doi: 10.1126/science.1222483.

G. R. V. Hammond, M. P. Machner, and T. Balla. A novel probe for phosphatidylinositol 4-phosphate reveals multiple pools beyond the Golgi. *J Cell Biol*, 205(1):113–126, Apr. 2014. ISSN 0021-9525, 1540-8140. doi: 10.1083/jcb.201312072.

K. Hanada, K. Kumagai, S. Yasuda, Y. Miura, M. Kawano, M. Fukasawa, and M. Nishijima. Molecular machinery for non-vesicular trafficking of

ceramide. *Nature*, 426(6968):803–809, Dec. 2003. ISSN 0028-0836, 1476-4687. doi: 10.1038/nature02188.

R. Hardie and M. Postma. Phototransduction in Microvillar Photoreceptors of Drosophila and Other Invertebrates. In *The Senses: A Comprehensive Reference*, pages 77–130. Elsevier, 2008. ISBN 978-0-12-370880-9. doi: 10.1016/B978-012370880-9.00402-3.

R. C. Hardie and P. Raghu. Visual transduction in Drosophila. 413:8, 2001.

R. C. Hardie, Y. Gu, F. Martin, S. T. Sweeney, and P. Raghu. *In Vivo* Light-induced and Basal Phospholipase C Activity in *Drosophila* Photoreceptors Measured with Genetically Targeted Phosphatidylinositol 4,5-Bisphosphate-sensitive Ion Channels (Kir2.1). *Journal of Biological Chemistry*, 279(46):47773–47782, Nov. 2004. ISSN 0021-9258, 1083-351X. doi: 10.1074/jbc.M407525200.

J. Harwood and J. Hawthorne. The properties and subcellular distribution of phosphatidylinositol kinase in mammalian tissues. *Biochimica et Biophysica Acta (BBA) - Enzymology*, 171(1):75–88, Jan. 1969. ISSN 00052744. doi: 10.1016/0005-2744(69)90107-7.

C. P. Haskins and E. V. Enzmann. A Determination of the Magnitude of the Cell Sensitive Volume Associated with the White Eye Mutation in X-rayed Drosophila - II.pdf. *Proceedings of the National Academy of Sciences*, 22, 1936.

V. Haucke. Phosphoinositide regulation of clathrin-mediated endocytosis. *Biochemical Society Transactions*, 33:5, 2005.

P. T. Hawkins, T. R. Jackson, and L. R. Stephens. Platelet-derived growth factor stimulates synthesis of Ptdlns(3,4,S)P3 by activating a Ptdlns(4,S)P2 3-0H kinase. page 3, 1992.

J. N. Hawthorne and E. Chargaff. A Study of Inositol Containing Lipides.pdf. *Journal of Biological Chemistry*, 1954.

K. He, R. Marsland III, S. Upadhyayula, E. Song, S. Dang, B. R. Capraro, W. Wang, W. Skillern, R. Gaudin, M. Ma, and T. Kirchhausen. Dynamics of phosphoinositide conversion in clathrin-mediated endocytic traffic. *Nature*, 552(7685):410–414, Dec. 2017. ISSN 0028-0836, 1476-4687. doi: 10.1038/nature25146.

S. Hecht. THE VISUAL ACUITY AND INTENSITY DISCRIMINATION OF DROSOPHILA. *The Journal of General Physiology*, 17(4):517–547, Mar. 1934. ISSN 0022-1295, 1540-7748. doi: 10.1085/jgp.17.4.517.

M. Helmkamp, M. S. Harvey, W. A. Wirtz, and L. M. Van. Phospholipid Exchange between Membranes. *Journal of Biological Chemistry*, 249:9, 1974.

K. A. Hinchliffe, A. Ciruela, and R. F. Irvine. PIPkins, their substrates and their products: New functions for old enzymes. *Biochimica et Biophysica Acta*, page 18, 1998.

L. E. Hokin and M. R. Hokin. The Incorporation of 32P from Triphosphate into Polyphosphoinositides [g-32P]Adenosine and Phosphatidic Acid in Erythrocyte Membranes.pdf. *Biochimica et Biophysica Acta*, 1964.

M. R. Hokin and L. E. Hokin. Enzyme Secretion and Incorporation of P32 into Phospholipids of Pancreas Slices.pdf. *Journal of Biological Chemistry*, 1952.

Y. Hotta and S. Benzer. Abnormal Electroretinograms in Visual Mutants of Drosophila. *Nature*, 222(5191):354, Apr. 1969. ISSN 1476-4687. doi: 10.1038/222354a0.

N.-Y. Hsu, O. Ilnytska, G. Belov, M. Santiana, Y.-H. Chen, P. M. Takvorian, C. Pau, H. van der Schaar, N. Kaushik-Basu, T. Balla, C. E. Cameron, E. Ehrenfeld, F. J. van Kuppeveld, and N. Altan-Bonnet. Viral Reorganization of the Secretory Pathway Generates Distinct Organelles for RNA Replication. *Cell*, 141(5):799–811, May 2010. ISSN 00928674. doi: 10.1016/j.cell.2010.03.050.

F.-D. Huang, H. J. G. Matthies, S. D. Speese, M. A. Smith, and K. Broadie. Rolling blackout, a newly identified PIP2-DAG pathway lipase required for Drosophila phototransduction. *Nature Neuroscience*, 7(10):1070–1078, Oct. 2004. ISSN 1546-1726. doi: 10.1038/nn1313.

H. Inoue, T. Yoshioka, and Y. Hotta. Diacylglycerol Kinase Defect in a Drosophila Retinal Degeneration Mutant rdgA. *Journal of Biological Chemistry*, 264(10):5996–6000, 1989.

S. Iqbal. *The Role of Vitamin D in the Treatment of Diabetes and Pancreatic Cancer*. PhD thesis, Aligarh Muslim University, 2018.

N. Jin, C. Y. Chow, L. Liu, S. N. Zolov, R. Bronson, M. Davisson, J. L. Petersen, Y. Zhang, S. Park, J. E. Duex, D. Goldowitz, M. H. Meisler, and L. S. Weisman. VAC14 nucleates a protein complex essential for the acute interconversion of PI3P and PI(3,5)P2 in yeast and mouse. *The EMBO Journal*, 27(24):3221–3234, Dec. 2008. ISSN 0261-4189, 1460-2075. doi: 10.1038/emboj.2008.248.

D. R. Jones, Y. Bultsma, W.-J. Keune, J. R. Halstead, D. Elouarrat, S. Mohammed, A. J. Heck, C. S. D'Santos, and N. Divecha. Nuclear PtdIns5P as a Transducer of Stress Signaling: An In Vivo Role for PIP4Kbeta. *Molecular Cell*, 23(5):685–695, Sept. 2006. ISSN 10972765. doi: 10.1016/j.molcel.2006.07.014.

M. Jović, M. J. Kean, Z. Szentpetery, G. Polevoy, A.-C. Gingras, J. A. Brill, and T. Balla. Two phosphatidylinositol 4-kinases control lysosomal delivery of the Gaucher disease enzyme, β-glucocerebrosidase. *Molecular Biology of the Cell*, 23(8):1533–1545, Apr. 2012. ISSN 1059-1524, 1939-4586. doi: 10.1091/mbc.e11-06-0553.

G. Kadamur and E. M. Ross. Mammalian Phospholipase C. *Annual Review of Physiology*, 75(1):127–154, Feb. 2013. ISSN 0066-4278, 1545-1585. doi: 10.1146/annurev-physiol-030212-183750.

M. Kai, G. White, and J. Hawthorne. The phosphatidylinositol kinase of rat brain. *Biochemical Journal*, 101(2):328–337, Nov. 1966. ISSN 0264-6021, 1470-8728. doi: 10.1042/bj1010328.

S. Kawal, T. Nikaido, Y. Aoki', Y. Zhai, T. Kumagai, K. Furihata, S. Fujii, and K. Kiyosawa. Vitamin D analogues upmregulate p21 and p27 during growth inhibition of pancreatic cancer cell lines. *British Journal of Cancer*, page 6, 1997.

W. T. Kim, S. Chang, L. Daniell, O. Cremona, G. Di Paolo, and P. De Camilli. Delayed reentry of recycling vesicles into the fusion-competent synaptic vesicle pool in synaptojanin 1 knockout mice. *Proceedings of the National Academy of Sciences*, 99(26):17143–17148, Dec. 2002. ISSN 0027-8424, 1091-6490. doi: 10.1073/pnas.222657399.

Y. J. Kim, M. L. Guzman-Hernandez, E. Wisniewski, N. Echeverria, and T. Balla. Phosphatidylinositol and phosphatidic acid transport between the ER and plasma membrane during PLC activation requires the Nir2 protein. *Biochemical Society Transactions*, 44(1):197–201, Feb. 2016. ISSN 0300-5127, 1470-8752. doi: 10.1042/BST20150187.

W. A. Kimber, L. Trinkle-Mulcahy, P. C. F. Cheung, M. Deak, L. J. Marsden, A. Kieloch, S. Watt, R. T. Javier, A. Gray, C. P. Downes, J. M. Lucocq, and D. R. Alessi. Evidence that the tandem-pleckstrin-homology-domain-containing protein TAPP1 interacts with Ptd(3,4)P2 and the multi-PDZ-domain-containing protein MUPP1 in vivo. page 12, 2002.

C. E. King, L. R. Stephens, P. T. Hawkins, G. R. Guy, and R. H. Michell. Multiple metabolic pools of phosphoinositides and phosphatidate in human

erythrocytes incubated in a medium that permits rapid transmembrane exchange of phosphate. *Biochemical Journal*, 244(1):209–217, May 1987. ISSN 0264-6021, 1470-8728. doi: 10.1042/bj2440209.

C. E. King, P. T. Hawkins, L. R. Stephens, and R. H. Michell. Determination of the steady-state turnover rates of the metabolically active pools of phosphatidylinositol 4-phosphate and phosphatidylinositol 4,5-bisphosphate in human erythrocytes. *Biochemical Journal*, 259(3):893–896, May 1989. ISSN 0264-6021, 1470-8728. doi: 10.1042/bj2590893.

E. Klenk and R. Sakai. Inositmonophosphorsäure, ein Spaltprodukt der Sojabohnenphosphatide. [14. Mitteilung über Phosphatide]. *Hoppe-Seyler´s Zeitschrift für physiologische Chemie*, 258(1):33–38, Jan. 1939. ISSN 0018-4888. doi: 10.1515/bchm2.1939.258.1.33.

C. T. Koe, Y. S. Tan, M. Lönnfors, S. K. Hur, C. S. L. Low, Y. Zhang, P. Kanchanawong, V. A. Bankaitis, and H. Wang. Vibrator and PI4KIIIα govern neuroblast polarity by anchoring non-muscle myosin II. *eLife*, 7: e33555, Feb. 2018. ISSN 2050-084X. doi: 10.7554/eLife.33555.

S. Kolay, U. Basu, and P. Raghu. Control of diverse subcellular processes by a single multi-functional lipid phosphatidylinositol 4,5-bisphosphate [PI(4,5)P2]. *Biochemical Journal*, 473(12):1681–1692, June 2016. ISSN 0264-6021, 1470-8728. doi: 10.1042/BCJ20160069.

I. Lassing and U. Lindberg. Specific interaction between phosphatidylinositol 4,5-bisphosphate and profilactin. *Nature*, 314(6010):472–474, Apr. 1985. ISSN 0028-0836, 1476-4687. doi: 10.1038/314472a0.

J. A. Lees, Y. Zhang, M. S. Oh, C. M. Schauder, X. Yu, J. M. Baskin, K. Dobbs, L. D. Notarangelo, P. D. Camilli, T. Walz, and K. M. Reinisch. Architecture of the human PI4KIIIα lipid kinase complex. *Proceedings of the National Academy of Sciences*, page 201718471, Dec. 2017. ISSN 0027-8424, 1091-6490. doi: 10.1073/pnas.1718471115.

R. Levin, G. R. V. Hammond, T. Balla, P. D. Camilli, G. D. Fairn, and S. Grinstein. Multiphasic dynamics of phosphatidylinositol 4-phosphate during phagocytosis. *Molecular Biology of the Cell*, 28(1):128–140, Jan. 2017. ISSN 1059-1524, 1939-4586. doi: 10.1091/mbc.E16-06-0451.

T. P. Levine and S. Munro. Targeting of Golgi-Specific Pleckstrin Homology Domains Involves Both PtdIns 4-Kinase-Dependent and -Independent Components. *Current Biology*, 12(9):695–704, Apr. 2002. ISSN 09609822. doi: 10.1016/S0960-9822(02)00779-0.

J. Li. PTEN, a Putative Protein Tyrosine Phosphatase Gene Mutated in Human Brain, Breast, and Prostate Cancer. *Science*, 275(5308):1943–1947, Mar. 1997. ISSN 00368075, 10959203. doi: 10.1126/science.275.5308.1943.

Y.-S. Li, F. D. Porter, R. M. Hoffman, and T. F. Deuel. Separation and identification of two phosphatidylinositol 4-kinase activities in bovine uterus. *Biochemical and Biophysical Research Communications*, 160(1):202–209, Apr. 1989. ISSN 0006291X. doi: 10.1016/0006-291X(89)91641-0.

D. Lu, H.-q. Sun, H. Wang, B. Barylko, Y. Fukata, M. Fukata, J. P. Albanesi, and H. L. Yin. Phosphatidylinositol 4-Kinase IIα Is Palmitoylated by Golgi-localized Palmitoyltransferases in Cholesterol-dependent Manner. *Journal of Biological Chemistry*, 287(26):21856–21865, June 2012. ISSN 0021-9258, 1083-351X. doi: 10.1074/jbc.M112.348094.

H. Ma, T. Blake, A. Chitnis, P. Liu, and T. Balla. Crucial role of phosphatidylinositol 4-kinase IIIα in development of zebrafish pectoral fin is linked to phosphoinositide 3-kinase and FGF signaling. *Journal of Cell Science*, 122(23):4303–4310, Dec. 2009. ISSN 0021-9533, 1477-9137. doi: 10.1242/jcs.057646.

T. Maehama and J. E. Dixon. The Tumor Suppressor, PTEN/MMAC1, Dephosphorylates the Lipid Second Messenger, Phosphatidylinositol 3,4,5-Trisphosphate. *Journal of Biological Chemistry*, 273(22):13375–13378, May 1998. ISSN 0021-9258, 1083-351X. doi: 10.1074/jbc.273.22.13375.

R. S. McEwen. The reactions to light and to gravity in Drosophila and its mutants. *Journal of Experimental Zoology*, 25(1):49–106, Feb. 1918. ISSN 0022-104X, 1097-010X. doi: 10.1002/jez.1400250103.

J. M. McKibbin. A Monophosphoinositide of the Liver.pdf. *Journal of Biological Chemistry*, 1956.

B. Mesmin. A Four-Step Cycle Driven by PI(4)P Hydrolysis Directs Sterol/PI(4)P Exchange by the ER-Golgi Tether OSBP. *Cell*, 155:14, 2013.

R. H. Michell and J. N. Hawthorne. The Site of Diphosphinositide Synthesis in Rat Liver. *BIOCHEMICAL AND BIOPHYSICAL RESEARCH COMMUNICATIONS*, 21(4):6, 1965.

R. H. Michell, J. L. Harwood, R. Coleman, and J. N. Hawthorne. Characteristics of Rat Liver Phosphatidylinositol Kinase and its Presence in the Plasma Membrane.pdf. *Biochimica et Biophysica Acta*, 1967.

S. Minogue. Phosphatidylinositol 4-kinase is required for endosomal traffick-

ing and degradation of the EGF receptor. *Journal of Cell Science*, 119(3): 571–581, Feb. 2006. ISSN 0021-9533, 1477-9137. doi: 10.1242/jcs.02752.

M. Mishra and E. Knust. Analysis of the Drosophila Compound Eye with Light and Electron Microscopy. In B. H. F. Weber and T. Langmann, editors, *Retinal Degeneration*, volume 1834, pages 345–364. Springer New York, New York, NY, 2019. ISBN 978-1-4939-8668-2 978-1-4939-8669-9. doi: 10.1007/978-1-4939-8669-9_22.

T. H. Morgan. SEX LIMITED INHERITANCE IN DROSOPHILA. *Science*, 32(812):120–122, July 1910. ISSN 0036-8075, 1095-9203. doi: 10.1126/science.32.812.120.

D. K. Morrison, M. S. Murakami, and V. Cleghon. Protein Kinases and Phosphatases in the *Drosophila* Genome. *The Journal of Cell Biology*, 150 (2):F57–F62, July 2000. ISSN 0021-9525, 1540-8140. doi: 10.1083/jcb.150.2.F57.

T. Nakagawa, K. Goto, and H. Kondo. Cloning, Expression, and Localization of 230-kDa Phosphatidylinositol 4-Kinase. *Journal of Biological Chemistry*, 271(20):12088–12094, May 1996. ISSN 0021-9258, 1083-351X. doi: 10.1074/jbc.271.20.12088.

F. Nakatsu, J. M. Baskin, J. Chung, L. B. Tanner, G. Shui, S. Y. Lee, M. Pirruccello, M. Hao, N. T. Ingolia, M. R. Wenk, and P. D. Camilli. PtdIns4P synthesis by PI4KIIIα at the plasma membrane and its impact on plasma membrane identity. *J Cell Biol*, 199(6):1003–1016, Dec. 2012. ISSN 0021-9525, 1540-8140. doi: 10.1083/jcb.201206095.

E. Okuhara and T. Nakayama. Studies on the Conjugated Lipides - on the Structure of inositide phospholipide.pdf. *Journal of Biological Chemistry*, 1954.

A. T. Pagnamenta, M. F. Howard, E. Wisniewski, N. Popitsch, S. J. L. Knight, D. A. Keays, G. Quaghebeur, H. Cox, P. Cox, T. Balla, J. C. Taylor, and U. Kini. Germline recessive mutations in PI4KA are associated with perisylvian polymicrogyria, cerebellar hypoplasia and arthrogryposis. *Human Molecular Genetics*, 24(13):3732–3741, July 2015. ISSN 0964-6906. doi: 10.1093/hmg/ddv117.

W. L. Pak. Why Drosophila to Study Phototransduction? *Journal of Neurogenetics*, 24(2):55–66, July 2010. ISSN 0167-7063, 1563-5260. doi: 10.3109/01677061003797302.

W. Pan, S.-C. Choi, H. Wang, Y. Qin, L. Volpicelli-Daley, L. Swan, L. Lucast,

C. Khoo, X. Zhang, L. Li, C. S. Abrams, S. Y. Sokol, and D. Wu. Wnt3a-Mediated Formation of Phosphatidylinositol 4,5-Bisphosphate Regulates LRP6 Phosphorylation. *Science*, 321(5894):1350–1353, Sept. 2008. ISSN 0036-8075, 1095-9203. doi: 10.1126/science.1160741.

F. Pettersson, K. W. Colston, and A. G. Dalgleish. Differential and antagonistic effects of 9-cis-retinoic acid and vitamin D analogues on pancreatic cancer cells in vitro. *British Journal of Cancer*, 83(2):239–245, July 2000. ISSN 0007-0920, 1532-1827. doi: 10.1054/bjoc.2000.1281.

T. R. Pettitt, S. K. Dove, A. Lubben, S. D. J. Calaminus, and M. J. O. Wakelam. Analysis of intact phosphoinositides in biological samples. *Journal of Lipid Research*, 47(7):1588–1596, Jan. 2006. ISSN 0022-2275, 1539-7262. doi: 10.1194/jlr.D600004-JLR200.

V. Prpic and J. H. Extong. Phosphatidylinositol Breakdown Induced by Vasopressin and Epinephrine in Hepatocytes Is Calcium-dependent. *Journal of Biological Chemistry*, page 9, 1982.

Y. Qin, L. Li, W. Pan, and D. Wu. Regulation of Phosphatidylinositol Kinases and Metabolism by Wnt3a and Dvl. *Journal of Biological Chemistry*, 284(34):22544–22548, Aug. 2009. ISSN 0021-9258, 1083-351X. doi: 10.1074/jbc.M109.014399.

P. Raghu, S. Yadav, and N. B. N. Mallampati. Lipid signaling in Drosophila photoreceptors. *Biochimica et Biophysica Acta (BBA) - Molecular and Cell Biology of Lipids*, 1821(8):1154–1165, Aug. 2012. ISSN 1388-1981. doi: 10.1016/j.bbalip.2012.03.008.

L. E. Rameh, K. F. Tolias, B. C. Duckworth, and L. C. Cantley. A new pathway for synthesis of phosphatidylinositol-4,5-bisphosphate. *Nature*, 390(6656):192–196, Nov. 1997. ISSN 0028-0836, 1476-4687. doi: 10.1038/36621.

S. Reiss, C. Harak, I. Romero-Brey, D. Radujkovic, R. Klein, A. Ruggieri, I. Rebhan, R. Bartenschlager, and V. Lohmann. The Lipid Kinase Phosphatidylinositol-4 Kinase III Alpha Regulates the Phosphorylation Status of Hepatitis C Virus NS5A. *PLoS Pathogens*, 9(5):e1003359, May 2013. ISSN 1553-7374. doi: 10.1371/journal.ppat.1003359.

S. G. Rhee. Regulation of Phosphoinositide Specific PLC.pdf. *Annu. Rev. Biochem.*, 70:281–312, 2001.

D. Sarkes and L. E. Rameh. A novel HPLC-based approach makes possible the spatial characterization of cellular PtdIns5 P and other phosphoinosi-

tides. *Biochemical Journal*, 428(3):375–384, June 2010. ISSN 0264-6021, 1470-8728. doi: 10.1042/BJ20100129.

T. Sasaki, S. Takasuga, J. Sasaki, S. Kofuji, S. Eguchi, M. Yamazaki, and A. Suzuki. Mammalian phosphoinositide kinases and phosphatases. *Progress in Lipid Research*, 48(6):307–343, Nov. 2009. ISSN 01637827. doi: 10.1016/j.plipres.2009.06.001.

K. Scott and C. S. Zuker. Assembly of the Drosophila phototransduction cascade into a signalling complex shapes elementary responses. *Nature*, 395(6704):805–808, Oct. 1998. ISSN 0028-0836, 1476-4687. doi: 10.1038/27448.

H. G. Skinner. Vitamin D Intake and the Risk for Pancreatic Cancer in Two Cohort Studies. *Cancer Epidemiology Biomarkers & Prevention*, 15 (9):1688–1695, Sept. 2006. ISSN 1055-9965, 1538-7755. doi: 10.1158/1055-9965.EPI-06-0206.

C. R. Slack, P. G. Roughan, and N. Balasingham. Labelling of Glycerolipids in the Cotyledons of Developing Oilseeds by I1-_4ClAcetate and 12-3H1Glycerol. 170:13, 1978.

G. H. Sloane-Stanley. Anaerobic reactions of phospholipins in brain suspensions. *Biochemical Journal*, 53(4):613–619, Mar. 1953. ISSN 0264-6021, 1470-8728. doi: 10.1042/bj0530613.

S. Sridhar, B. Patel, D. Aphkhazava, F. Macian, L. Santambrogio, D. Shields, and A. M. Cuervo. The lipid kinase PI4KIIIβ preserves lysosomal identity. *The EMBO Journal*, 32(3):324–339, Dec. 2012. ISSN 0261-4189, 1460-2075. doi: 10.1038/emboj.2012.341.

B. K. Staley and K. D. Irvine. Hippo signaling in *Drosophila* : Recent advances and insights: Hippo Signaling in *Drosophila*. *Developmental Dynamics*, 241(1):3–15, Jan. 2012. ISSN 10588388. doi: 10.1002/dvdy.22723.

W. S. Stark, J. A. Walker, and W. A. Harris. Genetic dissection of the photoreceptor system in the compound eye of *Drosophila melanogaster*. *The Journal of Physiology*, 256(2):415–439, Apr. 1976. ISSN 00223751. doi: 10.1113/jphysiol.1976.sp011331.

L. Stephens, T. R. Jackson, and P. T. Hawkins. Activation of phosphatidylinositol 4,5-bisphosphate supply by agonists and non-hydrolysable GTP analogues. *Biochemical Journal*, 296(2):481–488, Dec. 1993. ISSN 0264-6021, 1470-8728. doi: 10.1042/bj2960481.

L. R. Stephens, K. T. Hughes, and R. F. Irvine. Pathway of phosphatidylinositol(3,4,5)-trisphosphate synthesis in activated neutrophils. *Nature*, 351(6321):33–39, May 1991. ISSN 0028-0836, 1476-4687. doi: 10.1038/351033a0.

L. R. Stephens, P. T. Hawkins, and A. McGregor. Phosphoinositide 3-kinases: Regulation by cell surface receptors and function of 3-phosphorylated lipids. In *Biology of Phosphinositides*. Oxford University Press, 2000.

R. Z. Stolzenberg-Solomon, E. J. Jacobs, A. A. Arslan, D. Qi, A. V. Patel, K. J. Helzlsouer, S. J. Weinstein, M. L. McCullough, M. P. Purdue, X.-O. Shu, K. Snyder, J. Virtamo, L. R. Wilkins, K. Yu, A. Zeleniuch-Jacquotte, W. Zheng, D. Albanes, Q. Cai, C. Harvey, R. Hayes, S. Clipp, R. L. Horst, L. Irish, K. Koenig, L. Le Marchand, and L. N. Kolonel. Circulating 25-Hydroxyvitamin D and Risk of Pancreatic Cancer: Cohort Consortium Vitamin D Pooling Project of Rarer Cancers. *American Journal of Epidemiology*, 172(1):81–93, July 2010. ISSN 0002-9262, 1476-6256. doi: 10.1093/aje/kwq120.

J. R. Strating and F. J. van Kuppeveld. Viral rewiring of cellular lipid metabolism to create membranous replication compartments. *Current Opinion in Cell Biology*, 47:24–33, Aug. 2017. ISSN 09550674. doi: 10.1016/j.ceb.2017.02.005.

H. Sunshine and M. L. Iruela-Arispe. Membrane lipids and cell signaling:. *Current Opinion in Lipidology*, 28(5):408–413, Oct. 2017. ISSN 0957-9672. doi: 10.1097/MOL.0000000000000443.

J. Tan, K. Oh, J. Burgess, D. R. Hipfner, and J. A. Brill. PI4KIIIα is required for cortical integrity and cell polarity during Drosophila oogenesis. *J Cell Sci*, 127(5):954–966, Mar. 2014. ISSN 0021-9533, 1477-9137. doi: 10.1242/jcs.129031.

G. M. Thomas, E. Cunningham, A. Fensome, A. Ball, N. F. Totty, O. Truong, J. Hsuan, and S. Cockcroft. An essential role for phosphatidylinositol transfer protein in phospholipase C-Mediated inositol lipid signaling. *Cell*, 74(5):919–928, Sept. 1993. ISSN 00928674. doi: 10.1016/0092-8674(93)90471-2.

W. Thompson and R. Dawson. The hydrolysis of triphosphoinositide by extracts of ox brain. *Biochemical Journal*, 91(2):233–236, May 1964. ISSN 0264-6021, 1470-8728. doi: 10.1042/bj0910233.

R. Tomlinson and C. E. Ballou. Complete Characterization of the Myo-

inositol Polyphosphates from Beef Brain Phosphoinositide.pdf. *Journal of Biological Chemistry*, 1961.

J. T. Tóth, G. Gulyás, D. J. Tóth, A. Balla, G. R. V. Hammond, L. Hunyady, T. Balla, and P. Várnai. BRET-monitoring of the dynamic changes of inositol lipid pools in living cells reveals a PKC-dependent PtdIns4P increase upon EGF and M3 receptor activation. *Biochimica et Biophysica Acta (BBA) - Molecular and Cell Biology of Lipids*, 1861(3):177–187, Mar. 2016. ISSN 1388-1981. doi: 10.1016/j.bbalip.2015.12.005.

A. Traynor-Kaplan, M. Kruse, E. J. Dickson, G. Dai, O. Vivas, H. Yu, D. Whittington, and B. Hille. Fatty-acyl chain profiles of cellular phosphoinositides. *Biochimica et Biophysica Acta (BBA) - Molecular and Cell Biology of Lipids*, 1862(5):513–522, May 2017. ISSN 1388-1981. doi: 10.1016/j.bbalip.2017.02.002.

P. Várnai and T. Balla. Visualization of Phosphoinositides That Bind Pleckstrin Homology Domains: Calcium- and Agonist-induced Dynamic Changes and Relationship to Myo-[3H]inositol-labeled Phosphoinositide Pools. *The Journal of Cell Biology*, 143(2):501–510, Oct. 1998. ISSN 0021-9525, 1540-8140. doi: 10.1083/jcb.143.2.501.

P. Várnai, G. Gulyás, D. J. Tóth, M. Sohn, N. Sengupta, and T. Balla. Quantifying lipid changes in various membrane compartments using lipid binding protein domains. *Cell Calcium*, 64(Supplement C):72–82, June 2017. ISSN 0143-4160. doi: 10.1016/j.ceca.2016.12.008.

R. Venditti, M. C. Masone, C. Wilson, and M. A. De Matteis. PI(4)P homeostasis: Who controls the controllers? *Advances in Biological Regulation*, 60(Supplement C):105–114, Jan. 2016. ISSN 2212-4926. doi: 10.1016/j.jbior.2015.09.007.

K. Venkateswarlu, P. B. Oatey, J. M. Tavare, T. R. Jackson, and P. J. Cullen. Identification of centaurin-$A1$ as a potential in vivo phosphatidylinositol 3,4,5-trisphosphate-binding protein that is functionally homologous to the yeast ADP-ribosylation factor (ARF) GTPase-activating protein, Gcs. page 5, 1999.

J. M. von Filseck, A. Čopič, V. Delfosse, S. Vanni, C. L. Jackson, W. Bourguet, and G. Drin. Phosphatidylserine transport by ORP/Osh proteins is driven by phosphatidylinositol 4-phosphate. *Science*, 349(6246):432–436, July 2015. ISSN 0036-8075, 1095-9203. doi: 10.1126/science.aab1346.

H. Wang, H.-Q. Sun, X. Zhu, L. Zhang, J. Albanesi, B. Levine, and H. Yin. GABARAPs regulate PI4P-dependent autophagosome:lysosome fusion.

Proceedings of the National Academy of Sciences, 112(22):7015–7020, June 2015. ISSN 0027-8424, 1091-6490. doi: 10.1073/pnas.1507263112.

J. Wang, H.-Q. Sun, E. Macia, T. Kirchhausen, H. Watson, J. S. Bonifacino, and H. L. Yin. PI4P Promotes the Recruitment of the GGA Adaptor Proteins to the *Trans* -Golgi Network and Regulates Their Recognition of the Ubiquitin Sorting Signal. *Molecular Biology of the Cell*, 18(7): 2646–2655, July 2007. ISSN 1059-1524, 1939-4586. doi: 10.1091/mbc.e06-10-0897.

K. Wang, Z. Yang, X. Liu, K. Mao, U. Nair, and D. J. Klionsky. Phosphatidylinositol 4-Kinases Are Required for Autophagic Membrane Trafficking. *Journal of Biological Chemistry*, 287(45):37964–37972, Nov. 2012. ISSN 0021-9258, 1083-351X. doi: 10.1074/jbc.M112.371591.

T. Wang and C. Montell. A Phosphoinositide Synthase Required for a Sustained Light Response. *Journal of Neuroscience*, 26(49):12816–12825, Dec. 2006. ISSN 0270-6474, 1529-2401. doi: 10.1523/JNEUROSCI.3673-06.2006.

Y. J. Wang, J. Wang, H. Q. Sun, M. Martinez, Y. X. Sun, E. Macia, T. Kirchhausen, J. P. Albanesi, M. G. Roth, and H. L. Yin. Phosphatidylinositol 4 Phosphate Regulates Targeting of Clathrin Adaptor AP-1 Complexes to the Golgi. *Cell*, 114(3):299–310, Aug. 2003. ISSN 00928674. doi: 10.1016/S0092-8674(03)00603-2.

Y. J. Wei, H. Q. Sun, M. Yamamoto, P. Wlodarski, K. Kunii, M. Martinez, B. Barylko, J. P. Albanesi, and H. L. Yin. Type II Phosphatidylinositol 4-Kinase β Is a Cytosolic and Peripheral Membrane Protein That Is Recruited to the Plasma Membrane and Activated by Rac-GTP. *Journal of Biological Chemistry*, 277(48):46586–46593, Nov. 2002. ISSN 0021-9258, 1083-351X. doi: 10.1074/jbc.M206860200.

S. J. Weiss and J. W. Putney. The relationship of phosphatidylinositol turnover to receptors and calcium-ion channels in rat parotid acinar cells. *Biochemical Journal*, 194(2):463–468, Feb. 1981. ISSN 0264-6021, 1470-8728. doi: 10.1042/bj1940463.

G. B. Willars, S. R. Nahorski, and R. A. J. Challiss. Differential Regulation of Muscarinic Acetylcholine Receptor-sensitive Polyphosphoinositide Pools and Consequences for Signaling in Human Neuroblastoma Cells. *Journal of Biological Chemistry*, 273(9):5037–5046, Feb. 1998. ISSN 0021-9258, 1083-351X. doi: 10.1074/jbc.273.9.5037.

B. M. Wolpin, K. Ng, Y. Bao, P. Kraft, M. J. Stampfer, D. S. Michaud,

J. Ma, J. E. Buring, H. D. Sesso, I.-M. Lee, N. Rifai, B. B. Cochrane, J. Wactawski-Wende, R. T. Chlebowski, W. C. Willett, J. E. Manson, E. L. Giovannucci, and C. S. Fuchs. Plasma 25-Hydroxyvitamin D and Risk of Pancreatic Cancer. *Cancer Epidemiology Biomarkers & Prevention*, 21 (1):82–91, Jan. 2012. ISSN 1055-9965, 1538-7755. doi: 10.1158/1055-9965.EPI-11-0836.

L. Wu, B. Niemeyer, N. Colley, M. Socolich, and C. S. Zuker. Regulation of PLC-mediated signalling in vivo by CDP-diacylglycerol synthase. *Nature*, 373, 1995.

X. Wu, R. J. Chi, J. M. Baskin, L. Lucast, C. G. Burd, P. De Camilli, and K. M. Reinisch. Structural Insights into Assembly and Regulation of the Plasma Membrane Phosphatidylinositol 4-Kinase Complex. *Developmental Cell*, 28(1):19–29, Jan. 2014. ISSN 1534-5807. doi: 10.1016/j.devcel.2013.11.012.

M. Xing, M. C. Peterman, R. L. Davis, K. Oegema, A. K. Shiau, and S. J. Field. GOLPH3 drives cell migration by promoting Golgi reorientation and directional trafficking to the leading edge. *Molecular Biology of the Cell*, 27(24):3828–3840, Dec. 2016. ISSN 1059-1524, 1939-4586. doi: 10.1091/mbc.E16-01-0005.

S. Yadav, K. Garner, P. Georgiev, M. Li, E. Gomez-Espinosa, A. Panda, S. Mathre, H. Okkenhaug, S. Cockcroft, and P. Raghu. RDGB , a PtdIns-PtdOH transfer protein, regulates G-protein-coupled PtdIns(4,5)P2 signalling during Drosophila phototransduction. *Journal of Cell Science*, 128 (17):3330–3344, Sept. 2015. ISSN 0021-9533, 1477-9137. doi: 10.1242/jcs.173476.

Y. Yan, N. Denef, C. Tang, and T. Schüpbach. Drosophila PI4KIIIalpha is required in follicle cells for oocyte polarization and Hippo signaling. *Development*, 138(9):1697–1703, May 2011. ISSN 0950-1991, 1477-9129. doi: 10.1242/dev.059279.

Y. Yang, M. Lee, and G. D. Fairn. Phospholipid subcellular localization and dynamics. *Journal of Biological Chemistry*, 293(17):6230–6240, Apr. 2018. ISSN 0021-9258, 1083-351X. doi: 10.1074/jbc.R117.000582.

S. Yoshida, M. Goebl, A. Nakano, and Y. Anraku. A Novel Gene,STT4, Encodes a Phosphatidylinositol 4-Kinase in the PKCl Protein Kinase Pathwayof Saccharomyces cerevisia.e. *Journal of Biological Chemistry*, page 7, 1994a.

S. Yoshida, Y. Ohya, A. Nakano, and Y. Anraku. Genetic interactions among

genes involved in the STT4-PKC1 pathway of Saccharomyces cerevisiae. *Molecular and General Genetics MGG*, 242(6):631–640, Mar. 1994b. ISSN 0026-8925, 1432-1874. doi: 10.1007/BF00283416.

J. P. Zewe, R. C. Wills, S. Sangappa, B. D. Goulden, and G. R. Hammond. SAC1 degrades its lipid substrate PtdIns4P in the endoplasmic reticulum to maintain a steep chemical gradient with donor membranes. *eLife*, 2018. doi: 10.7554/elife.35588.001.

L. Zhang, S. Malik, J. Pang, H. Wang, K. M. Park, D. I. Yule, B. C. Blaxall, and A. V. Smrcka. Phospholipase Cϵ Hydrolyzes Perinuclear Phosphatidylinositol 4-Phosphate to Regulate Cardiac Hypertrophy. *Cell*, 153 (1):216–227, Mar. 2013. ISSN 00928674. doi: 10.1016/j.cell.2013.02.047.

X. Zhang, P. A. Hartz, E. Philip, L. C. Racusen, and P. W. Majerus. Cell Lines from Kidney Proximal Tubules of a Patient with Lowe Syndrome Lack OCRL Inositol Polyphosphate 5-Phosphatase and Accumulate Phosphatidylinositol 4,5-Bisphosphate. *Journal of Biological Chemistry*, 273(3):1574–1582, Jan. 1998. ISSN 0021-9258, 1083-351X. doi: 10.1074/jbc.273.3.1574.

X. Zhang, W.-A. Wang, L.-X. Jiang, H.-Y. Liu, B.-Z. Zhang, N. Lim, Q.-Y. Li, and F.-D. Huang. Downregulation of RBO-PI4KIIIα Facilitates Aβ42 Secretion and Ameliorates Neural Deficits in Aβ42-Expressing Drosophila. *Journal of Neuroscience*, 37(19):4928–4941, May 2017. ISSN 0270-6474, 1529-2401. doi: 10.1523/JNEUROSCI.3567-16.2017.

J. Zou, J. Marjanovic, M. V. Kisseleva, M. Wilson, and P. W. Majerus. Type I phosphatidylinositol-4,5-bisphosphate 4-phosphatase regulates stress-induced apoptosis. *Proceedings of the National Academy of Sciences*, 104(43):16834–16839, Oct. 2007. ISSN 0027-8424, 1091-6490. doi: 10.1073/pnas.0708189104.

G. Zugmaier, R. Jäger, B. Grage, M. Gottardis, K. Havemann, and C. Knabbe. Growth-inhibitory effects of vitamin D analogues and retinoids on human pancreatic cancer cells. *British Journal of Cancer*, 73(11): 1341–1346, June 1996. ISSN 0007-0920, 1532-1827. doi: 10.1038/bjc.1996.256.

Chapter 2

Materials and Methods

2.1 Flywork

2.1.1 Fly Cultures

Flies (*Drosophila melanogaster*) were reared in media containing corn flour (80 g), D-glucose (20 g), sugar (40 g), yeast powder (15 g), agar (8 g), propionic acid (4 mL), methylparahydroxy benzoate (1 g in 5 mL ethanol) and orthophosphoric acid (0.6 mL) made up to 1 L with water. Flies were maintained at 25° C and 50% relative humidity. There was no internal illumination within the incubator and the flies were subjected to short light pulses only when the incubator door was opened.

2.1.2 Fly Stocks

The wild-type (WT) strain was Red Oregon-R. The details of fly stocks and strains used in this study have been listed in Table 2.1. The $PI4KIII\alpha^{XE45B}$ mutant and genomic rescue flies were obtained from Hugo Bellen (Baylor College of Medicine, USA). The Gal4-upstream activating sequence (UAS) binary expression system was used to drive expression of transgenic constructs. To drive expression in eyes, Rh1Gal4, 3xRh1Gal4 (a kind gift from Donald Ready, Purdue University, Indiana) and GMRGal4 (BL #1104) were used (Ellis et al., 1993).

Table 2.1 :
Table of Fly Strains

Fly Stock	Source	Full Genotype
Wild type - Red Oregon R	Padinjat Lab	+;;
Rh1Gal4	Padinjat Lab	;Rh1Gal4;;
UAS-Dicer2 - 24651	BDSC	w^{1118}; Pw[+mC]=UAS-Dcr-2.D10
3x-Rh1Gal4	Donald Ready, Purdue University	;;3xRh1Gal4;
GMRGal4 - 1104	BDSC	w[*]; Pw[+mC]=GAL4-ninaE.GMR12
CG2929 (PI4KIIα) UAS-RNAi – 110687/KK	VDRC	PKK101202VIE-260B
CG2929 (PI4KIIα) UAS-RNAi – 25459/GD	VDRC	w^{1118}; PGD9857v25459
CG2929 (PI4KIIα) UAS-RNAi – 25458/GD	VDRC	w^{1118}; PGD9857v25458/TM3
CG2929 (PI4KIIα) UAS-RNAi – 35278	BDSC	y[1] sc[*] v[1] sev[21]; Py[+t7.7] v[+t1.8]=TRiP.GL00179attP2
CG10260 (PI4KIIIα) UAS-RNAi – 105614/KK	VDRC	PKK100549VIE-260B
CG10260 (PI4KIIIα) UAS-RNAi – 15993/GD	VDRC	w^{1118}; PGD6917v15993
CG10260 (PI4KIIIα) UAS-RNAi – 35256	BDSC	y[1] sc[*] v[1] sev[21]; Py[+t7.7] v[+t1.8]=TRiP.GL00144attP2
CG10260 (PI4KIIIα) UAS-RNAi – 38242	BDSC	y[1] sc[*] v[1] sev[21]; Py[+t7.7] v[+t1.8]=TRiP.HMS01686attP40

Continued on next page

Table 2.1 – continued from previous page

CG10260 (PI4KIIIα) UAS-RNAi – 35643	BDSC	y[1] sc[*] v[1] sev[21]; Py[+t7.7] v[+t1.8]=TRiP.GLV21007attP2/ TM3, Sb[1]
CG7004 (PI4KIIIβ) UAS-RNAi - 27786/GD	VDRC	w^{1118}; PGD12100v27786
CG7004 (PI4KIIIβ) UAS-RNAi - 27785/GD	VDRC	w^{1118}; PGD12100v27785/TM3
CG7004 (PI4KIIIβ) UAS-RNAi - 110159/KK	VDRC	PKK102095VIE-260B
CG7004 (PI4KIIIβ) UAS-RNAi - 29396	BDSC	y[1] v[1]; Py[+t7.7] v[+t1.8]=TRiP.JF03329attP2
CG7004 (PI4KIIIβ) UAS-RNAi - 31187	BDSC	y[1] v[1]; Py[+t7.7] v[+t1.8]=TRiP.JF01701attP2
CG7004 (PI4KIIIβ) UAS-RNAi - 35257	BDSC	y[1] sc[*] v[1] sev[21]; Py[+t7.7] v[+t1.8]=TRiP.GL00145attP2
CG8739 (stmA) UAS-RNAi - 23618/GD	VDRC	w^{1118}; PGD14013v23618
CG8739 (stmA) UAS-RNAi - 23619/GD	VDRC	w^{1118}; PGD14013v23619
CG8739 (stmA) UAS-RNAi - 47750/GD	VDRC	w^{1118}; PGD14013v47750
CG8739 (stmA) UAS-RNAi - 47751/GD	VDRC	w^{1118}; PGD14013v47751
CG8739 (stmA) UAS-RNAi - 105391/KK	VDRC	PKK100493VIE-260B
CG8739 (stmA) UAS-RNAi - 39062	BDSC	[1] sc[*] v[1] sev[21]; Py[+t7.7] v[+t1.8]=TRiP.HMS01982attP40
CG8325 (TTC7) UAS-RNAi - 35881/GD	VDRC	w^{1118}; PGD13893v35881

Continued on next page

Table 2.1 – continued from previous page

CG8325 (TTC7) UAS-RNAi - 50604	BDSC	y[1] sc[*] v[1] sev[21]; Py[+t7.7] v[+t1.8]=TRiP.HMC02388attP2
CG8325 (TTC7) UAS-RNAi - 44482	BDSC	y[1] v[1]; Py[+t7.7] v[+t1.8]=TRiP.HMC02372attP40
CG8739 (stmA) temperature-sensitive allele - 34517	BDSC	$stmA^{1}$
CG8739 (stmA) temperature-sensitive allele - 34518	BDSC	$stmA^{2}$
CG8739 (stmA) temperature-sensitive allele - 34519	BDSC	$stmA^{18\text{-}2}$/CyO
CG3620 ($norpA^{H52}$) temperature-sensitive allele - 27334	BDSC	w[*] norpA[31]
PI4KIIIα^{XE45B}	Hugo Bellen	yw, PI4KIIIα^{XE45B}, FRT19A/ FM7c, KrGal4, UAS-GFP;;
PI4KIIIα Genomic Rescue	Hugo Bellen	yw, PI4KIIIα^{XE45B}, FRT19A;; PI4KIIIα Genomic Rescue WT VK33
GMR-hid, FRT19A; EGUF;	Hugo Bellen	PGMR-hidSS1, y1w*, PneoFRT19A, l(1)CL(1)/ FM7c, KrGal4, UAS-GFP; ey-FLP
UAS-3xFLAG::hPI4KIIIα	Padinjat Lab	w^{1118};; p[UAS-3xFLAG::hPI4KIIIα]attP2/ TM3Sb
UAS-HA::hPI4KIIIα^{KD}	Padinjat Lab	w^{1118};; p[UAS-HA::hPI4KIIIα^{KD}]attP2/TM3Sb
UAS-HA::mEfr3B	Padinjat Lab	w^{1118};; p[UAS-HA::mEfr3B]attP2/TM3Sb
UAS-hTTC7B::GFP	Padinjat Lab	w^{1118};; p[UAS-hTTC7B::GFP]attP2/TM3Sb
$rdgB^{9}$	David Hyde	$rdgB^{9}$;;
UAS-rdgB	Padinjat Lab	w^{1118}; P[w+, UAS-rdgB]/CyO

Continued on next page

Table 2.1 – continued from previous page

dPIP5K^{18}, FRT42D	Padinjat Lab	w^{1118}; P[neo+,FRT42D], P[w+,HRPC18]/CyO
BL.5251	BDSC	y[1] w[*]; Pry[+t7.2]=neoFRT42D Py[+t7.7] ry[+t7.2]=Car20y44B, Pw[+mC]=GMR-hidSS2, l(2)CL-R[1]/CyO; Pw[+m*]=GAL4-ey.HSS5, Pw[+mC]=UAS-FLP.DJD2
UAS-dPIP5K (DGRC 200386)	DGRC	y[1] w[67c23]; Pw[+mC]=GSV1GS2280 / SM1
norpA^{P24}	Padinjat Lab	norpA^{P24};;
rdgA^{3}	Roger Hardie	rdgA^{3};;
laza^{22}	Padinjat Lab	;;laza^{22A}
UAS-P4M::GFP	Padinjat Lab	w^{1118};;p[UAS-P4M::GFP]attP2/TM3Sb
trp::PLCδ PH::GFP	Padinjat Lab	w;;P[w+,trp-PH::GFP]

2.2 Molecular Biology

2.2.1 Molecular Biology

The list of constructs used are listed in Table 2.2. The human PI4KIIIα along with the FLAG epitope tag was amplified from the p3XFLAG::hPI4KIIIα-CMV10 construct, obtained from Pietro De Camilli (Yale School of Medicine, USA), and cloned using EcoRI and XhoI. The kinase-dead mutant of human PI4KIIIαwith the haemagglutinin (HA) epitope tag was amplified from the pcDNA3.1-HA::hPI4KIIIα^{KD} construct obtained from Tamas Balla (NIH, USA) and cloned using EcoRI and XhoI. The mouse Efr3B along with the HA epitope tag was amplified from the pcDNA3.0-HA::mEfr3B construct, obtained from Pietro De Camilli, and cloned using EcoRI and NotI. The human TTC7B was amplified from the iRFP::TTC7B construct, obtained from Addgene (Massachusetts, USA) (Plasmid #51615), and cloned using NotI and XhoI. The PI4P binding of SidM (P4M) domain was amplified from the GFP::P4M-SidM construct, also from Addgene (Plasmid #51469), and

Table 2.2 :
Table of Plasmid Constructs

Construct	Source Plasmid	Source Lab
pUAS-3xFLAG::hPI4KIIIα-attB	p3xFLAG::hPI4KIIIα-CMV10	Tamas Balla
pUAS-HA::hPI4KIIIα^{KD}-attB	pHA::hPI4KIIIα^{KD}	Tamas Balla
pUAS-HA::mEfr3B-attB	pcDNA3.0-HA::mEfr3B	Pietro De Camilli
pUAS-hTTC7B::GFP-attB	iRFP::TTC7B	Addgene - 51615
pUAS-GFP::P4M-attB	GFP::P4M-SidM	Addgene - 51469

cloned using NotI and XbaI. All transgenes were cloned into either pUAST-attB (Bischof et al., 2007) or pUAST-attB-GFP vectors using suitable restriction enzyme-based methods. Site-specific integration (Fly (*Drosophila*) Facility, NCBS, Bangalore) at an attP2 landing site on the third chromosome was used to generate transgenic flies (Bischof et al., 2007).

2.2.2 Western Immunoblotting

Heads from 1 day old flies were homogenized in 2X SDS-PAGE sample buffer followed by boiling at 95° C for 5 min. Samples were separated using SDS-PAGE and electroblotted onto nitrocellulose membrane [Hybond-C Extra; (GE Healthcare, Buckinghamshire, UK)] using semidry transfer assembly (BioRad, California, USA). Following blocking with 5% Blotto (sc-2325, Santa Cruz Biotechnology, Texas, USA), membranes were incubated overnight at 4° C in appropriate dilutions of primary antibodies as listed in Table 2.3 (Chakrabarti et al., 2015; Sanxaridis et al., 2007; Dasgupta et al., 2009). Protein immunoreacted with the primary antibody was visualized after incubation in 1:10000 dilution of appropriate secondary antibody coupled to horseradish peroxidase (Jackson ImmunoResearch Laboratories, Pennsylvania, USA) for 2 hours at room temperature. Blots were developed with ECL (GE Healthcare) and imaged using a LAS 4000 instrument (GE

Table 2.3 :
Table of Antibodies

Antibody	**Dilution**	**Identifier and Source**
α-tubulin	1:4000	E7 (DSHB, Iowa, USA)
α-Gq_{α}	1:1000	Padinjat Lab
α-TRP	1:5000	Padinjat Lab
α-Rh1	1:250	4C5 (DSHB, Iowa, USA)
α-INAD	1:1000	Susan Tsunoda
α-NORPA	1:1000	Jayaraj Acharya
Mouse α-GFP	1:2000	sc-9996 (Santa Cruz Biotechnology, Texas, USA)
Mouse α-HA	1:1000	2367S (CST, Massachusetts, USA)
Mouse α-FLAG	1:1000	F1804 (Sigma-Aldrich, Missouri, USA)

Healthcare).

2.2.3 RNA Extraction and Q-PCR Analysis

RNA was extracted from *Drosophila* retinae using TRIzol reagent (15596018, Life Technologies, California, USA). To obtain retinae, flies were flash frozen in liquid nitrogen for one minute, following which they were transferred to glass vials containing acetone and stored for 2 days at -80^{o} C. This was done to ensure optimal levels of desiccation of the retinae. Purified RNA was treated with amplification grade DNase I (18068015, Thermo Fisher Scientific, California, USA). cDNA conversion was done using SuperScript II RNase H– Reverse Transcriptase (18064014, Thermo Fisher Scientific) and random hexamers (N8080127, Thermo Fisher Scientific). Quantitative Polymerase Chain Reaction (Q-PCR) was performed using Power SybrGreen PCR mastermix (4367659, Applied Biosystems, Warrington, UK) in an Applied Biosystem 7500 Fast Real Time PCR instrument. Primers were designed at the exon-exon junctions following the parameters recommended for

Table 2.4 :
Table of Primers

Gene	Primer
RP49 Forward	CGGATCGATATGCTAAGCTGT
RP49 Reverse	GCGCTTGTTCGATCCGTA
CG10260 (PI4KIIIα) Forward	GAGGAACAGATCACGGAATGGCG
CG10260 (PI4KIIIα) Reverse	CCTCCTCATCAATGATCTCCGCG
CG2929 (PI4KIIα) Forward	TATGCACGGAGTTGTGACCCCC
CG2929 (PI4KIIα) Reverse	ACTTGTGGCTGCTCCACCCG
CG7004 (PI4KIIIβ) Forward	TTCGGGTGAGATGGATGCGG
CG7004 (PI4KIIIβ) Reverse	GTCCAATTCGGTGGAAGCGG
CG8739 (stmA) Forward	GTGGAAATGTCCTGCAACGA
CG8739 (stmA) Reverse	GTGGGGGAAGGAAATGGC
CG8325 (TTC7) Forward	GGAGACGGTAAAGCAAGGTCTG
CG8325 (TTC7) Reverse	CGTTCCCATCAAACTGCACA
Gq_{α} Forward	GAGAATCGAATGGAGGAATC
Gq_{α} Reverse	GCTGAGGACCATCGTATTC

Q-PCR. Transcript levels of the ribosomal protein 49 (RP49) were used for normalization across samples. Three separate samples were collected from each genotype, and duplicate measures of each sample were conducted to ensure the consistency of the data. The primers used are given in Table 2.4.

2.3 Electroretinography

Flies were cold anesthetized on ice and immobilized at the end of a disposable pipette tip using a drop of colorless nail varnish. Recordings were done using glass microelectrodes of resistance 1-10 MΩ (R0786, Harvard Apparatus, Massachusetts, USA) and filled with 0.8% w/v NaCl solution. Voltage changes were recorded between the surface of the eye and an electrode placed

on the thorax. One day old flies, both male and female, were used for recording. Following fixing and positioning, flies were dark adapted for 5 minutes. The electroretinogram (ERG) was recorded with 2 s flashes of green light (568nm; 33.16µW/cm^2}) stimulus, with 10 stimuli (flashes) per recording and 15 seconds of recovery time between two flashes of light}. Stimulating light was delivered from an LED light source to within 5 mm of the fly's eye through a fibre optic guide. Calibrated neutral density filters were used to vary the intensity of the light source, providing a spectrum of five light intensities, each one log order brighter than the previous one. Voltage changes were amplified using a DAM50 amplifier (SYS-DAM50, WPI, Florida, USA) and recorded using pCLAMP 10.7. Analysis of traces was performed using Clampfit 10.7 (Molecular Devices, California, USA).

For the temperature-dependent ERGs, a custom temperature controller was made by the in-house NCBS electronics workshop. The fly was immobilized, ventral side down, on paraffin wax, leaving the head free. The tip of a fine soldering iron was inserted into the wax just under the fly and used to maintain the fly at the required temperature (verified using a infrared thermometer). Once the set temperature was achieved, ERGs were recorded as described above. A known temperature-sensitive mutant fly was used ($norpA^{H52}$) to characterize the system (Wilson and Ostroy, 1987). As previously reported, this fly did not show an ERG response when the temperature was raised to 33° C but had a normal ERG response at 25° C, indicating that the temperature controller was working as expected.

2.4 Deep Pseudopupil Analysis

To monitor PI(4,5)P_2 at the rhabdomere membrane in live flies, transgenic flies expressing PH-PLCδ::GFP [PI(4,5)P_2 biosensor] (Chakrabarti et al., 2015) were anaesthetised and immobilized at the end of a pipette tip using a drop of colorless nail varnish and fixed in the light path of an Olympus IX71 microscope. The fluorescent Deep Pseudopupil (DPP) (a virtual image that sums rhabdomere fluorescence from ~20– 40 adjacent ommatidia) was focused and imaged using a 10X objective. After dark adaptation for 6 min, images were taken by exciting green fluorescent protein (GFP) using a 90 ms flash of blue light and collecting emitted fluorescence. Similarly, flies expressing P4M::GFP (PI4P biosensor) (Hammond et al., 2014) were subjected to the same protocol in order to monitor PI4P levels. The DPP intensity was measured using ImageJ from NIH (Bethesda, Maryland, USA). The area of the pseudopupil was measured and the mean intensity values per

unit area were calculated. Values are presented as mean ± s.e.m.

In order to perform the kinetic assay, the flies were immobilised as above and, following the first flash of blue light after 6 min of dark adaptation, a flash of blue light was administered every 30 seconds. Between every flash of blue light, the fly was exposed to red light to facilitate maximal conversion of metarhodopsin to rhodopsin. The schematic of the light administration protocol is outlined in **Fig.3.24A**.

2.5 Liquid Chromatography - Mass Spectrometry

2.5.1 Phosphoinositide measurement

Lipid Extraction:

Drosophila retinae were dissected under red light or white light (as indicated by dark/light treatment) and stored in 1X Phosphate Buffered Saline (PBS) on dry ice until ready for extraction. The retinae were homogenized in 950 µL phosphoinositide elution buffer (PEB), at which point the internal standards were added (mixture containing 50 ng PI/25 ng PI4P/50 ng PIP_2/0.2 ng PE per sample). Phase separation was achieved by adding 250 µL each of chloroform and 2.4M HCl, followed by centrifugation at 1000 g for 5 minutes (4° C). The organic phase was extracted and washed with 900 µL lower phase wash solution (LPWS) and centrifuged at 1000 g for 5 mins (4° C). Lipids from the remaining aqueous phase were extracted by phase separation once again. The organic phases were collected and dried in a vacuum centrifuge.

The dried lipid extracts were derivatized using 2M Trimethylsilyl (TMS)-diazomethane. 50 µL TMS-diazomethane (362832, Sigma Aldrich) was added to each tube and vortexed gently for 10 minutes. The reaction was neutralized using 10 µL glacial acetic acid.

Extraction Solvents:

- Phosphoinositide Elution Buffer (PEB) - 250 mL Chloroform: 500 mL Methanol : 200 mL 2.4M Hydrochloric acid
- Lower Phase Wash Solution (LPWS) - 235 mL Methanol : 245 mL 1M Hydrochloric acid : 15 mL Chloroform

Internal standards (IS):

- Phosphatidylethanolamine (PE) - 17:0/14:1 – Avanti (LM-110 (Alabama, USA)
- Phosphatidylinositol (PI) - 17:0/14:1 – Avanti (LM-1504)
- Phosphatidylinositol 4-phosphate (PI4P) - 17:0/20:4 – Avanti (LM-1901)
- d5 - Phosphatidylinositol 3,5 - bisphosphate [PI(3,5)P_2] – 16:0/16:0 – Avanti (850172)

Standard Curve Analysis:

Serial dilutions of three synthetic standards - PI (17:0/14:1), PI4P (17:0/20:4) and d5-PI(3,5)P_2 (16:0/16:0) - were prepared in 100% methanol. The dilutions contained 50 ng, 25 ng, 12.5 ng, 6.25 ng and 3.125 ng of the respective standards. These dilutions were subjected to the extraction and derivatisation protocol described above. The extracted standards were quantified using the LC-MS method described below.

Liquid Chromatography-Mass Spectrometry Analysis:

The experiment was performed on an ABSciex 6500 Q-Trap machine connected to a Waters Acquity LC system. A 45% to 100% acetonitrile in water (with 0.1% formic acid) gradient over 20 min was used for separation on an 1 mm x 100 mm Ultra Performance Liquid Chromatography (UPLC) C4 1.7µM from Acquity.

- Solvent A: Water + 0.1% Formic Acid
- Solvent B: Acetonitrile

MRMs:

- Polarity: Positive
- Ion Source: Turbo Spray IonDrive
- Resolution Q1: Unit
- Resolution Q3: Unit

Table 2.5 :
LC Gradient - Phosphoinositides

Time (min)	Flow Rate	% A	% B	Curve
0	0.1	55	45	-
5	0.1	55	45	6
10	0.1	0	100	6
15	0.1	0	100	6
16	0.1	55	45	6
20	0.1	55	45	-

Q-Trap 6500 Parameters (Set 1) :

- Curtain Gas: 40
- Ion Spray Voltage: 4000
- Temperature: 400
- GS1: 15
- GS2: 15
- Declustering Potential: 65
- Entrance Potential: 11.4
- Collision Gas Pressure: -2
- Collision Energy: 30
- Collision Exit Potential: 12

Q-Trap 6500 Parameters (Set 2) :

- Curtain Gas: 35
- Ion Spray Voltage: 5100
- Temperature: 300
- GS1: 15

Table 2.6 :
MRMs - Phosphoinositides

Q1 Mass (Da)	Q3 Mass (Da)	Dwell Time (ms)	Species
938.5	556.4	60	IS-PI4P (17:0/20:4)
957.5	575.5	60	PIP-34:2
955.5	573.5	60	PIP-34:3
985.6	603.6	60	PIP-36:2
983.6	601.6	60	PIP-36:3
981.5	599.5	60	PIP-36:4
1046.5	556.4	60	IS-d5-PI(3,5)P_2 (16:0/16:0)
1065.5	575.5	60	PIP_2-34:2
1063.5	573.5	60	PIP_2-34:3
1093.6	603.6	60	PIP_2-36:2
1091.6	601.6	60	PIP_2-36:3
1089.6	599.6	60	PIP_2-36:4
690.5	535.5	60	IS-PE (17:0/14:1)
730.5	575.5	20	PE-34:2
728.5	573.5	20	PE-34:3
758.5	603.5	20	PE-36:2
756.5	601.5	20	PE-36:3
754.5	599.5	20	PE-36:4

- GS2: 5
- Declustering Potential: 140
- Entrance Potential: 12
- Collision Gas Pressure: -2
- Collision Energy: 29
- Collision Exit Potential: 12

2.5.2 DAG Measurement

Lipid Extraction:

Adult flies were collected by carbon dioxide (CO_2) anaesthesia and flash frozen using liquid nitrogen. They were transferred to glass vials containing acetone and stored at -80° C for 24 hours. They were then dried at room temperature for a further 24 hours. Depending on whether they required light treatment or not, they were either exposed to light before flash freezing or were directly frozen after collection. After drying, the retinae were collected using a sharp blade and transferred to homogenization tubes. They were stored at room temperature for no more than 48 hours.

The retinae were homogenised in 300 µL of methanol, after which the internal standards were added (50 ng DAG/50 ng PA/0.2 ng PE per sample). Phase separation was achieved by adding 800 µL of chloroform and 400 µL of 0.88% KCl, followed by centrifugation at 1000 g for 5 minutes (4° C). The organic phase was collected and dried in a vacuum centrifuge.

The dried lipid extracts were derivatized using 2M TMS-diazomethane. 50 µL TMS-diazomethane (362832, Sigma Aldrich) was added to each tube and vortexed gently for 10 minutes. The reaction was neutralized using 10 µL glacial acetic acid. The mixture was dried in a vacuum centrifuge and the dried lipids were reconstituted with 150 µL methanol.

Internal standards (IS):

- Phosphatidylethanolamine (PE) - 17:0/14:1 – Avanti (LM-1104) (Alabama, USA)
- Phosphatidic acid (PA) - 17:0/14:1 – Avanti (LM-1404)
- Diacylglycerol (DAG) – 10:0/10:0 – Avanti (800810)

Standard Curve Analysis:

Serial dilutions of three synthetic standards - DAG (10:0/10:0), PA (17:0/14:1) and PE (17:0/14:1) - were prepared in 100% methanol. The dilutions contained 50 ng, 25 ng, 12.5 ng, 6.25 ng and 3.125 ng of the respective standards. These dilutions were subjected to the extraction and derivatisation protocol described above. The extracted standards were quantified using the LC-MS method described below.

Liquid Chromatography-Mass Spectrometry Analysis:

The experiment was performed on an ABSciex 6500 Q-Trap machine connected to a Waters Acquity LC system. A 40% to 100% acetonitrile and isopropanol (with 0.1% formic acid) gradient over 10 min was used for separation on a 2.1 mm x 50 mm UPLC C18 1µM from Acquity, maintained at 40° C.

- Solvent A: 60% acetonitrile, 40% water, 10 mM ammonium formate, 0.1% formic acid
- Solvent B: 10% acetonitrile, 90% isopropanol, 10 mM ammonium formate, 0.1% formic acid

Table 2.7 :
LC Gradient - DAG and PA

Time (min)	Flow Rate	% A	% B	Curve
0	0.2	60	40	-
0.5	0.2	60	40	6
5	0.2	0	100	6
7.5	0.2	0	100	6
7.6	0.2	60	40	6
10	0.2	60	40	-

MRMs:

- Polarity: Positive
- Ion Source: Turbo Spray IonDrive

- Resolution Q1: Unit
- Resolution Q3: Unit

Q-Trap 6500 Parameters:

- Curtain Gas: 45
- Ion Spray Voltage: 5500
- Temperature: 400
- GS1: 20
- GS2: 20
- Declustering Potential: 65
- Entrance Potential: 12
- Collision Gas Pressure: -2
- Collision Energy: 18
- Collision Exit Potential: 13.2

2.6 Immunohistochemistry

2.6.1 Immunohistochemistry

For immunofluorescence studies retinae from flies were dissected under low red light in phosphate buffer saline (PBS). Retinae were fixed in 4% paraformaldehyde in PBS with 1 mg/ml saponin at room temperature for 30 min. Fixed eyes were washed three times in PBST (1X PBS + 0.3% TritonX- 100) for 10 min each. The sample was then blocked in a blocking solution (5% Fetal Bovine Serum in PBST) for 2 hours at room temperature, after which the sample was incubated with primary antibody in blocking solution overnight at 4°C on a shaker. The following antibodies were used: mouse anti-HA (1:50; 2367S, CST), mouse anti-FLAG (1:100; F1804, Sigma) and chicken anti-GFP [1:5000; ab13970, Abcam (Cambridge, UK)]. Appropriate secondary antibodies conjugated with a fluorophore were used at 1:300 dilutions [Alexa Fluor 488/568/633 IgG, Molecular Probes (Oregon, USA)] and incubated for 4 hours at room temperature. Wherever required, during the incubation with secondary antibody, Alexa Fluor 568-phalloidin [1:200; A12380 (Thermo Fisher Scientific)] was also added to the tissues to stain the F-actin. After three washes in PBST, sample was mounted in 70% glycerol in

Table 2.8 :
MRMs - DAG and PA

Q1 Mass (Da)	Q3 Mass (Da)	Dwell Time (ms)	Species
633.5	534.4	20	IS-PA (17:0/14:1)
701.5	575.5	20	PA-34:2
699.5	573.5	20	PA-34:3
729.5	603.5	20	PA-36:2
727.5	601.5	20	PA-36:3
727.6	599.6	20	PA-36:4
418.3	383.3	20	IS-DAG (10:0/10:0)
610.5	575.5	20	DAG-34:2
608.5	573.5	20	DAG-34:3
638.5	603.5	20	DAG-36:2
636.5	601.5	20	DAG-36:3
634.6	599.6	20	DAG-36:4
690.5	535.5	20	IS-PE (17:0/14:1)
730.5	575.5	20	PE-34:2
728.5	573.5	20	PE-34:3
758.5	603.5	20	PE-36:2
756.5	601.5	20	PE-36:3
754.5	599.5	20	PE-36:4

1X PBS. Whole mounted preps were imaged on Olympus FV1000 confocal microscope using Plan-Apochromat 60x, NA 1.4 objective (Olympus, Tokyo, Japan).

2.6.2 Cell Culture

S2R+ cells stably expressing Actin-Gal4 (obtained from Satyajit Mayor's lab, NCBS, Bangalore) were split every 4–5 days and grown at 25° C. They were maintained in Schneider's *Drosophila* Insect Medium (SDM; 21720024, Gibco, Thermo Fisher Scientific) supplemented with 10% fetal bovine serum (FBS; 1600044, Gibco, Thermo Fisher Scientific) and penicillin - streptomycin - glutamine solution (10ml/L; G1146, Sigma-Aldrich). They were transfected using Effectene as a transfection agent [301425, Qiagen (Hilden, Germany)]. The cells were plated in 12 well plates and 0.5g of desired DNA construct was used for transfections. 48 hours post transfection, cells were allowed to adhere on glass cover slip dishes for 1 hour and fixed with 2.5% PFA in 1X M1 buffer (10X M1 buffer; 8.76 g sodium chloride, 0.373 g potassium chloride, 0.147 g calcium chloride, 0.203 g magnesium chloride, 4.76 g HEPES, 100 ml MilliQ water, pH 6.8–7) for 20 mins. They were washed and permeabilized with 0.37% Igepal (I3021, Sigma) in 1X M1 buffer for 13 mins. Blocking was performed in 1X M1 buffer containing 5% FBS and 1 mg/ml BSA for 1 hour at RT. The cells were then incubated with primary antibodies diluted in block solution for 2 hours at RT, washed with 1X M1 several times, and incubated with appropriate secondary antibodies for 1-2 hours at RT. Following this, they were stained with 4', 6 - diamidino - 2 - phenylindole (DAPI) (1:3000; D1306, Thermo Fisher Scientific) and washed with 1X M1 buffer. The following primary antibodies were used: mouse anti-HA (1:200: 2367S, CST) and mouse anti-FLAG (1:400; F1804, Sigma). Appropriate secondary antibodies conjugated with a fluorophore were used at 1:300 dilutions (A11001, Alexa Fluor 488 IgG, Molecular Probes). The cells imaged on Olympus FV1000 confocal microscope using Plan-Apochromat 60x, NA 1.4 objective (Olympus).

2.7 Bioinformatic analysis

The protein sequences for STMA, EFR3 and the DAG lipases were obtained from the NCBI protein database (species, protein and accession ID of the sequences used are listed below). For multiple sequence alignments (MSA), CLUSTALW was used. The lipase 3 region and active site of DAG lipase was assigned as outlined in the NCBI Conserved Domain Database (CDD). In

order to build the position-specific scoring matrix for the DAG lipase active site, we first ran the MSA through Consurf, which assigns conservation scores to each amino acid. We used those scores to guide the construction of a Position Specific Scoring Matrix (PSSM), for which we used the formula of

Score (position, amino acid) = (q + p)/ (N + B) , where

- q = observed counts for the amino acid
- p = pseudocounts = B*(overall frequency of an amino acid)
- N = total number of sequences
- B = total number of allocated pseudocounts = square root of N

We also cross-checked the consensus sequence derived from the PSSM with the NCBI PSSM viewer, which gave a consensus sequence for the human DAG lipase active site. The sequences differed only by four amino acids. We used ScanProsite to check for occurrence of the consensus sequence in the *Drosophila* proteome and in UniProt database. The maximum-likelihood phylogenetic tree was built using the Mega7 software, using the WAG+G model run for 1000 bootstraps.

List of proteins used to build MSA:

- *Anthurium amnicola*, DAGLA - A0A1D1YY70
- *Anthurium amnicola*, DAGLB - A0A1D1Y419
- *Anthurium amnicola*, EFR3A - A0A1D1ZJR9
- *Anthurium amnicola*, EFR3B - A0A1D1ZEH0
- *Apis mellifera*, DAGLA - XP_003250951.2
- *Apis mellifera*, DAGLB - XP_001122519.2
- *Apis mellifera*, EFR3 - XP_006571817.1
- *Aspergillus udagawae*, DAGLA - GAO84222.1
- *Aspergillus udagawae*, EFR3 - GAO84941.1
- *Atta colombica* , DAGLA - KYM75470.1
- *Atta colombica*, DAGLB - KYM81960.1
- *Atta colombica*, EFR3 - KYM87784.1
- *Bos taurus*, DAGLA - NP_001179512.1

- *Bos taurus*, DAGLB - NP_001076956.1
- *Bos taurus*, EFR3A - NP_001069515.1
- *Bos taurus*, EFR3B - NP_001069515.1
- *Caenorhabditis elegans*, DAGLA - NP_741085.1
- *Caenorhabditis elegans*, EFR3 - CCD66029.1
- *Ciona intestinalis*, DAGLA - XP_026696611.1
- *Ciona intestinalis*, EFR3B-like - XP_002129458.1
- *Cricetulus griseus*, DAGLA - ERE79003.1
- *Cricetulus griseus*, EFR3A - RLQ80005.1
- *Cricetulus griseus*, EFR3B - XP_016819663.2
- *Drosophila melanogaster*, INAE (E) - ACL82927.1
- *Drosophila melanogaster*, INAE (F) - ACL82928.1
- *Drosophila melanogaster*, STMA (A) - AAF59046.2
- *Drosophila melanogaster*, STMA (C) -AAX52723.1
- *Homo sapiens*, ANG2 - CAA77513.1
- *Homo sapiens*, DAGLA (X1) - XP_016873727.1
- *Homo sapiens*, DAGLA (X2) -XP_016873729.1
- *Homo sapiens*, DAGLB (1) - NP_631918.3
- *Homo sapiens*, DAGLB (2) - NP_001136408.1
- *Homo sapiens*, EFR3A - NP_001310482.1
- *Homo sapiens*, EFR3B - XP_011531003.1
- *Malassezia globosa*, LIP1 - EDP44990.1
- *Mus musculus*, DAGLA - NP_932782.2
- *Mus musculus*, DAGLB - NP_659164.2
- *Mus musculus*, EFR3A - NP_598527.2
- *Mus musculus*, EFR3B - NP_001075952.1
- *Pan paniscus*, DAGLA - XP_003828506.1

- *Pan paniscus*, DAGLB - XP_008956646.1
- *Pan paniscus*, EFR3A - XP_008953716.1
- *Pan paniscus*, EFR3B - XP_008950654.1
- *Pan troglodytes*, DAGLA - XP_016776509.1
- *Pan troglodytes*, DAGLB - XP_024213481.1
- *Pan troglodytes*, EFR3A - XP_003311971.1
- *Pan troglodytes*, EFR3B - XP_016803647.1
- *Penicillium brasilianum*, EFR3 - OOQ86473.1
- *Penicillium camembertii*, Lipase - AAB26004.1
- *Pongo abelii*, DAGLA - XP_002821724.1
- *Pongo abelii*, DAGLB - XP_024105788.1
- *Pongo abelii*, EFR3A - XP_002819481.2
- *Pongo abelii*, EFR3B - XP_024098572.1
- *Rattus norvegicus*, DAGLA - NP_001005886.1
- *Rattus norvegicus*, DAGLB - NP_001100590.1
- *Rattus norvegicus*, EFR3A - NP_001124036.1
- *Saccharomyces cerevisiae*, EFR3 - KZV09065.1
- *Zeugodacus cucurbitae*, DAGLA - A0A0A1XFQ0
- *Zeugodacus cucurbitae*, EFR3 - JAD08203.1

2.8 Statistics

Unpaired two-tailed t-test or Analysis of Variance (ANOVA), followed by Tukey's multiple comparison test, were carried out where applicable. Effect size was calculated using standard statistical methods. Sample size was calculated using G*Power 3.1 (available at http://www.gpower.hhu.de/en.html).

Bibliography

J. Bischof, R. K. Maeda, M. Hediger, F. Karch, and K. Basler. An optimized transgenesis system for Drosophila using germ-line-specific C31 integrases. *Proceedings of the National Academy of Sciences*, 104(9):3312–3317, Feb. 2007. ISSN 0027-8424, 1091-6490. doi: 10.1073/pnas.0611511104.

P. Chakrabarti, S. Kolay, S. Yadav, K. Kumari, A. Nair, D. Trivedi, and P. Raghu. A dPIP5K Dependent Pool of Phosphatidylinositol 4,5 Bisphosphate (PIP2) Is Required for G-Protein Coupled Signal Transduction in Drosophila Photoreceptors. *PLOS Genetics*, 11(1):e1004948, Jan. 2015. ISSN 1553-7404. doi: 10.1371/journal.pgen.1004948.

U. Dasgupta, T. Bamba, S. Chiantia, P. Karim, A. N. A. Tayoun, I. Yonamine, S. S. Rawat, R. P. Rao, K. Nagashima, E. Fukusaki, V. Puri, P. J. Dolph, P. Schwille, J. K. Acharya, and U. Acharya. Ceramide kinase regulates phospholipase C and phosphatidylinositol 4, 5, bisphosphate in phototransduction. *Proceedings of the National Academy of Sciences*, 106(47):20063–20068, Nov. 2009. ISSN 0027-8424, 1091-6490. doi: 10.1073/pnas.0911028106.

M. C. Ellis, E. M. O'Neill, and G. M. Rubin. Expression of Drosophila glass protein and evidence for negative regulation of its activity in non-neuronal cells by another DNA-binding protein. *Development*, 119(3):855–865, Nov. 1993. ISSN 0950-1991, 1477-9129.

G. R. V. Hammond, M. P. Machner, and T. Balla. A novel probe for phosphatidylinositol 4-phosphate reveals multiple pools beyond the Golgi. *J Cell Biol*, 205(1):113–126, Apr. 2014. ISSN 0021-9525, 1540-8140. doi: 10.1083/jcb.201312072.

P. D. Sanxaridis, M. A. Cronin, S. S. Rawat, G. Waro, U. Acharya, and S. Tsunoda. Light-induced recruitment of INAD-signaling complexes to detergent-resistant lipid rafts in Drosophila photoreceptors. *Molecular and Cellular Neuroscience*, 36(1):36–46, Sept. 2007. ISSN 1044-7431. doi: 10.1016/j.mcn.2007.05.006.

M. J. Wilson and S. E. Ostroy. Studies of the Drosophila norpA phototransduction mutant. *Journal of Comparative Physiology A*, 161(6):785–791, Nov. 1987. ISSN 0340-7594, 1432-1351. doi: 10.1007/BF00610220.

Chapter 3

PI4KIIIα is Required to Support *Drosophila* Phototransduction

3.1 Identification of a PI4K involved in phototransduction

The *Drosophila* genome encodes three isoforms of PI4K - *PI4KIIα* (CG2929), *PI4KIIIα* (CG10260) and *PI4KIIIβ* (CG7004). In order to determine which of the three kinases is involved in phototransduction, one would have to remove each kinase individually and analyse its effect on the same. Instead of generating loss-of-function mutants for each gene, a simpler alternative was to use RNA interference (RNAi) to knock down each gene and measure the signalling readout. When exposed to light, *Drosophila* photoreceptors undergo a large depolarisation which manifests as a measurable change in potential difference, which can be used a readout of signalling. A recording of this phenomenon is known as an electroretinogram (ERG; explained in detail in Methods - Section 2.3). One can infer the effect of genetic perturbations on the light response by quantifying the extent of the change in potential difference, which is referred to as the response amplitude. For the initial experiments to identify the PI4K isoform involved in phototransduction, we looked for significant differences between the response amplitudes of control flies and flies in which the PI4Ks were knocked down.

3.1.1 Knockdown using Rh1Gal4

We tested multiple UAS-RNAi constructs against all three PI4K genes and expressed them in the fly using eye-specific drivers. The list of RNAi lines that were tested are given in Table 2. To begin with, Rh1Gal4 (Rhodopsin-1) was used to drive expression exclusively in late pupal/adult photoreceptor cells. We combined Rh1Gal4 with UAS-Dicer2 to improve the efficiency of knockdown. With this combination, only RNAi against the *PI4KIIIα* gene resulted in a mild reduction of the ERG response amplitude. Knocking down the other two PI4Ks (*PI4KIIα* and *PI4KIIIβ*) had no impact on the response **(Fig.3.1)**. While this indicated that *PI4KIIIα* might have a role in phototransduction, the observation required validation by other means.

To check whether the reduction in ERG response could be exacerbated using a stronger driver, we used a 3xRh1Gal4 containing 3 copies of the Rh1 promoter (a kind gift from Donald Ready, Purdue University, Indiana). It was tested both with and without UAS-Dicer2. In both cases, RNAi against *PI4KIIIα* gave lower ERG responses than controls, but this was not consistent between individual flies. There was also a high day-to-day variation among the control genotypes in terms of the response amplitude **(Fig.3.2)**. This was possibly due to the strength of the promoter, which by itself caused a slight degeneration of the photoreceptors. Given the inconsistency of the ERG response using 3xRh1Gal4, we did not use it further.

3.1.2 Knockdown using GMRGal4

The second strong driver we tested was GMRGal4 [Glass Multimer Reporter (GMR)]. This drives expression in all eye cells, starting from late third larval instar, and lasts throughout eye development (Ellis et al., 1993). In contrast to Rh1Gal4, here the UAS-RNAi would be expressed much earlier on and for a longer time period. When RNAi against *PI4KIIIα* was driven using GMR-Gal4, the ERG amplitude of these flies was heavily reduced when compared to controls **(Fig.3.3A)**. There was no effect seen upon knocking down the other two PI4Ks using the same promoter **(Fig.3.3B and C)**. This clearly pointed to the involvement of PI4KIIIα, and not the other two PI4Ks, in phototransduction.

As *PI4KIIIα* emerged as the kinase most likely involved in phototransduction, it is important to note that complete deletion of the gene is cell lethal (Yan et al., 2011b). Therefore, in lieu of a null allele, we used the Gal4/UAS-RNAi combination that gave the maximum knockdown, as quantified using qPCR, and the strongest ERG phenotype. For *PI4KIIIα*, we chose a Bloom-

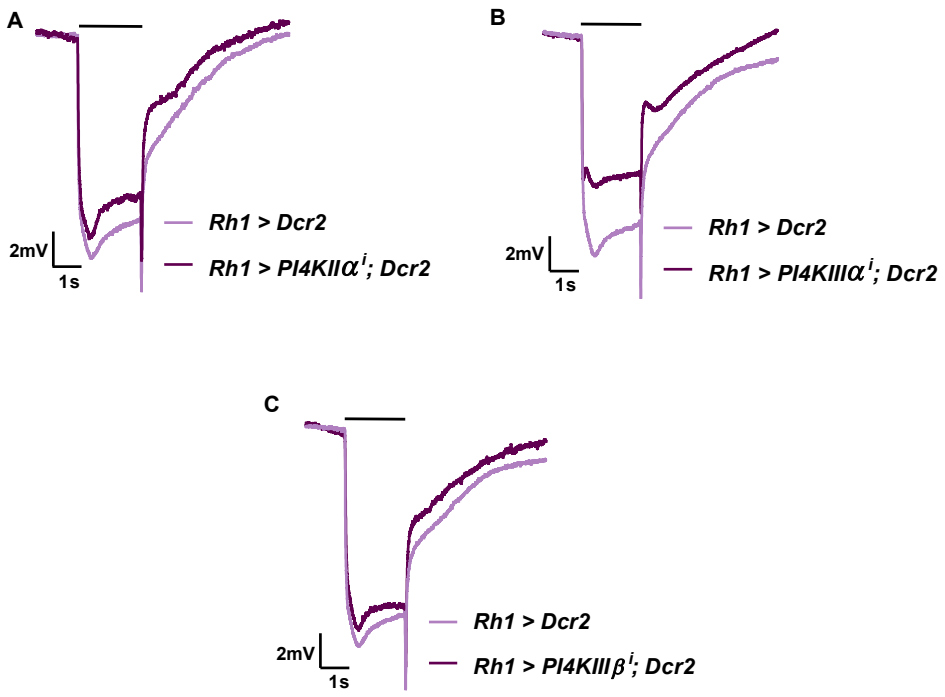

Figure 3.1 : Effect of knocking down PI4K in photoreceptors using Rh1Gal4

Representative ERG trace of the control genotype (Rh1 > Dcr2), shown in light purple, and the test genotype, shown in dark purple. The black bar on top indicates the duration of the light stimulus. The scale bar is shown in the bottom left corner. **(A) CG2929 (PI4KIIα)** Knocking down PI4KIIα using Rh1; UAS-Dcr2 did not affect the ERG response in any manner. **(B) CG10260 (PI4KIIIα)** Knocking down PI4KIIIα using Rh1; UAS-Dcr2 reduced the amplitude of the ERG response when compared to control flies. **(C) CG7004 (PI4KIIβ)** Knocking down PI4KIIβ using Rh1; UAS-Dcr2 did not affect the ERG response in any manner.

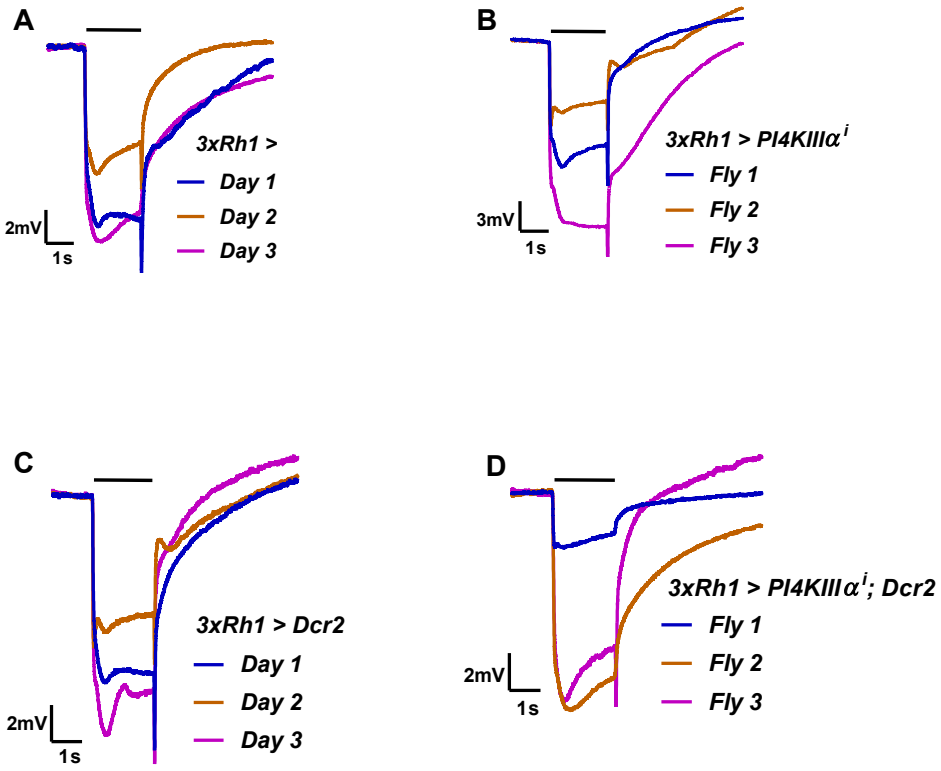

Figure 3.2 : Effect of knocking down PI4K in photoreceptors using 3x-Rh1Gal4
Representative ERG trace of flies expressing RNAi against PI4KIIIα driven by 3xRh1Gal4 either with or without UAS-Dicer2. The black bar on top indicates the duration of the light stimulus. The scale bar is in the bottom left corner. **(A)** The control genotype of 3xRh1 > displayed high day-to-day variation in ERG response amplitude. Each colour represents a recording from a different day. **(B)** Flies expressing RNAi against PI4KIIIα driven by 3xRh1Gal4 displayed high variation in the ERG response amplitude. Each colour represents a recording from a different fly, all < 24 h old and all recorded from on the same day. **(C)** The control genotype of 3xRh1 > Dcr2 displayed high day-to-day variation in ERG response amplitude. Each colour represents a recording from a different day. **(D)** Flies expressing RNAi against PI4KIIIα driven by 3xRh1Gal4 along with UAS-Dcr2 displayed high variation in the ERG response amplitude. Each colour represents a recording from a different fly, all < 24 h old and all recorded from on the same day.

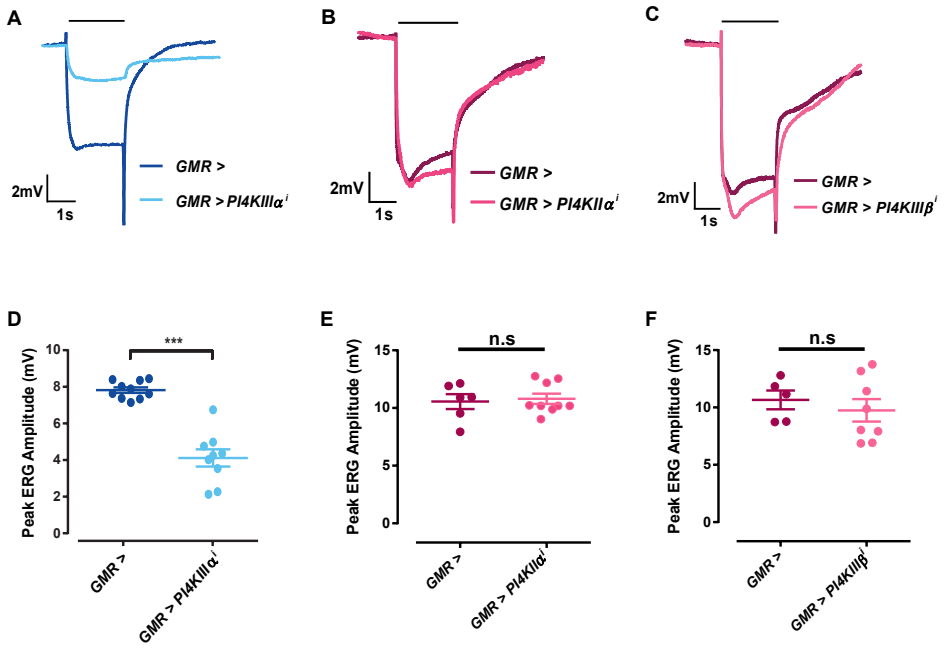

Figure 3.3 : Effect of knocking down PI4K in eyes using GMRGal4 Representative ERG trace of the control genotype (GMR >), shown in dark colours, and the test genotype, shown in light colours. The black bar on top indicates the duration of the light stimulus. The scale bar is in the bottom left corner. **(A) PI4KIIIα** Knocking down PI4KIIIα using GMRGal4 reduced the amplitude of the ERG response when compared to control flies. **(B) PI4KIIα** Knocking down PI4KIIα using GMRGal4 did not affect the ERG response in any manner. **(C) PI4KIIIβ** Knocking down PI4KIIIβ using GMRGal4 did not affect the ERG response in any manner. **(D-F)** Quantification of the peak ERG amplitude of control and the three PI4K isoform knockdown flies. x-axis represents genotype; y-axis represents response amplitude in mV. *** - $p < 0.001$, n.s = not significant as per two-tailed t-test, values are mean ± s.e.m., n = 7 minimum. Figure adapted from Balakrishnan *et al.*, 2018

ington TRiP line (#38242) that gave a knockdown of 60% **(Fig.3.4A)** in retinae when expressed using GMRGal4.

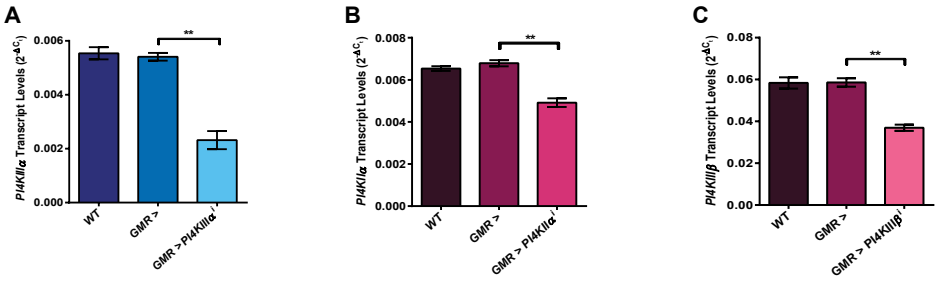

Figure 3.4 : Q-PCR estimation of transcript knockdown
The level of transcript knockdown in retinae as estimated using Q-PCR. x-axis represents genotype of the source tissue; y-axis represents $2^{-\Delta C_t}$ values for the described gene. **(A) PI4KIIIα** Knocking down PI4KIIIα using GMRGal4 reduced the transcript of the gene by 60% when compared to control flies. **(B) PI4KIIα** Knocking down PI4KIIα using GMRGal4 reduced the transcript of the gene by 30% when compared to control flies. **(C) PI4KIIIβ** Knocking down PI4KIIIβ using GMRGal4 reduced the transcript of the gene by 35% when compared to control flies. ** - $p < 0.01$ as per two-tailed t-test, values are mean ± s.e.m., n = 75 retinae per sample. Figure adapted from Balakrishnan *et al.*, 2018

The best RNAi lines for the other two PI4Ks were similarly validated, giving 30% and 35% knockdown for *PI4KIIα* and *PI4KIIIβ*, respectively **(Fig.3.4B and C)** . We also saw that knocking down *PI4KIIIα* (using BL #38242) did not affect the transcript levels of the other two PI4Ks in the eye **(Fig.3.5)**.

3.2 *PI4KIIIα* downregulation has characteristic ERG phenotypes

Historically, the electrical response to light in *Drosophila* photoreceptors has been used to identify molecular components involved in phototransduction, ranging from PLC (*norpA*) to RDGB (*rdgB*) (Hotta and Benzer, 1969; Stark et al., 1976; Yoon et al., 2004). Apart from using it to screen for genes affecting the photoresponse, one can take a closer look at the electroretinogram (ERG) waveform itself and make some mechanistic inferences.

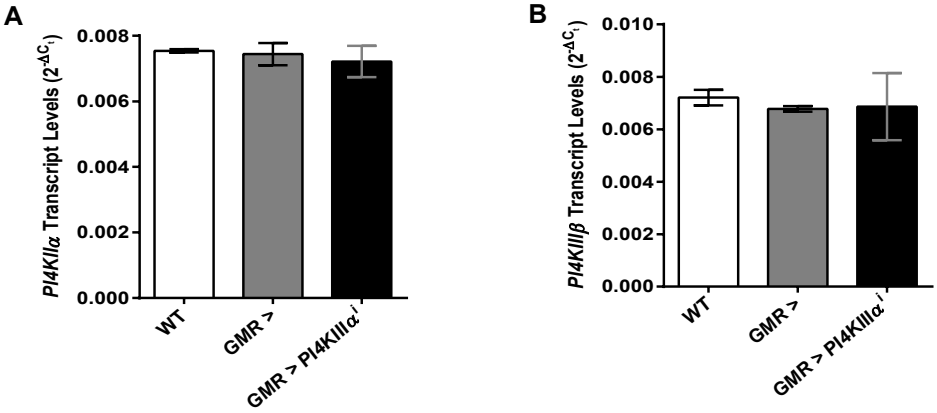

Figure 3.5 : Q-PCR estimation of transcript levels
The levels of PI4KIIα and PI4KIIIβ transcripts when PI4KIIIα has been knocked down in retinae, as measured using Q-PCR. x-axis represents genotype of the source tissue; y-axis represents $2^{-\Delta C_t}$ values for the described gene. **(A) PI4KIIα** Knocking down PI4KIIIα using GMRGal4 did not affect transcript levels of PI4KIIα, which were similar to those of control flies. **(B) PI4KIIIβ** Knocking down PI4KIIIα using GMRGal4 did not affect transcript levels of PI4KIIIβ, which were similar to those of control flies. Values are mean ± s.e.m., n = 75 retinae per sample. Figure adapted from Balakrishnan *et al.*, 2018

3.2.1 Quantifiable features of an ERG

A typical ERG has several characteristics that can be quantified. The most commonly measured feature is the amplitude of the response **(Fig.3.6a)**. When light-stimulated photoreceptors depolarise, the event is recorded as a sudden drop in potential. This depolarisation effect lasts as long as the light stimulus remains on and is abated only when the light stimulus is terminated. The amplitude of the drop in potential can inform on the efficiency of signalling. For instance, hypomorphs of PLC have highly reduced ERG amplitudes since PIP_2 hydrolysis occurs at very low rates in these mutants (Yoon et al., 2000).

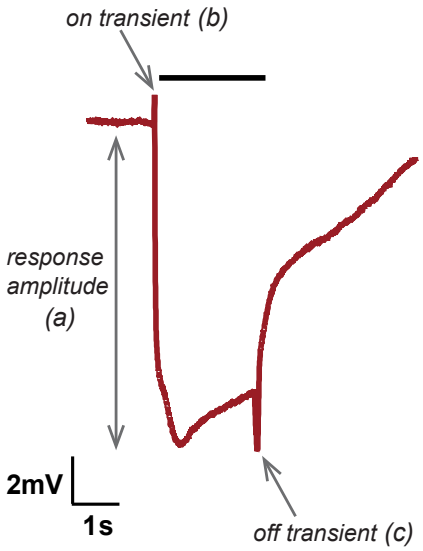

Figure 3.6 : Example ERG trace
The quantifiable features of an ERG trace are outlined. The black bar on top represents the duration of the light stimulus and the scale bar is on the bottom left. The depolarisation of photoreceptors in response to light causes a drop in potential, which is recorded as the response amplitude (**a**). The upward spike seen upon start of the light stimulus is the "on" transient (**b**) and the downward spike seen upon end of the light stimulus is the "off" transient (**c**).

The next obvious features are the spikes that occur at the start and end of the light stimulus **(Fig.3.6b and c)**. The upward spike seen at the start of the light stimulus is termed the "on transient" and the downward spike seen when the light is turned off is called the "off transient". Transients are

thought to reflect synaptic transmission in the laminar layers of the optic lobe (Heisenberg, 1971). Loss-of-function mutants for genes regulating this event, such as synaptojanin, have normal ERG amplitude but small or no transients (Verstreken et al., 2003).

ERGs can also be used to chart a stimulus-response curve, where one can subject the fly to light of different intensities and measure the response amplitude. Changes in the slope of the intensity response (IR) curve obtained here allows one to assess the sensitivity of the system. A classic example of this is the IR curve of white eyed flies, which has a much steeper slope than red eyed flies **(Fig.3.7)**. This is because white eyed flies lack screening pigments, making them much more sensitive to light (Stark and Wasserman, 1974). Additionally, one can quantify the kinetics of repolarisation of the photoreceptors, which reflect the speed of response termination. For example, after the stimulus is turned off, mutants for arrestin take much longer to revert to baseline than wild type flies (Dolph et al., 1993).

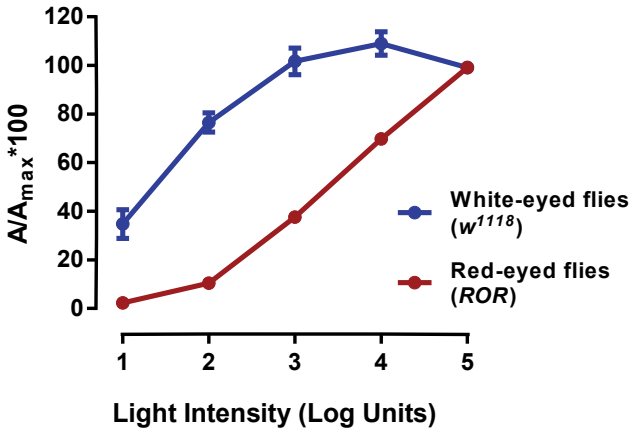

Figure 3.7 : Example intensity response curve
Quantification of the intensity response functions of red-eyed (ROR - red line) and white-eyed (w^{1118} - blue line) wild-type flies. x-axis represents light intensity in log units; y-axis represents the response amplitude at each intensity normalised to that at maximum intensity. The curve for the white-eyed flies has a much larger slope than that for the red-eyed flies, indicating that white-eyed flies have a higher sensitivity to light.

3.2.2 ERG phenotype of *GMR > PI4KIIIα^i* flies

Bearing the above parameters in mind, we took a closer look at the ERG waveform of flies in which *PI4KIIIα* was knocked down using GMRGal4. Henceforth, flies of this genotype will be referred to as *GMR > PI4KIIIα^i*. The Gal4 control flies for all our experiments are denoted as *GMR >*. When one day old flies were given a single flash of light for 2 s, the overall ERG amplitude of *GMR > PI4KIIIα^i* flies was lower than that of controls by ~50% **(Fig.3.8A, B, C)**. The ERGs also lacked the "on" and "off" transients. However, it is worth noting that ERGs with small amplitudes tend to lack transients, probably because the amplitude of the transients themselves are very small.

Apart from the overall reduction in amplitude, there was another notable phenotype in these flies. When subjected to a sequence of ten consecutive light flashes, the ERG amplitude of control flies was the same for every flash of light in the sequence. In the *GMR > PI4KIIIα^i* flies, not only was the response to the first flash smaller than controls, but the response for every subsequent flash of light was smaller than the preceding one **(Fig.3.8E)**. By the end of the light flash sequence, the amplitude of the tenth response was ~40% of the first response, whereas in control flies the first and tenth responses were identical. In order to check if this reduction in amplitude was permanent, flies that were subjected to the sequence of ten light flashes were allowed to dark adapt for five minutes. After dark adaptation, they were able to recover their initial response amplitudes **(Fig.3.8F)**.

We tested the sensitivity of *GMR > PI4KIIIα^i* flies by plotting an intensity response (IR) curve. Flies were given light stimuli of five different intensities, each approximately one order of magnitude brighter than the previous one. The responses were quantified by normalising the ERG amplitude for each flash to that of the last one. The IR curve of *GMR > PI4KIIIα^i* flies had a much lower slope than controls, indicating that these flies have reduced sensitivity to light **(Fig.3.8D)**. This implied that flies with lower levels of *PI4KIIIα* expression required higher amounts of stimulus to generate the same degree of response as a control fly.

Aside from the 2 s flash of light, we also tested whether prolonging the duration of the stimulus would further stress the system and enhance the phenotype. To do this, we subjected the flies to a light pulse that lasted for 5 s and measured the ERG amplitude. We observed that giving a longer light stimulus did not worsen the ERG phenotype of *GMR > PI4KIIIα^i* flies. Their response amplitudes for the 5 s light pulse were no different when

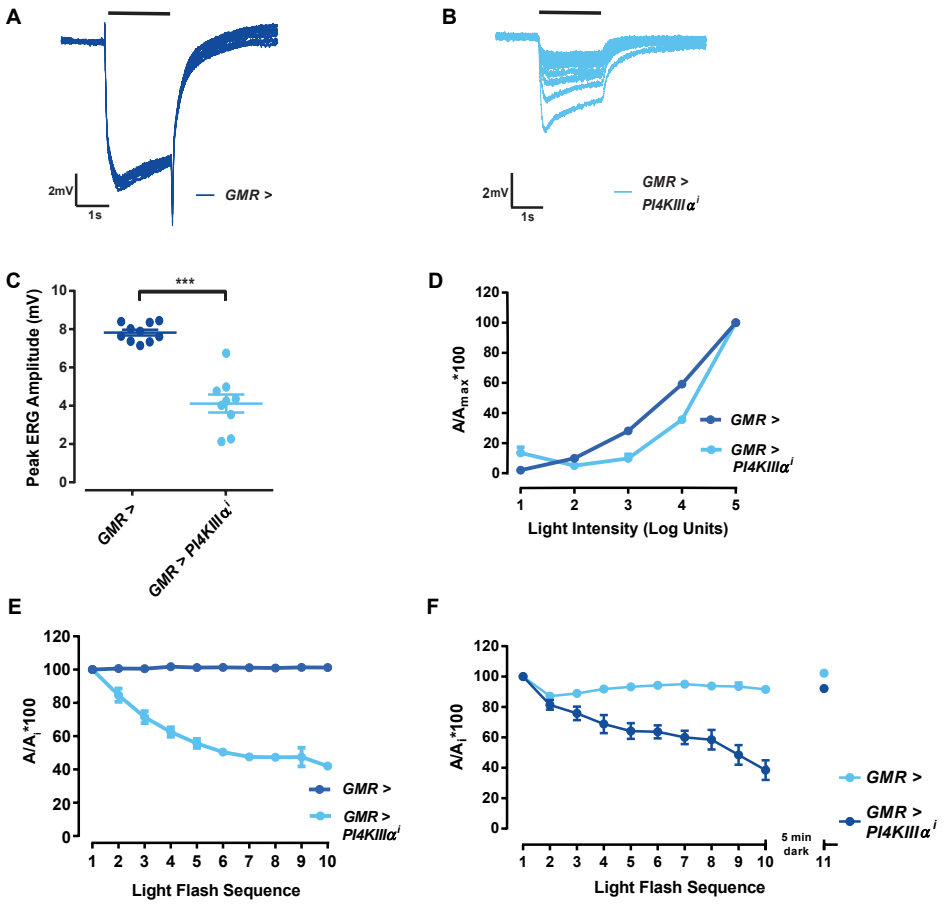

Figure 3.8 : ERG phenotype of *GMR > PI4KIIIα^i* flies
(A and B) Representative ERG traces of control (A) and *GMR > PI4KIIIα^i* (B) in response to ten consecutive light flashes. The black bar on top indicates duration of the light stimulus, scale bar is on the bottom left. **(C)** Quantification of the peak ERG amplitude of control and *GMR > PI4KIIIα^i* flies. x-axis represents genotype; y-axis represents response amplitude in mV. **(D)** Intensity response function of control and *GMR > PI4KIIIα^i* flies. x-axis represents light intensity in log units; y-axis represents the response amplitude at each intensity normalised to that at maximum intensity. **(E) and (F)** Quantification of the ERG amplitude of control and *GMR > PI4KIIIα^i* flies in response to ten consecutive light flashes. x-axis represents the light flash number; y-axis represents response amplitude for each light flash normalised to that at first light flash. *** - $p < 0.001$ as per two-tailed t-test, values are mean ± s.e.m., n = 10 flies per genotype.

compared to the 2 s light pulse **(Fig.3.9A)**. When we subjected these flies to five consecutive light flashes of 5 s each, the progressive reduction with every subsequent flash was seen. However, the extent of reduction was similar to that for the shorter light pulse, with the response to the final flash of light being ~50% of the response to the first flash **(Fig.3.9B)**.

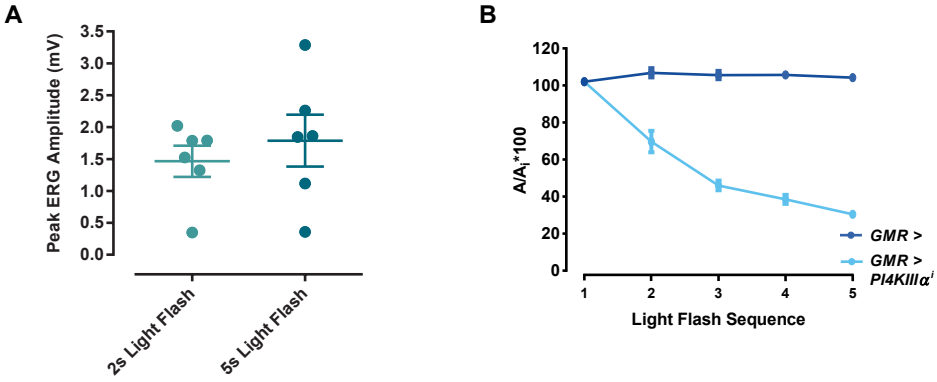

Figure 3.9 : ERG response of *GMR > PI4KIIIα^i* flies to 5 s light flash
(A) Quantification of the peak ERG amplitude of control and *GMR > PI4KIIIα^i* flies. x-axis represents duration of light stimulus; y-axis represents response amplitude in mV. **(B)** Quantification of the ERG amplitude of control and *GMR > PI4KIIIα^i* flies in response to five consecutive light flashes. x-axis represents the light flash number in the sequence; y-axis represents response amplitude for each light flash normalised to that at the first light flash. Values are mean ± s.e.m., n = 10 flies per genotype.

When we tested other ERG parameters, such as the depolarisation and repolarisation kinetics, we found that the *GMR > PI4KIIIα^i* flies had slightly higher rise times and decay slopes than the control flies **(Fig.3.10)**.

While it was tempting to directly attribute the ERG defects to *PI4KIIIα* downregulation, we first had to ensure that the main molecular components of phototransduction were intact in these flies. To check this, we performed Western blots for key proteins involved in phototransduction - Rh1, Gq_{α}, PLC, TRP, inactivation no afterpotential D (INAD) and dPIP5K - in one day old *GMR > PI4KIIIα^i* flies. We found that the levels of all these proteins were comparable between control and *GMR > PI4KIIIα^i* flies **(Fig.3.11)**. This indicated that the ERG phenotypes most likely arose due to reduced PI4KIIIα levels and not because of any perturbations in known phototransduction proteins.

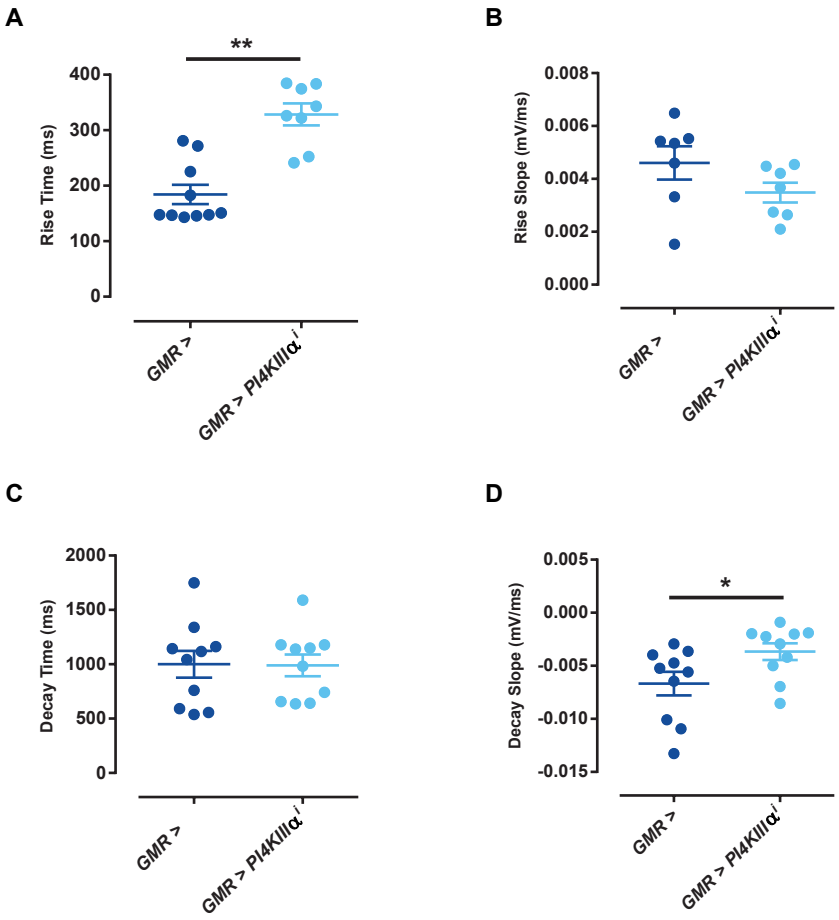

Figure 3.10 : Rise and decay kinetics of *GMR > PI4KIIIα^i* flies
(A) Quantification of rise time of control and *GMR > PI4KIIIα^i* flies. **(B)** Quantification of rise slope of control and *GMR > PI4KIIIα^i* flies. **(C)** Quantification of decay time of control and *GMR > PI4KIIIα^i* flies. **(D)** Quantification of decay slope of control and *GMR > PI4KIIIα^i* flies. ** - $p < 0.01$ as per two- tailed t-test, values are mean ± s.e.m., n = 10 flies per genotype.

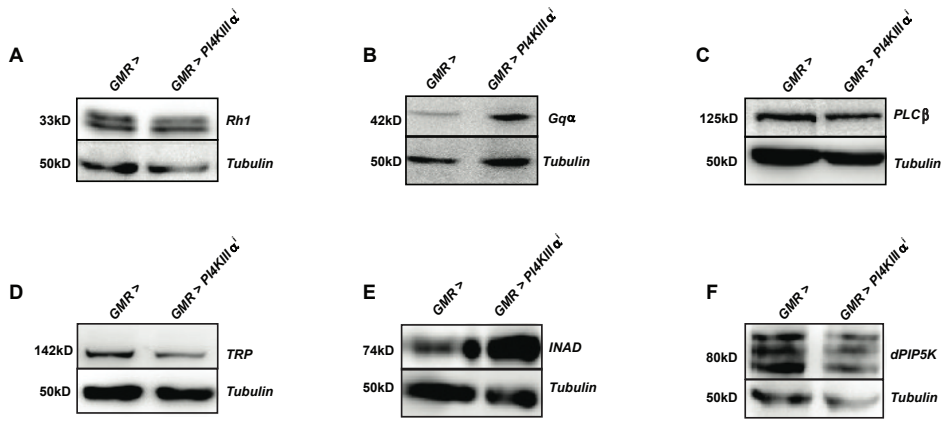

Figure 3.11 : Levels of key phototransduction proteins in *GMR > PI4KIIIα^i* flies
Western blots showing the levels of key phototransduction proteins extracted from the heads of *GMR > PI4KIIIα^i* flies as compared to GMR > flies. Tubulin is used as a loading control in all cases. **(A)** Rh1 **(B)** Gq_α **(C)** PLCβ **(D)** TRP **(E)** INAD **(F)** dPIP5K - protein was extracted from retinae and not heads to probe for dPIP5K.

3.3 The lipid kinase function of PI4KIIIα is required for its role in phototransduction

The main function of PI4KIIIα is to work as a lipid kinase that makes PI4P from PI. Having characterised the ERG phenotypes of *PI4KIIIα* downregulation, it was natural to wonder whether the defects arose merely due to absence of the protein or specifically due to loss of its enzymatic action. To test this, one would have to reconstitute a catalytically inactive protein in the PI4KIIIα depleted flies. If kinase activity does indeed contribute to PI4KIIIα function during the light response, then the catalytically dead mutant should not be able to rescue any of the ERG defects. However, a fully functional protein would be capable of restoring the response.

When using RNAi against the fly gene, one cannot reconstitute the system with a fly protein as that would get knocked down by the RNAi construct as well. To circumvent this, we expressed the tagged human PI4KIIIα (both wild-type and kinase-dead) in these flies **(Fig.3.12)** (Harak et al., 2014; Nakatsu et al., 2012; Pagnamenta et al., 2015). The kinase-dead allele contains a single residue mutation of aspartic acid (D) to alanine (A) at position 1957, which lies within the kinase domain of the protein and renders the

enzyme inactive (Harak et al., 2014; Pagnamenta et al., 2015). Using the human protein also allowed us to comment on the degree of conservation between the fly and human systems.

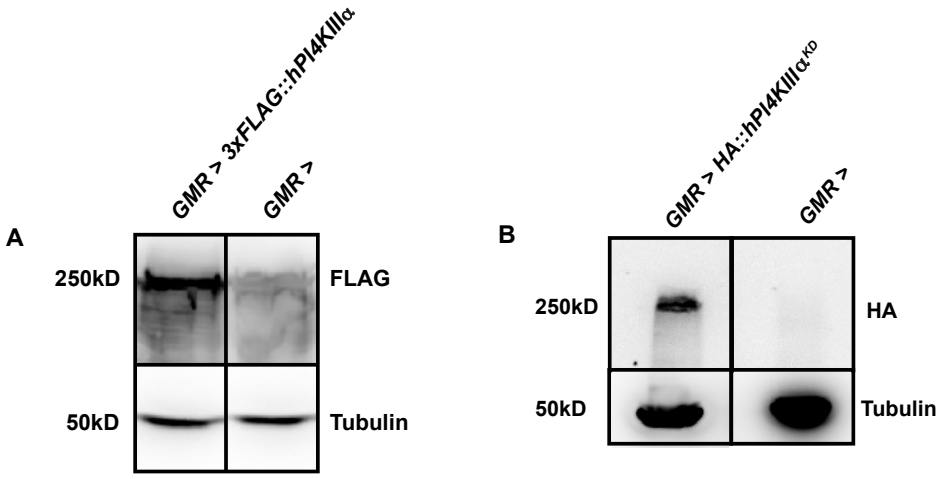

Figure 3.12 : Transgenic expression of tagged human PI4KIIIα
(A) Western blot showing the expression of 3xFLAG-tagged human PI4KIIIα, driven using GMRGal4. **(B)** Western blot showing the expression of HA-tagged kinase-dead human PI4KIIIα, driven using GMRGal4.

Transgenic flies expressing the wild-type human PI4KIIIα (hPI4KIIIα) under UAS promoter were made using site-specific integration as explained in Methods, Section 2.1. When expressed in the background of *GMR > PI4KIIIα^{i}*, we found that it completely rescued all the ERG defects associated with the knockdown. The ERG amplitude of *GMR > PI4KIIIα^{i} ; UAS-hPI4KIIIα* flies was comparable to that of controls **(Fig.3.13A and B)**. Importantly, the responses to ten sequential light flashes were no longer progressively reducing but were constant across all flashes, again like those of controls **(Fig.3.13C)**. The sensitivity of the system was also restored; the slope of the IR curve now resembled that of control flies **(Fig.3.13D)**. From these results, it was clear that the ERG defects were caused purely because of knockdown of *PI4KIIIα* and not due to any other perturbations or off-target effects. It is also vital to note that the human *PI4KIIIα* was capable of wholly rescuing the ERG defects in a *Drosophila* knockdown, signifying a high degree of functional conservation across these two systems.

To examine the necessity for the kinase function of PI4KIIIα during phototransduction, we expressed a catalytically inactive mutant of the human

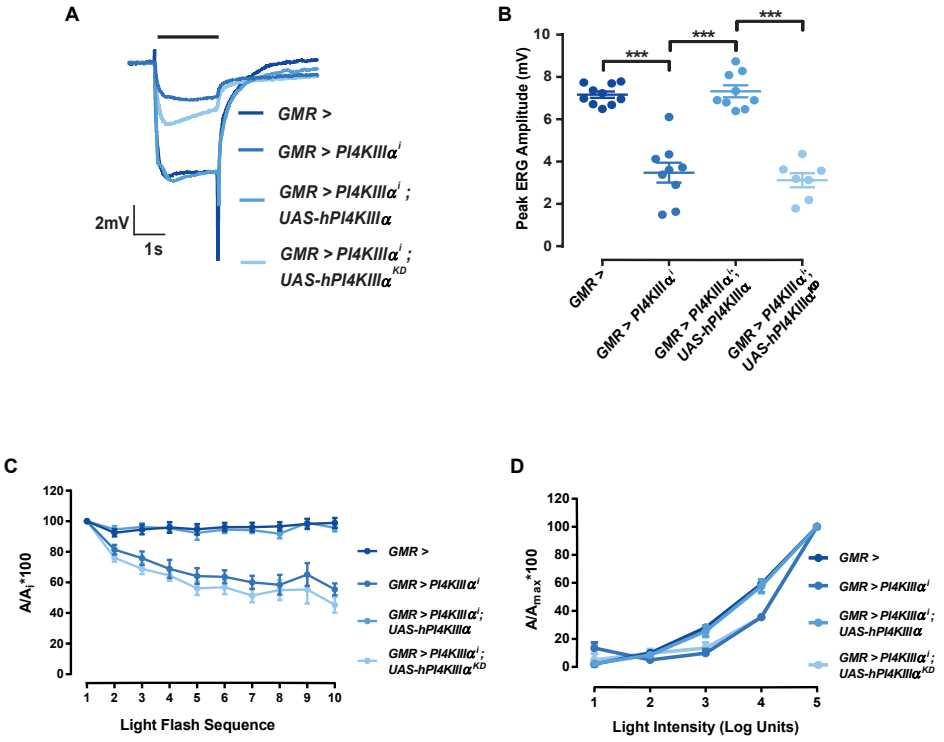

Figure 3.13 : Rescue of *GMR > PI4KIIIα^i* ERG phenotypes by full length hPI4KIIIα, but not by the kinase-dead allele
(A) Representative ERG traces of listed genotypes. Black bar on top indicates duration of light stimulus; scale bar is shown on bottom left. **(B)** Quantification of the peak ERG amplitude of indicated genotypes. x-axis represents genotype and y-axis represents response amplitude in mV. n = 7 flies per genotype. **(C)** Quantification of the ERG amplitude of indicated genotypes in response to ten consecutive light flashes. x-axis represents the light flash number in the sequence and y-axis represents response amplitude for each light flash normalised to that at the first light flash. n = 10 flies per genotype. **(D)** Quantification of the intensity response function of indicated genotypes. x-axis represents light intensity in log units and y-axis represents the response amplitude at each intensity normalised to that at maximum intensity. *** - $p < 0.001$ as per one way ANOVA followed by Tukey's multiple comparison test, values are mean ± s.e.m., n = 8 flies per genotype.

PI4KIIIα in *GMR > PI4KIIIα^{i}* flies. Unlike the wild-type protein, the kinase-dead hPI4KIIIα (hPI4KIIIα^{KD}) was incapable of rescuing any of the ERG defects **(Fig.3.13)**. In fact, the ERG responses of *GMR > PI4KIIIα^{i} ; UAS-hPI4KIIIα^{KD}* flies were no different from those of *GMR > PI4KIIIα^{i}* flies for any of the parameters quantified. This evidence highlighted the need for enzymatic activity of PI4KIIIα during the photoresponse, further pointing to a requirement for the lipid PI4P during signalling.

3.4 A mutant allele of *PI4KIIIα* can recapitulate the effects of RNAi knockdown

Complete removal of the *PI4KIIIα* gene in flies is cell lethal (Yan et al., 2011a). This was one of the main reasons for using RNAi against the gene in this study. There were also no viable *Drosophila* mutants suitable for use in photoreceptors when we began the study. In 2014, however, a viable mutant for *PI4KIIIα* was identified in a genetic screen for X-chromosome mutations involved in neuronal disorders (Yamamoto et al., 2014). Since the screen was performed using ERGs as a readout, the identification of *PI4KIIIα* was promising. It is important to note that the mutants could only be analysed as whole-eye mosaics, where only the eye tissue expresses mutant PI4KIIIα, whereas all other cells of the fly express the wild-type protein.

The mutant flies, henceforth referred to as *PI4KIIIα^{XE45B}*, were gifted to us from Hugo Bellen's laboratory, as were the other strains required to generate whole-eye mosaics. The mutation is a single amino acid substitution at position 2126, where glutamine (Q) is substituted by lysine (L) **(Fig.3.14)**. The amino acid lies just outside the catalytic domain, but we currently do not know whether it has any effect on the catalytic activity of the protein.

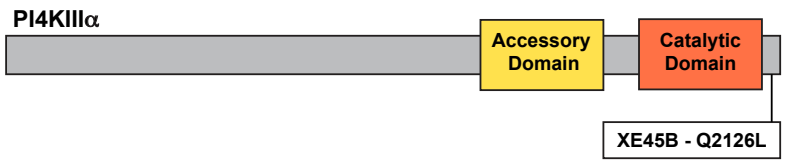

Figure 3.14 : PI4KIIIα^{XE45B} allele
The PI4KIIIα^{XE45B} allele carries a point mutation of glutamine (Q) to lysine (L) at amino acid position 2126, which is just outside the catalytic domain pf the protein.

To generate whole eye mosaics of $PI4KIII\alpha^{XE45B}$, we used the method as described in **Fig.3.15** (Stowers and Schwarz, 1999).

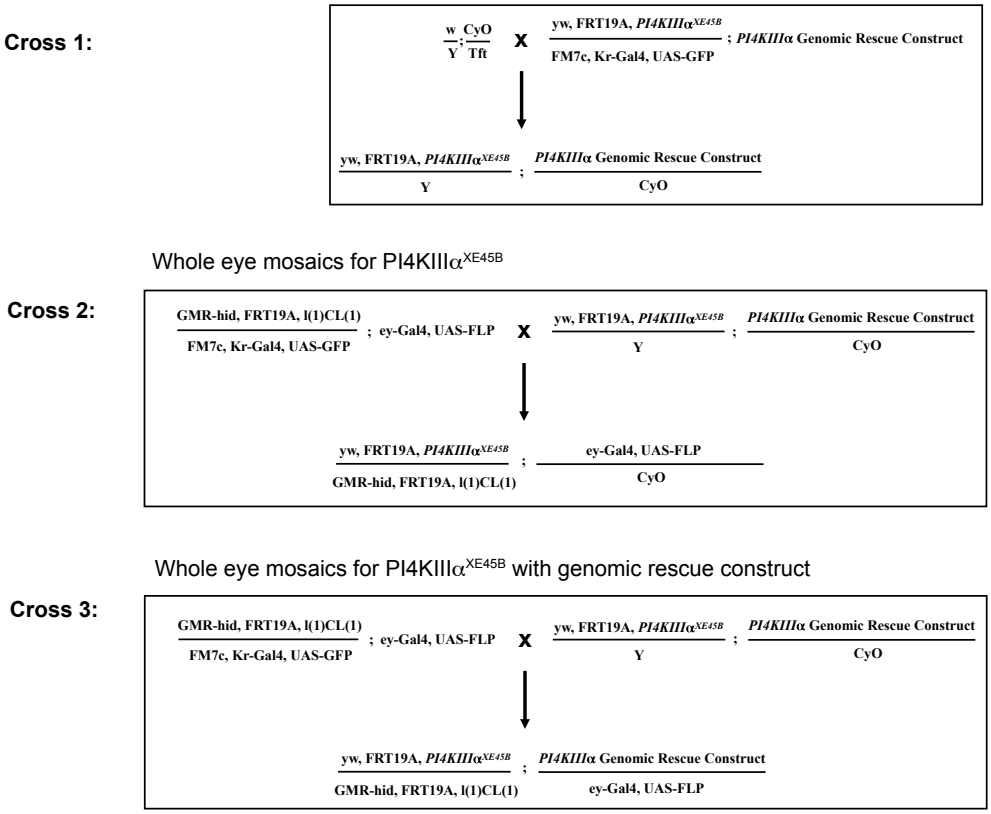

Figure 3.15 : Generation of whole eye mosaics for PI4KIIIα^{XE45B}
Schematic showing the sequence of crosses set up to generate whole eye mosaics for the PI4KIIIα^{XE45B} allele, either with or without the PI4KIIIα genomic rescue construct in the background.

Once flies of the desired genotypes were obtained, they were subjected to the same ERG analyses as the $GMR > PI4KIII\alpha^{i}$ flies. The $PI4KIII\alpha^{XE45B}$ behaved almost identically to the $GMR > PI4KIII\alpha^{i}$ flies for every parameter tested (**Fig.3.16**). The overall ERG amplitude was reduced when compared to the corresponding FRT controls. Notably, the responses to a sequence of ten light flashes became progressively smaller, mimicking the phenotype of $GMR > PI4KIII\alpha^{i}$ flies. In fact, the response to the last flash in the sequence was ~40% of the first response, which was identical to that of the $PI4KIII\alpha$ knockdown flies. The ability of the mutant to recapitulate the effect of RNAi lent further confidence to the results of those experiments.

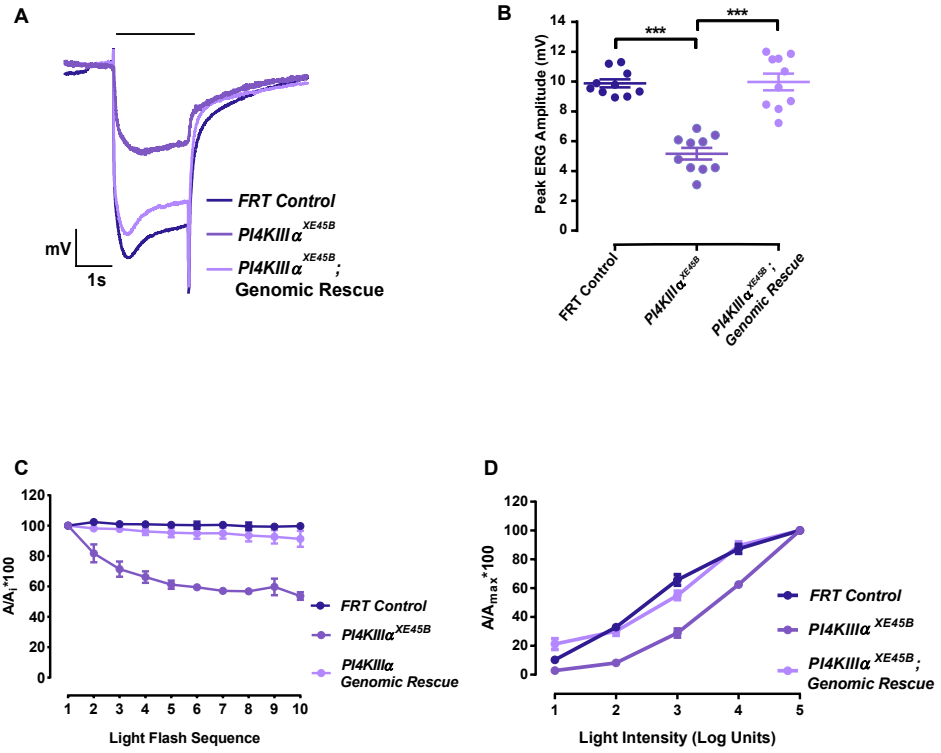

Figure 3.16 : ERG phenotypes of PI4KIIIα^{XE45B}
(A) Representative ERG traces of listed genotypes. Black bar on top indicates duration of light stimulus; scale bar is shown on bottom left. **(B)** Quantification of the peak ERG amplitude of indicated genotypes. x-axis represents genotype and y-axis represents response amplitude in mV. **(C)** Quantification of the ERG amplitude of indicated genotypes in response to ten consecutive light flashes. x-axis represents the light flash number in the sequence and y-axis represents response amplitude for each light flash normalised to that at the first light flash. **(D)** Quantification of the intensity response function of indicated genotypes. x-axis represents light intensity in log units and y-axis represents the response amplitude at each intensity normalised to that at maximum intensity. *** - $p < 0.001$ as per one way ANOVA followed by Tukey's multiple comparison test, values are mean ± s.e.m., n = 10 flies per genotype.

Despite the above results, it was technically possible that the ERG defects were a result of an undetected secondary mutation and not just the mapped *PI4KIIIα* mutation. To eliminate this possibility, we expressed a genomic construct of *Drosophila PI4KIIIα* in the background of the $PI4KIII\alpha^{XE45B}$ mutant. The genomic construct was able to completely rescue the ERG defects seen in the mutants, confirming that the phenotypes were due to the mapped mutation and not any others **(Fig.3.16)**.

The use of the mutant allele, coupled with RNAi, allowed us to perturb *PI4KIIIα* in photoreceptors using two independent genetic methods. The fact that both perturbations caused similar ERG defects further confirmed a role for *PI4KIIIα* during phototransduction.

3.5 Knocking down *PI4KIIIα* reduces the levels of PIP and PIP_2 in *Drosophila* retinae

A key function of PI4P is to act as the primary substrate for PIP_2 synthesis at the plasma membrane. If so, depleting cells of *PI4KIIIα* should reduce not only PI4P levels, but those of PIP_2 as well. To check this one would have to measure the levels of both lipids in *Drosophila* photoreceptors where *PI4KIIIα* is knocked down. Moreover, previous studies have shown that mutants with low levels of PIP_2 also have reduced ERG response amplitudes (Chakrabarti et al., 2015; Yadav et al., 2015). Hence, it is probable that the ERG defects seen in $GMR > PI4KIII\alpha^{i}$ flies are due to reduced PIP_2 levels. Quantifying the lipid levels would therefore, not only inform on the product of *PI4KIIIα* activity, but also enable us to deduce whether they modulate the ERG response or not.

For quantitative measurements of phosphoinositides, we turned to liquid chromatography - mass spectrometry (LC-MS). We adapted an existing method where the lipids are chemically derivatised, making them easier to separate and fragment **(Fig.3.17)** (Clark et al., 2011). Separation of molecules occurs on the basis of their mass-to-charge ratio (m/z), allowing for clear distinction between phosphatidylinositol (PI), phosphatidylinositol monophosphates (PIP) and phosphatidylinositol bisphosphates (PIP_2). One major caveat of this method is that it cannot distinguish between positional isomers, i.e., all PIPs (PI3P, PI4P and PI5P) have the same m/z and are detected as one species, as are all PIP_2s [$PI(3,5)P_2$, $PI(3,4)P_2$ and $PI(4,5)P_2$]. Fortunately PI4P and $PI(4,5)P_2$, the specific isomers we are interested in, constitute >90% of the cellular phosphatidylinositol phosphate (PIP) and phos-

phatidylinositol bisphosphate (PIP_2) pools, respectively (Lemmon, 2008). Therefore, any changes in these two lipids would likely be reflected in the total pool.

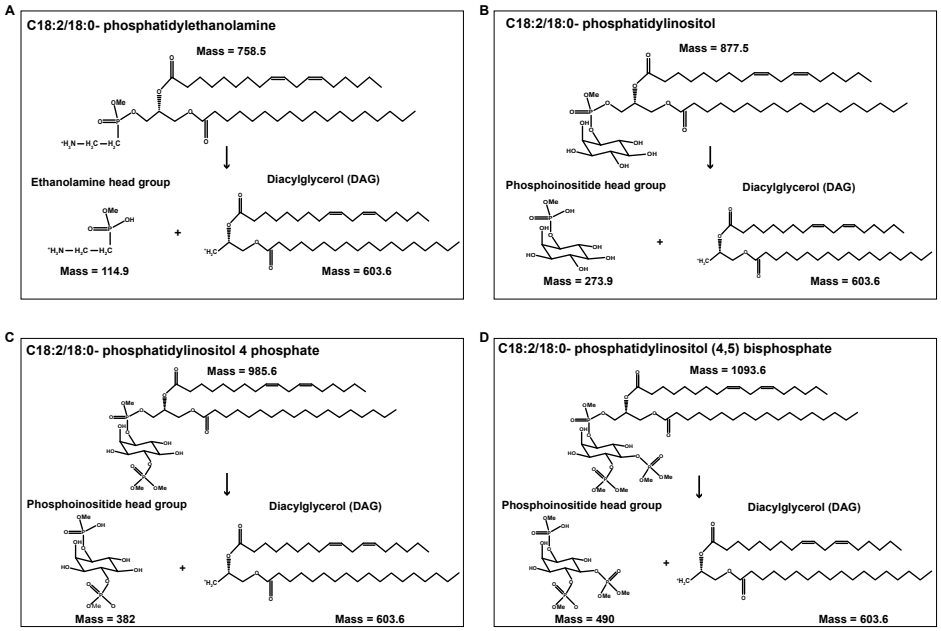

Figure 3.17 : Fragmentation pattern of phospholipids
(A) Phosphatidylethanolamine (PE) **(B)** Phosphatidyinositol (PI) **(C)** Phosphatidylinositol 4-phosphate (PI4P) **(D)** Phosphatidylinositol 4,5-bisphosphate [$PI(4,5)P_2$]

3.5.1 Standardisation and validation of LC-MS Method

We began by examining the sensitivity of the LC-MS method by plotting a standard curve with synthetic lipid standards. We prepared serial dilutions of synthetic standards for three phospholipids - PE, PIP and PIP_2 (molecular compositions listed in Section 2.5). These dilutions were subjected to an acidic lipid extraction (explained in detail in Section 2.5) and the extracted standards were quantified using the established LC-MS method. When the standard curves for each lipid class were plotted, they were found to be linear, with the r^2 values being ~0.98 **(Fig.3.18B-D)**. This analysis established the sensitivity and linearity of the method and we proceeded with experiments using biological samples.

Using retinal tissue as the source material, we extracted the lipids and subjected them to LC-MS analysis. We initially characterised the distribution

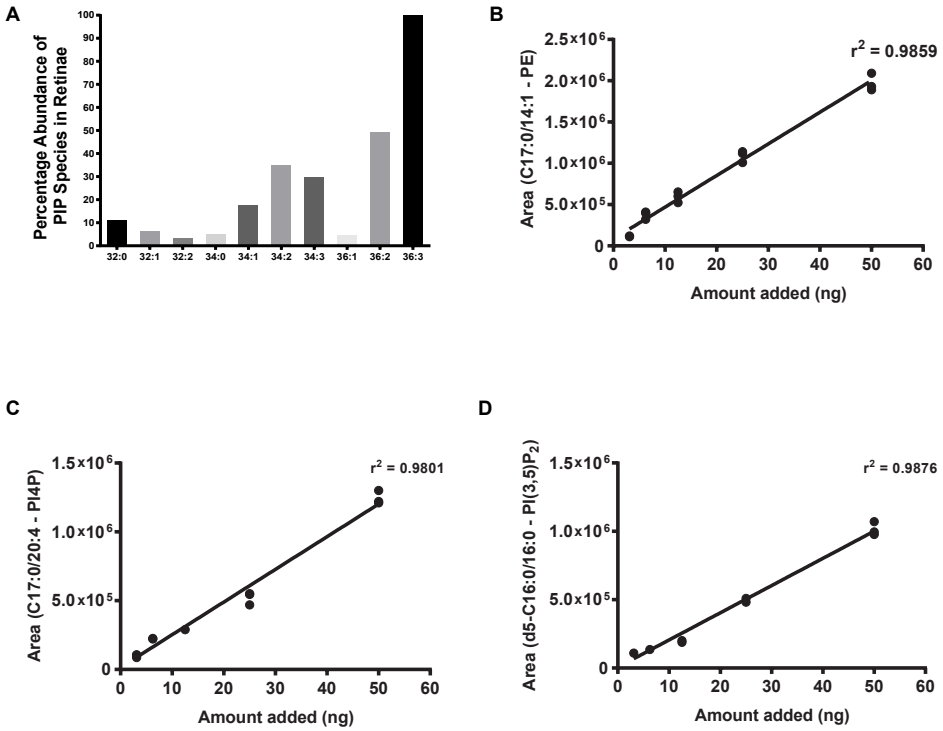

Figure 3.18 : Standard curve analysis
(A) Frequency distribution of different acyl chain species of PIP in *Drosophila* retinae **(B)** Standard curve of C(17:0/14:1) PI internal standard. x-axis represents amount in ng; y-axis represents area under curve. **(C)** Standard curve of C(17:0/20:4) PI4P internal standard. x-axis represents amount in ng; y-axis represents area under curve. **(D)** Standard curve of d5-C(16:0/16:0) $PI(3,5)P_2$ internal standard. x-axis represents amount in ng; y-axis represents area under curve.

of different phosphoinositide species, based on acyl chain composition, in wild-type (WT) retinae. The acyl chain composition of a lipid is represented as x:y, with x denoting the total number of carbon atoms between the two chains and y denoting the total number of double bonds in the acyl chains. In WT retinae, we were able to detect 32, 34 and 36 species for PI, PIP and PIP_2. However, 36:2 and 36:3 were the most abundant species in all three cases. Therefore, for subsequent experiments, we focussed mainly on these two species **(Fig.3.18A)**.

As positive controls, we first measured the lipid levels in mutants for *rdgB*, a PI-transfer protein known to supply PI for PIP_2 formation in photoreceptors. Severe hypomorphic mutants ($rdgB^9$) have been previously reported to have low PIP_2 levels since in these flies, there is not enough PI available for their synthesis (Yadav et al., 2015). When we perfomed LC-MS analysis of $rdgB^9$ retinal lipids, that is exactly what we saw. Both PIP and PIP_2 levels were reduced when compared to WT controls, indicating that the LC-MS method was capable of detecting cellular changes in phosphoinositides **(Fig.3.19A-D)**.

Since we were examining the role of these lipids during phototransduction, it was important to examine whether the light stimulus itself could cause any perceptible changes in their levels. We measured the lipids from a set of $rdgB^9$ flies that were reared and processed completely in the dark and another set that was exposed to a strong light flash before processing. To quantify and detect any changes caused by the light stimulus, we took a light:dark ratio of these lipids. In WT flies, the light:dark ratioes of both PIP and PIP_2 remained close to one, whereas the ratioes were ~0.5 in $rdgB^9$ flies **(Fig.3.19E and F)**.

We also used another well-characterised phototransduction mutant - $dPIP5K^{18}$ - to further validate the LC-MS method. dPIP5K is the enzyme that uses PI4P to make PIP_2 at the rhabdomeres; the protein null mutants ($dPIP5K^{18}$) are known to have reduced ERG responses (Chakrabarti et al., 2015). In these flies, it is presumed that most of the PI4P at the rhabdomere does not get converted to PIP_2. Therefore, we anticipated that upon measurement, we would see an increase in PI4P and decrease in PIP_2 in $dPIP5K^{18}$ null mutants. When we extracted retinal lipids from dark-reared $dPIP5K^{18}$ flies and subjected them to LC-MS analysis, we found that this was indeed the case **(Fig.3.20)**. Hence, using known mutants for single genes, we were able to demonstrate that the LC-MS method could be used to detect changes in phosphoinositide levels in *Drosophila* retinal tissue.

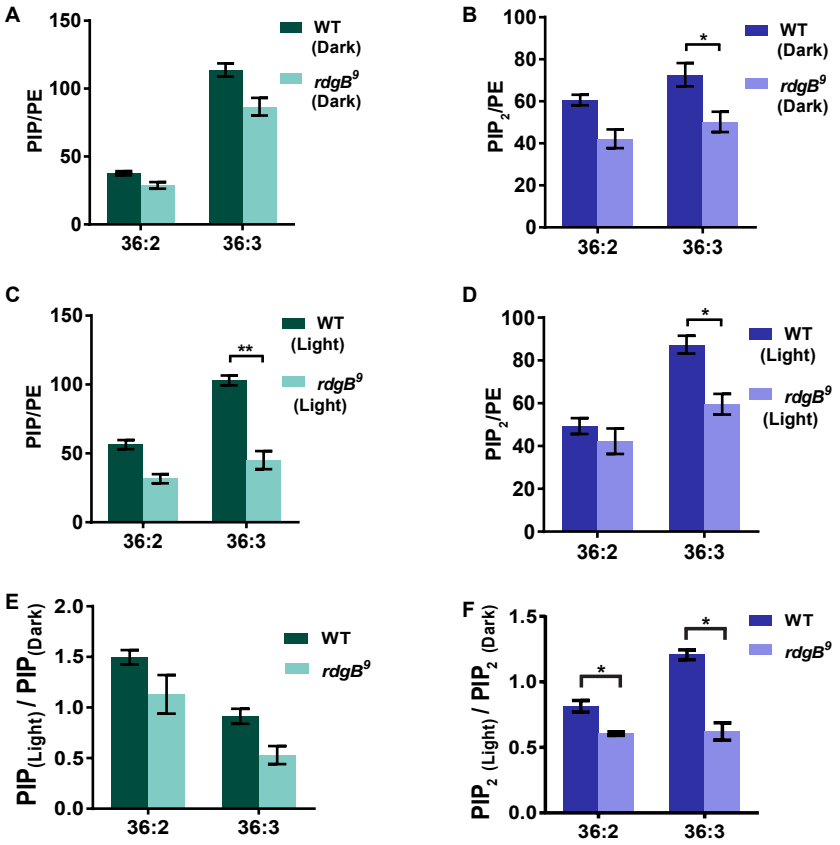

Figure 3.19 : LC-MS Measurement of PIP and PIP_2 from *rdgB*^{9} flies

Liquid chromatography-mass spectrometry measurement of PIP and PIP_2 levels in retinae of one-day old *rdgB*^{9} flies. The lipid levels for the two most abundant acyl chain species (36:2 and 36:3) are shown here. x-axis represents acyl chain species; y-axis represents ratio of PIP/PE and PIP_2/PE. **(A) and (B)** The flies were reared in dark and not exposed to any light during processing. **(C) and (D)** The flies were reared in dark and exposed to one minute of blue light before processing. **(E) and (F)** To highlight the effect of illumination on lipid levels, a ratio of the levels in light-exposed flies to those in dark-reared flies was taken. The $PIP_{(light)}$:$PIP_{(dark)}$ and $PIP_{2(light)}$:$PIP_{2(dark)}$ ratios for the 36:2 and 36:3 acyl chain species are shown. x-axis represents acyl chain species; y-axis represents ratio of light:dark lipid levels. * - $p < 0.05$ as per one way ANOVA followed by Tukey's multiple comparison test, values are mean ± s.e.m., n = 25 retinae per sample.

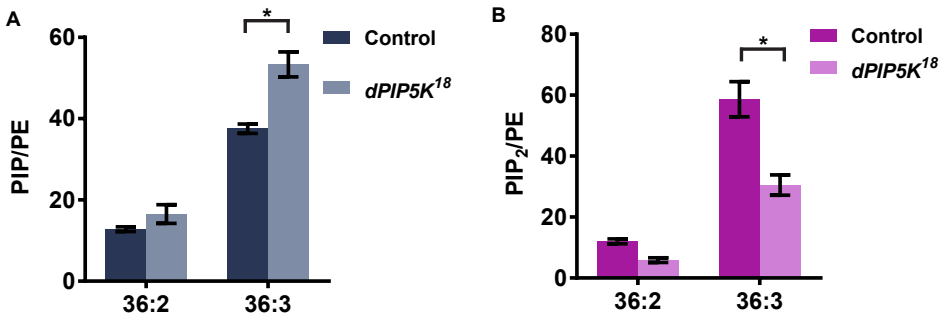

Figure 3.20 : LC-MS Measurement of PIP and PIP_2 from *dPIP5K*^{18} flies
(A) and (B) Liquid chromatography-mass spectrometry measurement of PIP (**A**) and PIP_2 (**B**) levels in retinae of one-day old *dPIP5K*^{18} flies. The flies were reared in dark and not exposed to any light during processing. The lipid levels for the two most abundant acyl chain species (36:2 and 36:3) are shown here. x-axis represents acyl chain species; y-axis represents ratio of PIP/PE and PIP_2/PE. * - $p < 0.05$ as per one way ANOVA followed by Tukey's multiple comparison test, values are mean ± s.e.m., n = 25 retinae per sample.

3.5.2 Lipid Measurement from *GMR > PI4KIIIα*^{i} flies

Having performed the appropriate controls, we finally measured the lipid levels in *GMR > PI4KIIIα*^{i} flies. Apart from measuring the baseline levels in dark-reared flies, we also measured them in flies that were exposed to a bright flash of light, as we did for *rdgB*^{9} mutants. In both conditions, there was a quantifiable reduction of PIP and PIP_2 levels in *GMR > PI4KIIIα*^{i} flies as compared to controls **(Fig.3.21A-D)**. This reduction could be completely rescued by expressing hPI4KIIIα in the background. A crucial result obtained from these experiments was that the decrease in lipid levels could not be reverted by expressing the kinase-dead hPI4KIIIα mutant, once again highlighting the requirement for enzymatic activity of PI4KIIIα in maintaining PIP and PIP_2 levels in photoreceptors **(Fig.3.21A-D)**.

We also quantified the light-induced changes in PIP and PIP_2 by taking a light:dark ratio of these lipids. In control flies, the ratioes were close to one, whereas in *GMR > PI4KIIIα*^{i} flies, the light:dark ratioes for both PIP and PIP_2 were significantly less than one. This decrease could by fully reversed by reconstituting the system with the *hPI4KIIIα*, but not the kinase-dead allele **(Fig.3.21E and F)**.

In essence, we were able to demonstrate a clear light-dependent decrease

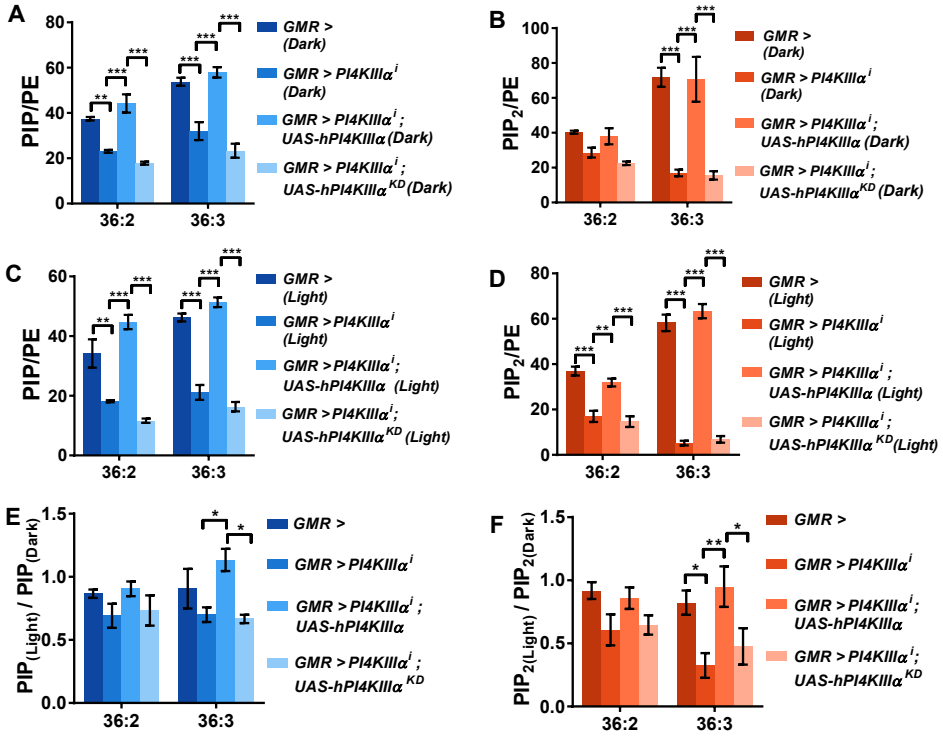

Figure 3.21 : LC-MS Measurement of PIP and PIP_2 from *GMR > PI4KIIIα^i* flies

Liquid chromatography-mass spectrometry measurement of PIP and PIP_2 levels in retinae of one-day old flies of the indicated genotypes. The lipid levels for the two most abundant acyl chain species (36:2 and 36:3) are shown here. x-axis represents acyl chain species; y-axis represents ratio of PIP/PE and PIP_2/PE. **(A) and (B)** The flies were reared in dark and not exposed to any light during processing. **(C) and (D)** The flies were reared in dark and exposed to one minute of blue light before processing. The lipid levels for the two most abundant acyl chain species (36:2 and 36:3) are shown here. **(E) and (F)** To highlight the effect of illumination on lipid levels, a ratio of the levels in light-exposed flies to those in dark-reared flies was taken. The $PIP_{(light)}$:$PIP_{(dark)}$ and $PIP_{2(light)}$:$PIP_{2(dark)}$ ratios for the 36:2 and 36:3 acyl chain species are shown. x-axis represents acyl chain species; y-axis represents ratio of light:dark lipid levels. * - $p < 0.05$ as per two way ANOVA followed by Tukey's multiple comparison test, values are mean ± s.e.m., n = 25 retinae per sample. Figure adapted from Balakrishnan *et al.*, 2018

in PIP and PIP_2 levels upon knocking down *PI4KIIIα*. These reduced lipid levels might be a major contributor to the ERG phenotypes seen in these flies.

3.6 Levels of plasma membrane PI4P and PIP_2 are reduced when *PI4KIIIα* is downregulated

In *Drosophila* photoreceptors the apical plasma membrane, known as the rhabdomere, houses the molecular machinery required for phototransduction. Given that knocking down *PI4KIIIα* has a strong effect on the light response of these flies, one might expect any light-induced changes in PI4P and PIP_2 to be reflected in the rhabdomeres. While the LC-MS analysis allowed accurate lipid measurements, they lacked spatial information as the extracts were made from total retinal tissue. Although it is not yet possible to get absolute quantifications solely from rhabdomeres, one can make relative measurements using specific lipid-binding probes. When tagged to fluorescent proteins like GFP, the probes can be monitored by their fluorescence intensities, which then act as a proxy for the cellular lipid levels (Várnai and Balla, 1998).

To observe these probes in photoreceptors, we harnessed a phenomenon known as the deep pseudopupil (DPP) that is seen in fly eyes. The ommatidia and rhabdomeres of the eye have a very stereotypic arrangement. Because of this, light rays passing through several adjacent ommatidia converge on a plane below the surface and form a single virtual image (Franceschini et al., 1981). This image is seen as one large ommatidium, with the rhabdomeres being the most prominent features. If one now expresses a fluorophore in photoreceptors and observes the DPP, the signal from the rhabdomeres can be recorded as fluorescence. Therefore, one need only measure the fluorescence intensity at the rhabdomere for different probes, allowing estimation of the relative lipid levels. To account for variations in the size of the pseudopupil, the fluorescence intensity is measured per unit area.

In order to monitor PI4P levels, we used the P4M domain of a bacterial protein (SidM) which specifically binds to PI4P (Hammond et al., 2014). Transgenic flies expressing the GFP-tagged P4M probe (P4M::GFP) under the UAS promoter were made and probe expression was driven using GMR-Gal4. Similarly for PIP_2, we used the pleckstrin homology (PH) domain of PLCδ, also fused to GFP (PLCδ-PH:GFP). This probe was generated previously in the lab and expressed under control of the *trp* promoter (Chakrabarti

et al., 2015).

3.6.1 Fluorescence intensity of lipid-binding probes at the rhabdomeres

We expressed the PI4P and PIP_2 probes individually in $GMR > PI4KIII\alpha^i$ flies and measured the fluorescence intensity of the DPP. When compared to controls, the fluorescence levels of both probes were reduced in the rhabdomeres of these flies **(Fig.3.22A and B)** and **(Fig.3.23A and B)**. It was possible that the reduced fluorescence was due to low expression of the probes and so, we performed Western blots to check the same. The probe expression was unchanged in both control and experimental flies **(Fig.3.22C)** and **(Fig.3.23C)**, suggesting that the low fluorescence in $GMR > PI4KIII\alpha^i$ flies was due to reduced binding of the probes at the rhabdomeres. This indicated that both PI4P and PIP_2 levels at the rhabdomere (apical plasma membrane) were decreased when *PI4KIIIα* was knocked down.

Since the human *PI4KIIIα* could completely rescue the ERG defects of$GMR > PI4KIII\alpha^i$ flies, we tested whether it could do the same for probe fluorescence levels. In keeping with previous observations, hPI4KIIIα was able to restore the levels of both probes in $GMR > PI4KIII\alpha^i$ flies to those of control flies. However, the kinase-dead allele of *hPI4KIIIα* could not rescue either PI4P or PIP_2 probe levels **(Fig.3.22)** and **(Fig.3.23)**. Thus, it was clear that *PI4KIIIα* is required to maintain PI4P and PIP_2 levels at the rhabdomere, and that it does so by virtue of its enzymatic activity.

3.6.2 Light-induced kinetics of lipid-binding probes

In addition to measuring the basal fluorescence levels, it is also possible to use lipid-binding probes to monitor the recovery kinetics of lipids after PLC stimulation. PLC stimulation results in PIP_2 hydrolysis, causing the PIP_2-binding probe to fall off the plasma membrane. This is recorded as a loss in plasma membrane fluorescence. Over time, as PIP_2 is resynthesised by the cell, the fluorescence levels at the plasma membrane recover. The kinetics of this recovery can be quantified, providing information on the rates of PIP_2 resynthesis. The same principle can be applied for monitoring PI4P recovery as well. The PI4P and PIP_2 probes used in this study have been effectively used in mammalian cells for similar purposes (Várnai and Balla, 1998, Tóth et al. (2016)).

In *Drosophila* photoreceptors, we have an additional advantage in that the same wavelength of light (488nm) can be used both to stimulate photore-

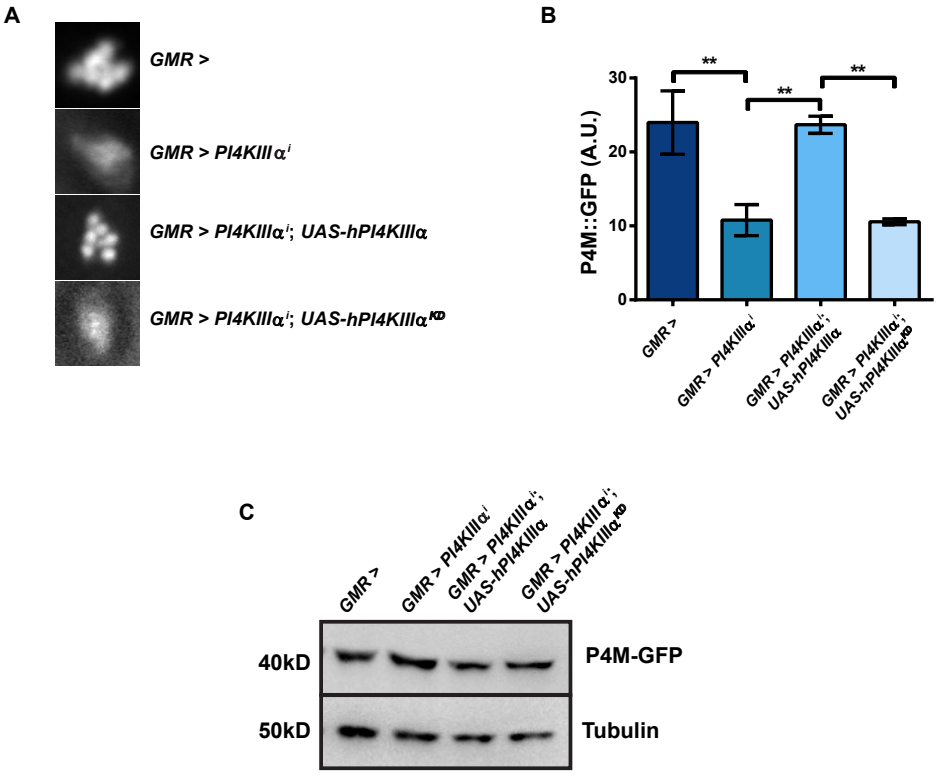

Figure 3.22 : PI4P levels at the rhabdomere of *GMR > PI4KIIIα^i* flies

(A) Representative images of the fluorescent deep pseudopupil from one day old flies, genotype as indicated. **(B)** Quantification of fluorescence intensity of P4M::GFP probe in the deep pseudopupil. x-axis indicates genotype, y-axis indicates fluorescence intensity per unit area. ** - $p < 0.01$ as per one way ANOVA followed by Tukey's multiple comparison test, values are mean ± s.e.m., n = 7 flies per genotype. **(C)** Western blot of head extracts made from flies expressing the P4M::GFP probe. Tubulin is used as a loading control. Figure adapted from Balakrishnan *et al.*, 2018

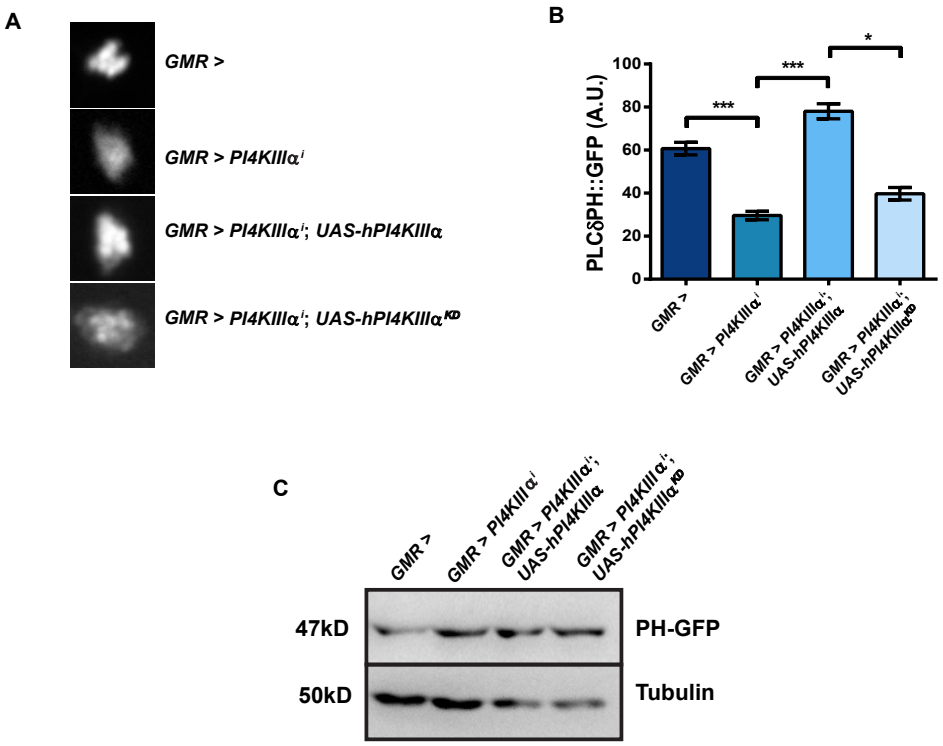

Figure 3.23 : PI(4,5)P_2 levels at the rhabdomere of *GMR > PI4KIIIα^{i}* flies

(A) Representative images of the fluorescent deep pseudopupil from one day old flies, genotype as indicated. **(B)** Quantification of fluorescence intensity of PLCδPH::GFP probe in the deep pseudopupil. x-axis indicates genotype, y-axis indicates fluorescence intensity per unit area. ** - $p < 0.01$ as per one way ANOVA followed by Tukey's multiple comparison test, values are mean ± s.e.m., n = 10 flies per genotype **(C)** Western blot of head extracts made from flies expressing the PLCδPH::GFP probe. Tubulin is used as a loading control. Figure adapted from Balakrishnan *et al.*, 2018

ceptors and excite GFP. This allowed the lab to develop an assay to track changes in PIP_2 levels at the rhabdomere, using probe fluorescence as a readout (described in detail in Methods - Section 2.4). Briefly, a dark-adapted fly is exposed to ten flashes of blue light, with incremental recovery periods between each flash of light. During all recovery periods except the first one, the fly is exposed to red light to terminate PLC signalling and allow conversion of metarhodopsin to rhodopsin **(Fig.3.24A)**. By depleting PIP_2 at the rhabdomere and assessing its recovery over different time periods, one can chart a time course for its resynthesis. The fluorescence intensity at each time point, normalised to basal levels, reflects the relative amounts of PIP_2 present at the rhabdomere **(Fig.3.24B)**.

From previous work in the lab, it is known that both $dPIP5K^{18}$ and $rdgB^{9}$ mutants (null allele and severe hypomorph, respectively) show delayed PIP_2 recovery kinetics as measured using PLCδPH::GFP (Chakrabarti et al., 2015; Yadav et al., 2015). Given that both these proteins play major roles in maintaining PIP_2 levels in photoreceptors, we anticipated a similar result for $GMR > PI4KIII\alpha^{i}$ flies. The recovery kinetics were measured in $GMR > PI4KIII\alpha^{i}$ flies expressing the PLCδPH::GFP probe. We saw that PIP_2 recovery indeed appeared to be slower in these flies **(Fig.3.25)**. However, what was more prominent was that after the first light stimulus, the loss of fluorescence was highly reduced in $GMR > PI4KIII\alpha^{i}$ flies when compared to controls. With respect to the first image, the control flies exhibited close to a 70% loss in probe fluorescence after the first flash of blue light whereas the fluorescence in $GMR > PI4KIII\alpha^{i}$ flies dropped only by ~30% **(Fig.3.25)**. Even though the extent of depletion is less when $PI4KIII\alpha$ is knocked down, the recovery to initial levels took longer in this case.

We next measured the recovery kinetics of PI4P in photoreceptors after light stimulation. The P4M::GFP probe had not been used in the lab for this assay before and hence, we first tested its kinetics in wild-type flies. The wild-type flies showed recovery kinetics that were similar to those of the PIP_2 probe **(Fig.3.26A)**. We next tested the P4M::GFP probe in the background of $norpA^{P24}$, a mutant for PLC. These mutants have been used as negative control for PIP_2 kinetics, since without PLC activity there is no PIP_2 hydrolysis and the probe remains at the rhabdomere throughout the protocol (Chakrabarti et al., 2015). When we expressed the PI4P probe in the backgorund of $norpA^{P24}$, we found that the probe fluorescence remained at the initial values for all light flashes, similar to the effect seen with PLCδPH::GFP **(Fig.3.26B)**.

Having tested the P4M::GFP probe, we expressed it in $GMR > PI4KIII\alpha^{i}$

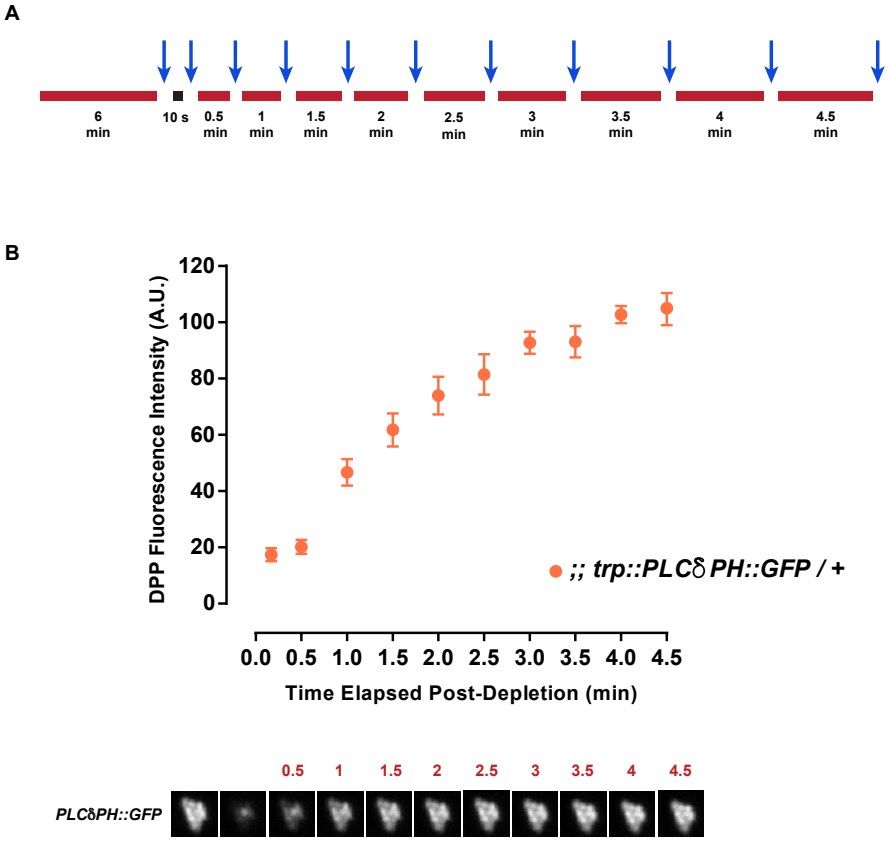

Figure 3.24 : Light induced PI(4,5)P_2 kinetics in wild-type *Drosophila* photoreceptors
(A) Representation of light stimulus delivered to the immobilised fly through the microscope objective. Red bars indicate duration of red light, black bar indicates no light, blue arrows indicate 90ms flash of blue light. **(B)** Recovery kinetics of the PLCδPH::GFP PI(4,5)P_2 probe when subjected to the above paradigm. x-axis indicates time in minutes after the very first flash of blue light; y-axis represents the fluorescence intensity per unit area of the deep pseudopupil at each instance, normalised to the intensity of the very first image. Representative images of each instance are shown below, with the time points of acquisition marked in red.

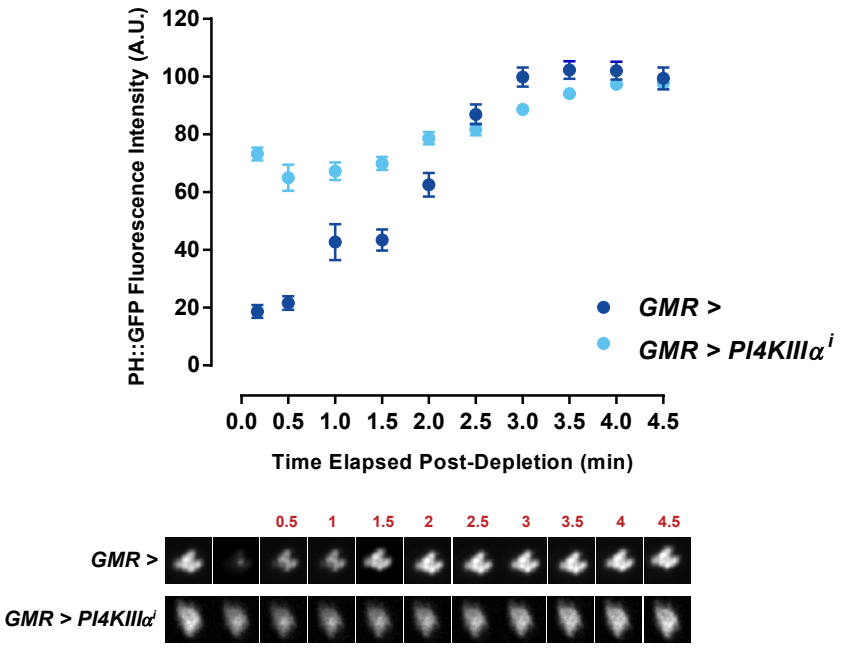

Figure 3.25 : Light induced PI(4,5)P_2 kinetics in *GMR > PI4KIIIα^i* flies

Recovery kinetics of the PLCδPH::GFP PI(4,5)P_2 probe when subjected to the light sequence described previously, genotype as indicated. x-axis indicates time in minutes after the very first flash of blue light; y-axis represents the fluorescence intensity per unit area of the deep pseudopupil at each instance, normalised to the intensity of the very first image. Representative images of each instance are shown below, with the time points of acquisition marked in red. Values are mean ± s.e.m., n = 10 flies per genotype.

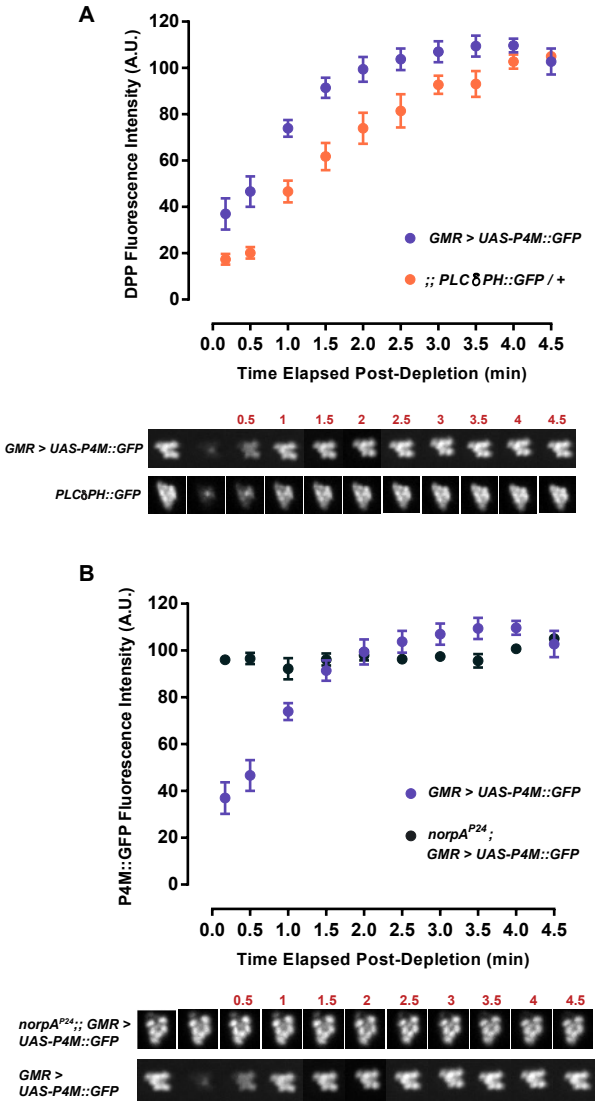

Figure 3.26 : Light induced PI4P kinetics in wild-type *Drosophila* photoreceptors
(A) Recovery kinetics of the PLCδPH::GFP $PI(4,5)P_2$ probe and P4M::GFP PI4P probe in wild-type flies and of the **(B)** P4M::GFP PI4P probe in both wild-type and $norpA^{P24}$ flies, when subjected to the light sequence described previously. x-axis indicates time in minutes after the very first flash of blue light; y-axis represents the fluorescence intensity per unit area of the deep pseudopupil at each instance, normalised to the intensity of the very first image. Representative images of each instance are shown below, with the time points of acquisition marked in red. Values are mean ± s.e.m., n = 10 flies per genotype.

flies and measured the recovery kinetics after light stimulation. Knocking down *PI4KIIIα* had a rather unexpected effect on PI4P kinetics. There was almost no loss of probe fluorescence after the first light stimulus - the control flies showed a drop in fluorescence intensity by ~60%, whereas the intensity of $GMR > PI4KIII\alpha^{i}$ flies did not drop from the basal values. Moreover, the fluorescence intensity of $GMR > PI4KIII\alpha^{i}$ flies remained constant for all events of light stimulation, similar to what was seen in $norpA^{P24}$ flies **(Fig.3.27)**.

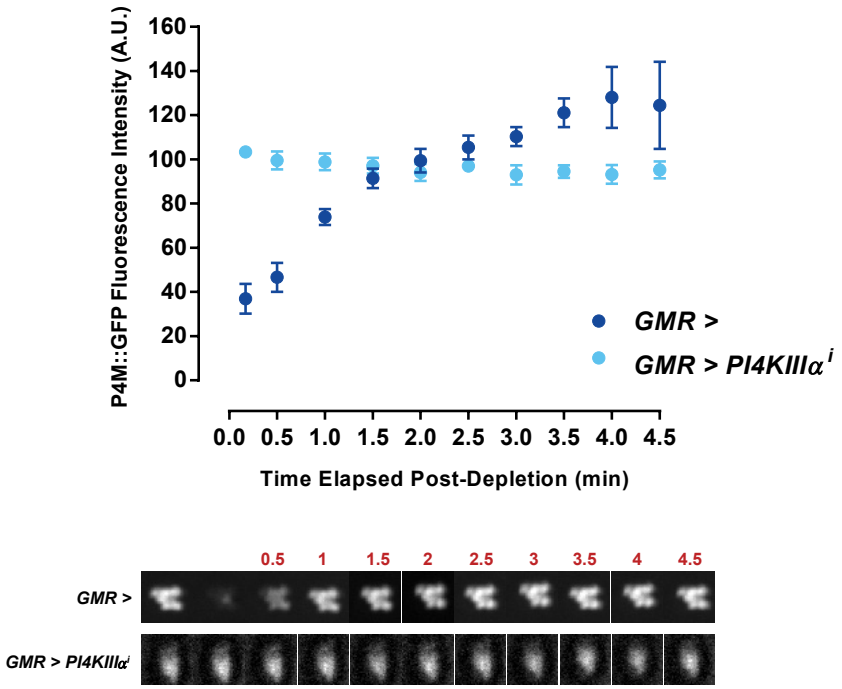

Figure 3.27 : Light induced PI4P kinetics in $GMR > PI4KIII\alpha^{i}$ flies

Recovery kinetics of the P4M::GFP PI4P probe when subjected to the light sequence described previously, genotype as indicated. x-axis indicates time in minutes after the very first flash of blue light; y-axis represents the fluorescence intensity per unit area of the deep pseudopupil at each instance, normalised to the intensity of the very first image. Representative images of each instance are shown below, with the time points of acquisition marked in red. Values are mean ± s.e.m., n = 10 flies per genotype.

In effect, it appeared that *PI4KIIIα* downregulation alters the light-induced kinetics of both PI4P and PIP_2, but have slightly different effects on each

lipid.

3.7 Localisation of PI4KIIIα in *Drosophila* photoreceptors

The PI4KIIIα enzyme has been very well characterised in yeast and mammalian systems. In yeast, the protein is constitutively present at the plasma membrane whereas in mammalian cells, it is present in the cytosol and recruited to the plasma membrane upon agonist-stimulation (Nakatsu et al., 2012). There is currently no information available about the localisation of PI4KIIIα in *Drosophila*. In our previous experiments, we showed that knocking PI4KIIIα down in photoreceptors has distinct effects on signalling events occurring at the rhabdomere. This indicated that PI4KIIIα most likely acts at the plasma membrane in *Drosophila* photoreceptors as well. However, this is an indirect inference and without explicit visualisation of the protein, we cannot make any claims about localisation.

Ideally, one would like to visualise the endogenous protein in wild-type (WT) photoreceptors using an antibody against the protein. Regrettably, our attempts to generate a functional antibody against *Drosophila* PI4KIIIα proved unsuccessful. We did, however, possess a tagged human PI4KIIIα that could be expressed in flies (Section 3.3). As the hPI4KIIIα was able to completely rescue both the ERG phenotypes and reduced lipid levels of *GMR > PI4KIIIα^{i}* flies, it is likely that the functions of the human and fly proteins are highly conserved.Therefore, in lieu of the fly protein, we examined the localisation of the tagged hPI4KIIIα (3xFLAG::hPI4KIIIα) in WT *Drosophila* photoreceptors (experiments performed by Rajan Thakur).

In dark-reared WT flies, i.e., those that have not received any light stimulation, the 3xFLAG::hPI4KIIIα was excluded from the rhabdomere and present in the cell body **(Fig.3.28B)**. This concurs with data from mammalian cells, where the protein is present in the cytosol until the cells are stimulated (Nakatsu et al., 2012). To supplement the data in photoreceptors, we also expressed the 3xFLAG::hPI4KIIIα in cultured *Drosophila* S2R+ cells (experiments perfomed by Urbashi Basu). In these unstimulated cells, hPI4KIIIα was seen in the cell body, once again mimicking its behaviour in mammalian cells **(Fig.3.28A)**.

In order to test whether a light stimulus could draw hPI4KIIIα to the plasma membrane, we subjected the flies to an intense flash of light before processing. In these photoreceptors, the 3xFLAG::hPI4KIIIα was present both at the

rhabdomere and basolateral plasma membrane **(Fig.3.28C)**. This clearly established that the human PI4KIIIα behaves identically in both mammalian systems and fly photoreceptors.

3.8 Conclusion

The molecular complexities of phototransduction in *Drosophila* have been extensively studied over the past few decades. Most of the elements of the PIP_2 resynthesis pathway were identified using mutants with distinct ERG phenotypes. Even so, there remain a few unanswered questions regarding the cycle, one of which we have tackled in this study.

3.8.1 Main conclusions

We know that biochemically, PI 4-kinase is required to convert PI to PI4P. However, since there are three isoforms of PI4K in flies, there was still the question of which one is active during phototransduction. We used electroretinograms (ERGs) as a readout to investigate which of the three PI4K isoforms is involved in the light response. By performing experiments with different UAS-RNAi/Gal4 combinations, we saw that only knocking down *PI4KIIIα* and not the other two isoforms reduced the ERG response. This allowed us to pinpoint *PI4KIIIα* as the enzymatic isoform required during phototransduction.

The ERG phenotypes of *PI4KIIIα* downregulation were further validated using a viable mutant allele for the gene ($PI4KIII\alpha^{XE45B}$). The $PI4KIII\alpha^{XE45B}$ mutant displayed identical ERG defects to the knockdown, and these effects could be rescued using a genomic construct. The mutant was also used to check for ultrastructural defects in the photoreceptors. Using transmission electron microscopy, it was found that the structural integrity of the mutant photoreceptors was no different from those of controls, indicating that there was no degeneration (Balakrishnan et al., 2018).

The relevance of the lipid kinase function of *PI4KIIIα* was addressed by reconstituting the $GMR > PI4KIII\alpha^{i}$ flies with a catalytically inactive human *PI4KIIIα*. This transgene could not rescue the effects of knocking down *PI4KIIIα*, but a fully functional *PI4KIIIα* could, confirming that the kinase activity of *PI4KIIIα* is required for its role in phototransduction. This was further underlined by the fact that PI4P and PIP_2 levels were low in $GMR > PI4KIII\alpha^{i}$ flies, as measured using both LC-MS and lipid-binding probes. These reduced lipid levels were increased upon expressing the wild-

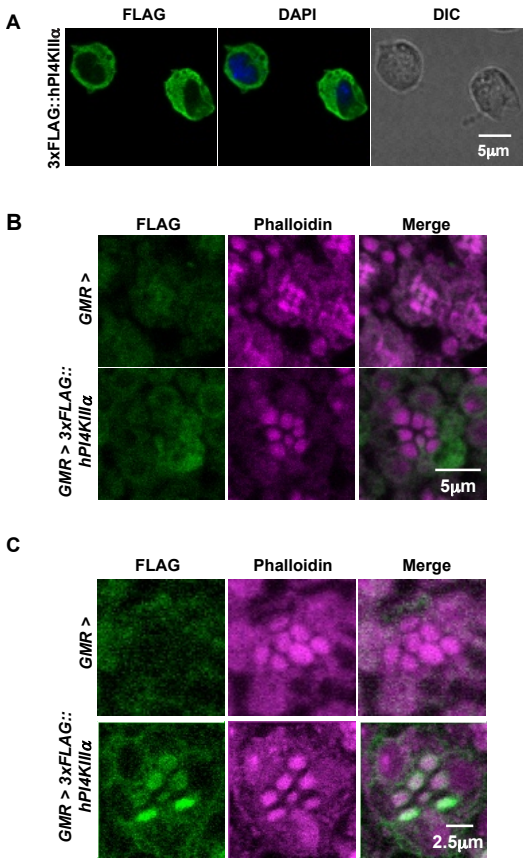

Figure 3.28 : Localisation of hPI4KIIIα in *Drosophila* photoreceptors
(A) Confocal images of S2R+ cells transfected with pUAST-3xFLAG::hPI4KIIIα, followed by staining with DAPI and α-FLAG. Blue represents DAPI, which marks the nucleus, and green represents FLAG. Scale bar - 5μm. **(B)** Confocal images of retinae from flies of the indicated genotypes, reared and processed completely in dark. The retinae have been stained with phalloidin (magenta) and α-FLAG (green). Scale bar - 5μm. **(C)** Confocal images of retinae from flies of the indicated genotypes, reared in dark and exposed to blue light for one minute before processing. The retinae have been stained with phalloidin (magenta) and α-FLAG (green). Scale bar - 2.5μm.

type *hPI4KIIIα*, but not the kinase-dead allele, reiterating the requirement for enzymatic activity of *PI4KIIIα*.

Having shown that *PI4KIIIα* exercises its function by controlling PI4P synthesis, we asked where in the cell the enzyme was acting. Using human *PI4KIIIα* in lieu of the fly protein, we saw that in light-stimulated *Drosophila* photoreceptors, the protein was present at the plasma membrane. This perfectly mirrored its behaviour in mammalian cells, pointing to a high degree of functional conservation between the human and fly proteins.

3.8.2 Molecular basis for ERG phenotypes

Knocking down PI4KIIIα in *Drosophila* photoreceptors had three major manifestations in terms of the ERG response:

- **Overall reduction in amplitude:** this effect was reminiscent of removing either *rdgB* or *dPIP5K* function in photoreceptors. Both these proteins are required for PIP_2 synthesis at the rhabdomere, and mutants for both (hypomorph for *rdgB* and null allele for *dPIP5K*) have been shown to have reduced PIP_2 levels (Section 3.5, (Chakrabarti et al., 2015; Yadav et al., 2015)). Low amounts of PIP_2 available for PLC to hydrolyse would reduce the signalling efficiency, resulting in low ERG amplitudes. Given that $GMR > PI4KIII\alpha^i$ flies also have reduced PIP_2 levels, it is possible that the diminished ERG response amplitude is a reflection of the lipid levels. However, the level of reduction in PIP_2 does not appear to correspond to the extent of decrease in ERG amplitude. $GMR > PI4KIII\alpha^i$ retinae have less PIP_2 than $rdgB^9$ retinae and yet, the response amplitude of $GMR > PI4KIII\alpha^i$ flies is higher than that of $rdgB^9$ flies. It is important to note here that the electrical response to light is a consequence of many molecular events following PIP_2 hydrolysis. Removing *rdgB* might affect some of these other events leading to photoreceptor depolarisation, causing a greater reduction in the response amplitude than knocking down *PI4KIIIα*. Additionally, in neither case is there a complete abrogation of protein synthesis; $rdgB^9$ mutants have ~10-20% protein present in the cell whereas $GMR > PI4KIII\alpha^i$ flies have close to 40% protein still produced. It is also curious that the reduced PIP_2 levels do not cause a response decay as seen in trp^{343} mutants. It has been established that the decay in this case is caused by excessive depletion of PIP_2, which in turn is mediated by a lack of inhibition by calcium. Since trp^{343} mutants have a much lower calcium influx than WT flies, the inhibition normally exercised by the ions on PLC is no longer as ef-

fective in this case. This presumably leads to unimpeded utilisation of the plasma membrane PIP_2 by PLC, eventually causing response decay and inactivation (Hardie et al., 2001). While we do not currently know the status of calcium concentrations in *GMR > PI4KIIIα*^{i} flies, it is possible that they are lower than those of control flies. *trp*^{343} mutants also show a characteristic response inactivation when exposed to bright light, which is mildly reflected by *GMR > PI4KIIIα*^{i} flies in that the response amplitude progressively reduces.

- **Progressive reduction in amplitude:** when subjected to a sequence of light flashes, the ERG response amplitude of *GMR > PI4KIIIα*^{i} flies decreased with each subsequent flash of light, unlike control flies where the amplitude was the same for every flash. One possible explanation is that this phenotype is independent of PI4P and PIP_2 levels and occurs due to some other cellular effect of knocking down *PI4KIIIα*. We have already demonstrated that *PI4KIIIα* controls the levels of PI4P and PIP_2 by virtue of its kinase activity. If these lipid levels do not contribute to the phenotype of progressive amplitude decrease in *GMR > PI4KIIIα*^{i} flies, we might have seen that reconstitution with catalytically inactive *PI4KIIIα* would rescue the ERG defect. However, presence of the kinase-dead *PI4KIIIα* did not alleviate the progressive reduction phenotype and we required a fully functional *PI4KIIIα* to rescue the ERG response. Given this, we conclude that the progressive reduction is indeed connected to the reduced PI4P and PIP_2 levels. Another explanation is that this phenotypes arises due to inefficient PIP_2 resynthesis during stimulation. If one considers PI4P synthesis to be a kinetically slower step than other reactions of the PIP_2 cycle, then when *PI4KIIIα* is depleted, the cell takes longer than normal to replenish PIP_2 during the short intervals between flashes. Given enough time, it should be able to recover the basal PIP_2 levels, but not within the 15 s given during the sequence. Indeed, after a sequence of 10 flashes, if the flies are allowed to dark adapt for 5 minutes then the first response amplitude is now back to initial values **(Fig.3.8F)**. Therefore, it is possible that removing *PI4KIIIα* slows down the whole PIP_2 resynthesis cycle, causing a progressive reduction in amplitudes due to insufficient recovery time.
- **Reduced sensitivity to light:** the intensity response curve of *GMR > PI4KIIIα*^{i} flies has a lower slope than that of controls, implying that they need a higher number of photons to elicit the same degree of response as a control fly. One reason could be reduced levels of the receptor molecule, which in this case is rhodopsin. However, we found

that the rhodopsin levels in *GMR > PI4KIIIα^i* flies were unaffected, as checked using Western blots. The levels of other major phototransduction proteins were also not altered in these flies. A similar scenario is seen in mutant flies carrying null alleles of *dPIP5K*, which also have reduced light sensitivity but unaltered levels of key phototransduction proteins. In both cases, PIP_2 levels are lower than normal, but it is not clear whether this has a direct impact on the light sensitivity. Given that the reduced sensitivity of *GMR > PI4KIIIα^i* flies could be rescued by the *hPI4KIIIα* but not by the kinase-dead allele, it appears that the signalling efficiency is dependent upon the levels of PI4P and PIP_2 available at the plasma membrane.

3.8.3 Altered lipid recovery kinetics in *GMR > PI4KIIIα^i* flies

In order to monitor the light-induced kinetics of PI4P and PIP_2 in photoreceptors, we used lipid-binding probes to track the changes in lipid levels. Knocking down *PI4KIIIα* had two major effects on the kinetics of these lipids:

- **Slower recovery kinetics of PIP_2:** this effect was anticipated, especially given that the ERG response of *GMR > PI4KIIIα^i* flies showed a progressive reduction in amplitude with multiple flashes of light. It is likely that limiting the amount of PI4P available for PIP_2 synthesis slows down the cycle, causing the probe fluorescence to recovery more slowly than controls.
- **Reduced depletion after light stimulation:** the fact that both PI4P and PIP_2 probe levels were depleted to very small extents in *GMR > PI4KIIIα^i* flies was rather unexpected. In *rdgB^9* and *dPIP5K^{18}* flies, the recovery kinetics of PIP_2 after light stimulation are slower than controls, but the level of probe depletion immediately after light stimulation is comparable to control flies (Chakrabarti et al., 2015; Yadav et al., 2015). In *GMR > PI4KIIIα^i* flies, the lack of depletion of PI4P and PIP_2 from the plasma membrane might reflect reduced activity of PLC. This would imply that downregulating *PI4KIIIα* affects not only the PIP_2 resynthesis phase, but the basal rate of signalling as well. This is also reiterated by the fact that the intensity response curve of *GMR > PI4KIIIα^i* flies has a lower slope than controls.

Interestingly, the lack of depletion was seen to a higher degree with the PI4P probe than with the PIP_2 probe. This could imply that the PI4P at the

rhabdomere, however low, is not further metabolised in *GMR > PI4KIIIα*^{i} flies. However, it is also possible that the probe has bound to the available PI4P and made it inaccessible to dPIP5K, which would convert it to PIP_2. While studies from mammalian cells largely negate the possibility of a dominant-negative effect of the P4M::GFP probe, it is possible that the levels of PI4P in *GMR > PI4KIIIα*^{i} flies are low enough to allow this effect.

3.8.4 Unaddressed Questions

Although we were able to definitively show that *PI4KIIIα* regulates *Drosophila* phototransduction by mediating PI4P synthesis, we could not demonstrate its localisation to the plasma membrane. Owing to a lack of reagents, we relied on the human protein to act as a proxy for the fly protein. Thus, localisation of the endogenous *Drosophila* PI4KIIIα still remains to be determined.

Another major finding from our experiments is that in photoreceptors, *PI4KIIIα* not only modulates PI4P levels, but those of PIP_2 as well. Knocking down *PI4KIIIα* reduces PIP_2 levels in retinae by more than half the normal amount. Apart from its signalling functions, PIP_2 at the plasma membrane controls a host of other cellular functions (Kolay et al., 2016). For example, in light-stimulated photoreceptors, rhodopsin is internalised via clathrin-dependent endocytosis. This type of endocytosis is regulated by PIP_2 (Haucke, 2005) and one might expect that reducing PIP_2 levels would perturb endocytosis. Therefore, it would be informative to see how *PI4KIIIα* depletion affects other PIP_2-dependent events.

In *Drosophila* photoreceptors, the GPCR rhodopsin undergoes clathrin - dependent endocytosis after activation by light (Orem and Dolph, 2002). The endocytosed rhodopsin is transported within the cell body as rhodopsin-loaded-vesicles (RLVs), which are either recycled to the plasma membrane or labelled for degradation (Satoh, 2005). The average number and size of RLVs in the cell body has previously been used in our lab as a readout of endocytosis in photoreceptors (Thakur et al., 2016; Kamalesh et al., 2017). An examination of RLV size and numbers in *GMR > PI4KIIIα*^{i} flies would provide some insight into whether such endocytic processes are affected in these flies or not.

Bibliography

S. S. Balakrishnan, U. Basu, D. Shinde, R. Thakur, M. Jaiswal, and P. Raghu. Regulation of PI4P levels by PI4KIIIα during G-protein-coupled PLC signaling in *Drosophila* photoreceptors. *Journal of Cell Science*, 131(15): jcs217257, Aug. 2018. ISSN 0021-9533, 1477-9137. doi: 10.1242/jcs.217257.

P. Chakrabarti, S. Kolay, S. Yadav, K. Kumari, A. Nair, D. Trivedi, and P. Raghu. A dPIP5K Dependent Pool of Phosphatidylinositol 4,5 Bisphosphate (PIP2) Is Required for G-Protein Coupled Signal Transduction in Drosophila Photoreceptors. *PLOS Genetics*, 11(1):e1004948, Jan. 2015. ISSN 1553-7404. doi: 10.1371/journal.pgen.1004948.

J. Clark, K. E. Anderson, V. Juvin, T. S. Smith, F. Karpe, M. J. O. Wakelam, L. R. Stephens, and P. T. Hawkins. Quantification of $PtdInsP_3$ molecular species in cells and tissues by mass spectrometry. *Nature Methods*, 8(3): 267, Mar. 2011. ISSN 1548-7105. doi: 10.1038/nmeth.1564.

P. Dolph, R. Ranganathan, N. Colley, R. Hardy, M. Socolich, and C. Zuker. Arrestin function in inactivation of G protein-coupled receptor rhodopsin in vivo. *Science*, 260(5116):1910–1916, June 1993. ISSN 0036-8075, 1095-9203. doi: 10.1126/science.8316831.

M. C. Ellis, E. M. O'Neill, and G. M. Rubin. Expression of Drosophila glass protein and evidence for negative regulation of its activity in non-neuronal cells by another DNA-binding protein. *Development*, 119(3):855–865, Nov. 1993. ISSN 0950-1991, 1477-9129.

N. Franceschini, K. Kirschfeld, and B. Minke. Fluorescence of Photoreceptor Cells Observed in vivo. *Science*, 213(4513):1264–1267, 1981.

G. R. V. Hammond, M. P. Machner, and T. Balla. A novel probe for phosphatidylinositol 4-phosphate reveals multiple pools beyond the Golgi. *J Cell Biol*, 205(1):113–126, Apr. 2014. ISSN 0021-9525, 1540-8140. doi: 10.1083/jcb.201312072.

C. Harak, D. Radujkovic, C. Taveneau, S. Reiss, R. Klein, S. Bressanelli, and V. Lohmann. Mapping of Functional Domains of the Lipid Kinase Phosphatidylinositol 4-Kinase Type III Alpha Involved in Enzymatic Activity and Hepatitis C Virus Replication. *Journal of Virology*, 88(17):9909–9926, Jan. 2014. ISSN 0022-538X, 1098-5514. doi: 10.1128/JVI.01063-14.

R. C. Hardie, P. Raghu, S. Moore, M. Juusola, R. A. Baines, and S. T. Sweeney. Calcium Influx via TRP Channels Is Required to Maintain PIP2

Levels in Drosophila Photoreceptors. *Neuron*, 30(1):149–159, Apr. 2001. ISSN 0896-6273. doi: 10.1016/S0896-6273(01)00269-0.

V. Haucke. Phosphoinositide regulation of clathrin-mediated endocytosis. *Biochemical Society Transactions*, 33:5, 2005.

M. Heisenberg. Separation of Receptor and Lamina Potentials in the Electroretinogram of Normal and Mutant Drosophila. *Journal of Experimental Biology*, 55:16, 1971.

Y. Hotta and S. Benzer. Abnormal Electroretinograms in Visual Mutants of Drosophila. *Nature*, 222(5191):354, Apr. 1969. ISSN 1476-4687. doi: 10.1038/222354a0.

K. Kamalesh, D. Trivedi, S. Toscano, S. Sharma, S. Kolay, and P. Raghu. Phosphatidylinositol 5-phosphate 4-kinase regulates early endosomal dynamics during clathrin-mediated endocytosis. *J Cell Sci*, 130(13): 2119–2133, July 2017. ISSN 0021-9533, 1477-9137. doi: 10.1242/jcs.202259.

S. Kolay, U. Basu, and P. Raghu. Control of diverse subcellular processes by a single multi-functional lipid phosphatidylinositol 4,5-bisphosphate [PI(4,5)P2]. *Biochemical Journal*, 473(12):1681–1692, June 2016. ISSN 0264-6021, 1470-8728. doi: 10.1042/BCJ20160069.

M. A. Lemmon. Membrane recognition by phospholipid-binding domains. *Nature Reviews Molecular Cell Biology*, 9(2):99–111, Feb. 2008. ISSN 1471-0072, 1471-0080. doi: 10.1038/nrm2328.

F. Nakatsu, J. M. Baskin, J. Chung, L. B. Tanner, G. Shui, S. Y. Lee, M. Pirruccello, M. Hao, N. T. Ingolia, M. R. Wenk, and P. D. Camilli. PtdIns4P synthesis by PI4KIIIα at the plasma membrane and its impact on plasma membrane identity. *J Cell Biol*, 199(6):1003–1016, Dec. 2012. ISSN 0021-9525, 1540-8140. doi: 10.1083/jcb.201206095.

N. R. Orem and P. J. Dolph. Epitope masking of rhabdomeric rhodopsin during endocytosis- induced retinal degeneration. *Molecular Vision*, page 7, 2002.

A. T. Pagnamenta, M. F. Howard, E. Wisniewski, N. Popitsch, S. J. L. Knight, D. A. Keays, G. Quaghebeur, H. Cox, P. Cox, T. Balla, J. C. Taylor, and U. Kini. Germline recessive mutations in PI4KA are associated with perisylvian polymicrogyria, cerebellar hypoplasia and arthrogryposis. *Human Molecular Genetics*, 24(13):3732–3741, July 2015. ISSN 0964-6906. doi: 10.1093/hmg/ddv117.

A. K. Satoh. Rab11 mediates post-Golgi trafficking of rhodopsin to the photosensitive apical membrane of Drosophila photoreceptors. *Development*, 132(7):1487–1497, Feb. 2005. ISSN 0950-1991, 1477-9129. doi: 10.1242/dev.01704.

W. S. Stark and G. S. Wasserman. Wavelength-specific ERG characteristics of pigmented- and white-eyed strains ofDrosophila. *Journal of Comparative Physiology*, 91(4):427–441, 1974. ISSN 0340-7594, 1432-1351. doi: 10.1007/BF00694472.

W. S. Stark, J. A. Walker, and W. A. Harris. Genetic dissection of the photoreceptor system in the compound eye of *Drosophila melanogaster*. *The Journal of Physiology*, 256(2):415–439, Apr. 1976. ISSN 00223751. doi: 10.1113/jphysiol.1976.sp011331.

R. S. Stowers and T. L. Schwarz. A Genetic Method for Generating Drosophila Eyes Composed Exclusively of Mitotic Clones of a Single Genotype. *Genetics*, 152(4):1631–1639, Aug. 1999. ISSN 0016-6731, 1943-2631.

R. Thakur, A. Panda, E. Coessens, N. Raj, S. Yadav, S. Balakrishnan, Q. Zhang, P. Georgiev, B. Basak, R. Pasricha, M. J. Wakelam, N. T. Ktistakis, and P. Raghu. Phospholipase D activity couples plasma membrane endocytosis with retromer dependent recycling. *eLife*, 5:e18515, Nov. 2016. ISSN 2050-084X. doi: 10.7554/eLife.18515.

J. T. Tóth, G. Gulyás, D. J. Tóth, A. Balla, G. R. V. Hammond, L. Hunyady, T. Balla, and P. Várnai. BRET-monitoring of the dynamic changes of inositol lipid pools in living cells reveals a PKC-dependent PtdIns4P increase upon EGF and M3 receptor activation. *Biochimica et Biophysica Acta (BBA) - Molecular and Cell Biology of Lipids*, 1861(3):177–187, Mar. 2016. ISSN 1388-1981. doi: 10.1016/j.bbalip.2015.12.005.

P. Várnai and T. Balla. Visualization of Phosphoinositides That Bind Pleckstrin Homology Domains: Calcium- and Agonist-induced Dynamic Changes and Relationship to Myo-[3H]inositol-labeled Phosphoinositide Pools. *The Journal of Cell Biology*, 143(2):501–510, Oct. 1998. ISSN 0021-9525, 1540-8140. doi: 10.1083/jcb.143.2.501.

P. Verstreken, T.-W. Koh, K. L. Schulze, R. Zhai, P. Hiesinger, Y. Zhou, S. Q. Mehta, Y. Cao, J. Roos, and H. J. Bellen. Synaptojanin Is Recruited by Endophilin to Promote Synaptic Vesicle Uncoating. *Neuron*, 40(4):733–748, Nov. 2003. ISSN 08966273. doi: 10.1016/S0896-6273(03)00644-5.

S. Yadav, K. Garner, P. Georgiev, M. Li, E. Gomez-Espinosa, A. Panda, S. Mathre, H. Okkenhaug, S. Cockcroft, and P. Raghu. RDGB , a PtdIns-

PtdOH transfer protein, regulates G-protein-coupled PtdIns(4,5)P2 signalling during Drosophila phototransduction. *Journal of Cell Science*, 128 (17):3330–3344, Sept. 2015. ISSN 0021-9533, 1477-9137. doi: 10.1242/jcs.173476.

S. Yamamoto, M. Jaiswal, W.-L. Charng, T. Gambin, E. Karaca, G. Mirzaa, W. Wiszniewski, H. Sandoval, N. A. Haelterman, B. Xiong, K. Zhang, V. Bayat, G. David, T. Li, K. Chen, U. Gala, T. Harel, D. Pehlivan, S. Penney, L. E. Vissers, J. de Ligt, S. N. Jhangiani, Y. Xie, S. H. Tsang, Y. Parman, M. Sivaci, E. Battaloglu, D. Muzny, Y.-W. Wan, Z. Liu, A. T. Lin-Moore, R. D. Clark, C. J. Curry, N. Link, K. L. Schulze, E. Boerwinkle, W. B. Dobyns, R. Allikmets, R. A. Gibbs, R. Chen, J. R. Lupski, M. F. Wangler, and H. J. Bellen. A Drosophila Genetic Resource of Mutants to Study Mechanisms Underlying Human Genetic Diseases. *Cell*, 159(1): 200–214, Sept. 2014. ISSN 00928674. doi: 10.1016/j.cell.2014.09.002.

Y. Yan, N. Denef, C. Tang, and T. Schüpbach. Drosophila PI4KIIIalpha is required in follicle cells for oocyte polarization and Hippo signaling. *Development*, 138(9):1697–1703, May 2011a. ISSN 0950-1991, 1477-9129. doi: 10.1242/dev.059279.

Y. Yan, N. Denef, C. Tang, and T. Schupbach. Drosophila PI4KIIIalpha is required in follicle cells for oocyte polarization and Hippo signaling. *Development*, 138(9):1697–1703, May 2011b. ISSN 0950-1991, 1477-9129. doi: 10.1242/dev.059279.

J. Yoon, H. C. Ben-Ami, Y. S. Hong, S. Park, L. L. R. Strong, J. Bowman, C. Geng, K. Baek, B. Minke, and W. L. Pak. Novel Mechanism of Massive Photoreceptor Degeneration Caused by Mutations in the trp Gene of Drosophila. *J Neuroscience*, page 11, 2000.

J. Yoon, H.-T. Leung, S. Lee, C. Geng, Y. Kim, K. Baek, and W. L. Pak. Specific molecular alterations in the norpA-encoded phospholipase C of Drosophila and their effects on electrophysiological responses in vivo. *Journal of Neurochemistry*, 89(4):998–1008, May 2004. ISSN 1471-4159. doi: 10.1111/j.1471-4159.2004.02384.x.

Chapter 4

Genetic Interaction of *PI4KIIIα* with *rdgB* and *dPIP5K*

4.1 Current models of PIP_2 resynthesis

The biochemical reactions required for PIP_2 resynthesis during *Drosophila* phototransduction have been extensively studied. Over the past few decades nearly all the components involved in the process, both in terms of enzymes and lipid intermediates, have been identified. The current architecture, however, does not account for potential feedbacks or other interactions between components of the cycle (Raghu et al., 2012). It is also assumed to be a closed loop, with no external reactions feeding into the process. Given that PIP_2 resynthesis is very tightly regulated, it is likely that there exists some cross-communication between the different components of the cycle.

In *Drosophila* photoreceptors, the entire PIP_2 resynthesis cycle is distributed over two different membranes - the plasma membrane (rhabdomere) and endoplasmic reticulum [sub-microvillar cisternae (SMC)] **(Fig.1.6)**. Without smooth coordination between these two compartments, the photoreceptors would not have sufficient PIP_2 for a sustained light response. RDGB, the protein that transfers PI from the SMC to the rhabdomere, has long been thought to be the main coordinator between these two organelles by virtue of its biochemical function. Mutants for RDGB have very low light responses and rhabdomeric PIP_2 levels, further lending support to this possibility (Yadav et al., 2015). Apart from the initial supply of PI for PIP_2 synthesis,

there is a second level of coordination required after PIP_2 hydrolysis. DAG generated by the process is converted to PA by a DAG-kinase encoded by the gene *rdgA* (Inoue et al., 1989). PA is then presumably transferred from the rhabdomere to the SMC by a transfer protein, most likely RDGB itself. While RDGB has been shown to bind PA using *in vitro* experiments, we lack conclusive evidence to show that it transfers PA *in vivo* (Yadav et al., 2015). Therefore, although RDGB is a promising candidate for regulating and coordinating the cycle both before and after PIP_2 hydrolysis, we cannot rule out the possibility of other players.

Even though the PIP_2 cycle is driven largely by enzymes, we do not yet have good kinetic information about them when PLC signalling is active. Existing biochemical characterisation studies, although they analyse the steady state turnover of PI4P and PIP_2, do not provide a clear candidate for the rate determining step in the cascade (King et al., 1989). We have some data on genetic interactions that confirm the current model, e.g. double mutants for *rdgB* and *dPIP5K* have a lower light response than either individual mutation (Chakrabarti et al., 2015). Such an additive effect clearly confirms that *rdgB* and *dPIP5K* function along the same pathway. However, there is also evidence to suggest alternate architectures for the cycle. Null mutants for *norpA*, the gene coding for PLC, have virtually no electrical response to light. This phenotype is partially suppressed by null mutants for *rdgA*, with the double mutants displaying a detectable light response (Hardie et al., 2003). This indicates a role for the DAG, which is a substrate for the protein encoded by *rdgA*, in regulating the electrical response to light. Such studies point to as yet uncharacterised cross-talk between elements of the PIP_2 cycle.

Additionally, a recent computational study from the lab has demonstrated that the closed-loop model of PIP_2 resynthesis may not be sufficient to explain all the phenotypes seen in mutants for different components of the cycle (Suratekar et al., 2018). Using mathematical models, the study concluded that the existing model of the PIP_2 cycle needs to be reimagined as an open cycle. For instance, a cycle with a constant external supply of PA to the SMC and a continuous clearing of DAG from the rhabdomere could explain the altered PA levels in loss-of-function mutants for *rdgA* and *laza* (PA-phosphatase) (Suratekar et al., 2018). Similar features, which are not part of conventional models, could help explain the lipid levels in other PIP_2 cycle mutants as well.

With respect to PI4P and PIP_2, the assumed sequence of events is one where RDGB supplies PI to the plasma membrane, where it is converted to PI4P by PI4KIIIα. At the same location, dPIP5K then acts on PI4P and makes PIP_2.

Biochemically, the sequential action of these three proteins is required, but their hierarchy and reaction rates *in vivo* are still unclear. To understand this, we investigated the genetic interactions of *PI4KIIIα* with *rdgB* and *dPIP5K* respectively. Examining the interaction of *PI4KIIIα* with its immediate predecessor and successor in the PIP_2 cycle would provide information about linearity of the reactions.

4.2 Genetic interaction of *PI4KIIIα* with *rdgB*

To study the *in vivo* functions of *rdgB*, a well characterised hypomorphic allele has traditionally been used in the lab. $rdgB^9$ mutants express only ~20% of protein when compared to wild-type flies. Apart from retinal degeneration, these flies display several other phenotypes. $rdgB^9$ flies have highly reduced ERG responses, lacking both the on and off transients. They also have low levels of both PIP and PIP_2, as measured using LC-MS (Section 3.5). Specifically, the rhabdomeric pool of PIP_2 is reduced in these flies, as seen with the PIP_2-binding probe PLCδ-PH:GFP (Yadav et al., 2015).

To assess the nature of the interaction between *rdgB* and *PI4KIIIα*, we knocked down *PI4KIIIα* in $rdgB^9$ photoreceptors and analysed the ERG response of these flies. When both manipulations were done together, we anticipated an additive effect as in the case of $rdgB^9$; $dPIP5K^{18}$ double mutants, where the ERG response was lower than either individual mutation (Chakrabarti et al., 2015). Since *rdgB* supplies the substrate for *PI4KIIIα*, a fly with low expression of both genes would presumably have much less PIP_2 available for signalling than the single manipulations.

One day old $rdgB^9$ flies in which *PI4KIIIα* was knocked down were subjected to 2 s light flashes, where we examined the initial response amplitude as well as the responses to a train of ten light flashes. When we performed the ERGs, the response of $rdgB^9$; $GMR > PI4KIIIα^i$ flies was not as expected. The initial response amplitude was not worse than the individual mutants but rather, similar to that of *PI4KIIIα* knockdown alone **(Fig.4.1A and B)**. Both $GMR > PI4KIIIα^i$ and $rdgB^9$; $GMR > PI4KIIIα^i$ had larger response amplitudes than $rdgB^9$ alone, implying that downregulating *PI4KIIIα* mildly suppresses the ERG phenotype of $rdgB^9$. Additionally, the sequential reduction of ERG amplitude in response to a series of light flashes was seen in $rdgB^9$; $GMR > PI4KIIIα^i$ flies **(Fig.4.1C)**. This second phenotype is absent in $rdgB^9$ flies, suggesting that downregulating *PI4KIIIα* overshadows the ef-

fect of removing rdgB function in photoreceptors. In terms of sensitivity, however, the *rdgB^{9}; GMR > PI4KIIIα^{i}* flies behaved similarly to *rdgB^{9}* flies **(Fig.4.1D)**.

We further explored this interaction by measuring the PIP and PIP_2 levels in *rdgB^{9}; GMR > PI4KIIIα^{i}* flies. Using the LC-MS method standardised earlier (Section 3.5), the amounts of PIP and PIP_2 in light-exposed retinae were quantified. There was a slight change in the MS parameters used in this experiment as compared to the previous one. A second round of parameter optimisation (listed in section 2.5 - QTRAP Parameters Set 2) enabled us to detect the 36:4 acyl species of PIP and PIP_2, which was previously not quantified. An assessment of the relative abundance of the 36:4 species showed that it was almost as abundant as the 36:3 species **(Fig.4.2)**. This led us to include this species in the analysis of lipid levels in subsequent experiments. Prior to extracting the lipids, the flies were reared in dark conditions and subjected to one minute of blue light before processing. There were two major observations made from these experiments. One was that the levels of PIP_2 were much lower in *GMR > PI4KIIIα^{i}* flies than in *rdgB^{9}* flies, but the PIP levels were reduced to similar extents in both genotypes **(Fig.4.3A)**. This was observed despite *rdgB^{9}* being a much stronger allele and having a more severe ERG phenotype. The second observation was that both PIP and PIP_2 levels in *rdgB^{9}; GMR > PI4KIIIα^{i}* flies closely mirrored those of *PI4KIIIα* downregulation alone, which corresponded well with the ERG results **(Fig.4.3B)**.

Given that only the PIP_2 levels reduced to different degrees in *rdgB^{9}* and *GMR > PI4KIIIα^{i}* flies, we examined the ratio of PIP:PIP_2 in these flies. In the control genotype, the ratio of PIP:PIP_2 was close to 0.4, implying that there is roughly 2.5 times more PIP_2 than PIP in the control flies. This ratio was maintained in *rdgB^{9}* mutants. In *GMR > PI4KIIIα^{i}* flies, the ratio of PIP:PIP_2 was increased to one, as was the case in *rdgB^{9}; GMR > PI4KIIIα^{i}* flies **(Fig.4.3C)**. Once again, the evidence pointed to a suppression of *rdgB^{9}* phenotypes by knocking down PI4KIIIα in the background.

Apart from simultaneously reducing the expression of both *rdgB* and *PI4KIIIα*, we checked whether overexpressing *rdgB* could alleviate the effects of downregulating *PI4KIIIα*. The ERG response amplitudes of *GMR > PI4KIIIα^{i}; UAS-rdgB* flies were no different from those of *GMR > PI4KIIIα^{i}* flies **(Fig.4.4A)**. Overexpressing *rdgB* also had no effect on the progressive response reduction phenotype of *GMR > PI4KIIIα^{i}* flies **(Fig.4.4B)**. It appeared that an excess of PI supply could not make up for a reduction in *PI4KIIIα* expression.

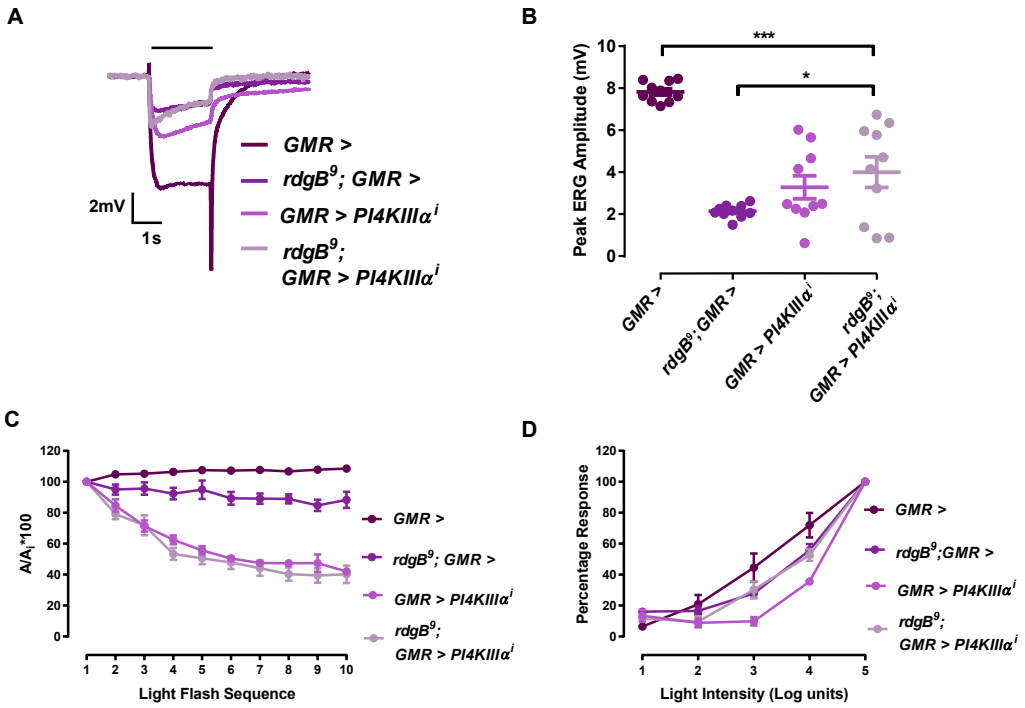

Figure 4.1 : Genetic interaction of *PI4KIIIα* with *rdgB*
(A) Representative ERG traces of listed genotypes. Black bar on top indicates duration of light stimulus; scale bar is shown on bottom left. **(B)** Quantification of the peak ERG amplitude of indicated genotypes. x-axis represents genotype and y-axis represents response amplitude in mV. **(C)** Quantification of the ERG amplitude of indicated genotypes in response to ten consecutive light flashes. x-axis represents the light flash number in the sequence and y-axis represents response amplitude for each light flash normalised to that at the first light flash. **(D)** Quantification of the intensity response function of indicated genotypes. x-axis represents light intensity in log units and y-axis represents the response amplitude at each intensity normalised to that at maximum intensity. * - $p < 0.05$ as per one way ANOVA followed by Tukey's multiple comparison test, values are mean ± s.e.m., n = 8 flies per genotype.

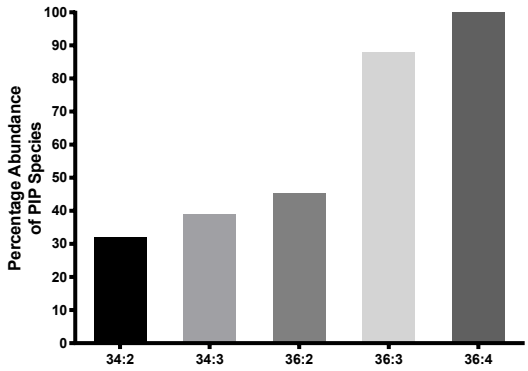

Figure 4.2 : Percentage abundance of acyl chain species
Frequency distribution of different acyl chain species of PIP in *Drosophila* retinae with optimised MS parameters

We also performed a complementary experiment where the human *PI4KIIIα* was overexpressed in the background of $rdgB^9$ mutants. The response amplitude of $rdgB^9$*; GMR > UAS-hPI4KIIIα* flies was slightly larger than $rdgB^9$ flies, indicating that an excess of PI4KIIIα could marginally rescue the effect of removing $rdgB^9$ function **(Fig.4.4C)**. Although the response amplitude was improved by the human *PI4KIIIα*, it had no effect on the reduced sensitivity of $rdgB^9$ flies **(Fig.4.4D)**.

4.3 Genetic interaction of *PI4KIIIα* with *dPIP5K*

The enzyme phosphatidylinositol 4-phosphate 5-kinase (PIP5K) synthesises PIP_2 using PI4P as a substrate. The *Drosophila* genome carries two genes coding for this activity - *dPIP5K* (CG3682) (Chakrabarti et al., 2015) and *sktl* (CG9985) (Hassan et al., 1998). Although both proteins catalyse the same reaction, only *dPIP5K* has been shown to be essential for phototransduction. From previous studies in the lab, *dPIP5K* expression is seen to be enriched in the eyes. A null allele for the gene was generated ($dPIP5K^{18}$), which was found to have low ERG response amplitudes. The mutants also have reduced levels of PIP_2 and higher levels of PIP than controls, as measured using LC-MS (Section 3.5). In contrast, hypomorphs for *sktl* do not have any impact on the light response. However, null mutants for *sktl* are cell lethal, implying that the PIP_2 produced by each enzyme feeds into different

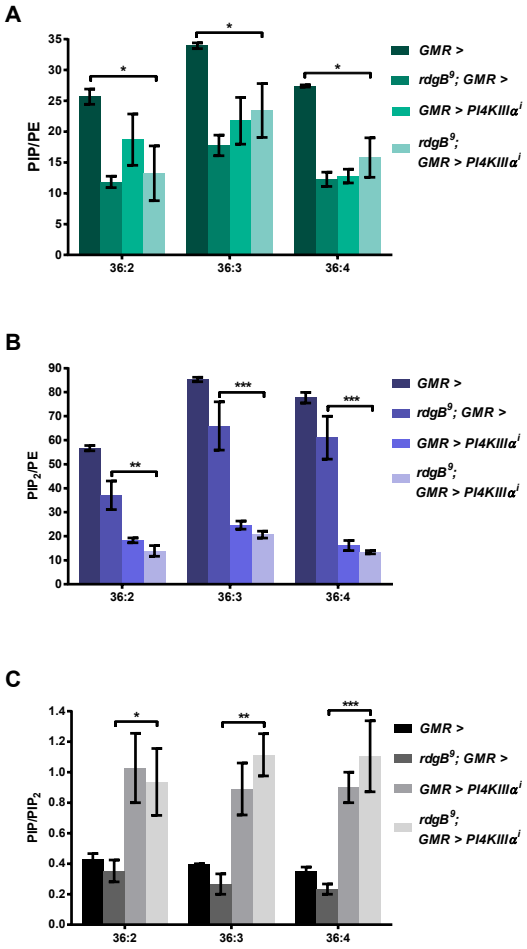

Figure 4.3 : LC-MS measurement of PIP and PIP_2 levels in *$rdgB^9$; $GMR > PI4KIII\alpha^i$* flies

(A) and (B) Liquid chromatography-mass spectrometry measurement of PIP and PIP_2 levels in retinae of one-day old flies of the indicated genotypes. The flies were reared in dark and exposed to one minute of blue light before processing. The lipid levels for the three most abundant acyl chain species (36:2, 36:3 and 36:4) are shown here. x-axis represents acyl chain species; y-axis represents ratio of PIP/PE and PIP_2/PE. **(C)** To highlight the effect of knocking down *PI4KIIIα* on the relative levels of lipids, we took a ratio of the PIP levels to PIP_2 levels in the tested genotypes. The x-axis represents acyl chain species; y-axis represents the ratio of PIP:PIP_2. * - $p < 0.05$ as per two way ANOVA followed by Tukey's multiple comparison test, values are mean ± s.e.m.

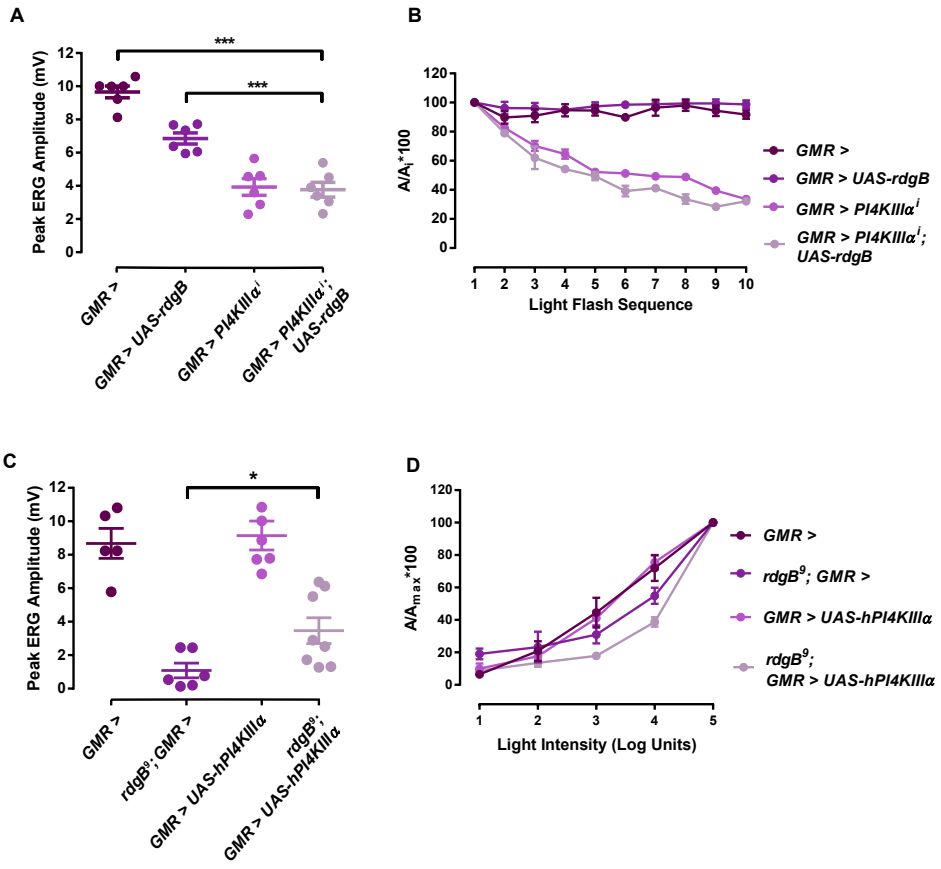

Figure 4.4 : Genetic interaction of *PI4KIIIα* with *rdgB*
(A) Quantification of the peak ERG amplitude of indicated genotypes. x-axis represents genotype and y-axis represents response amplitude in mV. **(B)** Quantification of the ERG amplitude of indicated genotypes in response to ten consecutive light flashes. x-axis represents the light flash number in the sequence and y-axis represents response amplitude for each light flash normalised to that at the first light flash. **(C)** Quantification of the peak ERG amplitude of indicated genotypes. x-axis represents genotype and y-axis represents response amplitude in mV. **(D)** Quantification of the intensity response function of indicated genotypes. x-axis represents light intensity in log units and y-axis represents the response amplitude at each intensity normalised to that at maximum intensity. * - $p < 0.05$ as per one way ANOVA followed by Tukey's multiple comparison test, values are mean ± s.e.m., n = 6 flies per genotype.

cellular functions (Chakrabarti et al., 2015).

In order to investigate the genetic interaction of *dPIP5K* and *PI4KIIIα*, we downregulated *PI4KIIIα* in the background of the $dPIP5K^{18}$ mutant. Since PI4KIIIα synthesises the substrate for dPIP5K, we anticipated that the double manipulation would drastically reduce the levels of PIP_2 available for signalling. We performed ERGs on these flies and examined the initial response amplitude as well as the responses to a train of ten light flashes. We found that the initial response amplitude was indeed lower than either the $dPIP5K^{18}$ mutant or *PI4KIIIα* knockdown alone **(Fig.4.5A and B)**. The progressive reduction in response amplitude that was seen in *GMR > PI4KIIIα*^{i} flies was also present when *PI4KIIIα* was knocked down in the $dPIP5K^{18}$ background **(Fig.4.5C)**. This implied that removing both *PI4KIIIα* and *dPIP5K* had an additive effect on the ERG response amplitude, but not on the ability to sustain the response, where the effect of knocking down *PI4KIIIα* was dominant.

Both PI4KIIIα and dPIP5K directly regulate the levels of PI4P and PIP_2 in photoreceptors and hence, we measured the levels of these lipids in flies where both genes were manipulated. Prior to extracting the lipids, the flies were reared in dark conditions and subjected to one minute of blue light before processing. We saw that the $dPIP5K^{18}$ mutants have higher PIP levels than control flies as there is reduced conversion of PI4P to PIP_2 in this condition. Conversely, *GMR > PI4KIIIα*^{i} flies have reduced PIP levels since this enzyme makes PI4P. Given that both enzymes have antagonistic functions with respect to PI4P, it was possible that reducing PI4KIIIα levels in the background of $dPIP5K^{18}$ could balance the PIP levels and restore them to those of controls. When we measured the PIP levels in $dPIP5K^{18}$; *GMR > PI4KIIIα*^{i} flies, we saw that they were lower than controls and nearly identical to those of *GMR > PI4KIIIα*^{i} flies **(Fig.4.6A)**. This implied that the effect of downregulating *PI4KIIIα* has a stronger effect on PIP levels than removing *dPIP5K*.

We observed a similar effect on the levels of PIP_2 in $dPIP5K^{18}$*; GMR > PI4KIIIα*^{i} flies. *GMR > PI4KIIIα*^{i} flies have lower PIP_2 levels than $dPIP5K^{18}$ mutants, which in turn are lower than control flies (Section 3.5). In flies where both genes were manipulated, we found that the levels of PIP_2 closely resembled those seen in *GMR > PI4KIIIα*^{i} flies **(Fig.4.6B)**. Therefore, knocking down *PI4KIIIα* has a more acute effect on lipid levels in photoreceptors than removing *dPIP5K*.

Since downregulating *PI4KIIIα* reduces but does not completely remove PI4P from the rhabdomere, we checked whether overexpressing *dPIP5K* in

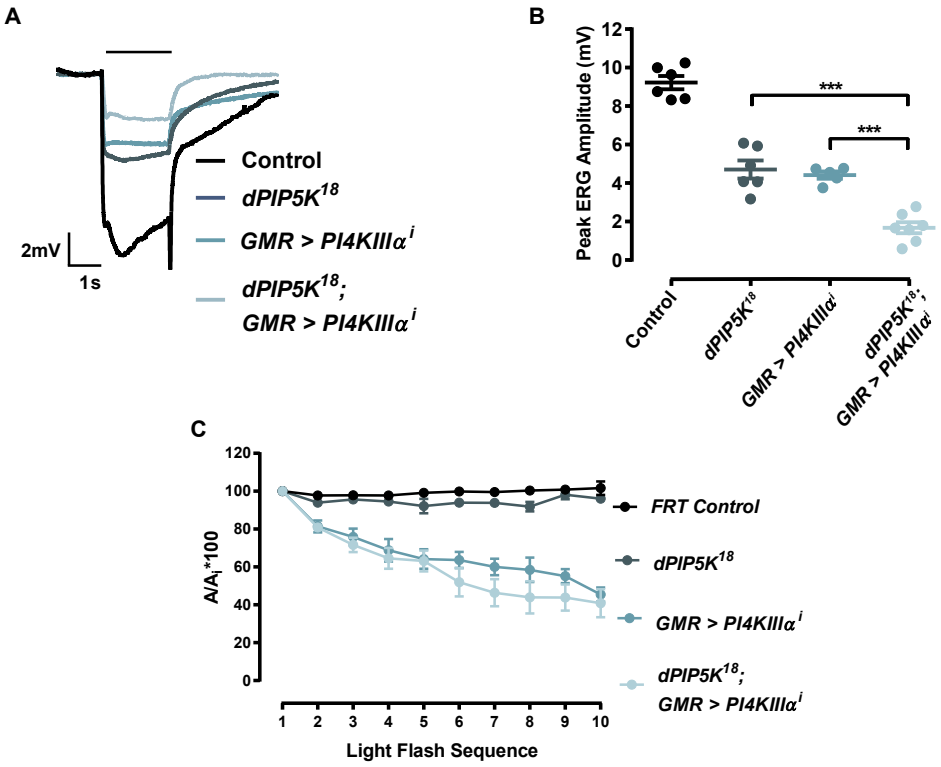

Figure 4.5 : Genetic interaction of *PI4KIIIα* with *dPIP5K*
(A) Representative ERG traces of listed genotypes. Black bar on top indicates duration of light stimulus; scale bar is shown on bottom left. **(B)** Quantification of the peak ERG amplitude of indicated genotypes. x-axis represents genotype and y-axis represents response amplitude in mV. **(C)** Quantification of the ERG amplitude of indicated genotypes in response to ten consecutive light flashes. x-axis represents the light flash number in the sequence and y-axis represents response amplitude for each light flash normalised to that at the first light flash. * - $p < 0.05$ as per one way ANOVA followed by Tukey's multiple comparison test, values are mean ± s.e.m., n = 6 flies per genotype.

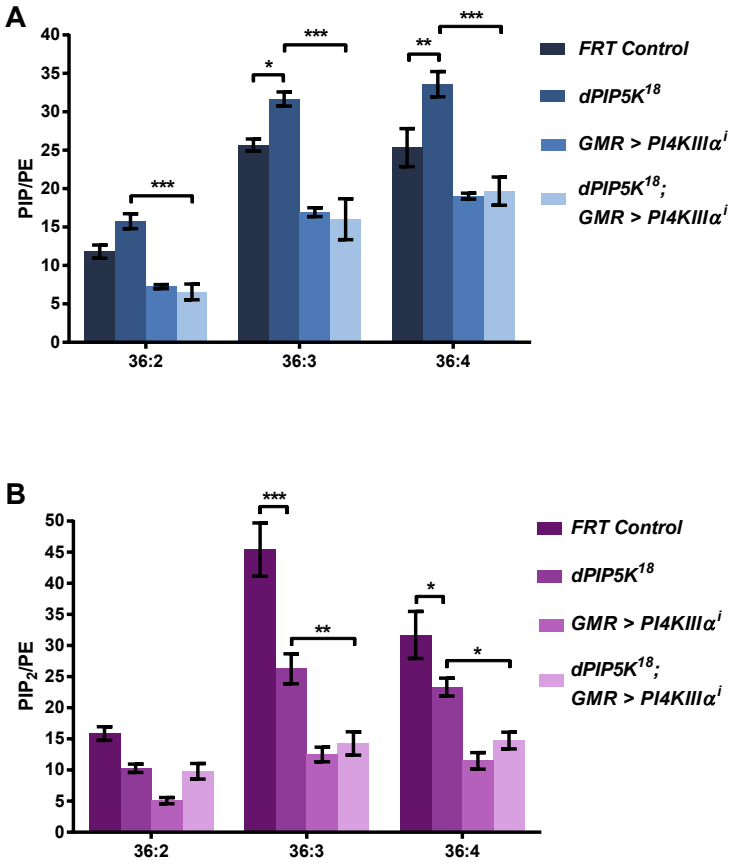

Figure 4.6 : LC-MS measurement of PIP and PIP_2 levels in *dPIP5K^{18}; GMR > PI4KIIIα^i* flies

(A) and (B) Liquid chromatography-mass spectrometry measurement of PIP (**A**) and PIP_2 (**B**) levels in retinae of one-day old flies of the indicated genotypes. The flies were reared in dark and exposed to one minute of blue light before processing. The lipid levels for the three most abundant acyl chain species (36:2, 36:3 and 36:4) are shown here. x-axis represents acyl chain species; y-axis represents ratio of PIP/PE and PIP_2/PE. * - $p < 0.05$ as per two way ANOVA followed by Tukey's multiple comparison test, values are mean ± s.e.m., n = 25 retinae per sample.

the background of *GMR > PI4KIIIα^{i}* could improve the ERG response. The response amplitude of *GMR > PI4KIIIα^{i}, UAS-dPIP5K* flies was no different from that of *GMR > PI4KIIIα^{i}* flies **(Fig.4.7A)**, implying that higher expression of *dPIP5K* could not improve the reduced ERG response of *GMR > PI4KIIIα^{i}* flies. *UAS-dPIP5K* also had no effect on the progressive reduction in response amplitude phenotype **(Fig.4.7B)**, which remained identical to that of *GMR > PI4KIIIα^{i}* flies.

Even though *dPIP5K* appears to be the main source of PIP_2 in rhabdomeres, the mutants still have an ERG response, albeit lower than control flies. This residual PIP_2 is probably synthesised by *sktl*, the other PIP5K in *Drosophila*. If *sktl* works as a low efficiency PIP5K in rhabdomeres, increasing the amount of substrate (PI4P) might raise the amount of PIP_2 at the membrane. To investigate this possibility, we overexpressed the human *PI4KIIIα* in the background of *dPIP5K^{18}*. We found that the human *PI4KIIIα* was able to marginally increase the ERG response amplitude of *dPIP5K^{18}* mutants **(Fig.4.7C)**. The effect, although small, was consistent across experimental replicates and statistically significant. This implied that an overabundance of *PI4KIIIα* could, to a minor extent, compensate for the lack of dPIP5K activity. While the human PI4KIIIα had a small impact on the response amplitude, it could not improve the reduced light sensitivity of *dPIP5K^{18}* mutants **(Fig.4.7D)**.

4.4 Conclusion

The architecture of the PIP_2 cycle in *Drosophila* photoreceptors has conventionally been regarded as a closed cycle with no discernible interactions between its components. A lack of information regarding in vivo enzyme kinetics has also restricted interpretations regarding the rate determining steps in the cycle. By investigating the nature of genetic interactions between *rdgB*, *PI4KIIIα* and *dPIP5K*, we have attempted to gain some insight into these questions.

4.4.1 Main Conclusions

The RDGB protein supplies PI at the rhabdomere for PI4KIIIα to act on. Hypomorphic mutants for *rdgB* have well characterised ERG defects and reduced levels of PIP_2 at the plasma membrane. When we knocked down *PI4KIIIα* in this background, we found that there was a mild suppression of the *rdgB^{9}* mutant phenotype. Despite *rdgB* functioning upstream of *PI4KIIIα* biochemically, the ERG phenotype of *PI4KIIIα* downregulation

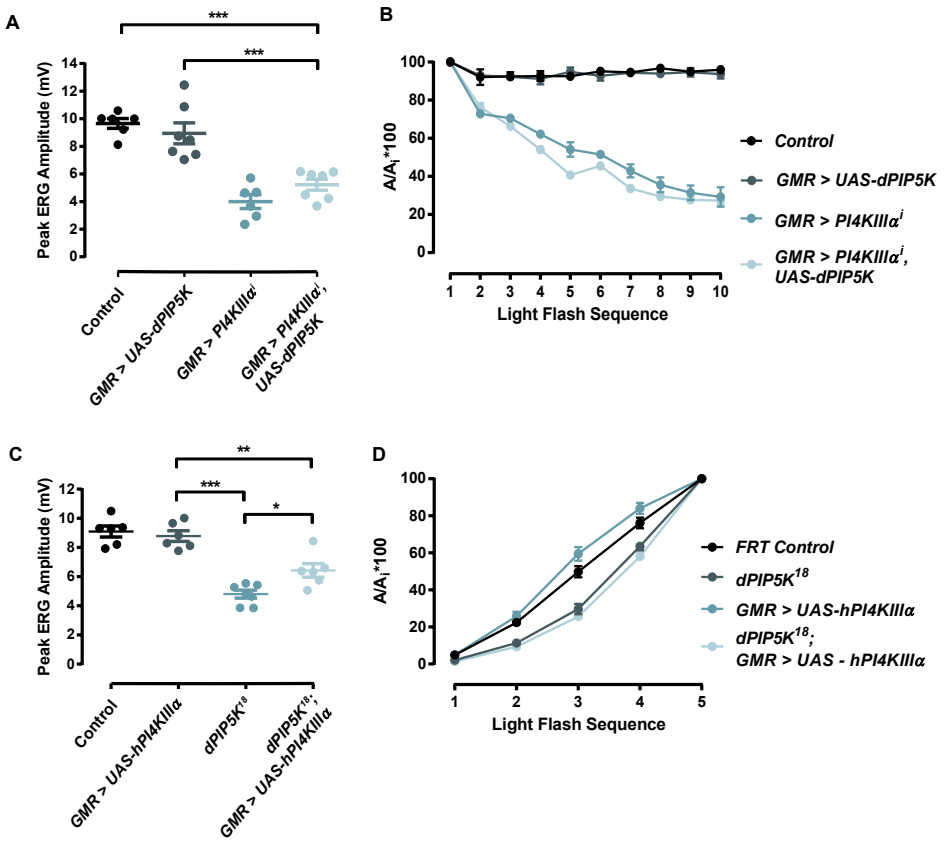

Figure 4.7 : Genetic interaction of *PI4KIIIα* with *dPIP5K*
(A) Quantification of the peak ERG amplitude of indicated genotypes. x-axis represents genotype and y-axis represents response amplitude in mV. **(B)** Quantification of the ERG amplitude of indicated genotypes in response to ten consecutive light flashes. x-axis represents the light flash number in the sequence and y-axis represents response amplitude for each light flash normalised to that at the first light flash. **(C)** Quantification of the peak ERG amplitude of indicated genotypes. x-axis represents genotype and y-axis represents response amplitude in mV. **(D)** Quantification of the intensity response function of indicated genotypes. x-axis represents light intensity in log units and y-axis represents the response amplitude at each intensity normalised to that at maximum intensity. * - $p < 0.05$ as per one way ANOVA followed by Tukey's multiple comparison test, values are mean $\pm$ s.e.m., n = 6 flies per genotype.

and not $rdgB^9$ was dominant. This effect was mirrored in the photoreceptor lipid levels of $rdgB^9$; $GMR > PI4KIII\alpha^i$ flies as well. Both PIP and PIP_2 levels in these flies resembled those of $GMR > PI4KIII\alpha^i$ flies and not those of $rdgB^9$ mutants.

The reduced ERG response of $rdgB^9$ mutants was also slightly alleviated by overexpressing the human $PI4KIII\alpha$ in the background. In effect, the response amplitude of these flies was higher than those of $rdgB^9$ flies, but still lower than those of controls.

The enzyme dPIP5K synthesises PIP_2 at the rhabdomere. The null mutants have low ERG response amplitudes, along with reduced rhabdomeral PIP_2 levels. Knocking down $PI4KIII\alpha$ in this background had an additive effect on the ERG response, with the amplitude being lower than either of the individual manipulations. The lipid levels in the retinae of these flies, however, did not show a similar trend. The $dPIP5K^{18}, GMR > PI4KIII\alpha^i$ flies had reduced PIP and PIP_2 levels, closely mirroring those of $GMR > PI4KIII\alpha^i$ flies. Additionally, overexpressing the human $PI4KIII\alpha$ in the background of $dPIP5K^{18}$ mutants could marginally suppress the reduced ERG response amplitude of $dPIP5K^{18}$ flies.

4.4.2 Molecular basis for ERG phenotypes

The classical model of PIP_2 resynthesis considers *rdgB* to be a key regulator and coordinator of the cycle. This is primarily because, as a transfer protein, RDGB is essential for the cycle to proceed across the rhabdomere and the SMC (Cockcroft and Raghu, 2016). Given that removing *rdgB* has dramatic structural and functional effects on photoreceptors, it emerged as a prime candidate for determining the rate of the cycle. This was further enforced by the additive effect seen in double mutants for *rdgB* and *dPIP5K* (Chakrabarti et al., 2015).

The suppression of $rdgB^9$ phenotypes by $PI4KIII\alpha$ knockdown runs contrary to this hypothesis. If *rdgB* is in fact the rate determining step in the cycle, then removing any components further downstream would only worsen the phenotype and not improve it. The fact that removing $PI4KIII\alpha$ increased the ERG response of $rdgB^9$ mutants strongly indicates that the reaction catalysed by PI4KIIIα might be more significant in regulating the PIP_2 cycle. In terms of the lipid levels, $PI4KIII\alpha$ downregulation was dominant over the effect of *rdgB* mutation, implying that the rates of lipid synthesis might also be limited by the activity of $PI4KIII\alpha$. This effect was also seen when $PI4KIII\alpha$ was knocked down in the background of $dPIP5K^{18}$ mutants, despite

dPIP5K^{18} being a complete null allele.

With respect to the ERG response, *PI4KIIIα* and *dPIP5K* appear to function in a linear manner. This clearly suggests that *PI4KIIIα* functions upstream of *dPIP5K*, as reflected in the lipid measurements. The ERG response of the doubly manipulated flies showed an additive effect, indicating that limiting the substrate, along with lack of PIP_2 production, severely reduces the signalling efficiency of the photoreceptors.

4.4.3 Unaddressed questions

The above experiments, while shedding some light on the nature of genetic interactions, still do not clearly highlight the hierarchy of the three genes under investigation. One major reason for this is nature of alleles used for each gene. The *rdgB* mutant is a strong hypomorph, whereas *dPIP5K*^{18} is a complete null allele. The *PI4KIIIα* manipulations have been performed using RNAi, which reduces the transcript by 60%. The interactions observed between *PI4KIIIα* and the other two mutants are a reflection not only of RNAi depletion but of the remaining functional protein in the cells as well. Ideally, such experiments would be performed with complete null alleles of all the genes in question, but given the lethality associated with deleting *PI4KIIIα*, RNAi was the best solution we had at hand. Further experiments using the point mutant allele of *PI4KIIIα* (Section 3.4) would go towards addressing the shortcomings of RNAi knockdowns.

In addition to *dPIP5K*, the *Drosophila* genome also encodes a second PIP5K known as *skittles*. *sktl* is known to be required for maintaining the PIP_2 pool that feeds into housekeeping functions of the cell, such as cytoskeletal regulation and endocytosis (Hassan et al., 1998). There is a possibility that the residual ERG response seen in *dPIP5K*^{18} mutants is due to *sktl* activity. Intriguingly, loss-of-function alleles of *sktl* do not show any ERG defects, nor do they seem to affect the rates of PIP_2 resynthesis when observed using PIP_2-specific probes (Liu et al., 2018; Chakrabarti et al., 2015). However, given that deletion of *sktl* results in cell lethality, it is currently not possible to evaluate the photoresponse in the complete absence of the gene. One could, however, investigate the interactions of the hypomorphic alleles with *PI4KIIIα* to potentially delineate the contributions coming from each PIP5K towards phototransduction.

We have also not investigated how the localisation of either RDGB or dPIP5K is affected when *PI4KIIIα* is knocked down in otherwise wild-type flies. In mammalian systems, it has been shown that knocking out *PI4KIIIα* results in

the misolocalisation of several plasma-membrane resident proteins (Nakatsu et al., 2012). If any phosphoinositide signatures are required for the presence of dPIP5K at the plasma membrane, there is a possibility that knocking down *PI4KIIIα* might disrupt dPIP5K localisation by perturbing the phosphoinositide cues.

Bibliography

P. Chakrabarti, S. Kolay, S. Yadav, K. Kumari, A. Nair, D. Trivedi, and P. Raghu. A dPIP5K Dependent Pool of Phosphatidylinositol 4,5 Bisphosphate (PIP2) Is Required for G-Protein Coupled Signal Transduction in Drosophila Photoreceptors. *PLOS Genetics*, 11(1):e1004948, Jan. 2015. ISSN 1553-7404. doi: 10.1371/journal.pgen.1004948.

S. Cockcroft and P. Raghu. Topological organisation of the phosphatidylinositol 4,5-bisphosphate–phospholipase C resynthesis cycle: PITPs bridge the ER–PM gap. *Biochemical Journal*, 473(23):4289–4310, Dec. 2016. ISSN 0264-6021, 1470-8728. doi: 10.1042/BCJ20160514C.

R. C. Hardie, F. Martin, S. Chyb, and P. Raghu. Rescue of Light Responses in the Drosophila "Null" Phospholipase C Mutant, norpAP24, by the Diacylglycerol Kinase Mutant, rdgA, and by Metabolic Inhibition. *Journal of Biological Chemistry*, 278(21):18851–18858, May 2003. ISSN 0021-9258, 1083-351X. doi: 10.1074/jbc.M300310200.

B. A. Hassan, S. N. Prokopenko, S. Breuer, B. Zhang, A. Paululat, and H. J. Bellen. Skittles, a Drosophila Phosphatidylinositol 4-Phosphate 5-Kinase, Is Required for Cell Viability, Germline Development and Bristle Morphology, But Not for Neurotransmitter Release. *Genetics*, 150(4):1527–1537, Dec. 1998. ISSN 0016-6731, 1943-2631.

H. Inoue, T. Yoshioka, and Y. Hotta. Diacylglycerol Kinase Defect in a Drosophila Retinal Degeneration Mutant rdgA. *Journal of Biological Chemistry*, 264(10):5996–6000, 1989.

C. E. King, P. T. Hawkins, L. R. Stephens, and R. H. Michell. Determination of the steady-state turnover rates of the metabolically active pools of phosphatidylinositol 4-phosphate and phosphatidylinositol 4,5-bisphosphate in human erythrocytes. *Biochemical Journal*, 259(3):893–896, May 1989. ISSN 0264-6021, 1470-8728. doi: 10.1042/bj2590893.

C.-H. Liu, M. K. Bollepalli, S. V. Long, S. Asteriti, J. Tan, J. A. Brill, and R. C. Hardie. Genetic dissection of the phophoinositide cycle in Drosophila photoreceptors. *Journal of Cell Science*, 131(8):35, 2018. doi: jcs214478.

F. Nakatsu, J. M. Baskin, J. Chung, L. B. Tanner, G. Shui, S. Y. Lee, M. Pirruccello, M. Hao, N. T. Ingolia, M. R. Wenk, and P. D. Camilli. PtdIns4P synthesis by PI4KIIIα at the plasma membrane and its impact on plasma membrane identity. *J Cell Biol*, 199(6):1003–1016, Dec. 2012. ISSN 0021-9525, 1540-8140. doi: 10.1083/jcb.201206095.

P. Raghu, S. Yadav, and N. B. N. Mallampati. Lipid signaling in Drosophila photoreceptors. *Biochimica et Biophysica Acta (BBA) - Molecular and Cell Biology of Lipids*, 1821(8):1154–1165, Aug. 2012. ISSN 1388-1981. doi: 10.1016/j.bbalip.2012.03.008.

R. Suratekar, A. Panda, P. Raghu, and S. Krishna. Evidence of sinks and sources in the phospholipase C-activated PIP $_2$ cycle. *FEBS Letters*, 592 (6):962–972, Mar. 2018. ISSN 00145793. doi: 10.1002/1873-3468.12998.

S. Yadav, K. Garner, P. Georgiev, M. Li, E. Gomez-Espinosa, A. Panda, S. Mathre, H. Okkenhaug, S. Cockcroft, and P. Raghu. RDGB , a PtdIns-PtdOH transfer protein, regulates G-protein-coupled PtdIns(4,5)P2 signalling during Drosophila phototransduction. *Journal of Cell Science*, 128 (17):3330–3344, Sept. 2015. ISSN 0021-9533, 1477-9137. doi: 10.1242/jcs.173476.

Chapter 5

stmA and *TTC7* are Required to Support *Drosophila* Phototransduction

5.1 *stmA* downregulation has characteristic ERG phenotypes

The protein eighty-five requiring 3 (Efr3) has been shown in other model systems to interact with PI4KIIIα and recruit it to the plasma membrane, where it produces PI4P (Nakatsu et al., 2012; Wu et al., 2014). The Efr3 orthologue in *Drosophila* is encoded by the gene *stmA* (CG8739). Having shown a role for PI4KIIIα in regulating phototransduction, we next tested whether Efr3 was also required for this function.

We first obtained RNAi lines against *stmA* from the VDRC and Bloomington stock centres (listed in Table 2). The constructs were expressed in photoreceptors using Rh1Gal4, along with UAS-Dicer2, and ERGs were performed on these flies. While we observed slight variations in the response amplitudes and transients, they were not significantly different from those of control flies **(Fig.5.1A)**. Knocking down *stmA* using *Rh1Gal4; UAS-Dcr2* did not display any gross ERG defects.

We then used GMRGal4, which is a stronger driver. We expressed all the previous RNAi constructs using GMRGal4 and performed ERGs on one-day old flies. As observed previously, different RNAi lines had different effects on the ERG response. One line had a slightly reduced response amplitude

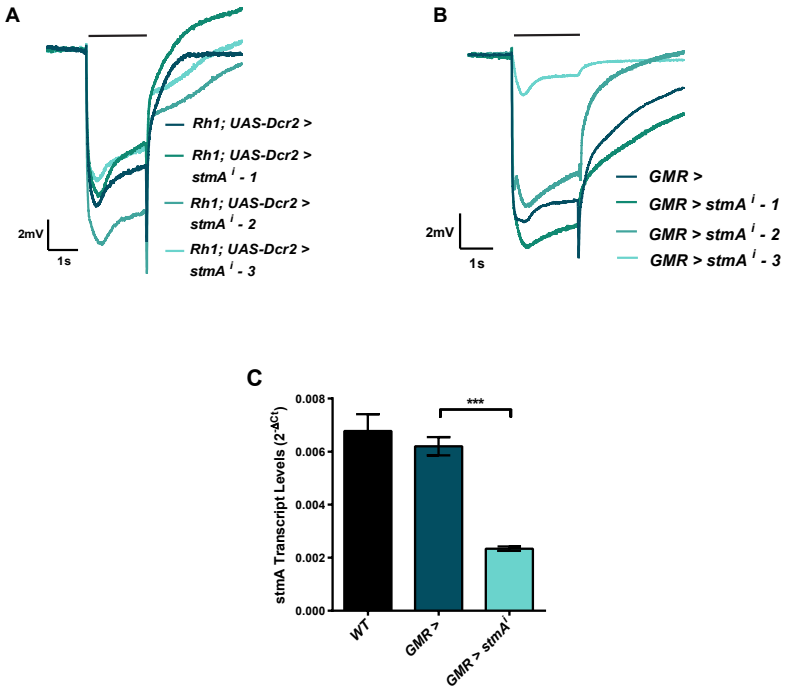

Figure 5.1 : Knocking down *stmA* in photoreceptors reduces the ERG response amplitude
(A) Knocking down *stmA* using Rh1; UAS-Dcr2 does not significantly impact the ERG response when compared to control flies. **(B)** Knocking down *stmA* using GMRGal4 significantly reduces ERG response in one of the RNAi lines tested when compared to control flies. **(C)** The level of transcript knockdown in retinae as estimated using Q-PCR has been shown. The x-axis represents the genotype of the source tissue; y-axis represents $2^{-\Delta C_t}$ values for the described gene. *** - $p < 0.001$ as per two-tailed t-test, values are mean $\pm$ s.e.m., n = 75 retinae per sample.

whereas the another had a normal response amplitude but had a slightly smaller "off" transient. Overall, the ERG responses of these lines were normal and did not have any notable defects. One line, however, had a highly reduced response amplitude when compared to controls. The ERG amplitude of these flies was only about a quarter of that of control flies **(Fig.5.1B and 5.2B)**. They also lacked both "on" and "off" transients, but that could also be attributed to the low amplitude itself. When we performed qPCRs from these retinae, we found that the *stmA* transcript was knocked down by ~60% using this RNAi line **(Fig.5.1C)**. Therefore, for all further experiments, the Bloomington TRiP line #39062 was used to downregulate *stmA* in photoreceptors, using GMRGal4.

Another key ERG phenotype seen upon knocking down *stmA* was a progressive reduction in amplitude when exposed to ten sequential light flashes. When subjected to a train of ten light flashes, the response amplitude of $GMR > stmA^{i}$ flies decreased with each subsequent flash, whereas the amplitude of control flies remained constant for every light flash **(Fig.5.2A-C)**. Additionally, when we examined the intensity response curve, the signalling sensitivity of $GMR > stmA^{i}$ flies was found to be lower than that of control flies **(Fig.5.2D)**.

The overall ERG phenotypes of $GMR > stmA^{i}$ flies was identical to those of $GMR > PI4KIII\alpha^{i}$ flies. The fact that knocking down both *PI4KIIIα* and *stmA* in photoreceptors produced identical effects on the ERG response pointed to a link between the two components.

In order to check whether the ERG defects of $GMR > stmA^{i}$ flies was purely due to the knockdown of *stmA* and not off-target effects, we expressed a mouse *mEfr3B* construct in the background of the RNAi **(Fig.5.3A)**. The mouse *mEfr3B* was placed downstream of a UAS promoter and transgenic flies expressing this construct were made. The amplitude of $GMR > stmA^{i}$*;UAS-mEfr3B* flies was not comparable to that of control flies, but it was markedly higher than that of $GMR > stmA^{i}$ flies **(Fig.5.3B and C)**. When subjected to a light train, the $GMR > stmA^{i}$*;UAS-mEfr3B* flies still exhibited a progressive decrease in response amplitude, but the extent of decrease was lower than that of $GMR > stmA^{i}$ flies**(Fig.5.3D)**. The light sensitivity of $GMR > stmA^{i}$*;UAS-mEfr3B* flies, however, were comparable to that of $GMR > stmA^{i}$ flies, indicating that the mouse construct could not rescue the reduced sensitivity of $GMR > stmA^{i}$ flies**(Fig.5.3E)**. Overall, the *mEfr3B* construct was able to partially rescue the ERG defects of $GMR > stmA^{i}$ flies, implying that off-target effects of the RNAi were unlikely.

We further tested whether the ERG phenotypes of $GMR > stmA^{i}$ flies arose

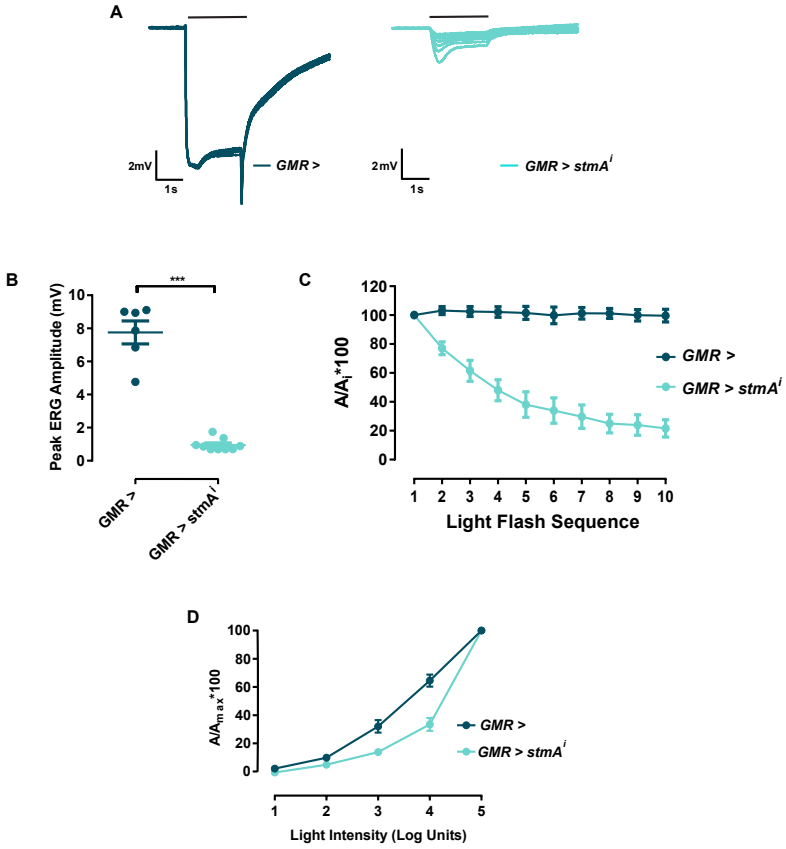

Figure 5.2 : ERG phenotypes of *GMR > stmA^i* flies
(A) Representative ERG amplitudes of control flies (dark coloured) and *GMR > stmA^i* flies (light coloured) in response to ten consecutive flashes of light. The black bar on top indicates duration of the light stimulus, scale bar is on the bottom left. **(B)** Quantification of the peak ERG amplitude of control and *GMR > stmA^i* flies. x-axis represents genotype and y-axis represents response amplitude in mV. **(C)** Quantification of the ERG amplitude of control and *GMR > stmA^i* flies in response to ten consecutive light flashes. x-axis represents the light flash number and y-axis represents response amplitude for each light flash normalised to that at the first light flash. **(D)** Intensity response function of control and *GMR > stmA^i* flies. x-axis represents light intensity in log units and y-axis represents the response amplitude at each intensity normalised to that at maximum intensity. * - $p < 0.05$ as per two-tailed t-test, values are mean ± s.e.m., n = 7 flies per genotype.

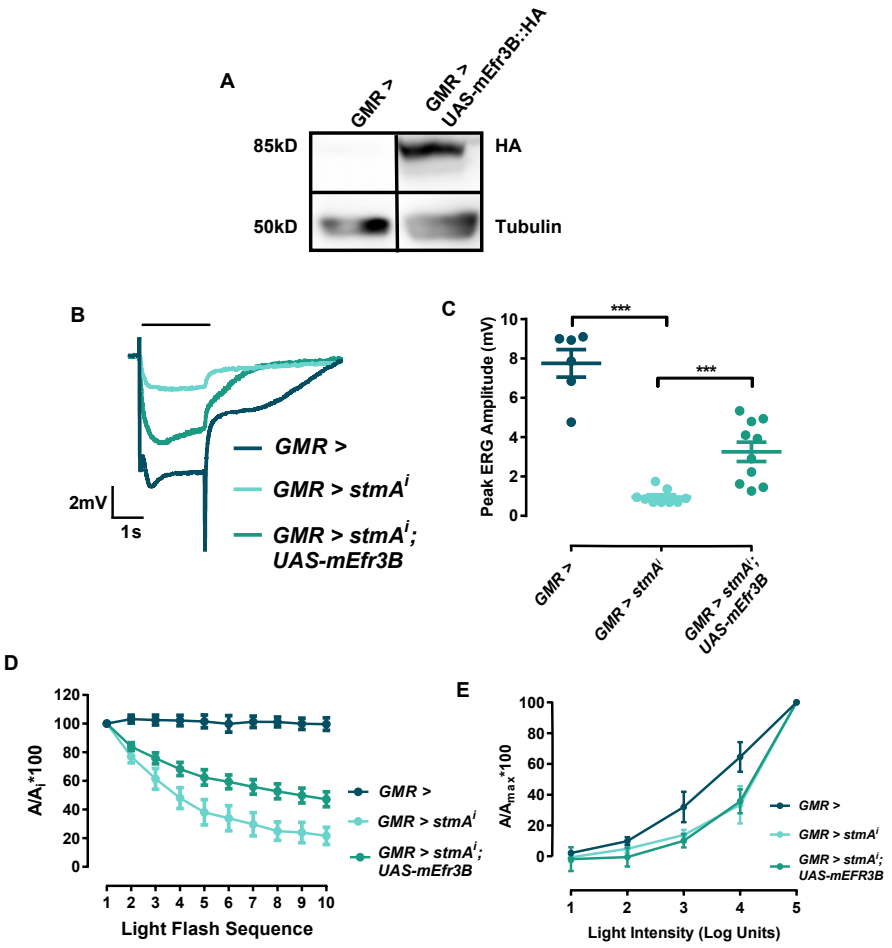

Figure 5.3 : Rescue of ERG phenotypes of *GMR > stmA^i* flies by mEfr3B

(A) Western blot showing the expression of HA-tagged mEfrB, driven using GMRGal4. **(B)** Representative ERG amplitudes of flies of indicated genotypes. The black bar on top indicates duration of the light stimulus, scale bar is on the bottom left. **(C)** Quantification of the peak ERG amplitude of flies of indicated genotypes. x-axis represents genotype and y-axis represents response amplitude in mV. **(D)** Quantification of the ERG amplitude of flies of indicated genotypes in response to ten consecutive light flashes. x-axis represents the light flash number and y-axis represents response amplitude for each light flash normalised to that at the first light flash. **(E)** Intensity response function of flies of indicated genotypes. x-axis represents light intensity in log units and y-axis represents the response amplitude at each intensity normalised to that at maximum intensity. * - $p < 0.05$ as one way ANOVA followed by Tukey's multiple comparison test, values are mean ± s.e.m., n = 8 flies per genotype.

due to altered expression of any key phototransduction proteins. We found that the levels of Rh1, PLC, TRP, INAD and dPIP5K in $GMR > stmA^i$ flies were similar to those of control flies **(Fig.5.4A-E)**. The only component which was affected was Gq_α, whose expression was reduced in $GMR > stmA^i$ flies**(Fig.5.4F)**. When we analysed the transcript levels of Gq_α in these flies, we found that the expression was identical in both control and $GMR > stmA^i$ flies **(Fig.5.4H)**, implying that the reduction in protein levels was not due to lower gene expression. While it is possible that this contributes to the ERG phenotype, it is important to note that Gq_α levels are normal in $GMR > PI4KIII\alpha^i$ flies **(Fig.3.11B)**. Despite the differences in Gq_α levels, the ERG defects of both $GMR > PI4KIII\alpha^i$ and $GMR >$ flies are the same, indicating a Gq_α independent mechanism behind the ERG phenotype.

5.2 A temperature-sensitive allele of *stmA* has a minimal photoresponse

Downregulation of *stmA* using GMRGal4 has a clear effect on phototransduction, as demonstrated in the previous section. The GMRGal4 driver is expressed from the late third instar larval stage and lasts throughout eye development (Ellis et al., 1993). This raises the possibility that the ERG defects seen in $GMR > stmA^i$ flies are due to developmental defects caused by reduced *stmA* transcript levels. In order to distinguish the role of *stmA* during development and adulthood, we turned to temperature sensitive mutant alleles of *stmA*. These mutants carry alleles of the gene that are fully functional as long as the fly is maintained at a permissive temperature (usually 25° C) and are only non-functional when placed at a restrictive temperature (usually 35-38° C) (Chandrashekaran and Sarla, 1993).

The *stmA* mutants were first isolated in 1985 in a screen of temperature-sensitive paralytic mutants on the second chromosome (Shyngle and Sharma, 1985). They undergo paralysis at the restrictive temperature (38° C), but are completely normal at the permissive temperature (25° C). This enables selective deactivation of *stmA* for small periods of time, ensuring that the gene is expressed normally during growth and eliminating any developmental effects. We obtained three well-characterised temperature sensitive (ts) alleles of *stmA* ($stmA^1$, $stmA^2$ and $stmA^{18\text{-}2}/CyO$) from the Bloomington stock centre. These specific alleles had been previously shown to have ERG defects when placed at 38° C (Huang et al., 2004).

In order to check whether *stmA* function is required during development for

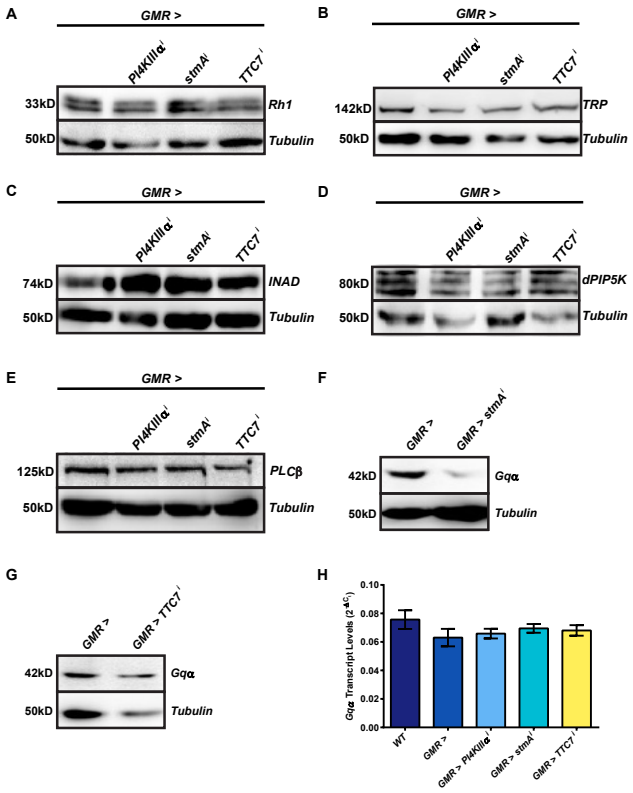

Figure 5.4 : Levels of key phototransduction proteins in *GMR > stmA^i* and *GMR > TTC7^i* flies
Western blots showing the levels of key phototransduction proteins extracted from the heads of *GMR > stmA^i* and *GMR > TTC7^i* flies as compared to GMR > flies. Tubulin is used as a loading control. **(A)** Rh1 **(B)** TRP **(C)** INAD **(D)** DPIP5K - protein was extracted from retinae and not heads to probe for DPIP5K. **(E)** PLCβ **(F)** Gq_α from heads of *GMR > stmA^i* flies **(G)** Gq_α from heads of *GMR > TTC7^i* flies **(H)** The level of Gq_α transcript in retinae as estimated using Q-PCR has been shown. The x-axis represents the genotype of the source tissue; y-axis represents $2^{-\Delta C_t}$ values for the Gq_α transcript. Values are mean ± s.e.m., n = 75 retinae per sample.

its role in phototransduction, we required a means of raising the temperature of the fly during the process of recording. A custom temperature controller was made by the NCBS electronics workshop and used for this experiment (details in Material and Methods). In order to test whether the controller was working as expected, we first performed ERGs on another temperature sensitive mutant. The $norpA^{H52}$ allele has been shown to have a negligible ERG response when placed at 33° C (Wilson and Ostroy, 1987). We obtained this fly and performed ERGs both at 25° C and 38° C, using the controller to maintain the desired temperature. As expected, the $norpA^{H52}$ flies showed normal ERG responses when placed at 25° C, but had no response when placed at 33° C or 38° C **(Fig.5.5B)**. In contrast, WT flies had normal ERGs at both temperatures, although the amplitude was marginally reduced at the higher temperature **(Fig.5.5A)**.

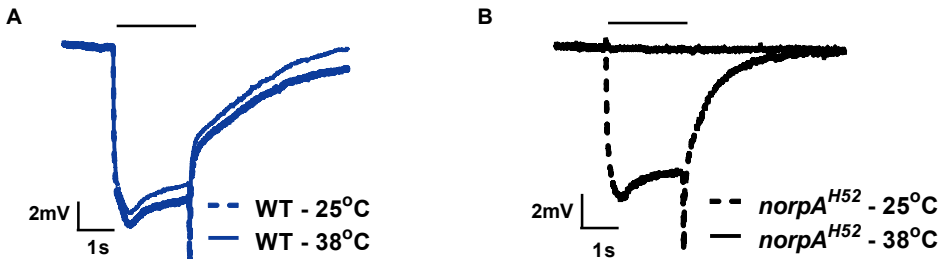

Figure 5.5 : Using the $norpA^{H52}$ temperature sensitive allele as a positive control
(A) and (B) Representative ERG amplitudes of flies of indicated genotypes. Dotted trace indicated 25° C and solid trace indicates 38°. The black bar on top indicates duration of the light stimulus, scale bar is shown on bottom left.

Having demonstrated the effectiveness of the temperature controller, we used it while performing ERGs on the *stmA* temperature-sensitive mutants. The flies were reared to adulthood at 25° C and placed at 38° C only during recording. While the response amplitudes of these flies was normal at 25° C, they were highly reduced at 38° C **(Fig.5.6A-C)**. Particularly, the $stmA^{18\text{-}2}$ mutant had only about one-tenth of the response at 38° C as it had at 25° C **(Fig.5.6C)**. For all ERGs, WT flies were used as controls and had comparable ERG responses at both temperatures. Since the $stmA^{18\text{-}2}$ allele showed the maximum decrease in ERG amplitude at 38° C, we used this allele for further experiments. The $stmA^{18\text{-}2}$ allele will henceforth be referred to as $stmA^{ts}$ in this thesis.

The reduction in response amplitude when *stmA* is inactivated only during

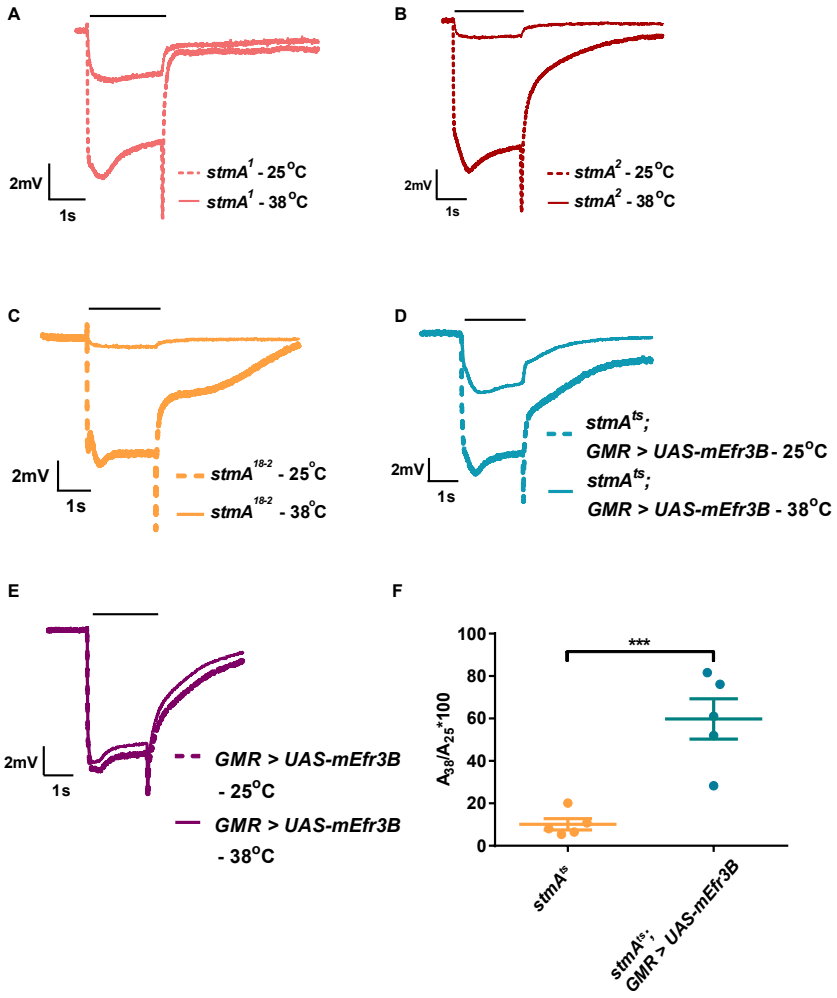

Figure 5.6 : ERG phenotypes of the $stmA^{ts}$ allele
(A) - (E) Representative ERG amplitudes of flies of indicated genotypes. Dotted trace indicated 25° C and solid trace indicates 38° C. The black bar on top indicates duration of the light stimulus, scale bar is shown on bottom left. $stmA^{ts}$ is equivalent to $stmA^{18\text{-}2}$. **(F)** Quantification of the ERG response amplitude of $stmA^{ts}$ and $stmA^{ts}$*; GMR > UAS-mEfr3B* flies. x-axis represents genotype; y-axis represents a ratio of peak ERG response amplitude at 38° C versus at 25° C. * - $p < 0.05$ as per two-tailed t-test, values are mean ± s.e.m., n = 5 flies per genotype

adulthood implies that the ERG defects do not arise from a role during development, but rather due to one in adult photoreceptors. Since the amplitude of the mutant flies at 38° C was extremely low to begin with, it was not possible to detect any progressive decrease in response to a light train. However, both the *GMR > stmA^i* and *stmA^{ts}* flies displayed low ERG amplitudes, indicating a role for *stmA* in adult photoreceptors.

We further tested whether the ERG response of *stmA^{ts}* flies could be rescued by expressing the mouse *Efr3B* construct in the background. The *stmA^{ts}; GMR > UAS-mEfr3B* and *GMR > UAS-mEfr3B* control flies had normal ERGs at 25° C **(Fig.5.6D - F)**. When placed at 38° C, the response amplitude was higher in*stmA^{ts}; GMR > UAS-mEfr3B* than that of *stmA^{ts}* mutants, but not as high as at 25° C **(Fig.5.6D and F)**. The mouse *Efr3B* was therefore able to partially alleviate the ERG defects of *stmA^{ts}* mutants. This further comfirmed that the ERG defects were most likely due to a specific loss of *stmA* function and not other secondary effects.

5.3 Knocking down *stmA* reduces the levels of PIP and PIP_2 in *Drosophila* retinae

The role of Efr3 as part of the PI4KIIIα complex has been well-studied in yeast and mammalian cell culture systems. In yeast, removing the ability of Efr3 to bind to the plasma membrane decreased the PI4P levels in the cell (Wu et al., 2014). In *Drosophila*, the role of *stmA* in phototransduction could be either dependent on or independent of PI4KIIIα. Given that knocking down both *stmA* and *PI4KIIIα* individually result in the same kind of ERG defects, it is likely that both elements function along the same pathway. If this is the case, it is also probable that downregulating *stmA* will have a direct impact on the plasma membrane levels of PI4P and PIP_2. In order to test this, we measured the lipid levels in *GMR > stmA^i* photoreceptors using two different methods.

5.3.1 Measurement of lipid levels using LC-MS

We first used LC-MS (described in Section 3.5) to measure the levels of PIP and PIP_2 in *GMR > stmA^i* retinae. We analysed two batches of flies, one of which was completely raised and processed in dark and another that was exposed to a bright flash of blue light before processing. In the dark-processed flies, the levels of PIP in *GMR > stmA^i* flies was lower than that of control flies **(Fig.5.7A)**. However, the PIP_2 levels were largely unchanged

and remained similar to those of controls **(Fig.5.7B)**. When exposed to a light flash, the PIP levels of $GMR > stmA^i$ flies were again lower than those of controls **(Fig.5.7C)**. There was also a significant reduction in the PIP_2 levels of $GMR > stmA^i$ flies, indicating that when the photoresponse is triggered in $GMR > stmA^i$ flies, they are unable to maintain the required amount of PIP_2 in retinae **(Fig.5.7D)**.

In order to quantify the changes brought on by light stimulation, we took a light:dark ratio of these lipids, as done in Section 3.5. In control flies, the light:dark ratio of PIP_2 was close to 1, whereas in $GMR > stmA^i$ flies this ratio dropped below 0.5 **(Fig.5.7F)**. This was similar to the drop seen in $GMR > PI4KIII\alpha^i$ flies as well. Unlike PIP_2, the light:dark ratio of PIP in $GMR > stmA^i$ flies remained similar to those of control flies **(Fig.5.7E)**. This is most likely because the PIP levels in $GMR > stmA^i$ flies were reduced to begin with and did not reduce much further upon light exposure.

5.3.2 Measurement of lipid levels using lipid-binding probes

The LC-MS measurements were complemented by a second set of semi-quantitative measurements using fluorescent-tagged lipid probes. These probes were expressed in the photoreceptors of control and $GMR > stmA^i$ flies and used as readouts of PI4P and PIP_2 levels at the rhabdomere. The P4M::GFP probe was used to monitor PI4P levels. In $GMR > stmA^i$ flies, the basal fluorescence intensity of the probe was lower at the rhabdomere **(Fig.5.8A)**. We also monitored the light-induced kinetics of the PI4P probe as done in Section 3.6. When compared to control flies, it was seen that the probe in $GMR > stmA^i$ flies did not undergo any depletion, nor did it display any discernible depletion and recovery kinetics **(Fig.5.8B)**. This almost perfectly mirrored the behaviour of the probe in the $GMR > PI4KIII\alpha^i$ background.

We used the PLCδPH::GFP probe to monitor PIP_2 levels. The fluorescence intensity of the probe in $GMR > stmA^i$ flies was significantly reduced when compared to controls **(Fig.5.9A)**. Additionally, when we measured the light-induced kinetics of the probe in $GMR > stmA^i$ flies, we found that the probe fluorescence did not change for the duration of the protocol, remaining at the initial intensity throughout **(Fig.5.9B)**. The PIP_2 kinetics in $GMR > stmA^i$ flies were identical to the PI4P kinetics, indicating that downregulating *stmA* impacts both PI4P and PIP_2 levels at the rhabdomere in a similar manner.

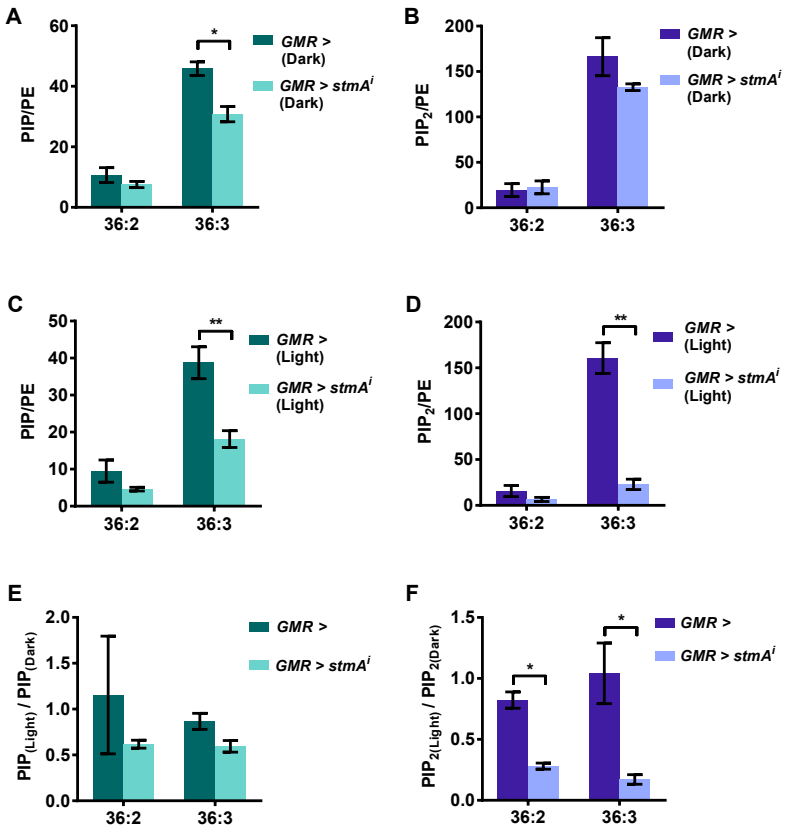

Figure 5.7 : LC-MS Measurement of PIP and PIP_2 from *GMR > stmA^i* flies

Liquid chromatography-mass spectrometry measurement of PIP and PIP_2 levels in retinae of one-day old *GMR > stmA^i* flies. The lipid levels for the two most abundant acyl chain species (36:2 and 36:3) are shown here. x-axis represents acyl chain species; y-axis represents ratio of PIP/PE and PIP_2/PE. **(A) and (B)** The flies were reared in dark and not exposed to any light during processing. **(C) and (D)** The flies were reared in dark and exposed to one minute of blue light before processing. **(E) and (F)** To highlight the effect of illumination on lipid levels, a ratio of the levels in light-exposed flies to those in dark-reared flies was taken. $PIP_{(light)}$:$PIP_{(dark)}$ and $PIP_{2(light)}$:$PIP_{2(dark)}$ ratios for the 36:2 and 36:3 acyl chain species are shown. x-axis represents acyl chain species; y-axis represents ratio of light:dark lipid levels. * - $p < 0.05$ as per one way ANOVA followed by Tukey's multiple comparison test, values are mean ± s.e.m., n = 25 retinae per sample.

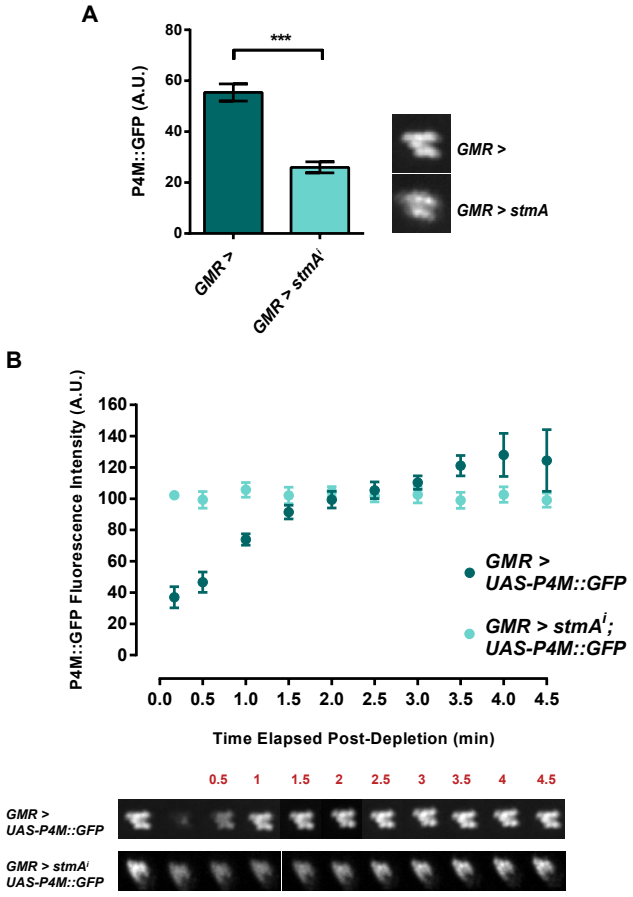

Figure 5.8 : PI4P levels at the rhabdomere of *GMR > stmA^i* flies **(A)** Quantification of fluorescence intensity of P4M::GFP probe in the deep pseudopupil. x-axis indicates genotype, y-axis indicates fluorescence intensity per unit area. Representative images of the deep pseudopupil for each genotype are shown beside the graph. **(B)** Recovery kinetics of the P4M::GFP PI4P probe when subjected to the light sequence described previously, genotype as indicated. x-axis indicates time in minutes after the very first flash of blue light; y-axis represents the fluorescence intensity per unit area of the deep pseudopupil at each instance, normalised to the intensity of the very first image. Representative images of each instance are shown below, with the time points of acquisition marked in red. *** - $p < 0.001$ as per two-tailed t-test, values are mean ± s.e.m., n = 8 flies per genotype.

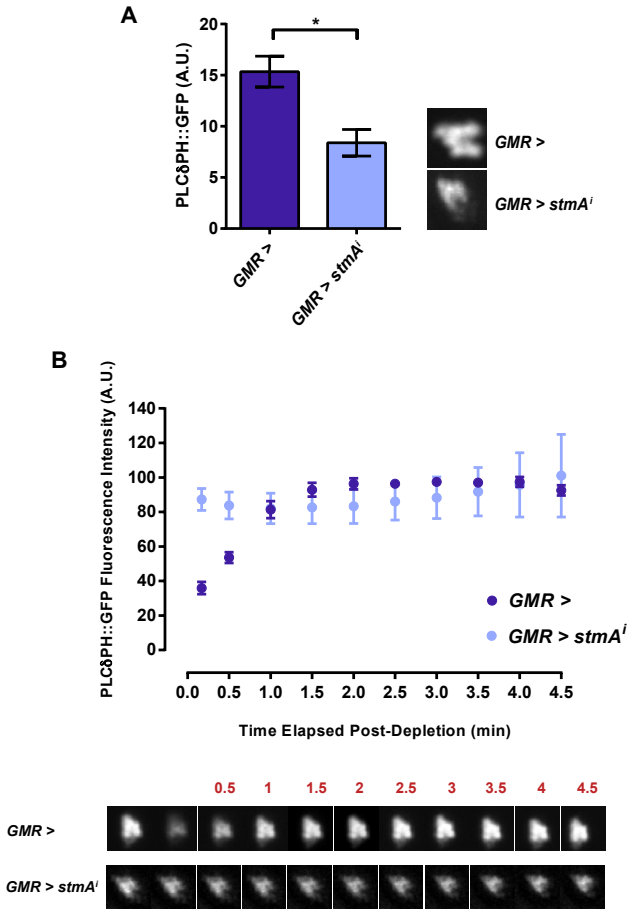

Figure 5.9 : $PI(4,5)P_2$ levels at the rhabdomere of *GMR > stmA^i* flies
(A) Quantification of fluorescence intensity of PLCδPH::GFP $PI(4,5)P_2$ probe in the deep pseudopupil. x-axis indicates genotype, y-axis indicates fluorescence intensity per unit area. Representative images of the deep pseudopupil for each genotype are shown beside the graph. **(B)** Recovery kinetics of the PLCδPH::GFP $PI(4,5)P_2$ probe when subjected to the light sequence described previously, genotype as indicated. x-axis indicates time in minutes after the very first flash of blue light; y-axis represents the fluorescence intensity per unit area of the deep pseudopupil at each instance, normalised to the intensity of the very first image. Representative images of each instance are shown below, with the time points of acquisition marked in red. * - $p < 0.05$ as per two-tailed t-test, values are mean ± s.e.m., n = 8 flies per genotype.

5.4 Localisation of mEfr3B in *Drosophila* photoreceptors

The LC-MS measurements and lipid-binding probes clearly pointed to a role for *stmA* in maintaining the levels of PI4P and PIP_2 at the rhabdomere. In other systems, Efr3 is shown to be constantly localised to the plasma membrane. In yeast, it does this by virtue of a patch of basic amino acids which bind to acidic lipid components in the plasma membrane (Wu et al., 2014). The mammalian Efr3 on the other hand, is palmitoylated owing to an N-terminus motif (Bojjireddy et al., 2015).

In *Drosophila*, we do not yet know the localisation of the STMA protein. In order to determine this, ideally one would visualise the endogenous protein, using either an antibody or an endogenous tag. Owing to a lack of functional reagents, we used the mouse Efr3B as a proxy readout for localisation of STMA. The mEfr3B construct was also able to partially rescue the ERG defects in $GMR > stmA^{i}$ and $stmA^{ts}$ flies, pointing to functional conservation between the fly and mammalian proteins.

We first transfected S2R+ cells with the HA::mEfr3B construct and found that the protein was localised to the plasma membrane (experiments performed by Urbashi Basu) **(Fig.5.10A)**. The tagged protein was then expressed in otherwise WT photoreceptors using GMRGal4. The mEFr3B was localised to both the rhabdomere and basolateral membrane, which together comprise the total plasma membrane of photoreceptors (experiments performed by Rajan Thakur) **(Fig.5.10B)**. This localisation corresponded well to that seen in mammalian cells (Nakatsu et al., 2012).

The above results show that the mEfr3B protein localises identically in both mammalian and *Drosophila* cells, which is most likely why it was able to partially rescue the ERG phenotypes of $GMR > stmA^{i}$ flies.

5.5 *TTC7* downregulation has characteristic ERG phenotypes

The tetratricopeptide containing 7 (TTC7) protein is the third component of the PI4KIIIα complex, as shown in mammalian and yeast systems (Nakatsu et al., 2012; Wu et al., 2014). In *Drosophila*, the orthologue is encoded by the gene CG8325, represented in this text as *TTC7*. As a putative interactor of PI4KIIIα in *Drosophila*, we investigated whether knocking down *TTC7* in fly photoreceptors would impact the photoresponse.

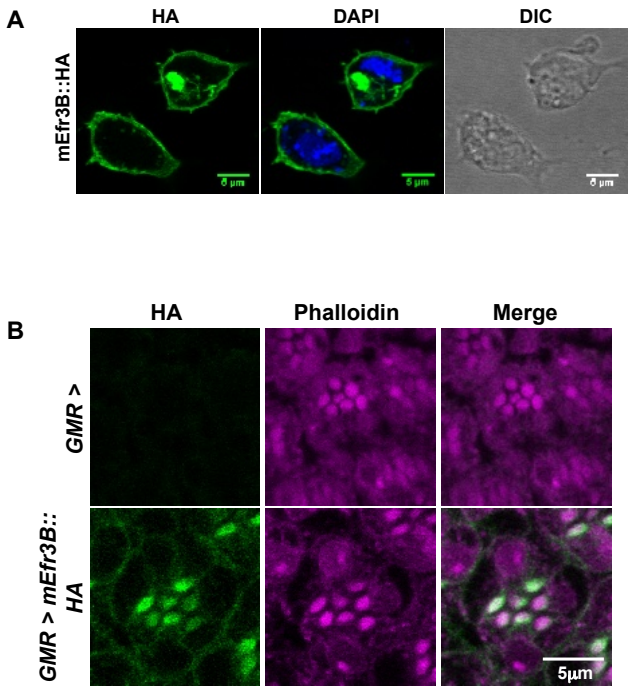

Figure 5.10 : Localisation of mEfr3B in *Drosophila* photoreceptors **(A)** Confocal images of S2R+ cells transfected with pUAST-HA::mEfr3B, followed by staining with DAPI and α-HA. Blue represents DAPI, which marks the nucleus, and green represents HA. Scale bar - 5 µm. **(B)** Confocal images of retinae from flies of the indicated genotypes, reared and processed completely in dark conditions. The retinae have been stained with phalloidin (magenta) and α-HA (green). Scale bar - 5 µm. Figure adapted from Balakrishnan *et al.*, 2018

As with *PI4KIIIα* and *stmA*, we screened multiple RNAi lines against *TTC7* by expressing the UAS-RNAi constructs in photoreceptors (listed in Table 2). As in previous cases, we initially used a combination of Rh1Gal4 and UAS-Dicer2 to drive the RNAi. When we performed ERGs on these flies, we did not observe any defects in the ERGs**(Fig.5.11A)**. We then used GMRGal4 to drive the RNAi constructs in all eye cells and found that one of the lines showed a highly reduced ERG response amplitude**(Fig.5.11B and 5.12B)**. We quantified the extent of *TTC7* transcript knockdown in the retinae of these flies and found it to be reduced by ~70% **(Fig.5.11C)**. Therefore, the Bloomington TRiP line #44482 was used for all further experiments.

Apart from the reduced amplitude, *GMR > TTC7^{i}* flies also exhibited the progressive decrease in amplitude when exposed to a light train of ten flashes **(Fig.5.12A and C)**. Additionally, the intensity response curve of *GMR > TTC7^{i}* flies had a lower slope than controls, implying lower sensitivity of the system to stimuli **(Fig.5.12D)**. Both these phenotypes were seen in *GMR > PI4KIIIα^{i}* and *GMR > stmA^{i}* flies as well. We also verified whether the ERG phenotypes arose due to reduced expression of key phototransduction proteins by performing Western blots from *GMR > TTC7^{i}* flies. We found that the levels of Rh1, Gq_{α}, PLC, TRP, INAD and dPIP5K were unchanged in *GMR > TTC7^{i}* flies, indicating that the ERG defects are likely due to *TTC7* downregulation itself **(Fig.5.4A-E, G)**.

In order to determine whether the ERG defects arose due to *TTC7* downregulation or any off-target effects, we expressed the human *TTC7B*construct in this background **(Fig.5.13A)**. The human *TTC7B* gene was placed downstream of a UAS promoter and transgenic flies expressing this construct were made. When we performed ERGs on *GMR > TTC7^{i}; UAS-hTTC7B* flies, we observed that the response amplitude was higher than that of *GMR > TTC7^{i}* flies, but still not as high as that of controls **(Fig.5.13B and C)**. However, *hTTC7B* was able to alleviate the progressive reduction phenotype, with *GMR > TTC7^{i}; UAS-hTTC7B* flies displaying a very small degree of progressive reduction in response to a series of light flashes**(Fig.5.13D)**. The human construct was also able to completely rescue the loss in sensitivity of *GMR > TTC7^{i}* flies **(Fig.5.13E)**. The ability of human *TTC7B* to rescue almost all the ERG defects associated with *TTC7* knockdown implied that the defects were not due to any off-target effects.

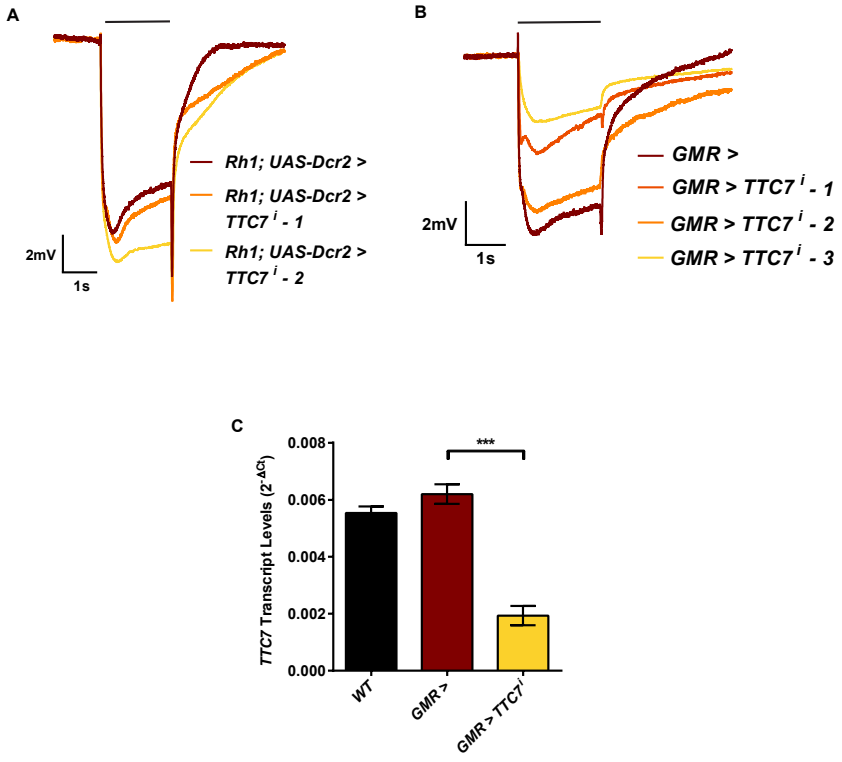

Figure 5.11 : Knocking down *TTC7* in photoreceptors reduces the ERG response amplitude
(A) Knocking down *TTC7* using Rh1; UAS-Dcr2 does not significantly impact the ERG response when compared to control flies. **(B)** Knocking down *TTC7* using GMRGal4 significantly reduces ERG response in one of the RNAi lines tested when compared to control flies. **(C)** The level of transcript knockdown in retinae as estimated using Q-PCR has been shown. The x-axis represents the genotype of the source tissue; y-axis represents $2^{-\Delta C_t}$ values for the described gene. *** - $p < 0.001$ as per two-tailed t-test, values are mean ± s.e.m., n = 75 retinae per sample.

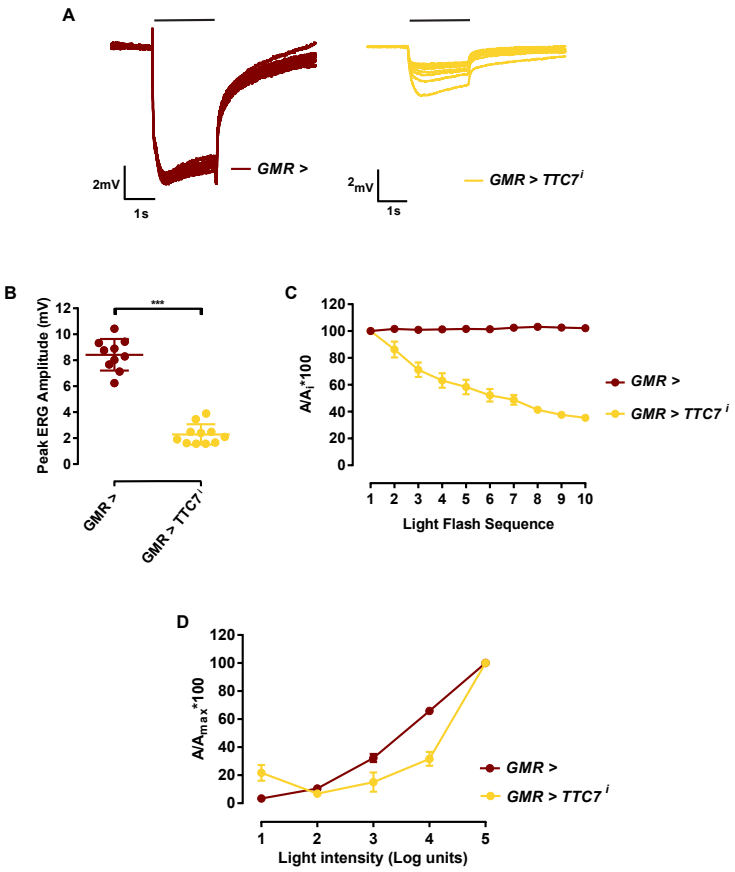

Figure 5.12 : ERG phenotypes of *GMR > TTC7^i* flies
(A) Representative ERG amplitudes of control flies (dark coloured) and *GMR > TTC7^i* flies (light coloured) in response to ten consecutive flashes of light. The black bar on top indicates duration of the light stimulus, scale bar is shown on bottom left. **(B)** Quantification of the peak ERG amplitude of control and *GMR > TTC7^i* flies. x-axis represents genotype and y-axis represents response amplitude in mV. **(C)** Quantification of the ERG amplitude of control and *GMR > TTC7^i* flies in response to ten consecutive light flashes. x-axis represents the light flash number in the sequence and y-axis represents response amplitude for each light flash normalised to that at the first light flash. **(D)** Intensity response function of control and *GMR > TTC7^i* flies. x-axis represents light intensity in log units and y-axis represents the response amplitude at each intensity normalised to that at maximum intensity. * - $p < 0.05$ as per two-tailed t-test, values are mean ± s.e.m., n = 10 flies per genotype.

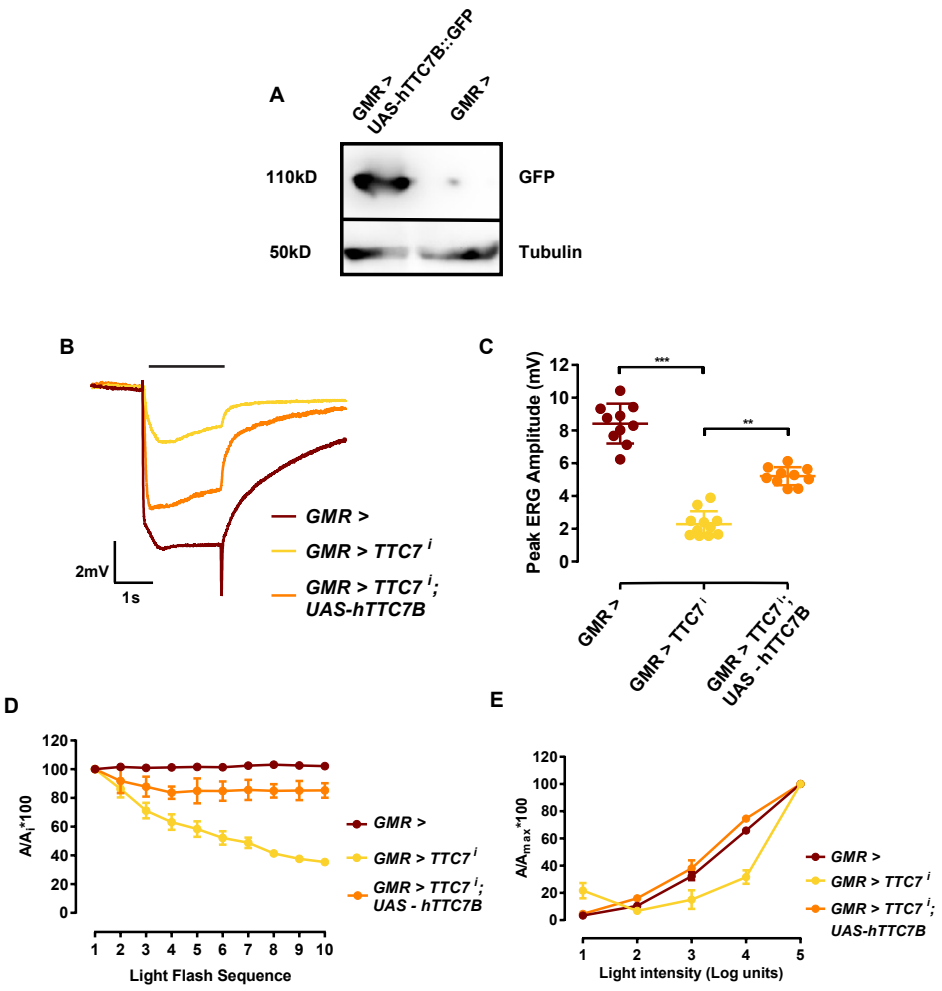

Figure 5.13 : Rescue of ERG phenotypes of *GMR > TTC7^{i}* flies by hTTC7B

(A) Western blot showing the expression of GFP-tagged hTTC7B, driven using GMRGal4. **(B)** Representative ERG amplitudes of flies of indicated genotypes. The black bar on top indicates duration of the light stimulus, scale bar is shown on bottom left. **(C)** Quantification of the peak ERG amplitude of flies of indicated genotypes. x-axis represents genotype and y-axis represents response amplitude in mV. **(D)** Quantification of the ERG amplitude of flies of indicated genotypes in response to ten consecutive light flashes. x-axis represents the light flash number in the sequence and y-axis represents response amplitude for each light flash normalised to that at the first light flash. **(E)** Intensity response function of flies of indicated genotypes. x-axis represents light intensity in log units and y-axis represents the response amplitude at each intensity normalised to that at maximum intensity. * - $p < 0.05$ as per two-tailed t-test, values are mean ± s.e.m., n = 10 flies per genotype.

5.6 Levels of plasma membrane PI4P and PIP_2 are reduced when *TTC7* is downregulated

The architecture of the PI4KIIIα complex as worked out in other model systems places TTC7 as a bridge between Efr3 and PI4KIIIα (Lees et al., 2017; Wu et al., 2014). A system lacking TTC7 thererfore would not be able to recruit PI4KIIIα to the plasma membrane, resulting in reduced PI4P synthesis. Indeed, yeast cells lacking functional TTC7 have been shown to have reduced PI4P and PIP_2 levels (Baird et al., 2008). In *Drosophila*, given that knocking down both *TTC7* and PI4KIIIα impact the light response in the same manner, it is likely that they affect the lipid levels similarly as well.

We measured the levels of PI4P and PIP_2 in the rhabdomeres of $GMR > TTC7^i$ flies using lipid-binding probes. The fluorescence intensity of the P4M::GFP probe, used to monitor PI4P, was significantly lower $GMR > TTC7^i$ flies when compared to controls **(Fig.5.14A)**. When we measured the light-induced kinetics of the PI4P probe in these flies, we found that the probe fluorescence did not undergo depletion, nor did it display any recovery kinetics, similar to the effect seen in $GMR > stmA^i$ and $GMR > PI4KIII\alpha^i$ flies **(Fig.5.14B)**.

We next measured the rhabdomeral PIP_2 levels, as reported by the PLCδPH::GFP probe. We found that they were only marginally reduced in $GMR > TTC7^i$ flies as compared to controls **(Fig.5.15A)**. The light-induced kinetics, however, were mostly stagnant and displayed minimal depletion and recovery kinetics, once again mirroring the effect seen in $GMR > stmA^i$ flies **(Fig.5.15B)**.

In terms of the kinetics of lipid recovery, knocking down *TTC7* had commensurate effects on both PI4P and PIP_2. Moreover, the lack of discernible kinetics corresponded well with the effects of downregulating both *PI4KIIIα* and *stmA*.

5.7 Localisation of hTTC7B in *Drosophila* photoreceptors

The TTC7 protein appears to lack any clear motifs or signals for binding directly to the plasma membrane. In mammalian cells, it is recruited to the membrane by binding to Efr3, which is constitutively membrane localised (Lees et al., 2017). The localisation of TTC7 in *Drosophila* is currently unknown. Since the human *TTC7B* was able to rescue almost all the ERG defects of knocking down *TTC7*, we used the tagged human protein as a

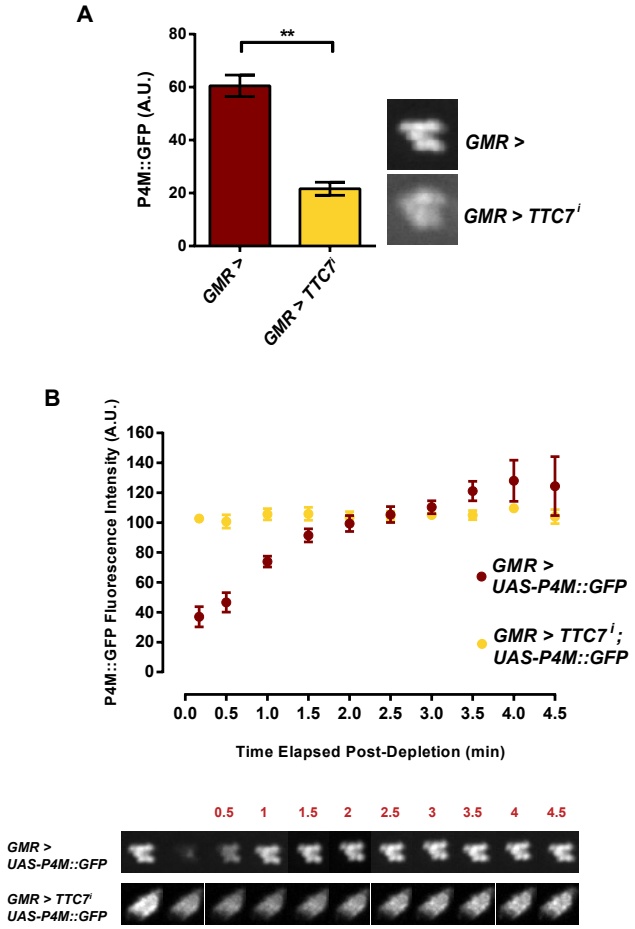

Figure 5.14 : PI4P levels at the rhabdomere of *GMR > TTC7^i* flies **(A)** Quantification of fluorescence intensity of P4M::GFP probe in the deep pseudopupil. x-axis indicates genotype, y-axis indicates fluorescence intensity per unit area. Representative images of the deep pseudopupil for each genotype are shown beside the graph. **(B)** Recovery kinetics of the P4M::GFP PI4P probe when subjected to the light sequence described previously, genotype as indicated. x-axis indicates time in minutes after the very first flash of blue light; y-axis represents the fluorescence intensity per unit area of the deep pseudopupil at each instance, normalised to the intensity of the very first image. Representative images of each instance are shown below, with the time points of acquisition marked in red. *** - $p < 0.001$ as per two-tailed t-test, values are mean ± s.e.m., n = 10 flies per genotype.

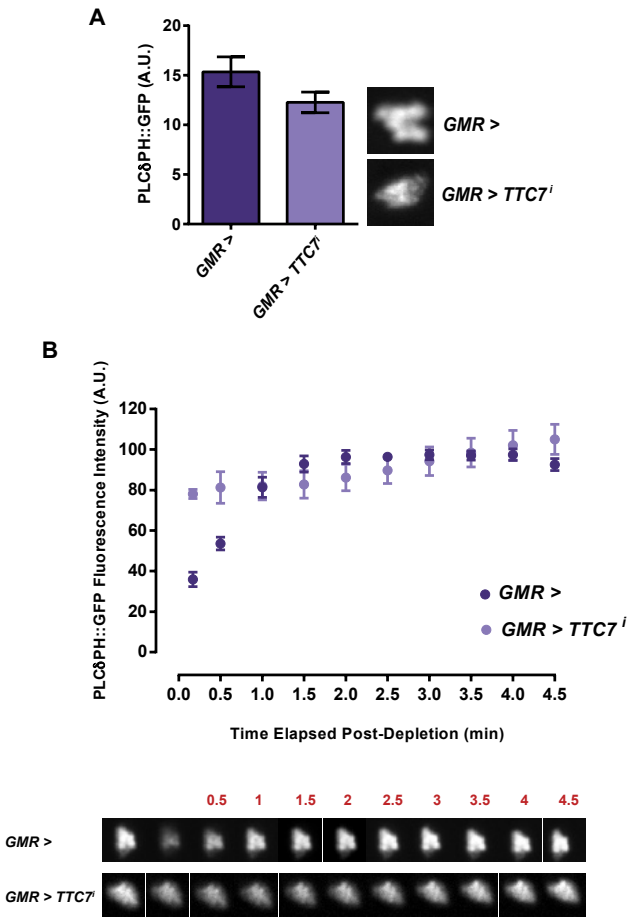

Figure 5.15 : $PI(4,5)P_2$ levels at the rhabdomere of *GMR > TTC7^i* flies

(A) Quantification of fluorescence intensity of PLCδPH::GFP $PI(4,5)P_2$ probe in the deep pseudopupil. x-axis indicates genotype, y-axis indicates fluorescence intensity per unit area. Representative images of the deep pseudopupil for each genotype are shown beside the graph. **(B)** Recovery kinetics of the PLCδPH::GFP $PI(4,5)P_2$ probe when subjected to the light sequence described previously, genotype as indicated. x-axis indicates time in minutes after the very first flash of blue light; y-axis represents the fluorescence intensity per unit area of the deep pseudopupil at each instance, normalised to the intensity of the very first image. Representative images of each instance are shown below, with the time points of acquisition marked in red. Values are mean ± s.e.m., n = 10 flies per genotype.

proxy for localisation in fly cells.

The human TTC7B::GFP was first transfected in *Drosophila* S2R+ cells. The protein was localised to the cytosol, as was expected (experiment performed by Urbashi Basu) **(Fig.5.16A)**. In mammalian cells, overexpression of TTC7B alone, without Efr3, also results in the protein in the cytosol (Nakatsu et al., 2012).

We then expressed the construct in otherwise WT flies using GMRGal4. We used two batches of flies, one of which were reared and processed in the dark and the other exposed to a bright flash of blue light and then further processed in light as well. In the dark reared flies, hTTC7B::GFP was seen to be excluded from the rhabdomere **(Fig.5.16B)**, as seen in the S2R+ cells as well (experiments performed by Rajan Thakur). In the light-exposed flies, however, the tagged protein was present both in the cell body as well as at the rhabdomere, indicating that in response to a light stimulus a fraction of hTTC7B translocates to the plasma membrane **(Fig.5.16C)**.

5.8 Conclusion

In this section, we investigated the requirement for stmA and TTC7, putative interactors of PI4KIIIα, for phototransduction. Both proteins are highly conserved across orders, and there is empirical data demonstrating their interaction with *PI4KIIIα* in both mammalian and yeast systems. Given this, it is likely that this paradigm holds true in *Drosophila* as well. However, there has till date been no experimental confirmation of the same. Here, we provide evidence in favour of stmA and TTC7 acting towards the same goal as PI4KIIIα in *Drosophila* photoreceptors.

5.8.1 Main Conclusions

We used RNAi-mediated knockdown to reduce the transcript levels of both *stmA* and *TTC7* in the photoreceptors. Flies in which these genes were knocked down individually showed a significant drop in the amplitude of their ERG responses. Moreover, both sets of flies showed a progressive decrease in response amplitude when subjected to a train of ten light flashes. These phenotypes clearly mimicked those of knocking down *PI4KIIIα*. Such an effect is anticipated in a scenario where multiple proteins are required to work together towards one common goal, which in this case would be generation of PI4P at the plasma membrane.

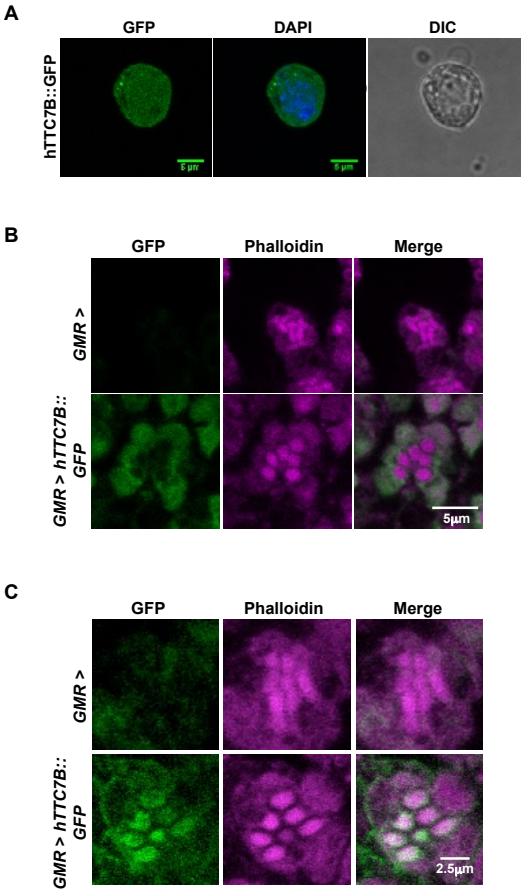

Figure 5.16 : Localisation of hTTC7B in *Drosophila* photoreceptors **(A)** Confocal images of S2R+ cells transfected with pUAST-hTTC7B:GFP, followed by staining with DAPI. Blue represents DAPI, which marks the nucleus, and green represents GFP. Scale bar - 5µm. **(B)** Confocal images of retinae from flies of the indicated genotypes, reared and processed completely in dark conditions. The retinae have been stained with phalloidin (magenta) and α-GFP (green). Magenta represents phalloidin, which marks the rhabdomere, and green represents FLAG. Scale bar - 5µm. **(C)** Confocal images of retinae from flies of the indicated genotypes, reared in dark and exposed to blue light for one minute before processing. The retinae have been stained with phalloidin (magenta) and α-GFP (green). Scale bar - 2.5µm.

With respect to lipid levels, we used a combination of fluorescent-tagged lipid-binding probes and LC-MS to quantify them. In flies where either *stmA* or *TTC7* were knocked down, we saw that the levels of PIP and PIP_2 were lower than in the respective controls. In $GMR > stmA^i$ flies, in fact, the decrease in PIP_2 levels after light stimulation was higher than in flies where *PI4KIIIα* itself was downregulated.

We also demonstrated a requirement for *stmA* function exclusively in adult photoreceptors using a temperature-sensitive loss-of-function mutant of the gene. We found that, when placed at restrictive temperature, the mutants had little or no light response. This was despite the fact that they were reared to adulthood at permissive temperatures, implying that the *stmA* gene was fully fucntional throughout development.

Additionally, we showed that the localisation of both mEfr3B and hTTC7B in fly photoreceptors was similar to that of mammalian cells, implying a deep conservation of function between the fly and mammalian proteins.

5.8.2 Molecular basis for phenotypes

The fact that both knocking down all three genes - *PI4KIIIα*, *stmA* and *TTC7* - elicited identical phenotypes in terms of both the light response and lipid levels strongly implies that all of them work either in concert or along parallel pathways. Therefore, it likely that the basis for the ERG phenotypes discussed in section 3.8 also hold true for the observations made here as well.

There is, however, one point of disparity in the results seen with *stmA* knockdown and *PI4KIIIα* knockdown. With respect to the intensity response curve of $GMR > stmA^i$ flies, it was observed that these flies were less sensitive to light than their corresponding controls. While this was also seen in $GMR > PI4KIII\alpha^i$ flies, the defect in these flies was fully rescued by the hPI4KIIIα. In contrast, the low sensitivity of $GMR > stmA^i$ flies was not mitigated to any degree by the mEfr3B construct. This could not be attributed to a general phenomenon of partial rescue, since in the case of $GMR > TTC7^i$ flies, even though the ERG response amplitude was only partially rescued, the reduced sensitivity was completely rescued by the *hTTC7B* construct.

We also observed that the $GMR > stmA^i$ flies had lower levels of Gq_α than control flies. It is possible that in this could be a contributing factor to the ERG phenotype in these flies, although it is probably independent of the changes in lipid levels; we see the same ERG phenotypes in $GMR > PI4KIII\alpha^i$ and $GMR > TTC7^i$ flies, even though the Gq_α levels in these flies are similar to those of controls.

The reason for the reduction in Gq_{α} could possibly be a consequence of STMA being a membrane-resident protein. In mammalian cells, there are indications that Efr3 can regulate the coupling of G proteins to their cognate receptors. Downregulation of *EFR3B* in HEK293 cells resulted in a faster uncoupling between the GPCR and its cognate G-protein. This implied that the receptor was desensitised faster than in normal cells, which also corresponded to a slower resensitisation. Given that Efr3B resides at the plasma membrane by virtue of palmitoylation, it has the opportunity to interact with the myriad resident proteins and lipids. This study also found that the rapid uncoupling was only seen when the full length receptor was used, and not one where the C-terminal tail was truncated, presenting a potential site for interaction of Efr3B with the GPCR (Bojjireddy et al., 2015). Given that Gq_{α} in *Drosophila* photoreceptors translocates to and from the cytosol during signalling (Cronin, 2004), STMA may play a role in restoring it to the membrane or even determining its initial association with rhodopsin.

5.8.3 Unaddressed questions

A key question that remains unaddressed in this thesis is the localisation of the endogenous *Drosophila* STMA and TTC7 proteins in photoreceptors. It would be especially informative to visualise all three proteins of the proposed complex - PI4KIIIα, STMA and TTC7 - both in wild-type conditions and when any one component has been removed. The possibility of the formation of a complex could be strengthened by proving a physical interaction between them, either through colocalisation studies or through co-immunoprecipitation experiments. One facet of this interaction has already been demonstrated in 2017, where STMA was co-immunoprecipitated with PI4KIIIα, proving that they do interact within the cell (Zhang et al., 2017).

A second aspect that merits further investigation is the reduction of Gq_{α} levels in $GMR > stmA^{i}$ flies. If *stmA* does indeed somehow regulate the coupling of Gq_{α} to rhodopsin, it would be informative to monitor the translocation of Gq_{α} to and from the cytosol during phototransduction. This phenomenon follows well-defined kinetics for specific regimes of light treatment (Cronin, 2004) and hence, could serve as a readout of Gq_{α} function in the background of *stmA* knockdown.

Bibliography

D. Baird, C. Stefan, A. Audhya, S. Weys, and S. D. Emr. Assembly of the PtdIns 4-kinase Stt4 complex at the plasma membrane requires Ypp1 and Efr3. *J Cell Biol*, 183(6):1061–1074, Dec. 2008. ISSN 0021-9525, 1540-8140. doi: 10.1083/jcb.200804003.

N. Bojjireddy, M. L. Guzman-Hernandez, N. R. Reinhard, M. Jovic, and T. Balla. EFR3s are palmitoylated plasma membrane proteins that control responsiveness to G-protein-coupled receptors. *J Cell Sci*, 128(1):118–128, Jan. 2015. ISSN 0021-9533, 1477-9137. doi: 10.1242/jcs.157495.

S. Chandrashekaran and N. Sarla. Phenotypes of lethal alleles of the recessive temperature sensitive paralytic mutant stambh A of Drosophila melanogaster suggest its neurogenic function. *Genetica*, 90(1):61–71, Feb. 1993. ISSN 0016-6707, 1573-6857. doi: 10.1007/BF01435179.

M. A. Cronin. Light-dependent subcellular translocation of Gq in Drosophila photoreceptors is facilitated by the photoreceptor-specific myosin III NINAC. *Journal of Cell Science*, 117(20):4797–4806, Oct. 2004. ISSN 0021-9533, 1477-9137. doi: 10.1242/jcs.01371.

M. C. Ellis, E. M. O'Neill, and G. M. Rubin. Expression of Drosophila glass protein and evidence for negative regulation of its activity in non-neuronal cells by another DNA-binding protein. *Development*, 119(3):855–865, Nov. 1993. ISSN 0950-1991, 1477-9129.

F.-D. Huang, H. J. G. Matthies, S. D. Speese, M. A. Smith, and K. Broadie. Rolling blackout, a newly identified PIP2-DAG pathway lipase required for Drosophila phototransduction. *Nature Neuroscience*, 7(10):1070–1078, Oct. 2004. ISSN 1546-1726. doi: 10.1038/nn1313.

J. A. Lees, Y. Zhang, M. S. Oh, C. M. Schauder, X. Yu, J. M. Baskin, K. Dobbs, L. D. Notarangelo, P. D. Camilli, T. Walz, and K. M. Reinisch. Architecture of the human PI4KIIIα lipid kinase complex. *Proceedings of the National Academy of Sciences*, page 201718471, Dec. 2017. ISSN 0027-8424, 1091-6490. doi: 10.1073/pnas.1718471115.

F. Nakatsu, J. M. Baskin, J. Chung, L. B. Tanner, G. Shui, S. Y. Lee, M. Pirruccello, M. Hao, N. T. Ingolia, M. R. Wenk, and P. D. Camilli. PtdIns4P synthesis by PI4KIIIα at the plasma membrane and its impact on plasma membrane identity. *J Cell Biol*, 199(6):1003–1016, Dec. 2012. ISSN 0021-9525, 1540-8140. doi: 10.1083/jcb.201206095.

J. Shyngle and R. Sharma. Studies on paralysis and development of sec-

ond chromosome temperature sensitive paralytic mutants of Drosophila melanogaster. *Indian Journal of Experimental Biology*, 23:235–240, 1985. ISSN 0019-5189.

M. J. Wilson and S. E. Ostroy. Studies of the DrosophilanorpA phototransduction mutant I. Electrophysiological changes and the offsetting effect of light. *J Comp. Physiol A*, page 7, 1987.

X. Wu, R. J. Chi, J. M. Baskin, L. Lucast, C. G. Burd, P. De Camilli, and K. M. Reinisch. Structural Insights into Assembly and Regulation of the Plasma Membrane Phosphatidylinositol 4-Kinase Complex. *Developmental Cell*, 28(1):19–29, Jan. 2014. ISSN 1534-5807. doi: 10.1016/j.devcel.2013.11.012.

X. Zhang, W.-A. Wang, L.-X. Jiang, H.-Y. Liu, B.-Z. Zhang, N. Lim, Q.-Y. Li, and F.-D. Huang. Downregulation of RBO-PI4KIIIα Facilitates Aβ42 Secretion and Ameliorates Neural Deficits in Aβ42-Expressing Drosophila. *Journal of Neuroscience*, 37(19):4928–4941, May 2017. ISSN 0270-6474, 1529-2401. doi: 10.1523/JNEUROSCI.3567-16.2017.

Chapter 6

Does *stmA* Function as a DAG Lipase During *Drosophila* Phototransduction?

6.1 Evidence for the requirement of a DAG lipase during phototransduction

Visual transduction in *Drosophila* is a phospholipase C (PLC)-mediated signalling pathway leading to the activation of ion channels. Light stimulation activates the GPCR rhodopsin, which triggers hydrolysis of the phosphoinositide PI(4,5)P_2 at the plasma membrane by PLCβ. The resulting cascade opens transient receptor potential (TRP and TRPL) channels, causing an influx of calcium and depolarisation of the photoreceptor cell (Hardie and Raghu, 2001). While most of the molecular elements involved in the cascade have been worked out over the years, certain aspects are yet to be deciphered.

PIP_2 hydrolysis generates second messengers diacylglycerol (DAG) and inositol(1,4,5)trisphosphate (IP_3), an immediate consequence of which is the opening of TRP channels. Initial attempts to identify the agent of excitation lead to DAG when the photoresponse of null alleles of *rdgA*, the gene encoding DAG kinase, was examined. Flies carrying the null allele $rdgA^{BS12}$ showed a constitutive inward current, which was attributed to a Ca^{2+} influx through TRP channels. Additionally, the $rdgA^{BS12}$ flies underwent severe retinal degeneration, which could be rescued by expressing loss-of-function *trp* and *trpl* alleles in the background. This triple mutant of $rdgA^{BS12}$*; trpl; trp*^{343} also no longer displayed the constitutive inward current seen in $rdgA^{BS12}$ mutants

alone, indicating that the TRP and TRPL channels were the source of the current. This relationship between DAG kinase (*rdgA*) and TRP channels implied that DAG is responsible for the activation of TRP channels, since null mutants for *rdgA* would be expected to have higher DAG levels than wild-type flies (Raghu et al., 2000).

A second line of evidence for came from a study which demonstrated that polyunsaturated fatty acids (PUFA) can excite TRP channels. The exogenous application of arachidonic and linolenic acids to dissociated ommatidial preparations from *Drosophila* eyes was able to trigger the activation of TRP channels. This activation occurred even in the absence of PLC, Gq_{α} and PKC, implying it occurs downstream of all these signalling elements (Chyb et al., 1999). In photoreceptors, DAG is a potential source of such fatty acids, as the action of a DAG lipase would release them from the glycerol backbone.

In both the above studies, however, there is no direct evidence for the claim, as seen in the case of mammalian TRPC channels. In this case, the exogenous application of DAG analogues was able to activate human TRPC6 channels expressed in CHO cells (Hofmann et al., 1999). In answer to this, it has recently been demonstrated in *Drosophila* that DAG can directly activate TRP channels when applied onto excised rhabdomeral patches. This activation was seen to be independent of PLC as both pharmacological inhibition and genetic deletion of PLC did not impact the action of DAG on TRP channels (Delgado et al., 2019).

In the light of such links between DAG and TRP channel activation, there have been attempts to characterise the connection in *Drosophila* photoreceptors. In 2008, the gene *inaE* was annotated as encoding a DAG lipase, which acts upon the sn-1 position of DAG to form 2-monoacylglycerol and a free fatty acid, as seen from *in vitro* protein activity experiments. Loss-of-function alleles for *inaE*, $inaE^{N125}$, displayed a response decay, similar to that seen in trp^{343} null mutants. The $inaE^{N125}$ flies also required more than 100 s of rest to recover the light response following an initial flash of light, as opposed to wild-type flies which only required 10 s of rest (Leung et al., 2008). While the gene *inaE* appears to be a viable prospect for a DAG lipase, there is also a second candidate in the running.

Prior to the annotation of *inaE*, a 2004 study identified the gene *stmA* as encoding a DAG lipase, mutants for which had a reduced light response (Huang et al., 2004). Quantification of DAG levels in the retinae of these mutants showed them to be lower than wild-type flies. This was counterintuitive to the assignment of *stmA* as a DAG lipase, since the absence of a lipase would

be expected to increase the levels of DAG, if not leave them undisturbed. A second question was raised based on the bioinformatic analysis of the *stmA* protein sequence. The annotation of the gene as a DAG lipase was initially done based on homology with previously characterised human DAG lipases. A closer look at the alignments revealed that the mammalian protein sequences used in the study were not in fact the DAG lipases alpha and beta, as claimed, but those of the protein Efr3 . The discrepancies in both the DAG measurements and sequence alignment of the protein led us to ask whether *stmA* does indeed function as a DAG lipase to regulate phototransduction.

The role of *stmA* as a regulator of phototransduction could be manifold. In this thesis, we have shown that downregulating *stmA* has a clear negative impact on the electrical response to light. We have also shown that *stmA* is involved in maintaining the levels of PI4P and PIP_2 at the plasma membrane, most likely through an association with PI4KIIIα. In this chapter, it has been investigated whether manipulating the levels of *stmA* also has a discernible effect on the levels of DAG in fly photoreceptors. We used LC-MS to quantify the lipid levels in retinae. The protein sequence of *stmA* is also examined in an attempt to demarcate any domains or motifs that would confer the protein with lipase activity.

6.2 Sequence analysis of the STMA protein

The STMA protein has been identified as an orthologue to the human proteins Efr3A and Efr3B. They share 39% sequence identity and have been shown to be functionally conserved as well (Nakatsu et al., 2012). In order to determine whether STMA bears any similarity to DAG lipases, we aligned the two longest isoforms of STMA with the two longest isoforms of human DAG lipases alpha and beta (sequence details given in Section 2.7). The human DAG lipase protein has three major characteristics that mark it as such - the lipase 3 domain, the catalytic triad and the nucleophilic elbow. An additional signature, more recently discovered, is the FxxH motif which confers substrate specificity to the enzyme **(Fig.6.1)**.

When the whole protein sequences were aligned using CLUSTALW, we did not find significant sequence identity between STMA and either of the human DAG lipases. The STMA sequence shared very poor identity with both the overall lipase 3 domain (marked in yellow) and the active site (marked in gray) of the DAG lipases **(Fig.6.2)**. Another key feature of a lipase is a catalytic triad consisting of highly conserved Ser-His-Asp residues (marked in blue) which are vital for the nucleophilic attack and hydrolytic activity of

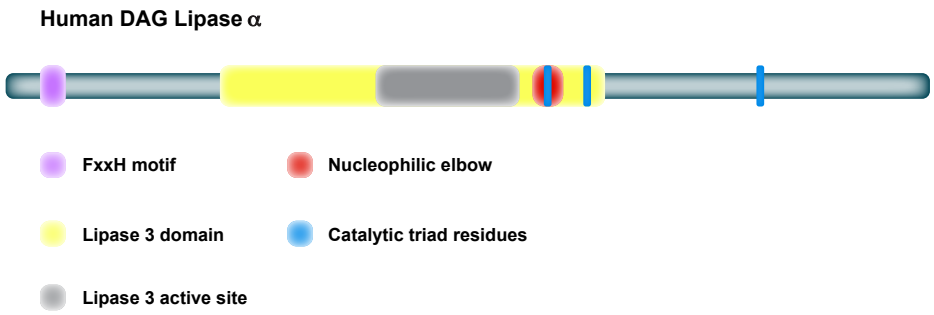

Figure 6.1 : Domain organisation of human DAG lipase α
The signature domains of DAG lipase α in humans. The yellow region marks the lipase 3 domain of DAG lipases. Gray marks the active site of the enzyme, red indicates the nucleophilic elbow and purple donates the FxxH motif. The residues of the catalytic triad have been marked in blue. All annotations have been made in accordance with the NCBI conserved domain database.

esterases (Cygler et al., 2008; Aitken, 1999) **(Fig.6.3)**. While we found the serine residue of human DAG lipases to be conserved in STMA, we failed to find histidine or aspartate residues at the corresponding positions **(Fig.6.3)**. However, better insight on the positions of His and Asp can only be provided based on structural data, since these are residues that directly interact with the substrate (DAG) and catalyse the reaction. One common feature shared by the proteins was a nucleophilic elbow (marked in red) **(Fig.6.2)**. This GxSxG motif is present in a large variety of proteins, ranging from esterases to proteases (Aitken, 1999). Although this motif can confer enzymatic activity to STMA, it may not correspond to that of a DAG lipase.

A simple protein sequence alignment may not account for variations in conserved sequences or motifs, which would show up as mismatches in conventional CLUSTAL based algorithms. In order to determine whether any variants of the lipase 3 active site (**Fig.6.2** - gray region) are present in STMA, we built a consensus sequence of the region. A consensus sequence denotes the most commonly occurring amino acids in a given protein stretch along with the range of possible substitutions. We used Consurf (Ashkenazy et al., 2016) to align DAG lipases (both α and β types) from 16 different organisms and mark the most highly conserved amino acids between these proteins (**Fig.6.4** - shaded regions correspond to earlier alignments). The conservation scores assisted us in building a position specific scoring matrix (PSSM - details in Section 2.8). The matrix assigns a score to every amino acid position based on frequency of occurrence, enabling us to incorporate allowed

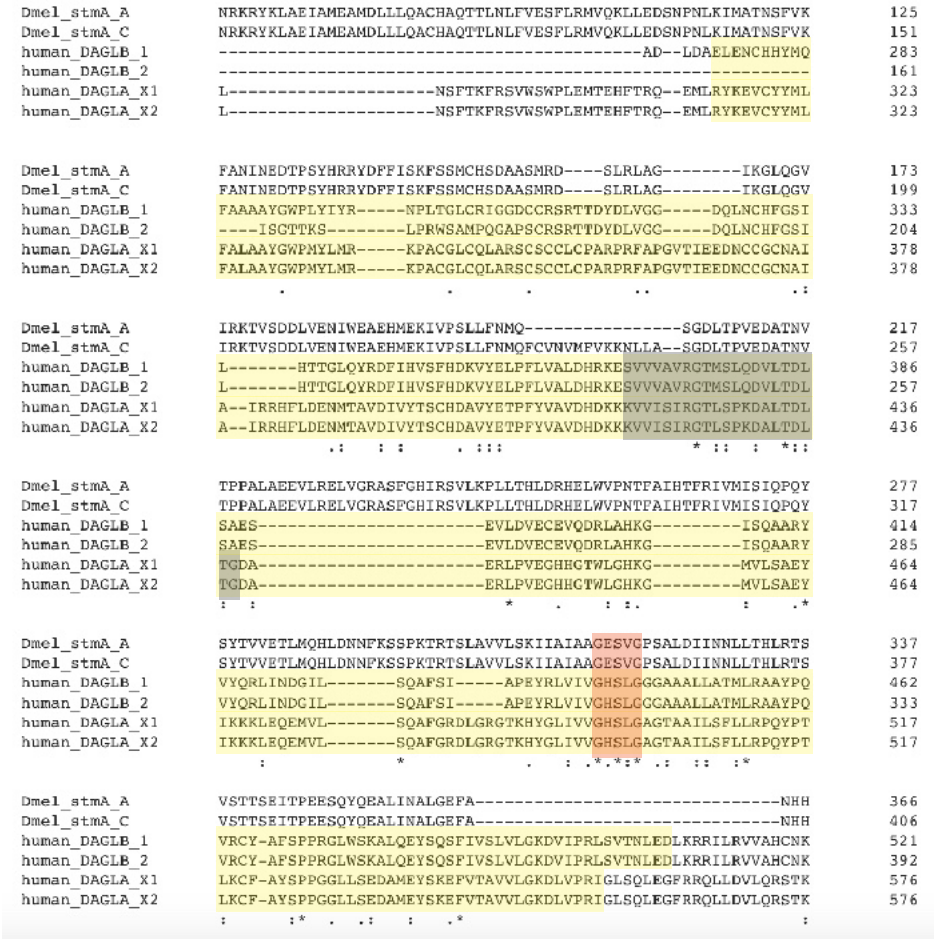

Figure 6.2 : Alignment of STMA with human DAG lipases
The longest STMA isoforms have been aligned with the longest DAG lipase α (DAGLA) and β (DAGLB) isoforms in humans. The yellow region marks the lipase 3 domain of DAG lipases. Gray marks the active site of the enzyme and red indicates the nucleophilic elbow. All annotations have been made in accordance with the NCBI conserved domain database.

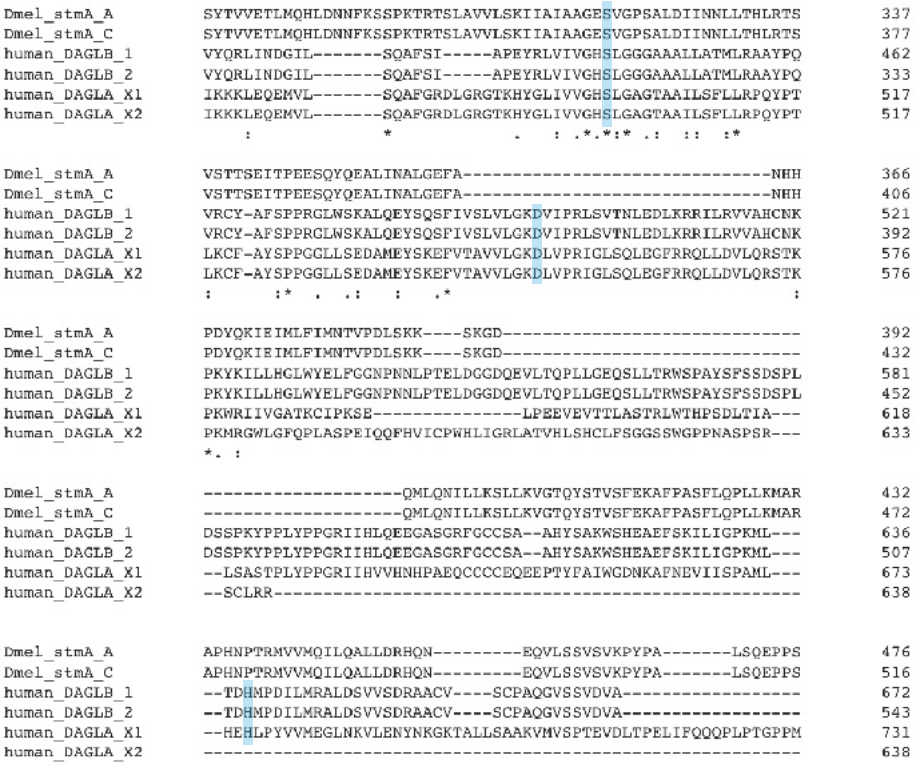

Figure 6.3 : Alignment of STMA with human DAG lipases
The longest STMA isoforms have been aligned with the longest DAG lipase α (DAGLA) and β (DAGLB) isoforms in humans. The yellow region marks the lipase 3 domain of DAG lipases. The blue residues mark the catalytic triad of Serine, Aspartate and Histidine required for the enzymatic activity of lipases.

substitutions and variations (Henikoff and Henikoff, 1994, 1996). Based on the Consurf alignments, the consensus sequence used for the active site was V-V-x(3)-R-G-T-x-S-x(2)-D-x-L-T-D. The PSSM was also validated using the NCBI tool for the same, which produced a very similar sequence of R-G-T-x-S-x(2)-D-x-L-T-D-L-T. Both consensus sequences were used as a queries in ScanPROSITE, which scans the UniProt protein database and returns any proteins matching the query (de Castro et al., 2006).

The consensus sequence of the human DAG lipase α active site did not return STMA as a hit, but it did return other mammalian and fungal DAG/TAG lipases, confirming that the consensus was correct. It also returned the protein INAE from *Drosophila*, which has been shown to have sn-1 specific DAG lipase activity *in vitro* (Leung et al., 2008). Further queries with shorter or more liberal sequences did not return any hits for STMA, indicating that STMA most likely does not contain a region corresponding to the DAG lipase active site. We also scanned all consensus sequences against only the STMA sequence and did not find any matching regions.

Apart from the lipase 3 domain, an additional FxxH motif in the C-terminus was also found to be vital for substrate selectivity in fungal lipases (**Fig.6.4** - purple region), enabling discrimination between triacylglycerols and di/monoacylglycerols (Liu et al., 2013). A single copy of this motif was conserved in almost all α-type DAG lipases, but not the β-type lipases. When used as a query in ScanPROSITE and scanned against the *Drosophila* proteome, the FxxH motif returned STMA as a hit, but the location of the motif was not in the C-terminus as in fungal lipases, nor in the N-terminus as in mammalian or other invertebrate DAG lipases **(Fig.6.5)**. In fact, the STMA protein had two copies of the FxxH motif in the middle region, which may be due to structural differences between DAG lipases and STMA **(Fig.6.6)**.

We next assessed the relatedness of the STMA and DAG lipases by building a phylogenetic tree. We performed a multiple alignment of protein sequences for DAG lipase α, DAG lipase β and Efr3 from 19 different organisms, ranging from fungi to humans. We used the human angiopoietin 2 as an outlier. We then constructed a maximum likelihood tree using the MEGA 7 software (Kumar et al., 2016). The resulting tree showed a clear separation of Efr3 and DAG lipases, with both sets of proteins forming different clusters. The STMA protein was present in the Efr3 cluster, implying that it is more related to Efr3 and not to DAG lipases **(Fig.6.7)**. On the other hand, INAE was seen in the DAG lipase cluster, confirming its annotation as a DAG lipase.

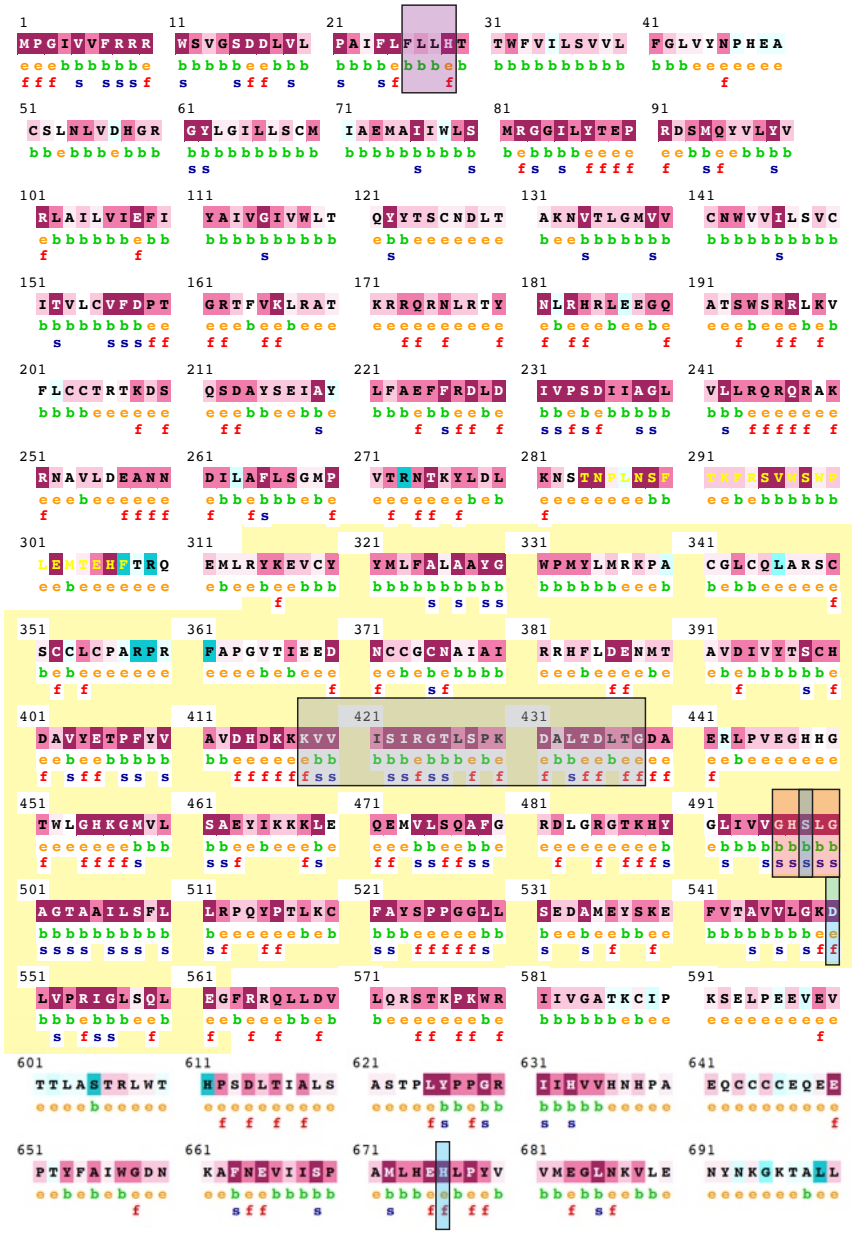

Figure 6.4 : Conserved residues in human DAG lipase α
Consensus amino acid sequence generated by Consurf, with the amino acids scored by degree of conservation. Darker shades of maroon indicate higher degree of conservation. Yellow highlights the lipase 3 domain, gray marks the active site, red indicated the nucleophilic elbow and blue marks the catalytic triad. Purple denotes the FxxH motif, which supposedly confers substrate specificity to lipases.

Figure 6.5 : ScanProsite results for FxxH motif
(A) FxxH motif is located towards the C-terminus of the DAG lipase protein in fungi. **(B)** A single FxxH motif is located towards the N-terminus of the DAG lipase α protein in invertebrates.

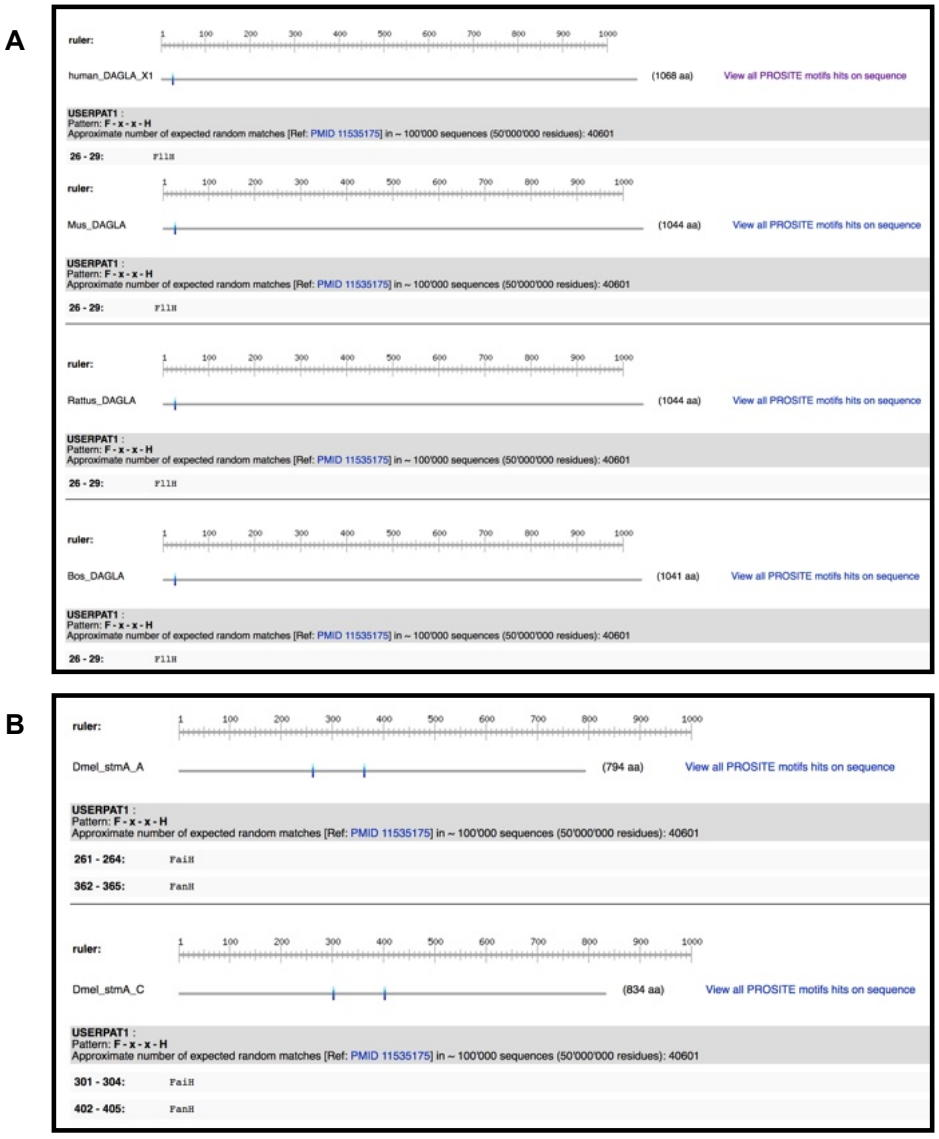

Figure 6.6 : ScanProsite results for FxxH motif
(A) A single FxxH motif is located towards the N-terminus of the DAG lipase α protein in mammals. **(B)** Two copies of the FxxH motif are located in the middle of the STMA protein in *Drosophila*.

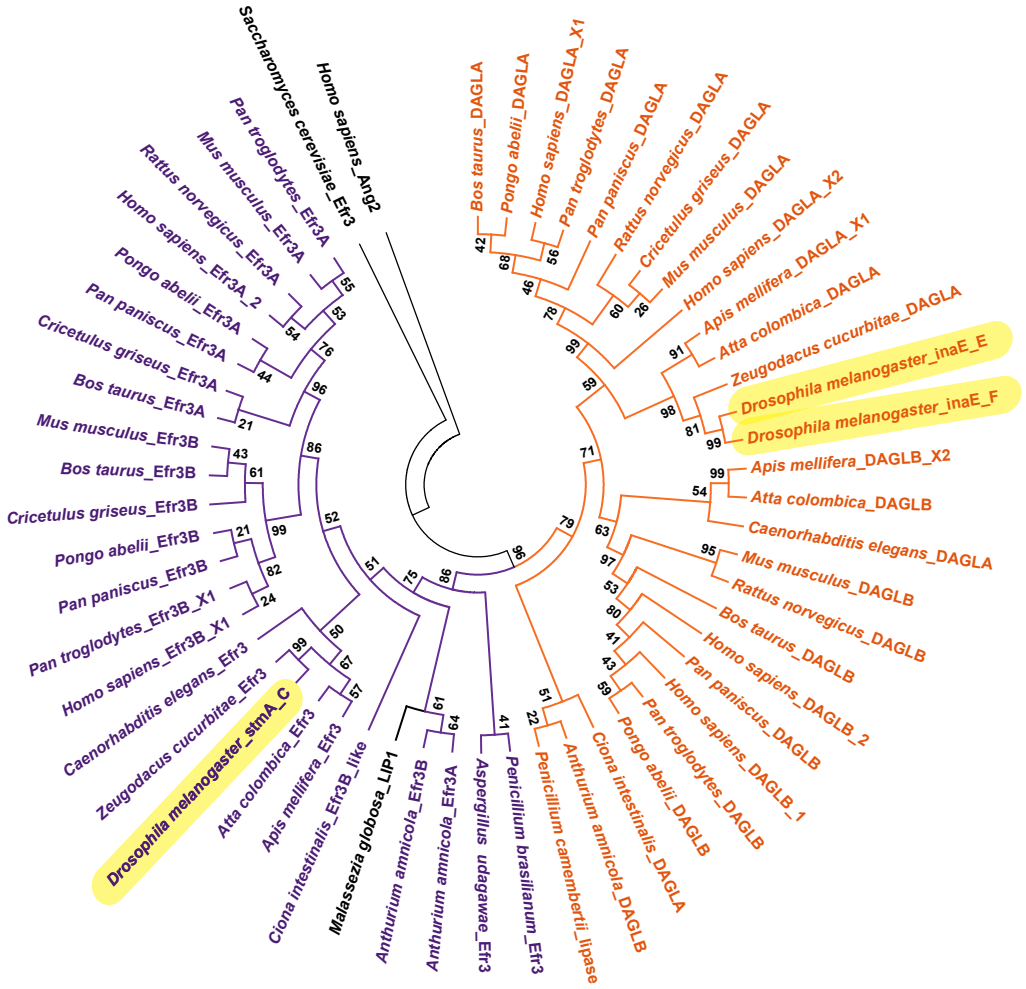

Figure 6.7 : Phylogenetic analysis of Efr3 and DAG lipases
The protein sequences of Efr3A and B isoforms and DAG lipase α and β isoforms from nineteen organisms spanning different orders were aligned and analysed. The *Drosophila* STMA and INAE sequences are highlighted in yellow. Mega7 was used to generate a nearest-neighbour phylogenetic tree; the analysis was performed using the WAG+G model run for 1000 bootstraps.

6.3 Knocking down *stmA* does not affect DAG and PA levels in *Drosophila* retinae

The role of *stmA* as a regulator of PI4P and PIP_2 was demonstrated earlier in this thesis using a combination of LC-MS and microscopy. If it is indeed a regulator of DAG levels as well, one might anticipate some discernible changes in the levels of DAG in the absence of *stmA* function. Additionally, if the DAG lipase activity is relevant to phototransduction, a correspondence in the acyl chain composition of DAG and PIP_2 is probable since DAG is a direct product of PIP_2 hydrolysis. During the PIP_2 resynthesis cycle, DAG is further converted to PA by the enzyme *rdgA*, implying that any significant changes in DAG levels would also be reflected in the levels of PA (Inoue et al., 1989; Yoshioka et al., 1984; Garcia-Murillas et al., 2006). Therefore, the amount of PA could serve as a secondary readout of DAG levels.

When we set out to quantify DAG in photoreceptors, we lacked a functional DAG-binding probe to work with. We therefore relied on LC-MS to quantify the lipid levels in retinae. We adapted a method developed by the NCBS Lipidomics Facility (Details in Materials and Methods). Fortunately, the same method could be used to quantify phosphatidic acid (PA) and phosphatidylethanol (PE) as well. The amount of PE in retinal tissue was used to normalise the levels of DAG and PA, as done in Section 3.5.

6.3.1 Standardisation of LC-MS method to quantify DAG and PA

We first assessed the sensitivity of the method by preparing serial dilutions of synthetic internal standards for DAG, PA and PE. These dilutions were subjected to a neutral lipid extraction and the extracted standards were quantified using the LC-MS method (details in Section 2.5). The standard curves for each lipid class were linear, with the r^2 values being ~0.98 **(Fig.6.8)**. With this, the sensitivity and linearity of the method was validated and we proceeded with experiments using biological samples.

Using freeze-dried retinal tissue as the source material, we extracted the lipids and subjected them to LC-MS analysis. Although we were able to detect multiple acyl chain species of DAG, PA and PE, we focussed solely on the species 36:2, 36:3 and 36:4, since these were also the most abundant species of PIP_2 in retinae (Sections 3.5, 4.2 and 4.3). Moreover, since we were quantifying DAG levels in the context of phototransduction, we chose to analyse only those acyl chains that had previously shown to be responsive

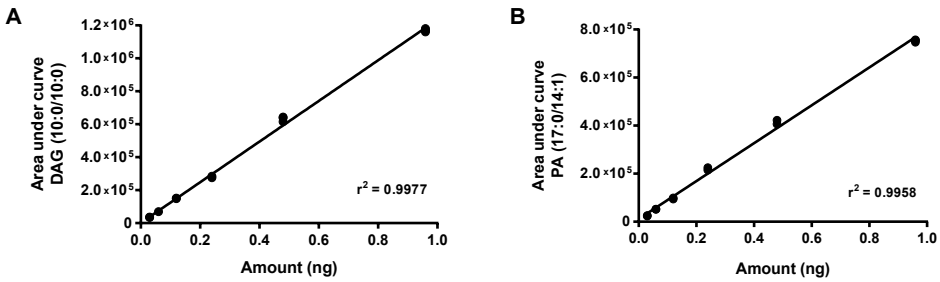

Figure 6.8 : Standard curve analysis of synthetic lipid standards (A) and (B) Response linearity curves for the synthetic lipid standards of C(10:0/10:0)DAG and C(17:0/14:1)PA, respectively. x-axis represents amount in ng; y-axis represents area under the curve.

to light in a sensitised background (Sections 3.5, 4.2 and 4.3).

In order to test the method using retinal tissue, we first analysed the levels of PA in wild-type flies that were subjected to two treatments - one group was reared and processed completely in dark and the other was reared in dark and then exposed to constant light for 12 hours after eclosion. It has been previously documented that WT flies exhibit an increase in PA levels upon exposure to light, as measured using LC-MS (Garcia-Murillas et al., 2006; Panda et al., 2018). In accordance with these reports, we also saw that the levels of PA in these flies were higher in the light treated group than in the dark-reared group. There was also a marginal increase in DAG levels, but they were not all statistically significant **(Fig.6.9A and B)**. The PE levels remained constant across light treatments **(Fig.6.9C)**, re-affirming its suitability as a control lipid for normalisation.

For the next set of positive control experiments, we used well-characterised mutants for known regulators of PA in photoreceptors. The gene *rdgA* encodes a DAG-kinase that converts DAG to PA in the photoreceptors (Inoue et al., 1989; Yoshioka et al., 1984). Null mutants for *rdgA* ($rdgA^3$) have been previously shown to have reduced levels of PA, using both traditional TLC and more recent LC-MS methods (Inoue et al., 1989; Yoshioka et al., 1984; Garcia-Murillas et al., 2006). We measured the levels of PA from WT controls and $rdgA^3$ mutants that were subjected to the same light-dark treatment as the initial WT control experiment. We found that the PA levels in the $rdgA^3$ flies were significantly lower than those of WT flies in both dark and light-exposed groups, confirming the previous results **(Fig.6.10A and C)**. We also found a corresponding increase in the DAG levels of light-exposed

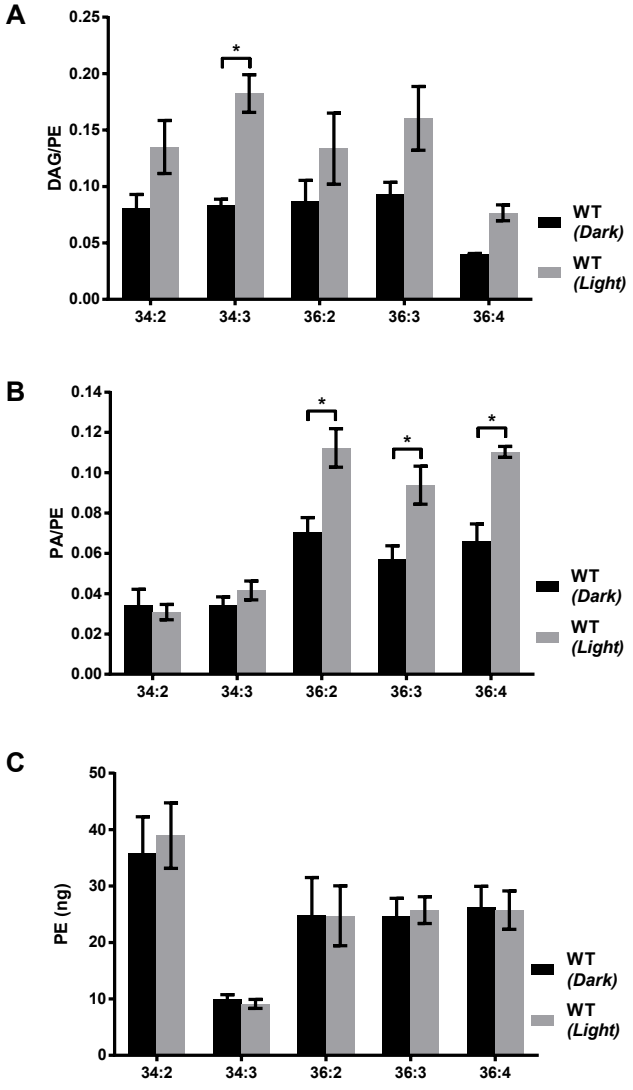

Figure 6.9 : LC-MS measurement of DAG and PA in wild-type *Drosophila* retinae
(A), (B) and (C) Liquid chromatography - mass spectrometry measurement of DAG, PA and PE levels respectively in retinae of wild-type dark-reared flies (black bars) and flies exposed to constant light for 12 h (grey bars) before processing. * - $p < 0.05$ as per one way ANOVA followed by Tukey's multiple comparison test, values are mean $\pm$ s.e.m., n = 40 retinae per sample.

rdgA^3 mutants, which was expected in a scenario where the conversion of DAG to PA was stalled **(Fig.6.10D)**.

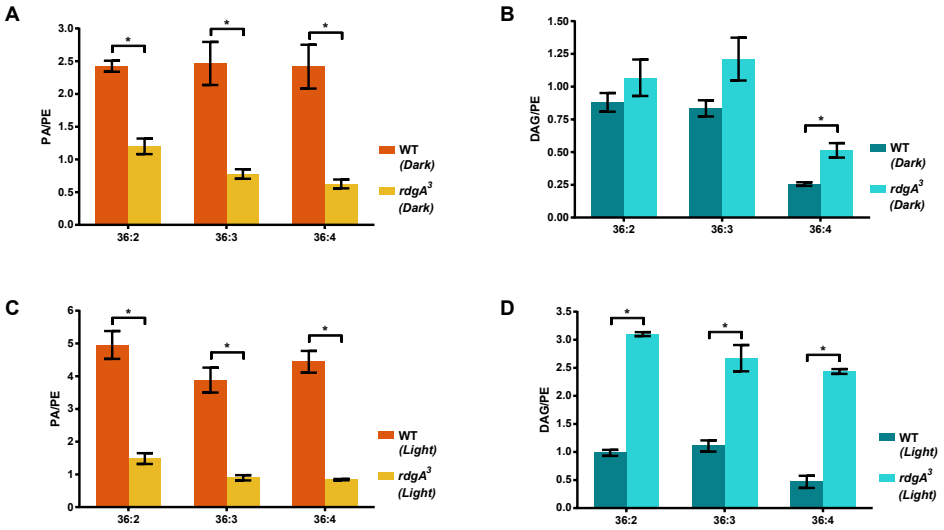

Figure 6.10 : LC-MS measurement of PA and DAG in *rdgA*^{3} retinae

Liquid chromatography - mass spectrometry measurement of PA and DAG levels in retinae of *rdgA*^{3} flies. **(A) and (B)** The flies were reared and processed in dark. **(C) and (D)** The flies were exposed to constant light for 12 h before processing. * - $p < 0.05$ as per one way ANOVA followed by Tukey's multiple comparison test, values are mean ± s.e.m., n = 40 retinae per sample.

We performed a final set of positive controls using loss-of-function mutants for the PA-phosphatase *lazaro* (*laza*^{22}), which converts PA to DAG in photoreceptors. Previous LC-MS measurements of PA levels from *laza*^{22} retinae have shown that they are significantly higher than those of WT flies (Garcia-Murillas et al., 2006). We performed similar experiments, where WT controls and *laza*^{22} flies were subjected to the same light treatment as *rdgA*^{3} mutants. When we analysed the PA levels, we found that they were higher in *laza*^{22} flies than in WT flies, for both dark-reared and light-exposed groups **(Fig.6.11A and C)**. The DAG levels in these flies were not significantly altered **(Fig.6.11B and D)**.

Hence, we were able to use two well-established mutants to prove that the developed LC-MS methods was capable of detecting changes in PA and DAG levels in photoreceptors.

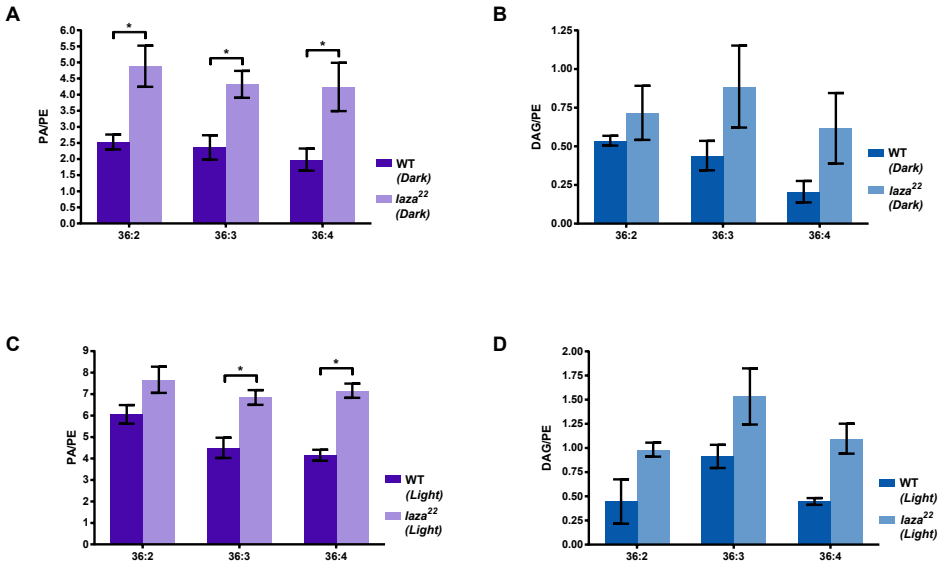

Figure 6.11 : LC-MS measurement of PA and DAG in *laza*^{22} retinae

Liquid chromatography - mass spectrometry measurement of PA and DAG levels in retinae of *laza*^{22} flies. **(A) and (B)** The flies were reared and processed in dark. **(C) and (D)** The flies were exposed to constant light for 12 h before processing. * - $p < 0.05$ as per one way ANOVA followed by Tukey's multiple comparison test, values are mean ± s.e.m., n = 40 retinae per sample.

6.3.2 Measurement of DAG and PA levels in *GMR > stmA^i* flies

Given that we lacked an existing positive control for changes in DAG levels, we proceeded directly with measurements from flies where *stmA* was downregulated. Having demonstrated that knocking down *stmA* results in ERG defects similar to those of the temperature-sensitive mutants (Section 5.1), we performed all measurements from *GMR > stmA^i* flies. This was also because we had the corresponding PIP and PIP_2 measurements from these flies. To maintain correspondence between the measured PIP and PIP_2 levels and future measurements of DAG and PA, we limited the duration of light exposure to one minute of blue light, as done in Section 5.3.

When we measured the DAG levels in *GMR > stmA^i* flies and their controls, we found that were no significant differences between the two genotypes, in either dark-reared or light-exposed flies. Both control and *GMR > stmA^i* flies did show a small increase in DAG upon light treatment, but this did not apply to all the acyl chain species **(Fig.6.12A and C)**. This lack of difference between *stmA* knockdown and control flies was also seen in terms of the PA levels **(Fig.6.12B and D)**. Neither genotype showed a light-dependent increase in PA levels, but this was probably due to the short duration of light exposure as compared to the experiments with WT flies.

The fact that downregulating *stmA* had no discernible effect on either DAG or PA levels in light-exposed photoreceptors indicates that it is most likely not a regulator of DAG during phototransduction, at least on the small timescales of PIP and PIP_2 changes.

6.4 Conclusion

We investigated the possibility of the STMA protein being a DAG lipase that is active during phototransduction, using a combination of bioinformatic and lipid quantification techniques.

6.4.1 Main Conclusions

Sequence analysis of the STMA protein revealed that it does not carry the key signatures of annotated DAG lipases, namely a lipase 3 active site and a conserved catalytic triad. The domain architecture of STMA does not correspond to those seen in mammalian or fungal DAG lipases. This implies that, based on protein sequence, it is unlikely that STMA hydrolyses DAG

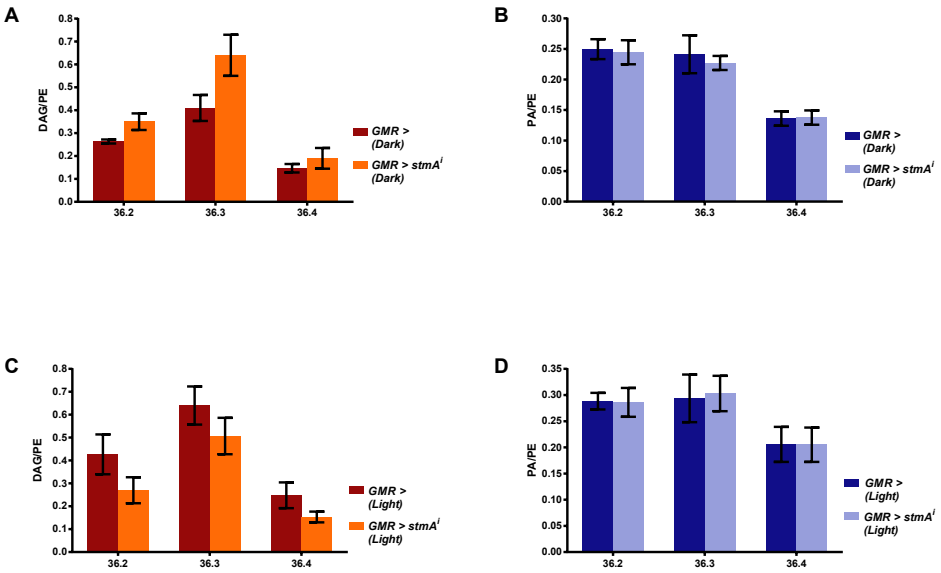

Figure 6.12 : LC-MS measurement of DAG and PA in *GMR > stmA^i* retinae

Liquid chromatography - mass spectrometry measurement of DAG and PA levels in retinae of *GMR > stmA^i* flies. **(A) and (B)** The flies were reared and processed in dark. **(C) and (D)** The flies were exposed to constant light for 12 h before processing. * - $p < 0.05$ as per one way ANOVA followed by Tukey's multiple comparison test, values are mean ± s.e.m., n = 40 retinae per sample.

to produce free fatty acids and monoacylglycerol. Phylogenetic analysis also showed that STMA is more similar to the Efr3 family of proteins rather than that of DAG lipases. Based on queries using a consensus sequence for the lipase 3 active site, we found that the protein INAE, encoded by the gene *inaE*, in *Drosophila*, is most likely the orthologue of DAG lipase. It shares sequence similarity with the human DAG lipases in regions both within and outside of the active site (Leung et al., 2008) and also clustered with the DAG lipases in the phylogenetic tree that was generated.

We further quantified the levels of DAG and PA in flies that had low levels of STMA transcripts. These flies had previously been shown to have ERG defects similar to those of $stmA^{ts}$ mutants. Neither the DAG nor the PA levels in $GMR > stmA^{i}$ flies showed any change when compared to control flies. This held true irrespective of whether the flies were reared in dark or whether they were exposed to light upon eclosion.

6.4.2 Domain architecture of STMA

While the most important contributors to lipase activity seemed to be missing in STMA, we did find a short motif which was thought to confer substrate specificity to fungal lipases. The FxxH motif was present in all α-type DAG lipases, along with the fungal lipases and STMA as well. However, the position and copy numbers of the motif differed between the lipases and STMA. Given a lack of structural information, it is difficult to make further inferences about the relevance of this motif in STMA.

The STMA protein in flies is poorly characterised in terms of molecular function. Although there exist studies pointing to a role in regulating endocytosis and neurogenesis, there are no mechanistic insights into these possibilities. Currently, we do have evidence of a role for *stmA* in regulating PLC signalling, by virtue of its association with PI4KIIIα. Downregulation of *stmA* clearly reduces the amount of PIP and PIP_2 in retinae, coupled with a distinct defect in the light response. Both of these effects of *stmA* knockdown echo those of *PI4KIIIα* knockdown, strengthening the probability that the two proteins work together in photoreceptors.

Owing to lack of a crystal structure, it is also unclear as to how the protein is localised to the plasma membrane. Initially predicted to be a transmembrane protein, this was later called into question upon seeing that neither the mouse nor yeast orthologues possessed any transmembrane helices. Moreover, both mouse and yeast proteins have different mechanisms of plasma membrane localisation - the mouse Efr3 undergoes palmitoylation at the N-terminus,

whereas the yeast Efr3 has a patch of basic amino acids at the N-terminus which binds to the negatively charged lipids in the plasma membrane.

When the secondary structure of STMA was predicted using PSIPRED, we found that STMA has two alpha helices which could potentially be transmembrane helices. It also has a signature for palmitoylation at the N-terminus, which is closely aligned with that of mammalian Efr3. Further insights into the architecture of STMA would require either rigorous modelling or solving the crystal structure to determine the three dimensional organisation of the amino acids.

Bibliography

A. Aitken. Protein consensus sequence motifs. *MOLECULAR BIOTECHNOLOGY*, 12:13, 1999.

H. Ashkenazy, S. Abadi, E. Martz, O. Chay, I. Mayrose, T. Pupko, and N. Ben-Tal. ConSurf 2016: An improved methodology to estimate and visualize evolutionary conservation in macromolecules. *Nucleic Acids Research*, 44(W1):W344–W350, July 2016. ISSN 0305-1048, 1362-4962. doi: 10.1093/nar/gkw408.

S. Chyb, P. Raghu, and R. C. Hardie. Polyunsaturated fatty acids activate the Drosophila light-sensitive channels TRP and TRPL. *Nature*, 397(6716):255–259, Jan. 1999. ISSN 0028-0836, 1476-4687. doi: 10.1038/16703.

M. Cygler, J. D. Schrag, J. L. Sussman, M. Harel, I. Silman, M. K. Gentry, and B. P. Doctor. Relationship between sequence conservation and three-dimensional structure in a large family of esterases, lipases, and related proteins. *Protein Science*, 2(3):366–382, Dec. 2008. ISSN 09618368, 1469896X. doi: 10.1002/pro.5560020309.

E. de Castro, C. J. A. Sigrist, A. Gattiker, V. Bulliard, P. S. Langendijk-Genevaux, E. Gasteiger, A. Bairoch, and N. Hulo. ScanProsite - detection of PROSITE signature matches and ProRule associated functional and structural residues in proteins.pdf. *Nucleic Acids Research*, 34, 2006.

R. Delgado, M. G. Delgado, L. Bastin-Héline, A. Glavic, P. M. O'Day, and J. Bacigalupo. Light-Induced Opening of the TRP Channel in Isolated Membrane Patches Excised from Photosensitive Microvilli from Drosophila Photoreceptors. *Neuroscience*, 396:66–72, Jan. 2019. ISSN 03064522. doi: 10.1016/j.neuroscience.2018.11.017.

I. Garcia-Murillas, T. Pettitt, E. Macdonald, H. Okkenhaug, P. Georgiev, D. Trivedi, B. Hassan, M. Wakelam, and P. Raghu. Lazaro Encodes a Lipid Phosphate Phosphohydrolase that Regulates Phosphatidylinositol Turnover during Drosophila Phototransduction. *Neuron*, 49(4):533–546, Feb. 2006. ISSN 08966273. doi: 10.1016/j.neuron.2006.02.001.

R. C. Hardie and P. Raghu. Visual transduction in Drosophila. 413:8, 2001.

J. G. Henikoff and S. Henikoff. Using substitution probabilities to improve position-specific scoring matrices. *Bioinformatics*, 12(2):135–143, 1996. ISSN 1367-4803, 1460-2059. doi: 10.1093/bioinformatics/12.2.135.

S. Henikoff and J. G. Henikoff. Position-based sequence weights. *Journal of Molecular Biology*, 243(4):574–578, Nov. 1994. ISSN 00222836. doi: 10.1016/0022-2836(94)90032-9.

T. Hofmann, A. G. Obukhov, M. Schaefer, C. Harteneck, T. Gudermann, and G. Schultz. Direct activation of human TRPC6 and TRPC3 channels by diacylglycerol. *Letters to Nature*, 397, 1999.

F.-D. Huang, H. J. G. Matthies, S. D. Speese, M. A. Smith, and K. Broadie. Rolling blackout, a newly identified PIP2-DAG pathway lipase required for Drosophila phototransduction. *Nature Neuroscience*, 7(10):1070–1078, Oct. 2004. ISSN 1546-1726. doi: 10.1038/nn1313.

H. Inoue, T. Yoshioka, and Y. Hotta. Diacylglycerol Kinase Defect in a Drosophila Retinal Degeneration Mutant rdgA. *Journal of Biological Chemistry*, 264(10):5996–6000, 1989.

S. Kumar, G. Stecher, and K. Tamura. MEGA7: Molecular Evolutionary Genetics Analysis Version 7.0 for Bigger Datasets. *Molecular Biology and Evolution*, 33(7):1870–1874, July 2016. ISSN 0737-4038, 1537-1719. doi: 10.1093/molbev/msw054.

H.-T. Leung, J. Tseng-Crank, E. Kim, C. Mahapatra, S. Shino, Y. Zhou, L. An, R. W. Doerge, and W. L. Pak. DAG Lipase Activity Is Necessary for TRP Channel Regulation in Drosophila Photoreceptors. *Neuron*, 58(6): 884–896, June 2008. ISSN 08966273. doi: 10.1016/j.neuron.2008.05.001.

L. Liu, D. Lang, Q. Wang, C. Gao, Z. Li, B. Yang, and Y. Wang. A "bridge-like" structure responsible for the substrate selectivity of mono- and diacylglycerol lipase from Aspergillus oryzae.pdf. *Journal of Molecular Catalysis B: Enzymatic*, 97:144–149, 2013.

F. Nakatsu, J. M. Baskin, J. Chung, L. B. Tanner, G. Shui, S. Y. Lee, M. Pirruccello, M. Hao, N. T. Ingolia, M. R. Wenk, and P. D. Camilli. PtdIns4P synthesis by PI4KIIIα at the plasma membrane and its impact on plasma membrane identity. *J Cell Biol*, 199(6):1003–1016, Dec. 2012. ISSN 0021-9525, 1540-8140. doi: 10.1083/jcb.201206095.

A. Panda, R. Thakur, H. Krishnan, A. Naik, D. Shinde, and P. Raghu. Functional analysis of mammalian phospholipase D enzymes. *Bioscience Reports*, 38(6):BSR20181690, Dec. 2018. ISSN 0144-8463, 1573-4935. doi: 10.1042/BSR20181690.

P. Raghu, K. Usher, S. Jonas, S. Chyb, A. Polyanovsky, and R. C. Hardie. Constitutive Activity of the Light-Sensitive Channels TRP and TRPL

in the Drosophila Diacylglycerol Kinase Mutant, rdgA. *Neuron*, 26(1): 169–179, Apr. 2000. ISSN 08966273. doi: 10.1016/S0896-6273(00)81147-2.

T. Yoshioka, H. Inoue, and Y. Hotta. Absence of diglyceride kinase activity in the photoreceptor cells of Drosophila mutants. *Biochemical and Biophysical Research Communications*, 119(1):389–395, Feb. 1984. ISSN 0006291X. doi: 10.1016/0006-291X(84)91664-4.

Chapter 7

Discussion

7.1 Main conclusions of this study

In this thesis, the function of the *PI4KIIIα* gene and its activity in the regulation of *Drosophila* phototransduction has been analysed. The main conclusions are as follows:

- RNAi-mediated downregulation of *PI4KIIIα* specifically in the retinal tissue negatively impacts the electrical response to light in *Drosophila*. The amplitude of the light response, as well as overall sensitivity of the eye to light, is reduced in these flies. The decrease in light response was accompanied by a significant drop in the levels of PI4P and PIP_2 in the rhabdomeres of these flies. This was further validated by quantitative measurements using LC-MS. All of the described defects could be completely rescued by reconstituting the system with the human *PI4KIIIα*. A kinase-dead allele of human *PI4KIIIα* could not rescue any of the defects, highlighting the requirement for kinase activity of the protein in the eye. Essentially, we were able to demonstrate a requirement for a kinase-dependent function of *PI4KIIIα* during phototransduction in *Drosophila* photoreceptors.
- We examined the genetic interactions of *PI4KIIIα* with the elements immediately upstream and downstream to its function in the PIP_2 resynthesis pathway. The immediate upstream element, *rdgB*, is a PI transfer protein that supplies the substrate PI for PI4KIIIα to convert to PI4P. We found that *PI4KIIIα* downregulation was able to marginally suppress the effect of a hypomorphic allele of *rdgB*, both in terms of the light response and lipid levels. On the other hand,

the interaction of *PI4KIIIα* with its immediate downstream element, *dPIP5K*, showed an additive effect. Knocking down *PI4KIIIα* in the background of *dPIP5K* null mutants simply worsened the reduced light response of the mutants. However, in terms of the lipid levels, the effect of knocking down *PI4KIIIα* appeared to dominate the effect of removing *dPIP5K*.

- In other model systems, PI4KIIIα has been shown to be recruited to the plasma membrane as a complex with two other proteins - Efr3 and TTC7. We investigated whether the *Drosophila* orthologues of these two proteins (STMA and TTC7) had a role to play in the same cellular processes that require PI4KIIIα function. Knocking down both *stmA* and *TTC7* exhibited identical phenotypes to knocking down *PI4KIIIα*. The light response in these flies was highly reduced, as was the sensitivity of the system. Importantly, both PI4P and PIP_2 levels were reduced in the rhabdomeres of these flies, indicating that a lack of these proteins impacts the ability of the cell to produce sufficient amounts of PI4P at the plasma membrane. The defects associated with the light response could be partially rescued by reconstituting the system with the mammalian orthologues of *stmA* and *TTC7*, pointing to a specificity of the effect.

- The gene *stmA* has previously been annotated as a DAG lipase, based on biochemical measurements of DAG from conditional loss-of-function mutant fly photoreceptors. We attempted to verify this annotation by using LC-MS to measure DAG and PA in *Drosophila* retinae where *stmA* was knocked down. We standardised and validated the method using loss-of-function mutants for members of the PIP_2 cycle that display known changes in PA levels. We were unable to show any conclusive changes in the DAG or PA levels of *stmA* downregulated flies, strongly indicating that *stmA* is not a modulator of DAG. These flies, however, do show a clear decrease in PIP and PIP_2 levels upon being subjected to a light stimulus. Therefore, the effects on the light response in these flies are most likely a product of impaired PI4P synthesis.

7.2 PI4K as the rate limiting step in the PIP_2 resynthesis cycle

The idea of PIP_2 resynthesis as a closed loop is rooted in early experiments from the 1960s, where it was demonstrated that ^{32}P labelled ATP was incorporated into phosphoinositides and phosphatidic acid of erythrocyte ghosts (Hokin and Hokin, 1964). Subsequent studies monitoring the depletion and recovery of both PI4P and PIP_2 cemented the idea of a cycle involving continuous breakdown and synthesis of these lipids (Downes et al., 1982; Creba et al., 1983; Willars et al., 1998). Two decades later, studies on the inhibitory effect of lithium on myo-inositol synthesis gave rise to the "lithium hypothesis", which proposed that recycling of IP_3 to inositol is required for PIP_2 resynthesis as well (Berridge et al., 1982, 1989). The traditional view of PIP_2 resynthesis as a closed cycle persists even today, with the model being used to make inferences in signalling systems ranging from hormone receptors to phototransduction (Cockcroft and Raghu, 2016; Tóth et al., 2016).

Recent computational work from our lab has demonstrated this closed architecture of the cycle is likely flawed as it cannot recapitulate the lipid dynamics as measured in known mutants. This prompted the construction of a second type of cycle with an open architecture, where there is an additional source and sink attached to the closed cycle. The source feeds into the cycle and the sink leads away from it. This open cycle was able to capture the lipid dynamics of well characterised mutants, further validating the model (Suratekar et al., 2018). The new model, along with the genetic interaction data from this thesis, prompts some rethinking of the traditional PIP_2 cycle.

7.2.1 Evidence for increased PI4K and PIP5K activity upon PLC stimulation

Experiments performed both in mammalian cells and this thesis show that upon PLC stimulation, both PIP_2 and PI4P are depleted from the plasma membrane with very closely matched kinetics (Creba et al., 1983; Willars et al., 1998; Balla et al., 2008, Section 3.6). Using the earlier described mathematical model, it appeared that incorporation of feedback interactions between enzymes and lipids was a possible way of recapturing the PIP_2 and PI4P dynamics, which was otherwise not possible using just the open cycle model. It was seen that some modulation of the activities of PI4K, dPIP5K and/or PLC could explain the depletion of both PIP_2 and PI4P during PLC activation (Suratekar, 2018).

This prediction from the model already has some biological evidence to support it. Several studies have indicated that the activities of both PI4K and PIP5K are increased upon agonist stimulation. Early work from rat kidney cells used a combination of biochemical measurements and first order kinetic modelling to show that the activities of the PI4K and PIP5K in the system were greater under conditions of stimulation. In these experiments, radiolabelled PIP and PIP_2 levels were measured before, during and after termination of PLC signalling. They found that when signalling was initiated, both the lipid levels dropped, but then recovered to a steady state that was maintained until termination of signalling. The kinetic modelling indicated that, in order to maintain the lipid levels, the enzymatic activities of both PI4K and PIP5K would have to be significantly higher during signalling (Chahwala et al., 1987). Another study conducted in human platelets tracked the levels of radiolabelled PIP and PIP_2 in the cells before and after treatment with thrombin and reached similar conclusions (Steen et al., 1989).

More recent work from *Xenopus* oocytes has shown that membrane depolarisation increases the levels of PIP_2 at the plasma membrane, which in turn is required for the activity of KCNQ2/3 potassium channels. The increase in PIP_2 and subsequent potassium channel current was abolished by the chemical inhibition of the class III PI 4-kinases by wortmannin, implying that the increase in PIP_2 was a consequence of increased PI4K activity (Zhang et al., 2010).

Another set of studies in neuronal cell cultures used a voltage sensitive phosphatase (VSP) to selectively dephosphorylate PIP_2 at the fifth position, leaving the cell with reduced PIP_2 and high amounts of PI4P. The recovery of PIP_2 in this scenario would chiefly be dependent on the activity of a PIP 5-kinase, since the substrate PI4P is already available. When PIP_2 recovery was monitored, it was found to be of the order of 11 s. However, when PLC signalling was triggered in the same cells using the M3 muscarinic receptor and PIP_2 levels monitored, the recovery took much longer, about 130 s. The key difference was the presence of PI4P, which was already at the plasma membrane in the first case, whereas in the second case PI4P needed to be synthesised from PI before being converted to PIP_2. Assuming equivalent levels of PIP5K activity, it would appear that the additional PI 4-kinase activity in the second scenario contributes the delay in PIP_2 recovery, implying that it is a catalytically slower step than PIP5K that requires a boost in activity during stimulation to keep up with the rate of PIP_2 synthesis and hydrolysis (Falkenburger et al., 2010).

7.2.2 Synthesis of PI4P by PI4KIIIα as a potential rate limiting step

All of the above evidence indicates that, during PLC activation, there are some slow steps in the PIP_2 resynthesis cycle that need to be sped up in order to explain the measured levels of PIP_2 and PI4P. While the "rate-limiting step" traditionally refers to the slowest catalytic step in a series of reactions, more recent definitions bypass the need for the step to be enzymatically slow. Rather, the current definition of rate-limiting step is that it is the most sensitive step in the cascade (Ray, 1983). This simply refers to the step which, when perturbed in small amounts, elicits large changes in the overall cascade.

With respect to the PIP_2 cycle, this definition could potentially apply to PI4KIIIα. A small change in the amount of protein, as effected using RNAi, reduces the electrical response to light almost to the same extent as severe mutants of *rdgB* and *dPIP5K*. Moreover, when *PI4KIIIα* was downregulated in the background of *rdgB* mutants, the lipid levels in these flies were similar to those in $GMR > PI4KIII\alpha^i$ flies and not those of $rdgB^9$ flies. The prevalence of the $GMR > PI4KIII\alpha^i$ phenotype was also seen in the case of a double manipulation with *dPIP5K*. Both the PIP and PIP_2 levels of the $dPIP5K^{18}$; $GMR > PI4KIII\alpha^i$ flies were identical to those in $GMR > PI4KIII\alpha^i$ flies alone. The fact that the lipid levels appear to be dependent on *PI4KIIIα* rather than its immediate upstream or downstream elements points to a greater relevance for *PI4KIIIα* activity in regulating these lipids at the plasma membrane.

Another piece of evidence that points to a possible role for *PI4KIIIα* in controlling the cycle is the ERG phenotype of $GMR > PI4KIII\alpha^i$ flies. Apart from a low response amplitude, these flies show a progressive decline in amplitude when subjected to a train of light flashes. The steady decrease in ERG amplitude points to a system that is incapable of sustaining a robust response in the absence of *PI4KIIIα*. Such an effect is not seen in any of the other mutants for elements of the PIP_2 cycle. In the case of both *rdgB* and *dPIP5K* loss-of-function mutants, the initial low response is maintained throughout the light train and does not get any worse with time. However, when either of these mutants are used in combination with *PI4KIIIα* knockdown, the progressive decrease in amplitude is immediately seen. This once again points to a dependency on *PI4KIIIα* rather than on other elements.

Given the above data, it is possible that the rate of activity of PI4KIIIα could set the tone of the PIP_2 cycle, especially when signalling is active. This might

also justify the need for tight regulation of the enzyme by virtue of its binding partners - Efr3 and TTC7 - both of which, when knocked down, mimic the effects of knocking down *PI4KIIIα*. A multi-protein complex such as this one generally indicates a highly controlled cellular event, which would be required in this case. We also observed that the human PI4KIIIα is present in the cytosol in dark-reared flies and migrates to the plasma membrane upon light treatment. Such a light-dependent translocation highlights an additional level of regulation, where recruitment to the appropriate membrane would ensure more production of PI4P during signalling, as opposed to a lower rate when the cell is at rest. A similar mechanism of location-dependent activity increase is also seen in the case of a phospholipase D (PLD), specifically, human PLD1, an enzyme which converts PC to PA. Upon receptor stimulation, hPLD1, which is otherwise present on internal vesicles, is recruited to the plasma membrane, where it exhibits higher catalytic activity by virtue of binding to PIP_2 (Brown et al., 1998).

It is also important to note that, while most other components of the PIP_2 cycle are constitutively present at either the rhabdomere or the SMC, PI4KIIIα is likely the only one that is present in the cytosol and periodically recruited to the plasma membrane. This additional difference between PI4KIIIα and other enzymes in the cycle indicate an added layer of control specifically at this reaction, further strengthening the possibility of it being a rate determinant for the PIP_2 cycle.

7.3 Relevance of performing the study in a whole organism system

The role of PI4KIIIα in maintaining PI4P at the plasma membrane has been shown in multiple model systems; be it yeast, mammalian cells, both in culture and *in vivo*, and even in *Drosophila* oocytes. However, a role in PI4P homeostasis in the cell does not necessarily correspond to a role in regulating PI4P levels during stimulation. Recent work from the lab has demonstrated that the same enzyme can have different physiological functions depending on the context. The enzyme phosphatidylinositol 5 - phosphate 4 - kinase (PIP4K), which synthesises PIP_2 from PI5P, has been shown to control cell size and growth in *Drosophila* larvae. Here, dPIP4K performs this function in a kinase-dependent manner, with the levels of PI5P being markedly higher in null mutants when compared to wild-type flies. In this scenario, the kinase-dead allele was unable to rescue the defects associated with the null mutant, whereas the wild-type allele could do so (Gupta et al., 2013). In *Drosophila*

photoreceptors, dPIP4K regulates the endocytosis of rhodopsin, with the null mutants showing an accumulation of larger rhodopsin loaded vesicles than control flies. This defect, however, could be rescued equally well by the expression of both a wild-type dPIP4K and a kinase-dead allele (Kamalesh et al., 2017).

Both the above studies were conducted in the same model organism, but demonstrated a context-dependent difference in the requirement for a single enzyme. In one case, the catalytic activity is required, whereas in the other the activity is dispensable. Given the existence of such functional contrasts, it becomes even more important to clearly outline the role of a protein in varying scenarios, especially if the claim is that the same protein functions identically in different contexts.

Although the role of PI4KIIIα in PLC signalling has been studied in mammalian cells as well, data about its catalytic activity comes largely from *in vitro* measurements (Nakagawa et al., 1996; Harak et al., 2014). Work from our lab has demonstrated that there is not always a one-to-one correspondence between *in vitro* measurements and *in vivo* observations. For example, the enzyme dPIP4K, as mentioned earlier, regulates cell size and growth in *Drosophila* larvae. Null mutants for the gene have been shown to have reduced salivary gland cell size (Gupta et al., 2013). The mammalian orthologue of this gene has three isoforms, each of which have three different specific activities as measured *in vitro*, with the least activity being up to 2000x less than the highest one. It would seem apparent that the isoform with the highest activity is the most physiologically active one. However, when each mammalian isoform was reconstituted in *Drosophila* null mutants for the gene, all of them were able to rescue the defects to the same extent (Mathre et al., 2019). This pointed to agents of activity regulation that were possibly missed when the enzymes were analysed *in vitro*, further stressing the relevance of carrying out parallel experiments in an endogenous system.

A second example comes from the studies on vitamin D as a potential chemotherapeutic agent against pancreatic cancer, as discussed in the introduction, Section 1.2.4. The dispute about the therapeutic properties of vitamin D largely stem from disparate observations made in cell culture systems versus in live human subjects; the pancreatic cancer cell lines experienced growth inhibition in upon vitamin D treatment whereas the human subjects showed an increased risk of developing the cancer upon vitamin D treatment (Kawal et al., 1997; Skinner, 2006). In an attempt to ensure genetic uniformity, vitamin D was administered to mice suffering from drug-induced pancreatic cancer, but showed no therapeutic effects (Iqbal, 2018).

Collectively, these studies offer a confounding picture of the relationship between vitamin D and pancreatic cancer, which was partly resolved by the experiments in mice. However, more conclusive evidence towards the same end remains wanting.

The above examples clearly indicate a lack of cohesion between experiments conducted within and outside of whole organisms. In this thesis, we were able to bypass any of the potentially distracting effects of a cell culture system by studying the requirement of PI4KIIIα in *Drosophila* phototransduction. Furthermore, a combination of electrophysiology and quantitative measurement has been used to show that the kinase activity of PI4KIIIα is required both for homeostasis and for regulating PLC signalling in *Drosophila* photoreceptors.

7.4 Conservation of the PI4KIIIα-Efr3-TTC7 protein complex

The binding of PI4KIIIα to Efr3 and TTC7 to form a protein complex at the plasma membrane is a phenomenon that is very well conserved in both yeast and mammalian systems (Baird et al., 2008; Nakatsu et al., 2012). In *Drosophila*, although we lack evidence of direct binding, we have shown in this study that removing any one of these three proteins from photoreceptors causes identical defects, be it in terms of electrical output or phosphoinositide levels. This points to a clear codependence of the three components on one another, most likely through the formation of a complex. Importantly, a study conducted in 2017 demonstrated that the fly PI4KIIIα and Efr3 proteins do indeed physically interact, as seen in co-immunoprecipitation experiments (Zhang et al., 2017).

Additional work from mammalian cell culture systems has shown that the PI4KIIIα complex has some other interactors as well. The FAM126A and TMEM150A proteins have also been shown to bind to and regulate formation of the PI4KIIIα protein complex. TMEM150A is the mammalian orthologue of the yeast Sfk1 protein, which is a suppressor of the temperature sensitivity of the $stt4^{ts}$ (PI4KIIIα in yeast) mutant (Audhya and Emr, 2002). In mammalian cells, TMEM150A serves as a potential substitute for TTC7 at the plasma membrane (Chung et al., 2015). FAM126A, on the other hand, binds to the PI4KIIIα-TTC7-Efr3 complex at the plasma membrane, contributing a further layer of regulation to the system (Baskin et al., 2016). The fact that this complex is so tightly regulated is curious, since the group II PI4Ks

do not appear to require so many interactors to function. This paradigm of complex formation is true for the other group III PI4K - PI4KIIIβ - as well. It has been shown to bind to and be regulated by proteins such as Rab11 and Arf1 (Chalupska et al., 2019).

There a several possible scenarios that necessitate multiple binding partners. One reason is to localise the enzyme to the correct membrane; unlike the group II enzymes, the group III PI4Ks lack clear membrane-binding motifs and instead, are recruited to the appropriate membranes by virtue of their interactions with other proteins. The architecture of the PI4KIIIα complex, as worked out from yeast and mammalian cells, is such that Efr3 sits at the plasma membrane and binds to TTC7, which in turn binds to PI4KIIIα (Wu et al., 2014). Hence, TTC7 acts as a bridge between the other two proteins and PI4KIIIα does not directly bind to the membrane. A possible advantage of such architecture could be that it allows flexibility and conformational changes in PI4KIIIα as it performs its catalysis. The catalytic domain of PI4KIIIα is at its C-terminus, whereas the binding region for TTC7 is at the N-terminus (Nakagawa et al., 1996). This leaves the protein free to reach out and catalyse conversion of PI to PI4P at the plasma membrane, with minimal steric hindrance from surrounding components. Similarly for PI4KIIIβ, current models drawn from cell culture systems predict that the enzyme is tethered to other proteins at its N-terminus, leaving rest of the protein free to access its substrate (Burke et al., 2014).

The second facet of such tight regulation could be temporal control. Experiments from the 1980s on kinetic activity suggest that the group III enzymes have a higher affinity for ATP and a faster catalysis rate (Endemann et al., 1987). In such cases, the cell might only require the activity of the enzyme for a limited time period and hence, a need-based recruitment to the site of activity would offer a means to control the process. We do not yet have any evidence suggesting that a constitutive presence of PI4KIIIα at the plasma membrane is detrimental to the cell; in fact, in yeast cells STT4 is present at the plasma membrane at all times (Audhya and Emr, 2002). However, it is possible that in systems requiring fine kinetic coordination between multiple processes, such an event might throw coordination off-balance. The group II enzymes are also more susceptible to inhibition by adenosine, suggesting that they are more easily regulated by soluble cellular components and may not require control at the level of recruitment (Endemann et al., 1987).

7.5 Other cellular functions of *stmA* and *TTC7*

The proteins Efr3 and TTC7 are very well conserved across eukaryotic systems, ranging from yeast to mammals (Baird et al., 2008; Nakatsu et al., 2012; Chandrashekaran and Sarla, 1993). While it is possible that their chief function is to act as scaffolds for the PI4KIIIα complex, there is evidence to support independent cellular functions for these genes.

7.5.1 Efr3 (*stmA*)

Early work on the *Drosophila* orthologue of Efr3 - *stmA* - showed that it is an essential gene required for embryonic survival. A failure to generate germline clones implied that the gene was required for cell viability as well (Faulkner et al., 1998). Further work in *Drosophila* involved the generation of temperature-sensitive mutants, allowing one to maintain gene function throughout development and selectively inactivate it during the adult stage. Inactivation of the gene at restrictive temperatures resulted in paralysis of the flies, indicating a neuronal function. Certain alleles also showed neural hypertrophy, prompting the assignment of a neurogenic function to the gene (Chandrashekaran and Sarla, 1993; Kumar et al., 2001; Shyngle and Sharma, 1985). The *stmA* gene is also speculated to regulate synaptic vesicle recycling, as the temperature-sensitive mutants were observed to have defects in both exocytosis and bulk endocytosis at neuromuscular junctions (Huang et al., 2006; Vijayakrishnan et al., 2009). Additional evidence for a requirement of the gene in neurons came when it was shown that *stmA*, in combination with PI4KIIIα, regulates the secretion of Aβ42 amyloid peptides from *Drosophila* brain tissue, a key causative agent of Alzheimer's disease (Zhang et al., 2017).

More recent work in mammalian cells also mirrored the findings in *Drosophila*. The mammalian genome codes for two isoforms of the gene - *EFR3A* and *EFR3B*. The *EFR3A* gene has been associated with autism spectrum disorders (ASD), as per data from whole exome sequencing. The sequences were obtained from cohorts of individuals exhibiting ASD as well as control populations. They found that certain deleterious mutations for *EFR3A* were more common in cases positive for ASD as compared to control cases. It was also seen that *EFR3A* was co-expressed in cortical neurons, in a pattern closely matching that of a module of ASD-related genes (Gupta et al., 2014). While the nature of this association remains unknown, it offers a promising route of investigation into the cell biology of ASD.

Curiously, another set of studies on *EFR3A* function in the mouse brain found that conditionally deleting the gene in adult brains promoted neuroge-

nesis of hippocampal neurons. Removing the gene also conferred a protective effect in terms of apoptosis and drug-induced neuronal degeneration. These effects likely resulted from an upregulation of brain-derived neurotrophic factor (BDNF) and its related signalling pathways (Hu et al., 2017; Qian et al., 2017). This evidence runs contrary to the data from *Drosophila*, where the gene appeared to be required for neurogenesis. However, it is important to note that the proliferation was only observed in hippocampal neurons and other regions of the brain did not show this effect. It is possible that there is an isoform-specific requirement of Efr3 in different brain regions. Moreover, the *EFR3B* isoform is still present in the brains lacking *EFR3A* and could potentially compensate for the deletion. *EFR3B* is, in fact, more highly expressed in mammalian brain tissue than *EFR3A*. As *Drosophila* have only a single copy of the gene, any manipulations would have more severe effect due to a lack of compensation by a second isoform.

The *EFR3B* isoform, despite being highly expressed in the brain, has been implicated in regulating GPCR signalling rather than neurogenesis. A study from mammalian cells indicate that *EFR3B* might regulate receptor resensitisation, possibly by interacting with its C-terminus and controlling the phosphorylation status (Bojjireddy et al., 2015). Further studies in this context would inform on the role of Efr3 in regulating cell signalling, as discussed in Section 5.8.3. Given that the photoreceptors of *Drosophila* are also primary sensory neurons, it is possible that the neuronal functions of *stmA* hold good in these cells as well. While we demonstrated a role for *stmA* in regulating PI4P and PIP_2 levels, this does not rule out other functions for the gene. A more detailed characterisation of the $stmA^{ts}$ allele, for instance, would aid in understanding the relevance of this protein and its functions in *Drosophila*.

7.5.2 TTC7

The TTC7 gene in mammals is also present as two isoforms - *TTC7A* and *TTC7B*. The gene appears to be expressed in almost all tissues except muscles, with relatively higher expression in kidney and liver tissue (TAKABAYASHI et al., 2007).The *TTC7A* gene has been associated with multiple genetic disorders, the most prominent being those related to intestinal health. Whole-exome sequencing data from patient samples has shown that mutations in *TTC7A* are seen repeatedly in cases of multiple intestinal atresia, a fatal disease involving intestinal obstructions and immune deficiencies (Chen et al., 2013; Samuels et al., 2013). An investigation into the mechanistic basis for the disorder pointed to a PI4P-dependent mechanism, where point mutants

for *TTC7A* showed reduced levels of PI4KIIIα in enterocytes, as well as low levels of PI4P in intestinal cell lines. These point mutations were isolated from sequencing data of patients positive for very early onset inflammatory bowel disease (Avitzur, 2014).The mutations also disrupt cell polarity of intestinal epithelia, possibly as a consequence of low PI4P levels (Bigorgne et al., 2014).

Apart from contributing to intestinal health, mutations in TTC7 ave been known to cause flaky skin syndrome in mice. These mice are also used as model systems for psoriasis and autoimmune disorders (TAKABAYASHI et al., 2007; Helms et al., 2005).

The cellular role of TTC7 in flies has been rather poorly studied till date. Given its association with intestinal health in mice, it would be valuable to study its function in *Drosophila*, especially since the fly genome only carries a single isoform of the gene and would eliminate any compensatory effects from other isoforms seen in mice.

Bibliography

A. Audhya and S. D. Emr. Stt4 PI 4-Kinase Localizes to the Plasma Membrane and Functions in the Pkc1-Mediated MAP Kinase Cascade. *Developmental Cell*, 2(5):593–605, May 2002. ISSN 1534-5807. doi: 10.1016/S1534-5807(02)00168-5.

Y. Avitzur. Mutations in Tetratricopeptide Repeat Domain 7A Result in a Severe Form of Very Early Onset Inflammatory Bowel Disease.pdf. *Gastroenterology*, 146:1028–1039, 2014.

D. Baird, C. Stefan, A. Audhya, S. Weys, and S. D. Emr. Assembly of the PtdIns 4-kinase Stt4 complex at the plasma membrane requires Ypp1 and Efr3. *J Cell Biol*, 183(6):1061–1074, Dec. 2008. ISSN 0021-9525, 1540-8140. doi: 10.1083/jcb.200804003.

A. Balla, Y. J. Kim, P. Varnai, Z. Szentpetery, Z. Knight, K. M. Shokat, and T. Balla. Maintenance of Hormone-sensitive Phosphoinositide Pools in the Plasma Membrane Requires Phosphatidylinositol 4-Kinase IIIα. *Molecular Biology of the Cell*, 19(2):711–721, Jan. 2008. ISSN 1059-1524, 1939-4586. doi: 10.1091/mbc.E07-07-0713.

J. M. Baskin, X. Wu, R. Christiano, M. S. Oh, C. M. Schauder, E. Gazzerro, M. Messa, S. Baldassari, S. Assereto, R. Biancheri, F. Zara, C. Minetti, A. Raimondi, M. Simons, T. C. Walther, K. M. Reinisch, and P. De Camilli. The leukodystrophy protein FAM126A (hyccin) regulates PtdIns(4)P synthesis at the plasma membrane. *Nature Cell Biology*, 18 (1):132–138, Jan. 2016. ISSN 1476-4679. doi: 10.1038/ncb3271.

M. J. Berridge, C. P. Downes, and M. R. Hanley. Lithium amplifies agonist-dependent phosphatidylinositol responses in brain and salivary glands. *Biochemical Journal*, 206(3):587–595, Sept. 1982. ISSN 0264-6021, 1470-8728. doi: 10.1042/bj2060587.

M. J. Berridge, C. Downes, and M. R. Hanley. Neural and developmental actions of lithium: A unifying hypothesis. *Cell*, 59(3):411–419, Nov. 1989. ISSN 00928674. doi: 10.1016/0092-8674(89)90026-3.

A. E. Bigorgne, H. F. Farin, R. Lemoine, N. Mahlaoui, N. Lambert, M. Gil, A. Schulz, P. Philippet, P. Schlesser, T. G. Abrahamsen, K. Oymar, E. G. Davies, C. L. Ellingsen, E. Leteurtre, B. Moreau-Massart, D. Berrebi, C. Bole-Feysot, P. Nischke, N. Brousse, A. Fischer, H. Clevers, and G. de Saint Basile. TTC7A mutations disrupt intestinal epithelial apicobasal polarity. *Journal of Clinical Investigation*, 124(1):328–337, Jan. 2014. ISSN 0021-9738. doi: 10.1172/JCI71471.

N. Bojjireddy, M. L. Guzman-Hernandez, N. R. Reinhard, M. Jovic, and T. Balla. EFR3s are palmitoylated plasma membrane proteins that control responsiveness to G-protein-coupled receptors. *J Cell Sci*, 128(1):118–128, Jan. 2015. ISSN 0021-9533, 1477-9137. doi: 10.1242/jcs.157495.

F. D. Brown, N. Thompson, K. M. Saqib, J. M. Clark, D. Powner, N. T. Thompson, R. Solari, and M. J. Wakelam. Phospholipase D1 localises to secretory granules and lysosomes and is plasma-membrane translocated on cellular stimulation. *Current Biology*, 8(14):835–838, July 1998. ISSN 09609822. doi: 10.1016/S0960-9822(98)70326-4.

J. E. Burke, A. J. Inglis, O. Perisic, G. R. Masson, S. H. McLaughlin, F. Rutaganira, K. M. Shokat, and R. L. Williams. Structures of PI4KIIIβ complexes show simultaneous recruitment of Rab11 and its effectors. *Science*, 344:5, 2014.

S. B. Chahwala, L. F. Fleischman, and L. Cantley. Kinetic analysis of guanosine 5'-O-(3-thiotriphosphate) effects on phosphatidylinositol turnover in NRK cell homogenates. *Biochemistry*, 26(2):612–622, Jan. 1987. ISSN 0006-2960, 1520-4995. doi: 10.1021/bi00376a037.

D. Chalupska, B. Różycki, J. Humpolickova, L. Faltova, M. Klima, and E. Boura. Phosphatidylinositol 4-kinase IIIβ (PI4KB) forms highly flexible heterocomplexes that include ACBD3, 14-3-3, and Rab11 proteins. *Scientific Reports*, 9(1), Dec. 2019. ISSN 2045-2322. doi: 10.1038/s41598-018-37158-6.

S. Chandrashekaran and N. Sarla. Phenotypes of lethal alleles of the recessive temperature sensitive paralytic mutant stambh A of Drosophila melanogaster suggest its neurogenic function. *Genetica*, 90(1):61–71, Feb. 1993. ISSN 0016-6707, 1573-6857. doi: 10.1007/BF01435179.

R. Chen, S. Giliani, G. Lanzi, G. I. Mias, S. Lonardi, K. Dobbs, J. Manis, H. Im, J. E. Gallagher, D. H. Phanstiel, G. Euskirchen, P. Lacroute, K. Bettinger, D. Moratto, K. Weinacht, D. Montin, E. Gallo, G. Mangili, F. Porta, L. D. Notarangelo, S. Pedretti, W. Al-Herz, W. Alfahdli, A. M. Comeau, R. S. Traister, S.-Y. Pai, G. Carella, F. Facchetti, K. C. Nadeau, M. Snyder, and L. D. Notarangelo. Whole-exome sequencing identifies tetratricopeptide repeat domain 7A (TTC7A) mutations for combined immunodeficiency with intestinal atresias. *Journal of Allergy and Clinical Immunology*, 132(3):656–664.e17, Sept. 2013. ISSN 00916749. doi: 10.1016/j.jaci.2013.06.013.

J. Chung, F. Nakatsu, J. M. Baskin, and P. D. Camilli. Plasticity of PI4KIIIα

interactions at the plasma membrane. *EMBO reports*, 16(3):312–320, Mar. 2015. ISSN 1469-221X, 1469-3178. doi: 10.15252/embr.201439151.

S. Cockcroft and P. Raghu. Topological organisation of the phosphatidylinositol 4,5-bisphosphate–phospholipase C resynthesis cycle: PITPs bridge the ER–PM gap. *Biochemical Journal*, 473(23):4289–4310, Dec. 2016. ISSN 0264-6021, 1470-8728. doi: 10.1042/BCJ20160514C.

J. A. Creba, C. P. Downes, P. T. Hawkins, G. Brewster, R. H. Michell, and C. J. Kirk. Rapid breakdown of phosphatidylinositol 4-phosphate and phosphatidylinositol 4,5-bisphosphate in rat hepatocytes stimulated by vasopressin and other Ca^{2+} -mobilizing hormones. *Biochemical Journal*, 212(3):733–747, June 1983. ISSN 0264-6021, 1470-8728. doi: 10.1042/bj2120733.

C. P. Downes, P. T. Hawkins, and R. H. Michell. Measurement of the metabolic turnover of the 4- and 5-phosphates of phosphatidylinositol 4,5-bisphosphate in erythrocytes. *Biochemical Society Transactions*, 10(4): 250–251, Aug. 1982. ISSN 0300-5127, 1470-8752. doi: 10.1042/bst0100250.

G. Endemann, S. N. Dunn, and L. C. Cantley. Bovine brain contains two types of phosphatidylinositol kinase. *Biochemistry*, 26(21):6845–6852, Oct. 1987. ISSN 0006-2960, 1520-4995. doi: 10.1021/bi00395a039.

B. H. Falkenburger, J. B. Jensen, and B. Hille. Kinetics of PIP2 metabolism and KCNQ2/3 channel regulation studied with a voltage-sensitive phosphatase in living cells. *The Journal of General Physiology*, 135(2):99–114, Feb. 2010. ISSN 0022-1295, 1540-7748. doi: 10.1085/jgp.200910345.

D. L. Faulkner, T. C. Dockendorff, and T. A. Jongens. Clonal analysis ofcmp44E, which encodes a conserved putative transmembrane protein, indicates a requirement for cell viability inDrosophila. *Developmental Genetics*, 23(4):264–274, 1998. ISSN 0192-253X, 1520-6408. doi: 10.1002/(SICI)1520-6408(1998)23:4<264::AID-DVG2>3.0.CO;2-6.

A. Gupta, S. Toscano, D. Trivedi, D. R. Jones, S. Mathre, J. H. Clarke, N. Divecha, and P. Raghu. Phosphatidylinositol 5-phosphate 4-kinase (PIP4K) regulates TOR signaling and cell growth during Drosophila development. *Proceedings of the National Academy of Sciences*, 110(15):5963–5968, Sept. 2013. ISSN 0027-8424, 1091-6490. doi: 10.1073/pnas.1219333110.

A. R. Gupta, M. Pirruccello, F. Cheng, H. Kang, T. V. Fernandez, J. M. Baskin, M. Choi, L. Liu, A. Ercan-Sencicek, J. D. Murdoch, L. Klei, B. M. Neale, D. Franjic, M. J. Daly, R. P. Lifton, P. De Camilli, H. Zhao, N. Šestan, and M. W. State. Rare deleterious mutations of the gene EFR3A

in autism spectrum disorders. *Molecular Autism*, 5(1):31, 2014. ISSN 2040-2392. doi: 10.1186/2040-2392-5-31.

C. Harak, D. Radujkovic, C. Taveneau, S. Reiss, R. Klein, S. Bressanelli, and V. Lohmann. Mapping of Functional Domains of the Lipid Kinase Phosphatidylinositol 4-Kinase Type III Alpha Involved in Enzymatic Activity and Hepatitis C Virus Replication. *Journal of Virology*, 88(17):9909–9926, Jan. 2014. ISSN 0022-538X, 1098-5514. doi: 10.1128/JVI.01063-14.

C. Helms, S. Pelsue, L. Cao, E. Lamb, B. Loffredo, P. Taillon-Miller, B. Herrin, L. M. Burzenski, B. Gott, B. L. Lyons, D. Keppler, L. D. Shultz, and A. M. Bowcock. The Tetratricopeptide Repeat Domain 7 Gene is Mutated in Flaky Skin Mice: A Model for Psoriasis, Autoimmunity, and Anemia. *Experimental Biology and Medicine*, 230(9):659–667, Oct. 2005. ISSN 1535-3702, 1535-3699. doi: 10.1177/153537020523000908.

L. E. Hokin and M. R. Hokin. The Incorporation of 32P from Triphosphate into Polyphosphoinositides [g-32P]Adenosine and Phosphatidic Acid in Erythrocyte Membranes.pdf. *Biochimica et Biophysica Acta*, 1964.

H. Hu, B. Ye, L. Zhang, Q. Wang, Z. Liu, S. Ji, Q. Liu, J. Lv, Y. Ma, Y. Xu, H. Wu, F. Huang, and M. Xiang. Efr3a Insufficiency Attenuates the Degeneration of Spiral Ganglion Neurons after Hair Cell Loss. *Frontiers in Molecular Neuroscience*, 10, Mar. 2017. ISSN 1662-5099. doi: 10.3389/fnmol.2017.00086.

F.-D. Huang, E. A. Woodruff III, R. Mohrmann, and K. Broadie. Rolling Blackout Is Required for Synaptic Vesicle Exocytosis.pdf. *Journal of Neuroscience*, 26(9):2369–2379, 2006.

S. Iqbal. *The Role of Vitamin D in the Treatment of Diabetes and Pancreatic Cancer*. PhD thesis, Aligarh Muslim University, 2018.

K. Kamalesh, D. Trivedi, S. Toscano, S. Sharma, S. Kolay, and P. Raghu. Phosphatidylinositol 5-phosphate 4-kinase regulates early endosomal dynamics during clathrin-mediated endocytosis. *J Cell Sci*, 130(13):2119–2133, July 2017. ISSN 0021-9533, 1477-9137. doi: 10.1242/jcs.202259.

S. Kawal, T. Nikaido, Y. Aoki', Y. Zhai, T. Kumagai, K. Furihata, S. Fujii, and K. Kiyosawa. Vitamin D analogues upmregulate p21 and p27 during growth inhibition of pancreatic cancer cell lines. *British Journal of Cancer*, page 6, 1997.

M. Kumar, M. Joseph, and S. Chandrashekaran. Effects of mutations at the

stambh A locus of Drosophila melanogaster. *Journal of Genetics*, 80(2): 83–95, Aug. 2001. ISSN 0022-1333, 0973-7731. doi: 10.1007/BF02728334.

S. Mathre, K. B. Reddy, V. Ramya, H. Krishnan, A. Ghosh, and P. Raghu. Functional analysis of the biochemical activity of mammalian phosphatidylinositol 5 phosphate 4-kinase enzymes. *Bioscience Reports*, 39 (2):BSR20182210, Feb. 2019. ISSN 0144-8463, 1573-4935. doi: 10.1042/BSR20182210.

T. Nakagawa, K. Goto, and H. Kondo. Cloning, Expression, and Localization of 230-kDa Phosphatidylinositol 4-Kinase. *Journal of Biological Chemistry*, 271(20):12088–12094, May 1996. ISSN 0021-9258, 1083-351X. doi: 10.1074/jbc.271.20.12088.

F. Nakatsu, J. M. Baskin, J. Chung, L. B. Tanner, G. Shui, S. Y. Lee, M. Pirruccello, M. Hao, N. T. Ingolia, M. R. Wenk, and P. D. Camilli. PtdIns4P synthesis by PI4KIIIα at the plasma membrane and its impact on plasma membrane identity. *J Cell Biol*, 199(6):1003–1016, Dec. 2012. ISSN 0021-9525, 1540-8140. doi: 10.1083/jcb.201206095.

Q. Qian, Q. Liu, D. Zhou, H. Pan, Z. Liu, F. He, S. Ji, D. Wang, W. Bao, X. Liu, Z. Liu, H. Zhang, X. Zhang, L. Zhang, M. Wang, Y. Xu, F. Huang, B. Luo, and B. Sun. Brain-specific ablation of Efr3a promotes adult hippocampal neurogenesis *via* the brain-derived neurotrophic factor pathway. *The FASEB Journal*, 31(5):2104–2113, May 2017. ISSN 0892-6638, 1530-6860. doi: 10.1096/fj.201601207R.

W. J. Ray. Rate-Limiting Step: A Quantitative Definition. Application to Steady-State Enzymic Reactionst. *Biochemistry*, page 13, 1983.

M. E. Samuels, J. Majewski, N. Alirezaie, I. Fernandez, F. Casals, N. Patey, H. Decaluwe, I. Gosselin, E. Haddad, A. Hodgkinson, Y. Idaghdour, V. Marchand, J. L. Michaud, M.-A. Rodrigue, S. Desjardins, S. Dubois, F. Le Deist, P. Awadalla, V. Raymond, and B. Maranda. Exome sequencing identifies mutations in the gene *TTC7A* in French-Canadian cases with hereditary multiple intestinal atresia. *Journal of Medical Genetics*, 50(5):324–329, May 2013. ISSN 0022-2593, 1468-6244. doi: 10.1136/jmedgenet-2012-101483.

J. Shyngle and R. Sharma. Studies on paralysis and development of second chromosome temperature sensitive paralytic mutants of Drosophila melanogaster. *Indian Journal of Experimental Biology*, 23:235–240, 1985. ISSN 0019-5189.

H. G. Skinner. Vitamin D Intake and the Risk for Pancreatic Cancer in

Two Cohort Studies. *Cancer Epidemiology Biomarkers & Prevention*, 15 (9):1688–1695, Sept. 2006. ISSN 1055-9965, 1538-7755. doi: 10.1158/1055-9965.EPI-06-0206.

V. M. Steen, O. B. Tysnes, and H. Holmsen. Evidence for tight metabolic control of the receptor-activated polyphosphoinositide cycle in human platelets. *Biochemical Journal*, 263(2):621–624, Oct. 1989. ISSN 0264-6021, 1470-8728. doi: 10.1042/bj2630621.

R. Suratekar. *Understanding Structure and Dynamics of the Drosophila PI(4,5)P2 Cycle Using Mathematical Models*. Doctor of Philosophy, Tata Institute of Fundamental Research, 2018.

R. Suratekar, A. Panda, P. Raghu, and S. Krishna. Evidence of sinks and sources in the phospholipase C-activated PIP $_2$ cycle. *FEBS Letters*, 592 (6):962–972, Mar. 2018. ISSN 00145793. doi: 10.1002/1873-3468.12998.

S. TAKABAYASHI, S. IWASHITA, T. HIRASHIMA, and H. KATOH. The Novel Tetratricopeptide Repeat Domain 7 Mutation, Ttc7 fsn-Jic, with Deletion of the TPR-2B Repeat Causes Severe Flaky Skin Phenotype. page 7, 2007.

J. T. Tóth, G. Gulyás, D. J. Tóth, A. Balla, G. R. V. Hammond, L. Hunyady, T. Balla, and P. Várnai. BRET-monitoring of the dynamic changes of inositol lipid pools in living cells reveals a PKC-dependent PtdIns4P increase upon EGF and M3 receptor activation. *Biochimica et Biophysica Acta (BBA) - Molecular and Cell Biology of Lipids*, 1861(3):177–187, Mar. 2016. ISSN 1388-1981. doi: 10.1016/j.bbalip.2015.12.005.

N. Vijayakrishnan, E. A. Woodruff III, and K. Broadie. Rolling blackout is required for bulk endocytosis in non-neuronal cells and neuronal synapses.pdf. *Journal of Cell Science*, 122:114–125, 2009.

G. B. Willars, S. R. Nahorski, and R. A. J. Challiss. Differential Regulation of Muscarinic Acetylcholine Receptor-sensitive Polyphosphoinositide Pools and Consequences for Signaling in Human Neuroblastoma Cells. *Journal of Biological Chemistry*, 273(9):5037–5046, Feb. 1998. ISSN 0021-9258, 1083-351X. doi: 10.1074/jbc.273.9.5037.

X. Wu, R. J. Chi, J. M. Baskin, L. Lucast, C. G. Burd, P. De Camilli, and K. M. Reinisch. Structural Insights into Assembly and Regulation of the Plasma Membrane Phosphatidylinositol 4-Kinase Complex. *Developmental Cell*, 28(1):19–29, Jan. 2014. ISSN 1534-5807. doi: 10.1016/j.devcel.2013.11.012.

X. Zhang, X. Chen, C. Jia, X. Geng, X. Du, and H. Zhang. Depolarization Increases Phosphatidylinositol (PI) 4,5-Bisphosphate Level and KCNQ Currents through PI 4-Kinase Mechanisms. *Journal of Biological Chemistry*, 285(13):9402–9409, Mar. 2010. ISSN 0021-9258, 1083-351X. doi: 10.1074/jbc.M109.068205.

X. Zhang, W.-A. Wang, L.-X. Jiang, H.-Y. Liu, B.-Z. Zhang, N. Lim, Q.-Y. Li, and F.-D. Huang. Downregulation of RBO-PI4KIIIα Facilitates Aβ42 Secretion and Ameliorates Neural Deficits in Aβ42-Expressing Drosophila. *Journal of Neuroscience*, 37(19):4928–4941, May 2017. ISSN 0270-6474, 1529-2401. doi: 10.1523/JNEUROSCI.3567-16.2017.

Appendix A

Representative Chromatograms

A.1 PIP, PIP_2 and PE

Representative chromatograms for the five main PIP, PIP_2 and PE species detected using liquid chromatography - mass spectrometry **(Fig.A.1, A.2, A.3, A.4, A.5 and A.6)**. The left column is representation from a blank sample, containing no biological material. The right column represents a lipid sample extracted from the retinae of WT flies.

A.2 DAG, PA and PE

Representative chromatograms for the five main DAG, PA and PE species detected using liquid chromatography - mass spectrometry **(Fig.A.7, A.8, A.9, A.10, A.11 and A.12)**. The left column is representation from a blank sample, containing no biological material. The right column represents a lipid sample extracted from the retinae of WT flies.

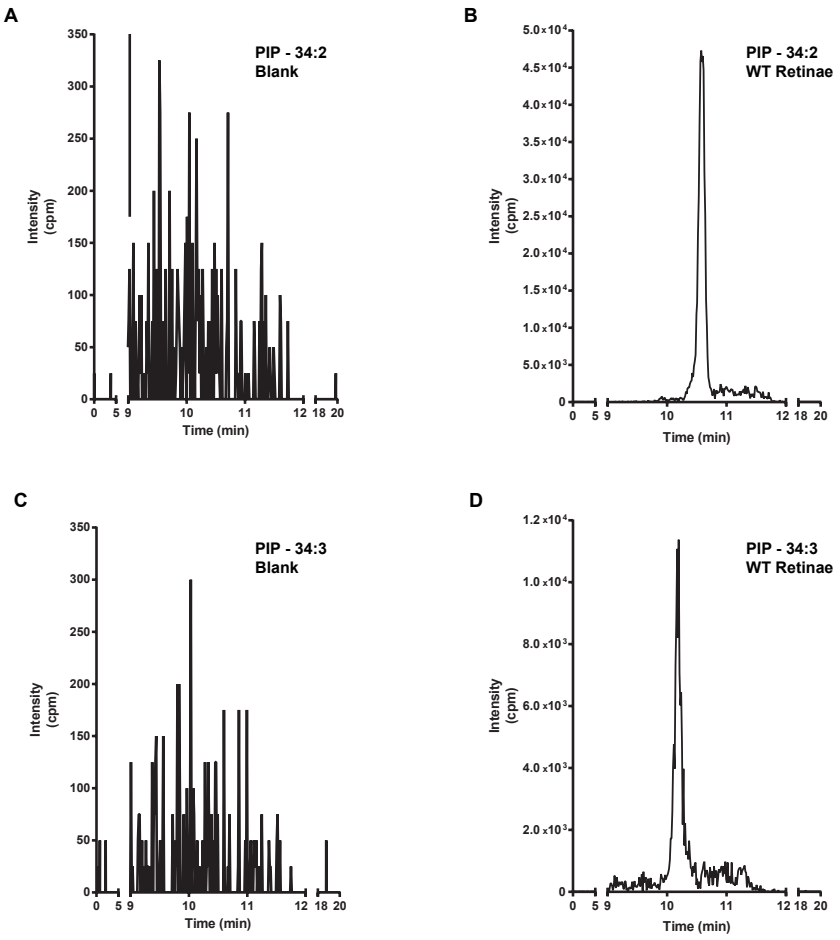

Figure A.1 : Representative chromatograms - PIP (34 species)
The x-axis represents elution time; y-axis represents intensity in counts per minute. The x-axis has been cropped to focus on the elution time for each species.

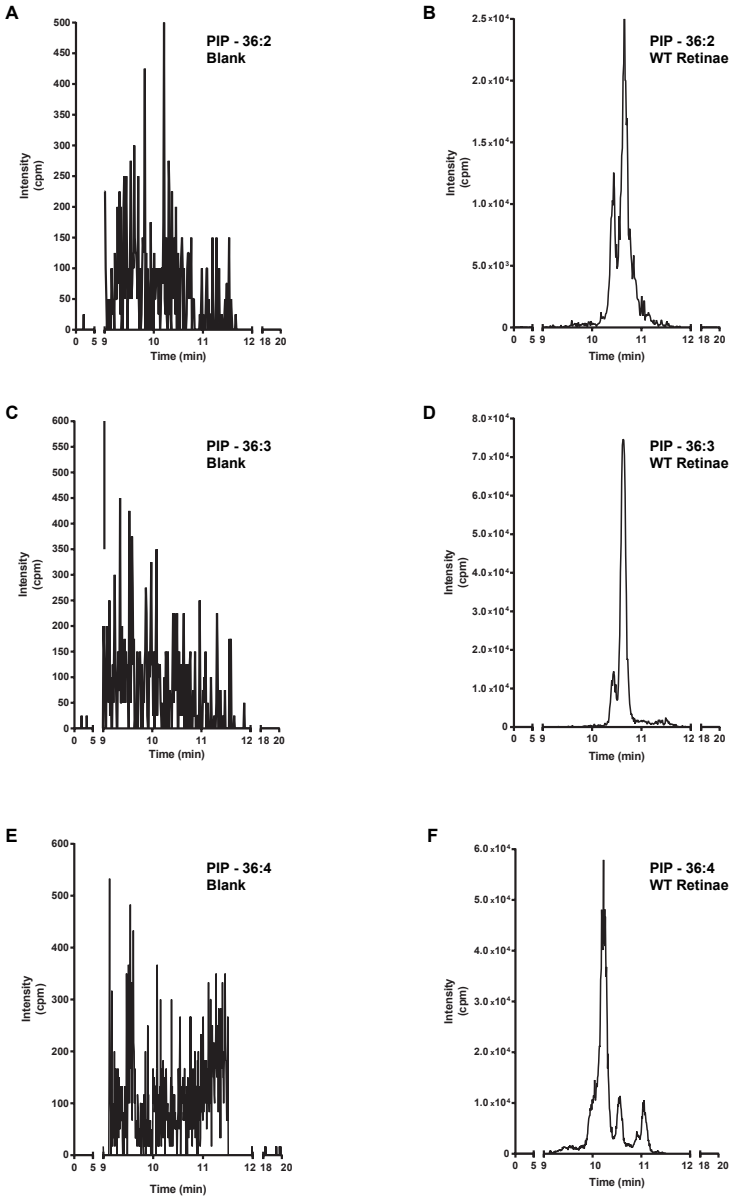

Figure A.2 : Representative chromatograms - PIP (36 species)
The x-axis represents elution time; y-axis represents intensity in counts per minute. The x-axis has been cropped to focus on the elution time for each species.

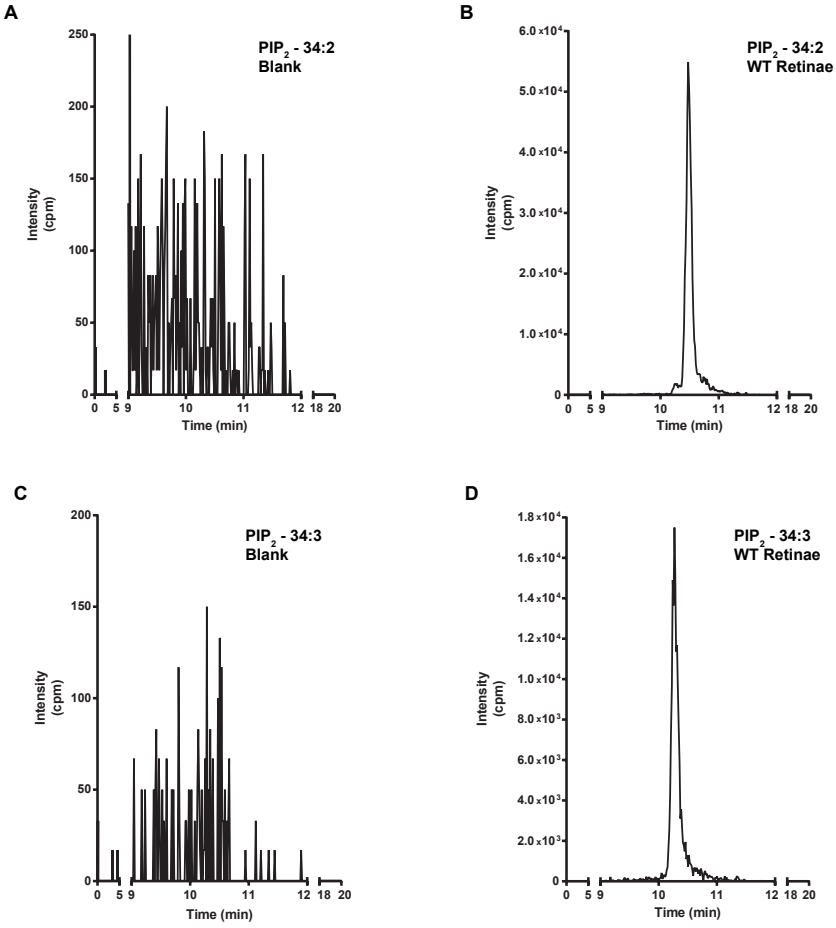

Figure A.3 : Representative chromatograms - PIP_2 (34 species)
The x-axis represents elution time; y-axis represents intensity in counts per minute. The x-axis has been cropped to focus on the elution time for each species.

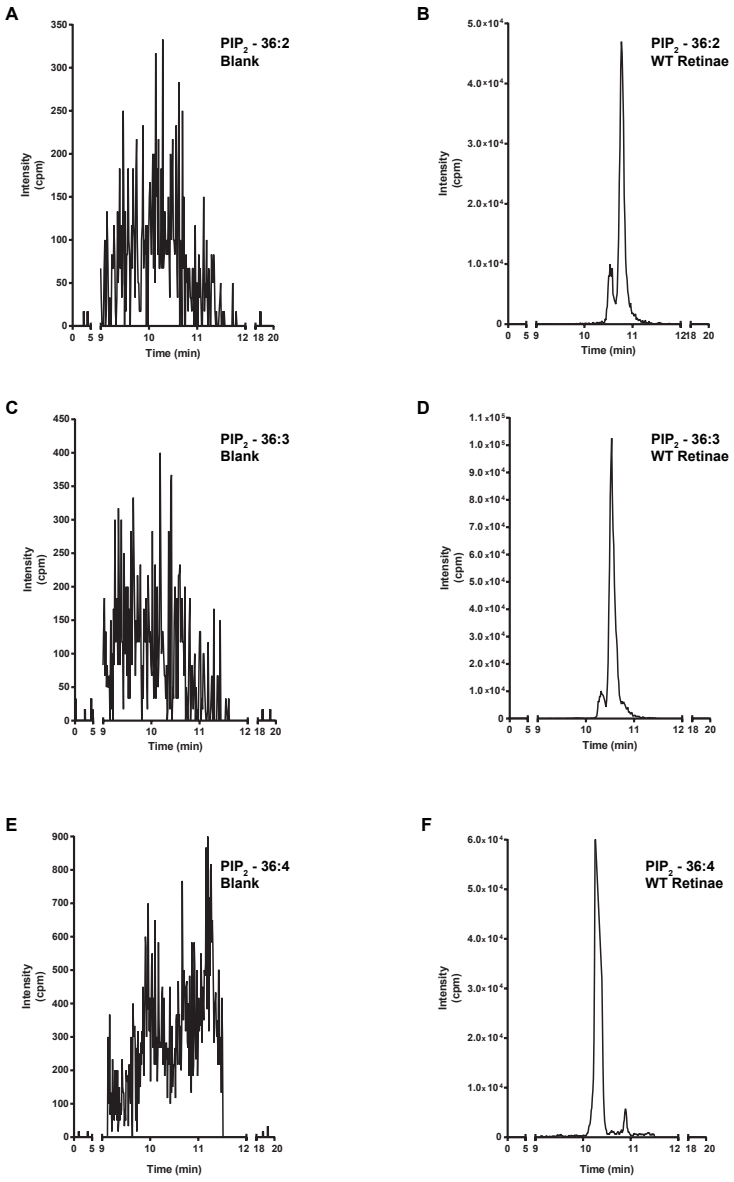

Figure A.4 : Representative chromatograms - PIP_2 (36 species)
The x-axis represents elution time; y-axis represents intensity in counts per minute. The x-axis has been cropped to focus on the elution time for each species.

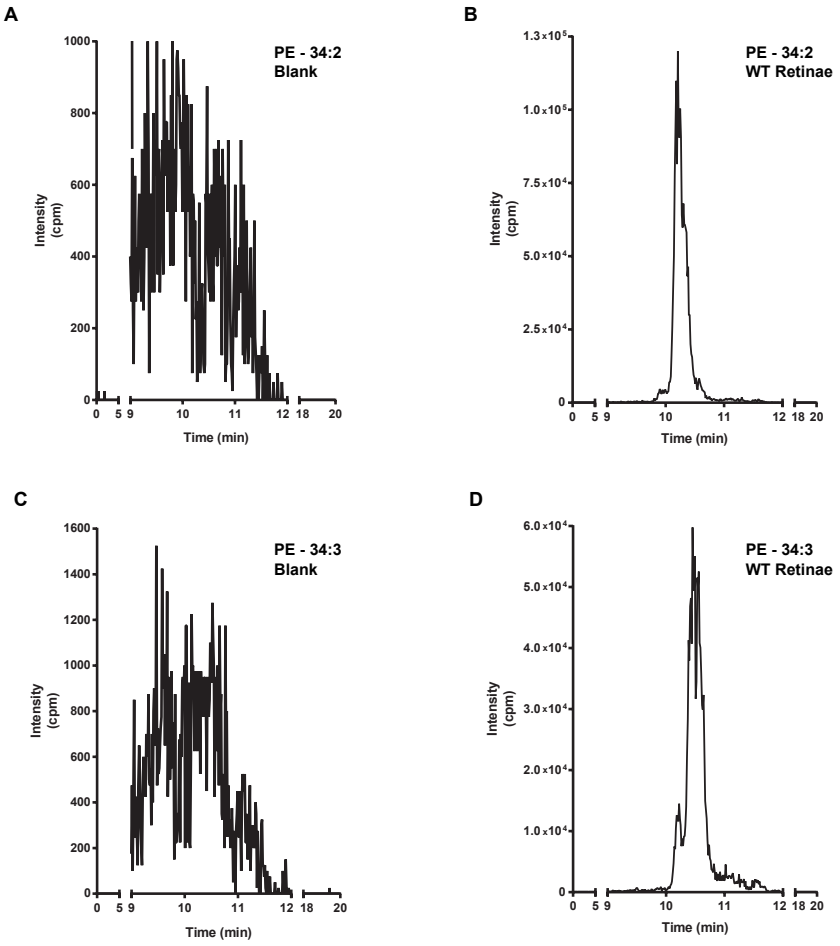

Figure A.5 : Representative chromatograms - PE (34 species)
The x-axis represents elution time; y-axis represents intensity in counts per minute. The x-axis has been cropped to focus on the elution time for each species.

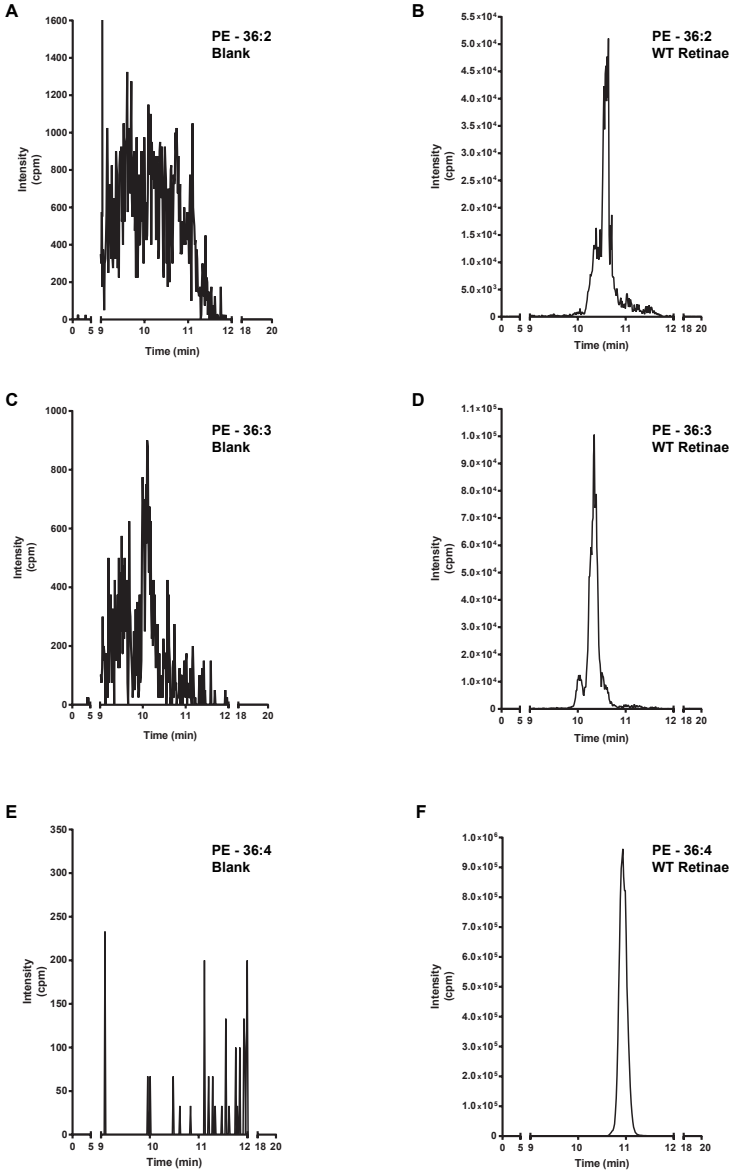

Figure A.6 : Representative chromatograms - PE (36 species)
The x-axis represents elution time; y-axis represents intensity in counts per minute. The x-axis has been cropped to focus on the elution time for each species.

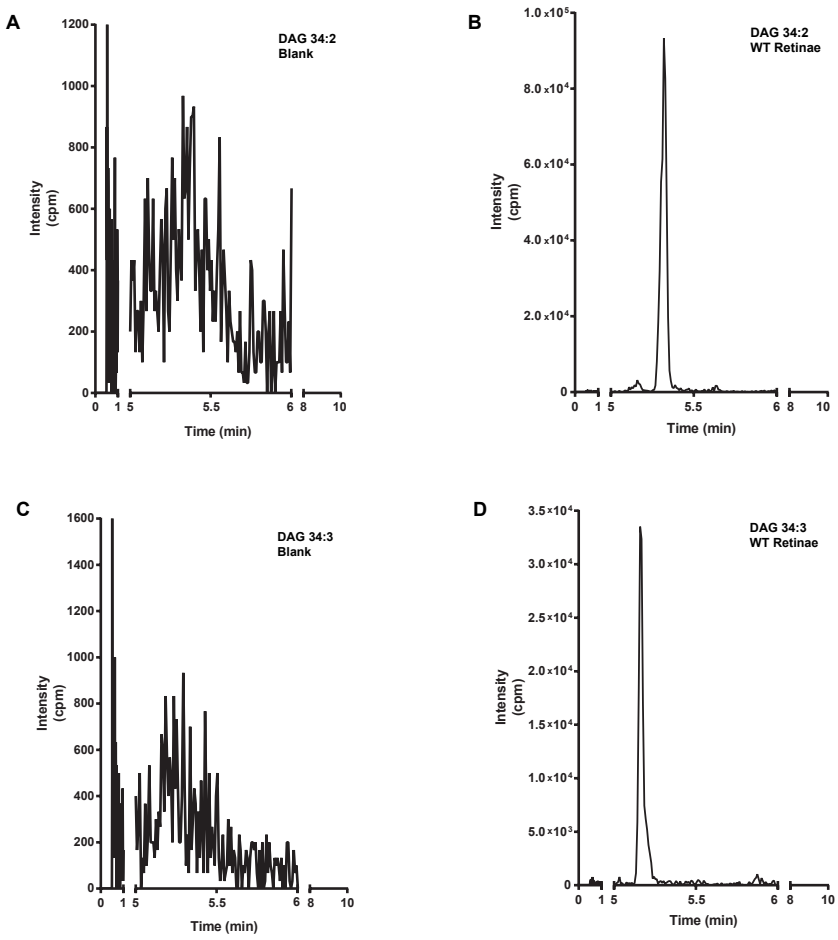

Figure A.7 : Representative chromatograms - DAG (34 species) The x-axis represents elution time; y-axis represents intensity in counts per minute. The x-axis has been cropped to focus on the elution time for each species.

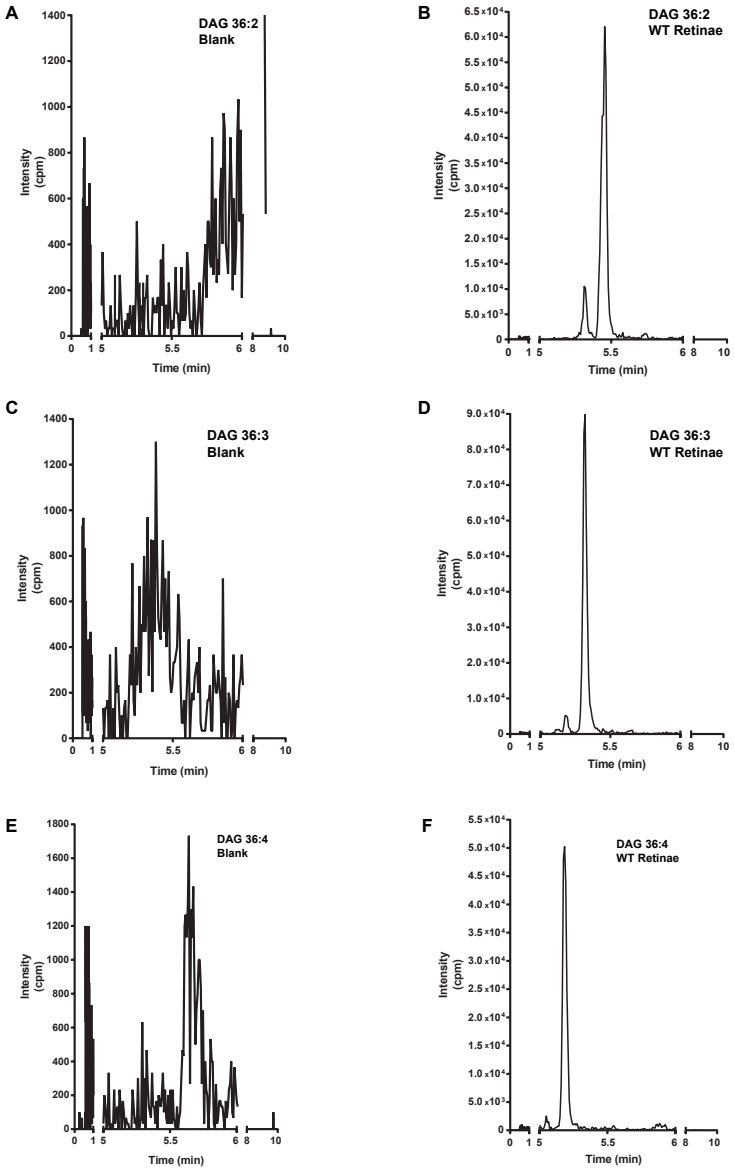

Figure A.8 : Representative chromatograms - DAG (36 species)
The x-axis represents elution time; y-axis represents intensity in counts per minute. The x-axis has been cropped to focus on the elution time for each species.

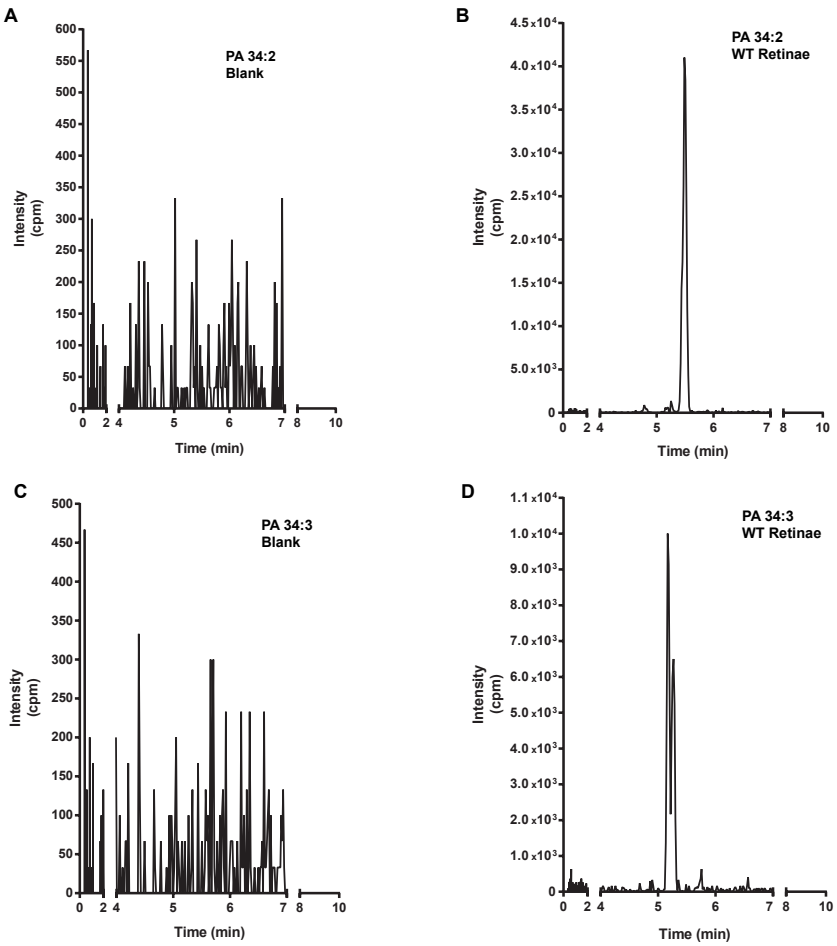

Figure A.9 : Representative chromatograms - PA (34 species)
The x-axis represents elution time; y-axis represents intensity in counts per minute. The x-axis has been cropped to focus on the elution time for each species.

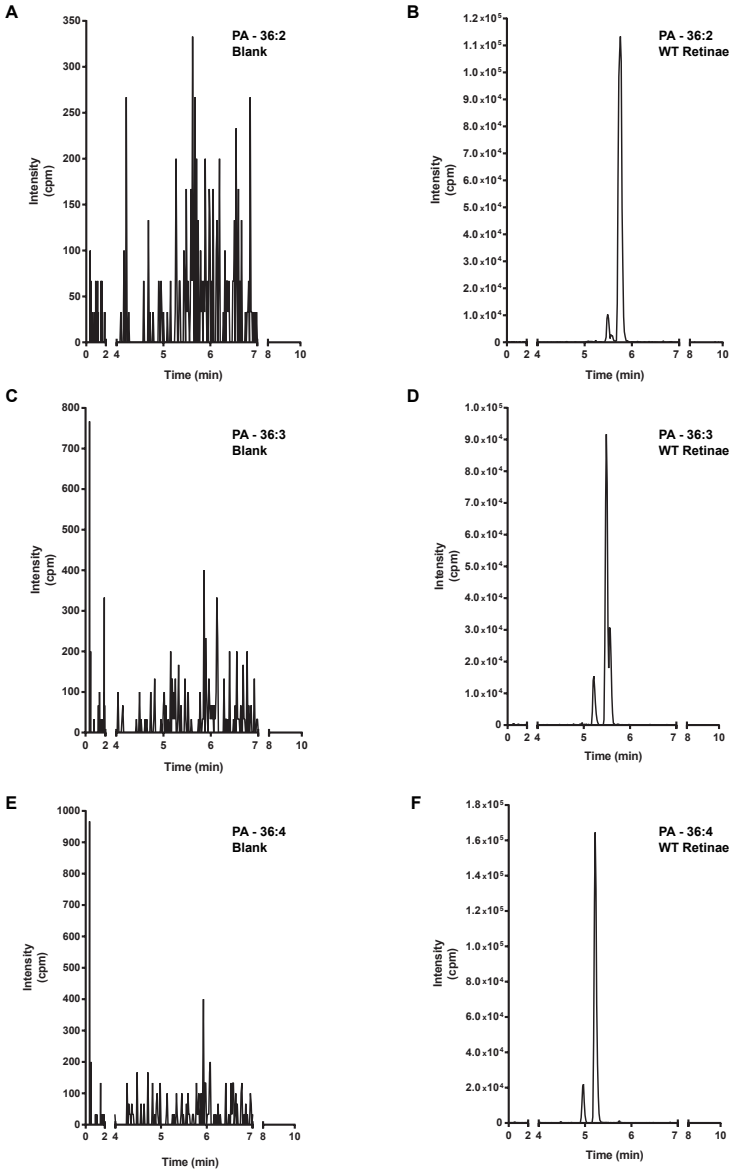

Figure A.10 : Representative chromatograms - PA (36 species)
The x-axis represents elution time; y-axis represents intensity in counts per minute. The x-axis has been cropped to focus on the elution time for each species.

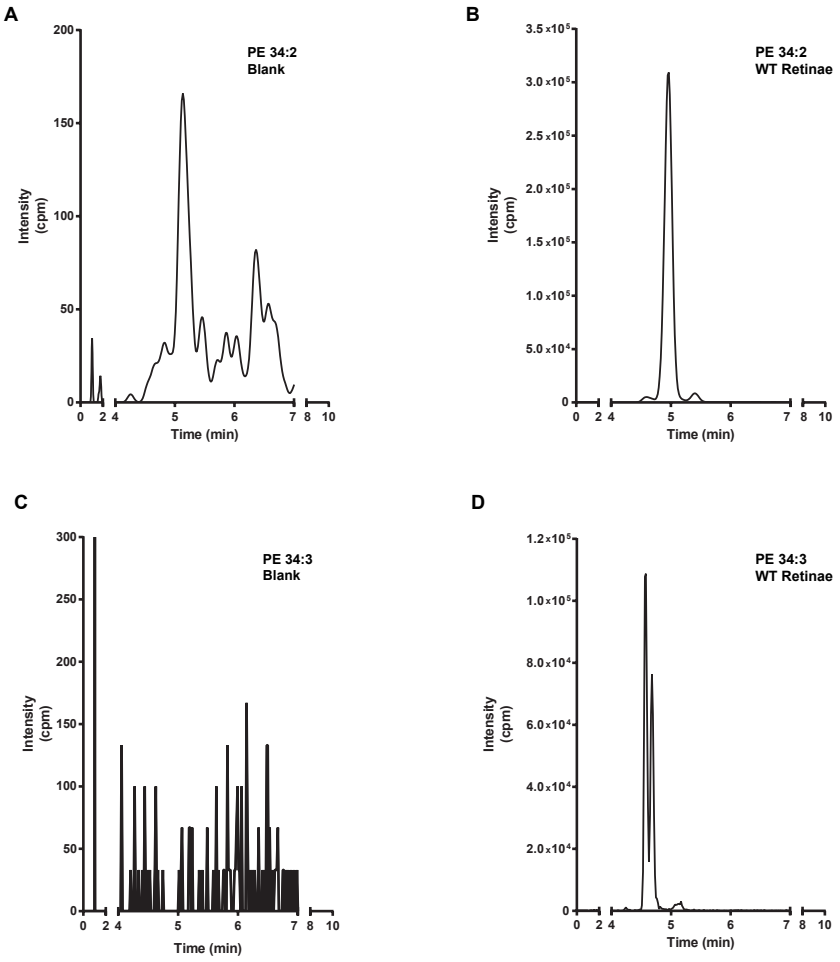

Figure A.11 : Representative chromatograms - PE (34 species) The x-axis represents elution time; y-axis represents intensity in counts per minute. The x-axis has been cropped to focus on the elution time for each species.

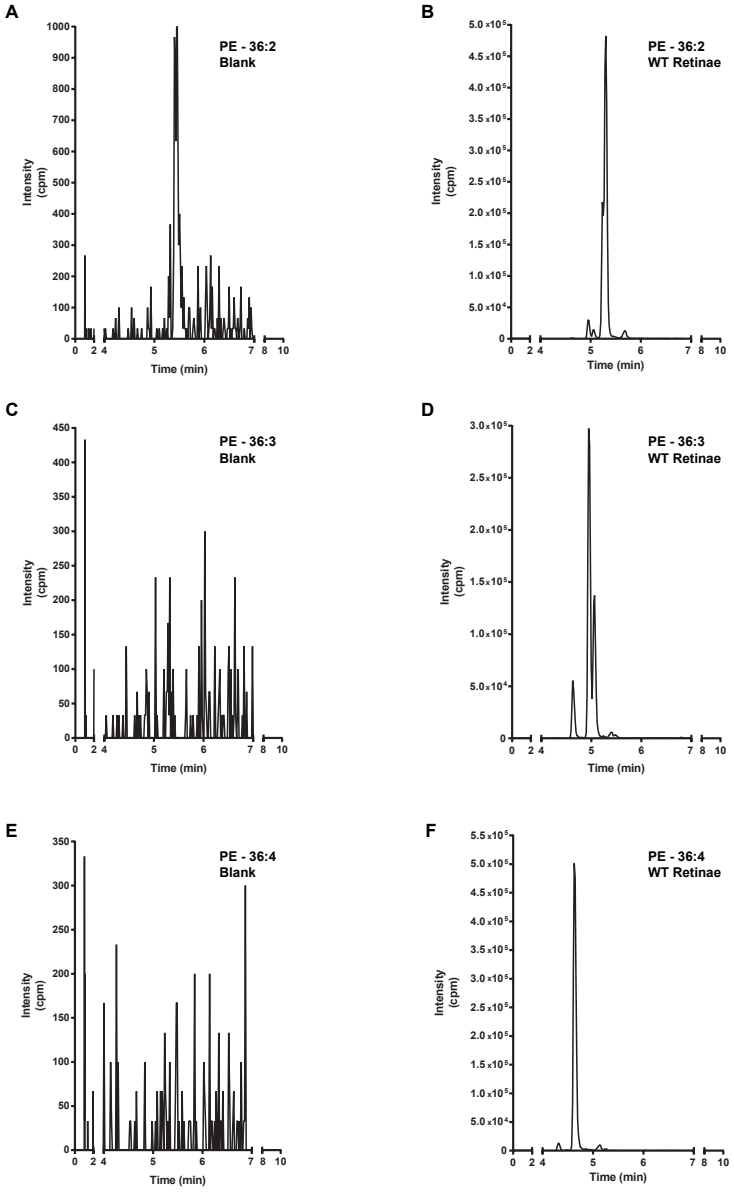

Figure A.12 : Representative chromatograms - PE (36 species) The x-axis represents elution time; y-axis represents intensity in counts per minute. The x-axis has been cropped to focus on the elution time for each species.